

University of Exeter

Hierarchy in Honeycombs

Submitted by Christopher Michael Taylor, to the University of Exeter as a thesis for the degree of Doctor of Philosophy in Engineering

In July 2012

It is a requirement of the project sponsor that the contents of this thesis are not made publicly available due to commercial sensitivities, The External Examiner will be required to sign a confidentiality agreement.

I certify that all material in this thesis which is not my own work has been identified and that no material has previously been submitted and approved for the award of a degree by this or any other University.

.....

Christopher Michael Taylor

Abstract

The main aim of this project was to examine the effects of introducing hierarchy into honeycombs and determining the variables that preside over the global response of the structure. Specifically to understand how the in and out-of-plane elastic and non-linear plastic properties of honeycombs were affected by hierarchy. Analytical analysis of hierarchical honeycombs has been used to explain and predict the response of finite element simulations validated by experimental investigations.

The early stage of the investigation focused on finding if the elastic modulus could be maintained or improved on an equal density basis due to the introduction of hierarchy. It is clear that honeycombs are sensitive to hierarchical sub-structures, particularly the fraction of mass shared between the super-and sub-structures. Introduction of an additional level of hierarchy without reducing performance is difficult, but was possible by functional grading. Another original result was that it was determined when the sub-structure could be assumed to be a continuum of the super-structure. Meaning the material properties from a single unit sub-cell could be used as the constituent material properties of the super-structure, as in previous work by (Lakes 1993) and (Carpinteri *et al* 2009) for example.

Work investigating the in-plane, non-linear plastic response of hierarchical honeycombs showed that the introduction of hierarchy into honeycombs can have the effect of delaying the onset of elastic buckling, which is a common failure mechanism for low relative density structures. As such it was possible to achieve a marked increase in the recoverable energy absorbed by hierarchical honeycombs prior to elastic buckling or plastic yield. The potential benefits are less *apparent* in higher relative density structures due to the onset of plasticity becoming the first mode of failure. The out-of-plane properties also investigated showed no increase in the elastic properties due to the introduction of hierarchy, but showed a marked increase in the out-of-plane elastic buckling stress of 60% when compared to a conventional hexagonal honeycomb of the same relative density.

Contents

Title Page	i
Abstract	ii
Contents	iii
List of Figures	viii
List of Tables	xxi
Nomenclature	xxii
Acknowledgements	xxvii
Dissemination	xxviii
Chapter 1. Introduction & Literature Review	1
1.1 Introduction	1
1.2 Cellular Solids	1
1.2.1 Honeycombs.....	4
1.3 Hierarchy	21
Chapter 2. Modelling	32
2.1 Introduction	32
2.2 Method.....	36
2.2.1 Wire Elements	36
2.2.2 Shell Elements	40
2.3 Results	42
2.3.1 Wire Elements	42
2.3.2 Boundary Conditions and Sample Size	44
2.3.3 Shell Elements	46
2.3.4 Boundary Conditions and Sample Size	49
2.4 Discussion.....	51
2.4.1 Wire Elements	51
2.5 Shell Elements	51

2.6	Conclusion	53
Chapter 3. Introducing Hierarchy into Honeycombs		54
3.1	Introduction	54
3.2	Methods	55
3.2.1	Hierarchical Length Ratio	55
3.2.2	Co-ordination number.....	58
3.2.3	Mass Distribution	59
3.2.4	Functional Grading	61
3.2.5	Functional Grading and Co-Ordination Number	63
3.2.6	Functional Grading, Co-ordination Number and HLR	65
3.2.7	Functional Grading, Co-ordination Number and Change in Aspect Ratio.....	68
3.3	Analytical.....	71
3.3.1	Conventional honeycombs.....	71
3.3.2	Hierarchical honeycombs.....	72
3.4	Results	75
3.4.1	Hierarchical Length Ratio	75
3.4.2	Co-ordination number.....	76
3.4.3	Mass Distribution	77
3.4.4	Functional Grading	78
3.4.5	Functional Grading and Co-ordination Number HLR	80
3.4.6	Functional Grading and Co-ordination Number, Change in Aspect Ratio.....	83
3.5	Discussion.....	87
3.5.1	Hierarchical Length Ratio and Mass Distribution.....	87
3.5.2	Co-ordination number.....	87
3.5.3	Functional Grading	88
3.5.4	Functional Grading and Co-ordination Number HLR	89
3.5.5	Functional Grading and Co-ordination Number, Change in Aspect Ratio.....	89
3.6	Conclusion	92
Chapter 4. In-Plane Change in The Sub-Structure Poisson's Ratio		93
4.1	Introduction	93
4.2	Method.....	96
4.2.1	Hierarchical Length Ratio	96

4.2.2	Investigating Change in ϑ_{sub}	98
4.2.3	Investigating Change in h/l	99
4.3	Analytical.....	101
4.4	Results	104
4.4.1	Hierarchical Length Ratio	104
4.4.2	Investigating Change in ϑ_{sub}	105
4.4.3	Investigating Change in h/l	107
4.5	Discussion.....	110
4.6	Conclusion.....	113
Chapter 5. In-Plane Functionally Graded Hierarchical Honeycombs.....		114
5.1	Introduction	114
5.2	Methods	117
5.2.1	Finite Element Model.....	117
5.3	Analytical models	122
5.3.1	Conventional honeycombs.....	122
5.3.2	Hierarchical honeycombs.....	123
5.3.3	Functionally graded hierarchical honeycombs	124
5.4	Results	128
5.4.1	FE models	128
5.4.2	Analytical models	134
5.5	Discussion.....	139
5.6	Conclusion.....	141
Chapter 6. In-Plane Plasticity and Non-Linear Response.....		142
6.1	Introduction	142
6.2	Method.....	143
6.2.1	Functionally Graded	143
6.2.2	NPR.....	145
6.2.3	Finite Element Model.....	145
6.3	Results	149
6.3.1	Stress Strain and Internal Energy for $\rho^*_{rel} = 0.00577$	149
6.3.2	Stress, Strain and Internal Energy for $\rho^*_{rel} = 0.0577$	157

6.3.3	Triangular Super-Structure Triangular Sub-Structure Aluminium and Steel (6–6)	167
6.3.4	Negative Poisson’s Ratio Sub-Structure	169
6.4	Discussion	173
6.4.1	Functional Grading for Co-ordination Numbers for $\rho_{rel}^* = 0.00577$	173
6.4.2	Functional Grading for Co-ordination Numbers for $\rho_{rel}^* = 0.0577$	178
6.4.3	Poisson’s Ratio Sub-Structure	182
6.5	Conclusion	184
Chapter 7. Out-of-Plane Plasticity and Non-Linear Response.....		185
7.1	Introduction	185
7.2	Method.....	187
7.2.1	Elastic Models, Functional Grading and HLR.....	187
7.2.2	Functional Grading and Change in Aspect Ratio	189
7.2.3	Plastic Models	193
7.3	Analytical.....	195
7.3.1	Linear-Elastic Deformation of Conventional honeycombs.....	195
7.3.2	Linear-Elastic Deformation of Hierarchical honeycombs.....	195
7.3.3	Non-Linear-Elasticity: Elastic Buckling.....	196
7.3.4	Plastic Collapse.....	197
7.4	Results	199
7.4.1	Elastic Regime, Functional Grading and HLR.....	199
7.4.2	Functional Grading and Change in Aspect Ratio	200
7.4.3	Plastic Regime	201
7.5	Discussion.....	206
7.5.1	Elastic Models, hierarchical Length Ratio and Super-Structure Aspect Ratio...	206
7.5.2	Plasticity and Non-Linear Geometry Models	206
7.6	Conclusion	209
Chapter 8. Experimental Validation.....		210
8.1	Introduction	210
8.2	Method.....	211
8.2.1	Manufacture of Hierarchical Honeycombs	211
8.2.2	Characterisation of Continuum Material	213

8.2.3	In-plane Change in the HLR Experimental.....	214
8.2.4	In-plane Change in the Super-Structure Aspect Ratio α_{sup} Experimental	217
8.2.5	In-plane Discussion of Experimental Procedure	219
8.2.6	In-plane Discussion of Finite Element models	220
8.2.7	Out-of-plane Change in the Super-Structure Aspect Ratio α_{sup} Experimental..	223
8.2.8	Out-of-plane Discussion of Experimental Procedure.....	225
8.2.9	Out-of-plane Discussion to Finite Element models.....	225
8.3	Results	230
8.3.1	In-plane Change in the HLR Experimental.....	230
8.3.2	In-plane Change in the Super-Structure Aspect Ratio α_{sup} Experimental	236
8.3.3	Out-of-plane Change in the Super-Structure Aspect Ratio α_{sup} Experimental..	245
8.4	Discussion.....	251
8.4.1	In-plane change in HLR.....	251
8.4.2	In-plane Change in Super-Structure Aspect Ratio α_{sup}	252
8.4.3	Out-of-plane Change in Super-Structure Aspect Ratio α_{sup}	253
8.5	Conclusion	255
Chapter 9.	Discussion.....	256
9.1	In-Plane	256
9.2	Out-of-Plane	261
Chapter 10.	Conclusion	262
10.1	Further Work.....	263
References		

List of Figures

Figure 1.1: Polygons found in two dimensional cellular materials .	2
Figure 1.2: Packing of two-dimensional cells to fill a plane.	3
Figure 1.3: Three-dimensional polyhedral cells.	3
Figure 1.4: Shows the terminology and co-ordinate system used by Gibson & Ashby.	6
Figure 1.5: Shows the terminology and co-ordinate system used by Gibson & Ashby.	7
Figure 1.6: Comparison of measured and calculated force-displacement responses.	10
Figure 1.7: Shows the out-of-plane buckling of a hexagonal honeycomb.	15
Figure 1.8: Shows the terminology and dimensions used by Gibson and Ashby.	15
Figure 1.9: Shows the analytical and experimental out-of-plane crush response.	18
Figure 1.10: Shows the expansion method for manufacturing low density honeycombs.	20
Figure 1.11: Shows the corrugation manufacturing process.	20
Figure 1.12: Shows a slot and strip method.	21
Figure 1.13: Shows hierarchical structure in human compact bone over multiple size scales.	23
Figure 1.14: Shows the hierarchical structure in the Eiffel tower.	23
Figure 1.15: Show the Sierpinski carpet.	26
Figure 1.16: Shows photographs of (a) first and (b) second order corrugated cores.	27
Figure 1.17: Shows Nomenclature for solid and sandwich struts of honeycombs.	28
Figure 1.18: Shows hierarchical honeycomb.	29

Figure 1.19: Shows hierarchical honeycombs.	30
Figure 1.20: Shows level n hierarchical honeycombs as presented.	31
Figure 2.1: Shows a conventional honey annotated according to Gibson and Ashby.	33
Figure 2.2: Shows a unit cell for a conventional triangular honeycomb.	35
Figure 2.3: Shows hexagonal honeycombs from a quarter unit cell to an 8x8 array.	37
Figure 2.4: Shows triangular honeycombs from a half unit cell to an 8x8 array.	38
Figure 2.5: Shows the cross sectional area and terminology of ribs.	39
Figure 2.6: Shows the Boundary conditions applied to honeycombs.	40
Figure 2.7: Shows an example mesh for a quarter cell hexagonal honeycomb.	41
Figure 2.8: Shows an example mesh of a hexagonal and triangular honeycomb.	42
Figure 2.9: Shows a convergence graph for the Young's modulus of a hexagonal.	43
Figure 2.10: Shows a convergence graph for the Young's modulus of a hexagonal.	44
Figure 2.11: Shows a convergence graph for the Young's modulus of a triangular.	45
Figure 2.12: Shows a convergence graph for the Young's modulus of a triangular.	45
Figure 2.13: Shows Young's modulus against the relative density ρ^*_{rel} of honeycombs.	46
Figure 2.14: Shows Young's modulus against the relative density ρ^*_{rel} of honeycombs.	46
Figure 2.15: Shows a convergence graph for the Young's modulus of a honeycomb.	47
Figure 2.16: Shows a convergence graph for the Young's modulus of a honeycomb.	48

Figure 2.17: Shows a convergence graph for the Young's modulus of a honeycomb.	49
Figure 2.18: Shows a convergence graph for the Young's modulus of a honeycomb.	49
Figure 2.19: Shows Young's modulus against the relative density ρ^*_{rel} for honeycombs.	50
Figure 2.20: Shows Young's modulus against the relative density ρ^*_{rel} for honeycombs.	50
Figure 3.1: Shows the geometry for hierarchical hexagonal honeycombs.	55
Figure 3.2: Shows the geometry for hierarchical honeycombs with different HLR's.	56
Figure 3.3: Shows 2D honeycombs of different connectivity and co-ordination number.	58
Figure 3.4: Shows the geometry of hierarchical structures with different co-ordination.	59
Figure 3.5: Shows the mass distribution between the sub and super-structure.	60
Figure 3.6: Shows hexagonal hierarchical honeycombs.	61
Figure 3.7: Shows triangular hierarchical.	62
Figure 3.8: a) Shows the cell geometry and parameters for a conventional honeycomb.	63
Figure 3.9: Shows hierarchical honeycombs with 100% of the mass in the sub-structure.	64
Figure 3.10: Shows how the HLR changes for a (3-3) hierarchical honeycomb.	66
Figure 3.11: Shows how the HLR changes for a (3-6) hierarchical honeycomb.	66

Figure 3.12: Shows how the HLR changes for a (6-6) hierarchical honeycomb.	67
Figure 3.13: Shows how the HLR changes for a (6-3) hierarchical.	68
Figure 3.14: Shows how the sub and super-structure dimensions change.	69
Figure 3.15: Shows how the sub and super-structure dimensions change.	69
Figure 3.16: Shows how the sub and super-structure dimensions change.	70
Figure 3.17: Shows how the sub and super-structure dimensions change.	70
Figure 3.18: The elastic modulus for a hierarchical hexagonal honeycomb.	75
Figure 3.19: The elastic modulus for a hierarchical equilateral triangle honeycomb.	76
Figure 3.20: Shows the elastic modulus normalised to a conventional honeycomb.	77
Figure 3.21: Shows the Young's modulus normalised to a conventional hexagonal honeycomb of equivalent mass against the mass distribution within the sub-structure.	78
Figure 3.22: The elastic modulus normalised to a conventional hexagonal honeycomb of equivalent mass for hierarchical hexagonal structures with multiple mass distributions.	79
Figure 3.23: The elastic modulus normalised against a conventional triangular honeycomb of equivalent mass for hierarchical equilateral triangular structures for multiple mass distributions.	79
Figure 3.24: The FE predicted Young's modulus of a hexagonal super-structure and a hexagonal sub-structure HHs (normalised with respect to a conventional hexagonal.	80
Figure 3.25: The FE predicted Young's modulus of a hexagonal super-structure and a triangular sub-structure HHs (normalised with respect to a conventional hexagonal honeycomb of the same relative density) vs the number of sub-cells spanning the super-structure.	81

Figure 3.26: The FE predicted Young's modulus of a (6-6).	82
Figure 3.27: The FE predicted Young's modulus of a (6-3).	83
Figure 3.28: Shows the Young's moduli vs the super-cell rib thickness t_{sup} .	83
Figure 3.29: Shows the Young's moduli vs the super-cell rib thickness t_{sup} .	84
Figure 3.30: Shows the Young's moduli vs the super-cell rib thickness t_{sup} .	85
Figure 3.31: Shows the Young's moduli vs the super-cell rib thickness t_{sup} .	86
Figure 4.1: Compares an auxetic and a conventional material under tension	93
Figure 4.2: Shows a hierarchical honeycomb with a NPR sub-structure.	94
Figure 4.3: Shows the HLR of the hierarchical honeycomb with a NPR sub-structure.	97
Figure 4.4: Shows the HLR of the hierarchical honeycomb with a NPR sub-structure.	97
Figure 4.5: Shows the HLR of the hierarchical honeycomb with a NPR sub-structure.	98
Figure 4.6: Shows a hierarchical honeycomb with a re-entrant sub-structure.	99
Figure 4.7: Shows a hierarchical honeycomb with a re-entrant sub-structure.	100
Figure 4.8: Shows a hierarchical honeycomb with a re-entrant sub-structure.	100
Figure 4.9: Shows the Young's modulus of a honeycomb with NPR sub-structure.	104
Figure 4.10: Shows Young's modulus E_1 and E_2 normalized to conventional honeycomb.	105
Figure 4.11: Shows Young's modulus E_1 and E_2 normalized to conventional honeycomb.	106
Figure 4.12: The anisotropy present in re-entrant hierarchical structures as a polar plot.	107

Figure 4.13: Shows a polar plot of Young's modulus for on axis and off axis.	108
Figure 4.14: Shows a polar plot of Young's modulus for on axis and off.	108
Figure 4.15: Shows a polar plot of Young's modulus for on axis and off axis.	109
Figure 5.1: Shows the cell geometry and parameters for a conventional hexagonal honeycomb.	118
Figure 5.2: A hierarchical unit cell with a distribution of sub-cell rib thicknesses.	119
Figure 5.3: The properties of the sub-cells in a super-structure rib, as shown in and the layers.	125
Figure 5.4: Shows the mass distribution across the super-structure rib thickness.	128
Figure 5.5: The row number of the sub-cells across the super-structure.	130
Figure 5.6: The row number of the sub-cells across the super-structure.	131
Figure 5.7: Shows multiple functionally graded hierarchical structures.	132
Figure 5.8: Shows multiple functionally graded hierarchical structures.	133
Figure 5.9: Shows multiple functionally graded hierarchical structures.	134
Figure 5.10: The FE and analytical model of Young's moduli vs the super-cell thickness.	135
Figure 5.11: The deformed FE mesh of a hierarchical honeycomb.	135
Figure 5.12: The FE and analytical model predictions of in-plane Young's modulus.	136
Figure 5.13: Shows the deformation of a functionally graded hierarchical honeycomb.	136
Figure 5.14: The FE and analytical model prediction of in-plane Young's modulus vs t_{sup} .	137

Figure 5.15: Shows the deformation of a functionally graded hierarchical honeycomb.	138
Figure 6.1: Shows how the sub and super-structure dimensions.	144
Figure 6.2: Shows how the sub and super-structure dimensions change.	144
Figure 6.3: Shows how the sub and super-structure dimensions change.	144
Figure 6.4: Shows how the sub and super-structure dimensions change.	145
Figure 6.5: Shows the Stress Strain response of hierarchical honeycombs.	150
Figure 6.6: Shows the internal energy absorbed by models against applied strain.	151
Figure 6.7: Shows a deformation plot of a (3-3) hierarchical honeycomb.	151
Figure 6.8: Shows the Stress Strain response of hierarchical honeycombs.	152
Figure 6.9: Shows the internal energy absorbed by models against applied strain.	153
Figure 6.10: Shows a deformation plot of a (3-6) hierarchical honeycomb.	153
Figure 6.11: Shows the Stress Strain response of hierarchical honeycomb.	154
Figure 6.12: Shows the internal energy absorbed by models against applied strain.	155
Figure 6.13: Shows a deformation plot of a (6-6) hierarchical honeycomb.	155
Figure 6.14: Shows the Stress Strain response of hierarchical honeycombs.	156
Figure 6.15: Shows the internal energy absorbed by models against applied strain.	156
Figure 6.16: Shows a deformation plot of a (6-3) hierarchical honeycomb.	157
Figure 6.17: Shows the Stress Strain response of hierarchical honeycombs.	158
Figure 6.18: Shows the internal energy absorbed by models against applied strain.	159
Figure 6.19: Shows the extent of plastic energy absorption of internal energy.	159
Figure 6.20: Shows the Stress Strain response of hierarchical honeycombs.	161

Figure 6.21: Shows the internal energy absorbed by models against applied strain.	161
Figure 6.22: Shows the extent of plastic energy absorption of internal energy.	162
Figure 6.23: Shows the Stress Strain response of hierarchical honeycombs.	163
Figure 6.24: Shows the internal energy absorbed by models against applied strain.	163
Figure 6.25: Shows the Stress Strain response of hierarchical honeycombs.	164
Figure 6.26: Shows the internal energy absorbed by models against applied strain.	165
Figure 6.27: Shows the extent of plastic energy absorption of internal energy.	165
Figure 6.28: Shows the Stress Strain response of 52100 steel hierarchical honeycombs.	166
Figure 6.29: Shows the Stress Strain response of AA356.0 hierarchical honeycombs.	167
Figure 6.30: Shows the stress strain response of NPR sub-structures with a MD of 25%.	168
Figure 6.31: Shows the stress strain response of NPR sub-structures with a MD of 50%.	169
Figure 6.32: Shows the stress strain response of NPR sub-structures with a MD of 75%.	169
Figure 6.33: Shows internal energy against strain for NPR sub-structures.	170
Figure 6.34: Shows internal energy against strain for NPR sub-structures.	171
Figure 6.35: Shows internal energy against strain for NPR sub-structures.	171
Figure 7.1: Shows how the HLR changes for a (3-3) hierarchical honeycomb.	187

Figure 7.2: Shows how the HLR changes for a (3-3) hierarchical honeycomb.	187
Figure 7.3: Shows how the HLR changes for a (3-3) hierarchical honeycomb.	188
Figure 7.4: Shows how the sub and super-structure dimensions change.	189
Figure 7.5: Shows a 2D plan view of a hexagonal honeycomb array.	190
Figure 7.6: Shows the boundary conditions applied to the top and bottom face of a conventional honeycomb.	191
Figure 7.7: a) Shows how the boundary conditions were applied to the vertical edges of a conventional hexagonal honeycomb.	192
Figure 7.8: Shows the out-of-plane Young's modulus of hierarchical honeycombs.	198
Figure 7.9: Shows the Young's modulus of a functionally graded hierarchical honeycomb normalised to a conventional hexagonal honeycomb against the super-structure t_{sup} .	199
Figure 7.10: Shows the out-of-plane stress strain response of hierarchical honeycombs.	201
Figure 7.11: Shows the Plastic Dissipation Energy / Internal Energy for functionally graded hierarchical honeycombs.	201
Figure 7.12: Shows the internal energy of functionally graded hierarchical honeycombs.	202
Figure 7.13: Shows the elastic buckling stress of functionally graded hierarchical honeycombs.	204
Figure 8.1: Shows the press used to forge corrugated strips	210
Figure 8.2: Shows the rotary corrugating machine	211

Figure 8.3: Shows an example hierarchical honeycomb manufactured by the process described in this section. Characterisation	212
Figure 8.4: Shows the material characterisation of the aluminium sheet used in the manufacture of hierarchical honeycombs along with a discretisation of the material for input into FE models.	212
Figure 8.5: Shows a hierarchical honeycomb with 2 sub-cells spanning the super-structure and hierarchical length ratio $\lambda = 0.25$.	214
Figure 8.6: Shows a hierarchical honeycomb with 3 sub-cells spanning the super-structure and hierarchical length ratio $\lambda = 0.167$.	214
Figure 8.7: Shows a hierarchical honeycomb with 4 sub-cells spanning the super-structure and hierarchical length ratio $\lambda = 0.125$.	214
Figure 8.8: Shows a hierarchical honeycomb with 5 sub-cells spanning the super-structure and hierarchical length ratio $\lambda = 0.1$.	215
Figure 8.9: Shows a hierarchical honeycomb with 6 sub-cells spanning the super-structure and hierarchical length ratio $\lambda = 0.0833$.	215
Figure 8.10: Shows a hierarchical honeycomb with a super-structure aspect ratio $\alpha_{sup} = 1.15$ and a hierarchical length ratio $\lambda = 0.5$.	216
Figure 8.11: Shows a hierarchical honeycomb with a super-structure aspect ratio $\alpha_{sup} = 1.73$ and a hierarchical length ratio $\lambda = 0.333$.	217
Figure 8.12: Shows a hierarchical honeycomb with a super-structure aspect ratio $\alpha_{sup} = 2.89$ and a hierarchical length ratio $\lambda = 0.1$.	217
Figure 8.13: Shows a hierarchical honeycomb with a super-structure aspect ratio $\alpha_{sup} = 5.77$ and a hierarchical length ratio $\lambda = 0.2$.	217
Figure 8.14: Shows a hierarchical honeycomb with a super-structure aspect ratio $\alpha_{sup} = 7.51$ and a hierarchical length ratio $\lambda = 0.077$.	218

Figure 8.15: Shows how the sub and super-structure dimensions change for a hexagonal super-structure and hexagonal sub-structure hierarchical honeycomb.	219
Figure 8.16: Shows how the sub and super-structure dimensions change for a hexagonal super-structure and hexagonal sub-structure hierarchical honeycomb.	219
Figure 8.17: Shows hierarchical honeycombs with multiple super-structure aspect ratio and hierarchical length ratio λ .	223
Figure 8.18: Shows how the sub and super-structure dimensions change.	224
Figure 8.19: Shows a 2D plan view of a hexagonal honeycomb array.	225
Figure 8.20: Shows the boundary conditions applied to the top and bottom face of a conventional honeycomb.	227
Figure 8.21 Shows Young's modulus normalised to the relative density against the number of sub-cells spanning the super-structure.	228
Figure 8.22: Shows the stress strain response for experimental and FE results.	229
Figure 8.23: Shows a comparison of the deformation between FE and experimental.	230
Figure 8.24: Shows the stress strain response for experimental and FE results.	231
Figure 8.25: Shows a comparison of the deformation between FE and experimental.	231
Figure 8.26: Shows the stress strain response for experimental and FE results.	232
Figure 8.27: Shows a comparison of the deformation between FE and experimental.	232
Figure 8.28: Shows the stress strain response for experimental and FE results.	233
Figure 8.29: Shows a comparison of the deformation between FE and experimental.	234
Figure 8.30: Shows the stress strain response for experimental and FE results.	235

Figure 8.31: Shows a comparison of the deformation between FE and experimental.	235
Figure 8.32: Shows the in-plane Young's modulus normalised to the relative density against the super-structure aspect ratio.	237
Figure 8.33: Shows the stress strain response for experimental and finite element results for a hierarchical honeycomb.	238
Figure 8.34: Shows a comparison of the deformation between FE analysis and experimental test for a hierarchical honeycomb with a super-structure aspect ratio $\alpha_{sup} = 1.15$, a relative density of 0.0300 and a HLR = 0.5.	239
Figure 8.35: Shows the stress strain response for experimental and finite element results for a hierarchical honeycomb.	240
Figure 8.36: Shows a comparison of the deformation between FE analysis and experimental test for a hierarchical honeycomb.	241
Figure 8.37: Shows the stress strain response for experimental and finite element results for a hierarchical honeycomb.	242
Figure 8.38: Shows a comparison of the deformation between FE analysis and experimental test for a hierarchical honeycomb.	242
Figure 8.39: Shows the stress strain response for experimental and finite element results for a hierarchical honeycomb.	243
Figure 8.40: Shows a comparison of the deformation between FE analysis and experimental test for a hierarchical honeycomb.	243
Figure 8.41: Shows the stress strain response for experimental and finite element results for a hierarchical honeycomb.	244
Figure 8.42: Shows a comparison of the deformation between FE analysis and experimental test for a hierarchical honeycomb.	244

Figure 8.43: Shows the in-plane Young's modulus normalised to the relative density against the super-structure aspect ratio for FE, experimental and analytical results.	245
Figure 8.44: Shows the stress strain response for experimental and finite element results for a hierarchical honeycomb.	246
Figure 8.45: Shows a comparison of the deformation between FE analysis and experimental test for a hierarchical honeycomb.	247
Figure 8.46: Shows the stress strain response for experimental and finite element results for a hierarchical honeycomb.	247
Figure 8.47: Shows a comparison of the deformation between FE analysis and experimental test for a hierarchical honeycomb.	248
Figure 8.48: Shows the stress strain response for experimental and finite element results for a hierarchical honeycomb.	248
Figure 8.49: Shows a comparison of the deformation between FE analysis and experimental test for a hierarchical honeycomb.	249
Figure 8.50: Shows the stress strain response for experimental and finite element results for a hierarchical honeycomb.	249
Figure 8.51: Shows a comparison of the deformation between FE analysis and experimental test for a hierarchical honeycomb.	250

List of Tables

Table 3.1: Shows the analytical equations applied to the sub and super-structure of hierarchical honeycombs of co-ordination number (3-3), (3-6), (6-6) and (6-3).....	74
Table 5.1: Shows the distributions studied as a percentage of rib thickness for each region....	120
Table 6.1: Shows the change in sub-structure aspect ratio dependent on the super-structure aspect ratio for a (3-3) hierarchical honeycomb.....	174
Table 6.2: Shows the change in sub-structure aspect ratio dependent on the super-structure aspect ratio for a (3-6) hierarchical honeycomb.....	176
Table 6.3: Shows the change in sub-structure aspect ratio dependent on the super-structure aspect ratio for a (3-6) hierarchical honeycomb.....	177
Table 8.1: Shows how the HLR and the relative density changes as the number of sub-cells spanning the super-structure changes.....	215
Table 8.2 Shows how the HLR and the relative density changes as the super-structure aspect ratio α_{sup} changes.....	218
Table 8.3: Shows how the plastic strain response was inputted into Abaqus	222
Table 8.4 Shows how the HLR and the relative density changes as the super-structure aspect ratio α_{sup} changes.....	224

Nomenclature

l	length of conventional honeycomb
h	height of conventional honeycomb
t	Thickness of conventional honeycomb
θ	Internal angle of conventional honeycomb
d	Depth of honeycomb
ρ_{rel}^*	Relative Density
ρ^*	Effective density of the cellular solid
ρ_s	Density of the constituent material
V	Number of vertices
E	Number of edges
F	Number of faces
C	Number of cells
E_s	Young's modulus of constituent material
ν_s	Poisson's Ratio of constituent material
G_s	Shear modulus of constituent material
E_1^*	Young's modulus in the 1 direction of honeycomb
E_2^*	Young's modulus in the 2 direction of honeycomb

ν_{12}^*	Poisson's Ratio in the 12 direction of honeycomb
G_{12}^*	Shear modulus in the 12 direction of honeycomb
ε_1	strain in the 1 direction
ε_2	strain in the 2 direction
σ_1	Stress in the 1 direction
σ_2	Stress in the 2 direction
σ_{el3}^*	elastic buckling stress in the 3 direction of honeycomb
σ_{pl3}^*	plastic collapse stress in the 3 direction of honeycomb
n	Hierarchical order number
k	Hierarchical multiplier coefficient dependant on the structure (Lakes 1993)
r	Hierarchical exponent coefficient dependant on the structure (Lakes 1993)
V_{con}	Volume of the constituent material
V_{cell}	Volume of a hexagonal unit cell
ρ_{con}	Density of the constituent material
ρ_{cell}	Density of a hexagonal unit cell
a	Profile dimension of rectangular beam
b	Profile dimension of rectangular beam

l_{sup}	Length of super-structure honeycomb
h_{sup}	Height of super-structure honeycomb
t_{sup}	Thickness of super-structure honeycomb
θ_{sup}	Internal angle of super-structure honeycomb
l_{sub}	Length of sub-structure honeycomb
h_{sub}	Height of sub-structure honeycomb
t_{sub}	Thickness of sub-structure honeycomb
θ_{sub}	Internal angle of sub-structure honeycomb
λ	Hierarchical length ratio
α	Aspect ratio of rib
α_{sup}	Aspect ratio of super-structure
α_{sub}	Aspect ratio of sub-structure
E^*_{1sup}	Young's modulus of super-structure in the 1 direction
E^*_{1sub}	Young's modulus of sub-structure in the 1 direction
ν^*_{12sub}	Poisson's Ratio of sub-structure in the 12 direction of honeycomb
Δl	Change in length
δx	Small displacement
P	Total force on super-structure

Q	Total force on sub-structure
F_{Total}	Total reaction force
A_{Total}	Total cross sectional area
t_1	Thickness in region 1
t_2	Thickness in region 2
t_3	Thickness in region 3
t_4	Thickness in region 4
h_1	Height of central functionally graded region
n_{12}	Ratio between region 1 Young's modulus and region 2 Young's modulus
n_{13}	Ratio between region 1 Young's modulus and region 3 Young's modulus
n_{14}	Ratio between region 1 Young's modulus and region 4 Young's modulus
n_{1i}	Ratio between region 1 Young's modulus and region i Young's modulus
I	Second moment of area
E_I	Internal energy
E_s	Recoverable strain energy and
E_p	Energy absorbed by plastic deformation
σ_{el3sub}^*	elastic buckling stress in the 3 direction of honeycomb of sub-structure
σ_{pl3sub}^*	plastic collapse stress in the 3 direction of honeycomb of sub-structure

σ_{el3sup}^*	elastic buckling stress in the 3 direction of honeycomb of super-structure
σ_{pl3sup}^*	plastic collapse stress in the 3 direction of honeycomb of super-structure
A_{sup}	cross sectional area of the super-structure
A_{cell}	cross sectional area of the cell

Acknowledgements

I would like to thank Professor K.E. Evans, Professor C.W. Smith and Dr Wayne Miller for their guidance and support throughout this project.

I gratefully acknowledge the support of Rolls-Royce Plc and Great Western Research.

I would also like to thank Mr Christophe Scoumaque for his part in the manufacture of hierarchical honeycombs along with the help and support from the workshop and stores.

Also thanks to Karen Pope and Liz Roberts.

Dissemination

During the course of this PhD several papers have been published in peer reviewed journals and several conferences presentations given.

Publications

C.M. Taylor, C.W. Smith, W. Miller, K.E. Evans, 2011, Effects of Hierarchy on the In-Plane Elastic Properties of Honeycombs, *International Journal of Solids and Structures*.

C.M. Taylor, C.W. Smith, W. Miller, K.E. Evans, 2012, Functional Grading in Hierarchical Honeycombs; Density Specific Elastic Performance, *Composite Structures*, 94, 2296–2305.

Conferences

C.M. Taylor, C.W. Smith, W. Miller, K.E. Evans, 2011, Hierarchy in Honeycombs, ICCS-16, 2011, Porto.

C.M. Taylor, C.W. Smith, W. Miller, K.E. Evans, 2009, Discrete Hierarchical Honeycomb Structures, Auxetics Conference, 2009, Bolton.

Chapter 1. Introduction & Literature Review

1.1 Introduction

Honeycombs are commonly used in lightweight structures and sandwich panels due to their excellent density specific elastic properties, and as a result have found application in structural roles in a variety of industries including aerospace, automotive, marine and construction industries (Wilson, 1990, Thompson and Matthews, 1995, Bitzer, 1994, Price and Timbrook., 2001). They also offer good damage tolerance and so are often used in structural roles where the ability to remain functional after damage such as an impact is critical (Gibson *et al* 1989, Triantafillou *et al* 1989). Many natural materials possess excellent compromises between density specific elastic properties and damage tolerance and/or toughness, and many of these seem to contain structural hierarchy either by accident of their manufacture or specifically to aid in damage tolerance (Fratzl and Weinkamer, 2007; Gao, 2006). Conventional hexagonal honeycombs are manufactured via a low cost route, specifically periodic adhesion of flat sheets with a subsequent in plane stretching process to open up hexagonal cells (Sypeck, 2005; Wadley, 2006). The present study investigates the effects of adding hierarchy into a structure, at the exact same density, on the elastic properties especially elastic modulus.

1.2 Cellular Solids

Cellular solids can be described as being made up of solid struts or plates which form a network, creating the edges and faces of cells. A so called two dimensional cellular solid can be created by tessellating an extruded unit cell in a plane. There are numerous cell shapes that can be tessellated, but only certain cell geometries and connectivity's fill a plane with no overlaps or gaps by a repeated single cell, the same is true in 3D space. Figure 1.1 shows some possible unit cells which can be packed in a plane, whilst Figure 1.2 shows alternative packing sequences for the cells. Likewise the same can be done with a three dimensional cell, where as opposed to using shapes in a plane, a 3D unit cell can be repeatedly packed into a space to create a cellular solid, Figure 1.3 shows possible unit cells which can be packed, (a - e) will tessellate, and (f - i) will create voids unless combined with another cell of a different shape (Gibson & Ashby 1997).

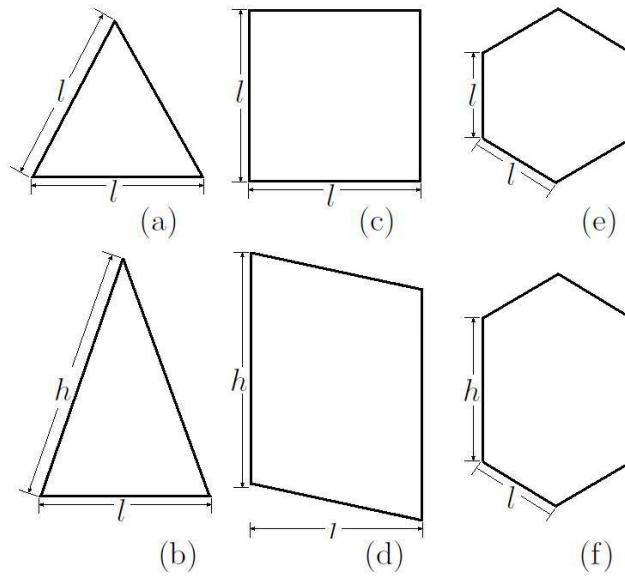


Figure 1.1: Polygons found in two dimensional cellular materials: (a) equilateral triangle, (b) isosceles triangle, (c) square, (d) parallelogram, (e) regular hexagon, (f) irregular hexagon (Gibson & Ashby 1997).

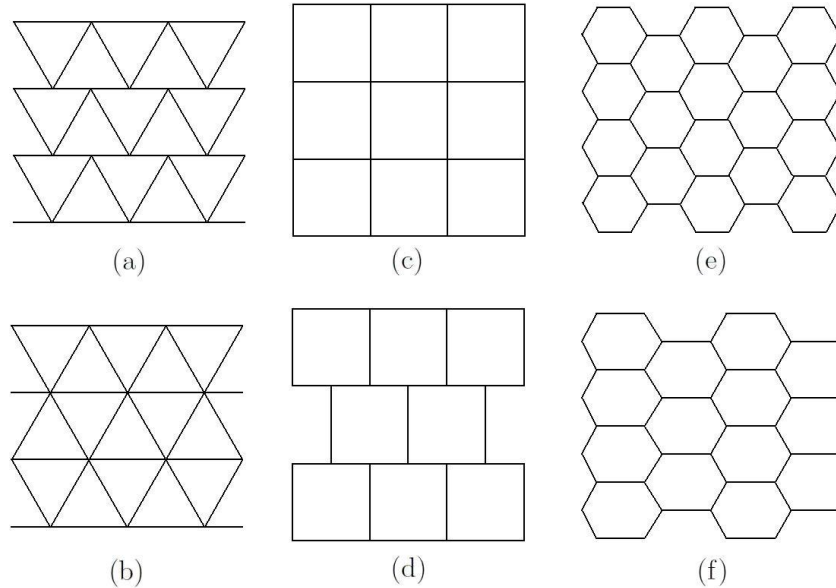


Figure 1.2: Packing of two-dimensional cells to fill a plane: (a, b) two packing's of equilateral triangles, (c, d) two packing's of squares, (e) packing of regular hexagons, (f) packing of irregular hexagons (Gibson & Ashby 1997).

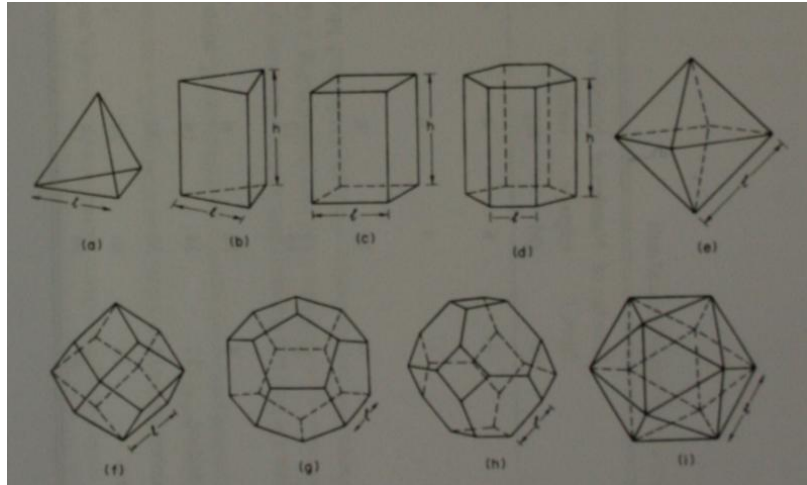


Figure 1.3: Three-dimensional polyhedral cells: (a) tetrahedron, (b) triangular prism, (c) rectangular prism, (d) hexagonal prism, (e) octahedron, (f) rhombic dodecahedron, (g) pentagonal dodecahedron, (h) tetrakaidodecahedron, (i) icosahedron (Gibson & Ashby 1997).

There are two main factors that preside over the properties of a cellular material. (i) The behaviour of the constituent material that makes the cell walls. (ii) The other is the geometric structure of the material including, the size and shape of cells along with the distribution throughout the material, the way in which matter is dispersed between the cell edges and faces, defining the relative density of the structure. The relative density ρ_{rel}^* is an important part of the characteristics of a cellular solid and is changeable by increasing the thickness of cell walls of the structure. This increases the volume of the constituent material to the void (usually composed of air or another fluid), as shown in Equation 1-1.

$$Relative\ Density\ \rho_{rel}^* = \frac{\rho^*}{\rho_s}$$

Equation 1-1

Where ρ^* is the effective density of the cellular solid and ρ_s is the density of the constituent material. The thickness of cell walls increase and the volume of pores decrease with a greater relative density, altering the material properties. When the relative density of a cellular solid is considered to be less than 0.3 as greater values are better modelled as a solid containing isolated pores (Gibson & Ashby 1997). We can

predict physical properties, notably elastic constants, by treating the unit cell as a structure formed by plates and or faces as done by Gibson and Ashby (Gibson & Ashby 1997); discussed later. There are rules governing the geometry and connectivity of 2D and 3D shapes such as Euler's Law of Connectivity where the geometry of cells and the topology by which they are connected and so is of importance to the behaviour of a cellular solid. It is necessary to determine the connectivity of a cellular solid, which can be considered as composing of vertices, joined by edges, which surround faces, which enclose cells. The number of edges which meet at a vertex is the edge-connectivity E and the number of faces that meet at an edge is the face-connectivity F . Euler's Law referenced from (Euler, 1746 and Lakatos, 1976) relates the number of vertices V , edges E , faces F and cells C by:

$$F - E + V = 1 \quad (2D)$$

Equation 1-2

$$-C + F - E + V = 1 \quad (3D)$$

Equation 1-3

Much work has been undertaken into the investigation of cellular materials and has been broken down into three main areas, honeycomb, foams and trusses. The main focuses of the current work involves honeycombs and are subsequently discussed, but similar techniques could be introduced into foams and trusses.

1.2.1 Honeycombs

1.2.1.1 In-plane Properties

Gibson and co-workers (Gibson *et al*, 1982) set out the fundamental underpinnings of the in-plane behaviour of honeycombs, and derived expressions for elastic modulus and several other physical properties for hexagonal honeycombs from beam mechanics equations for the Young's modulus, Poisson's ratio and the shear modulus are shown in Equation 1-4, Equation 1-5, Equation 1-6 and Equation 1-7. Figure 1.4 and Figure 1.5 shows hexagonal and equilateral triangle unit cells, annotated according to Gibson and Ashby's terminology.

$$\frac{E_1^*}{E_s} = \left(\frac{t}{l}\right)^3 \frac{\cos\theta}{(h/l + \sin\theta)\sin^2\theta}$$

Equation 1-4

$$\frac{E_2^*}{E_s} = \left(\frac{t}{l}\right)^3 \frac{h/l + \sin\theta}{\cos^3\theta}$$

Equation 1-5

$$v_{12}^* = -\frac{\epsilon_2}{\epsilon_1} = \frac{\cos^2\theta}{(h/l + \sin\theta)\sin\theta}$$

Equation 1-6

$$\frac{G_{12}^*}{E_s} = \left(\frac{t}{l}\right)^3 \frac{(h/l + \sin\theta)}{(h/l)^2(1 + 2 h/l)\cos\theta}$$

Equation 1-7

A similar approach was also implemented by Gibson & Ashby for a triangular honeycomb that is stretch dominated in Equation 1-8 (Gibson & Ashby 1997).

$$\frac{E_1^*}{E_s} = \frac{E_2^*}{E_s} = 1.15 \frac{t}{l}$$

Equation 1-8

Where t and l are the thickness and length of the cell walls respectively and θ is the internal angle of the hexagonal honeycomb and can be seen in Figure 1.4 and Figure 1.5.

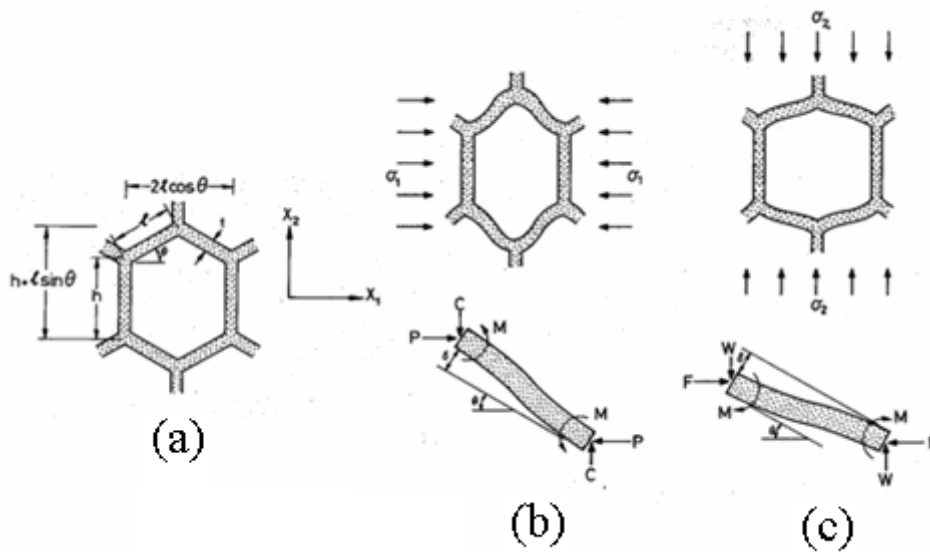


Figure 1.4: Shows the terminology and co-ordinate system used by Gibson & Ashby for an undeformed hexagonal honeycomb in (a) the bending caused by loads in the X_1 and X_2 directions are shown in (b) and (c) respectively (Gibson & Ashby 1997).

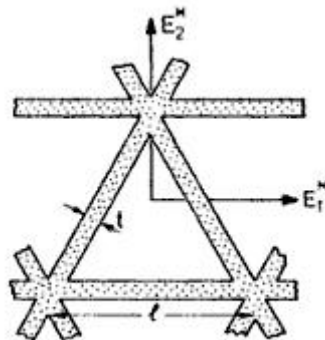


Figure 1.5: Shows the terminology and co-ordinate system used by Gibson & Ashby for a undeformed triangular honeycomb

Masters and Evans (Masters & Evans 1996, Evans 1991) later added some useful complexity to these models of in-plane properties by accounting for other deformation modes, specifically stretching/compression and hinging of ribs. In terms of elastic properties honeycombs can be sufficiently described by considering them as collections of beams or plates, usually deformed in flexure, and for which explicit relationships between deformation and force are known. The elastic response for a whole unit cell can be derived, and since a honeycomb is formed by tessellation of such unit cells, the

continuum elastic properties of a honeycomb can be represented very well by those of its unit cell.

Flexure is the dominant deformation mechanism of in-plane hexagonal honeycombs with conventionally slender ribs ($t/l < 0.1$) (Gibson and Ashby 1982, Evans 1991, Masters 1996). In flexure, the elastic modulus of such a structure is dominated by an aspect ratio term, specifically $(t/l)^3$, arising from the mechanics of beams in flexure. Notably, for triangular based unit cells Deshpande has shown deformation is stretch dominated (Deshpande 2001), as their particular connectivity means individual beams deform primarily by tension and compression. Square geometries are stretch dominated on-axis and flexure dominated of axis vs the cell architecture. Thus, stretch dominated structures are potentially attractive for applications despite their inherently higher manufacturing costs. Interestingly, flexure dominated structures can have greater energy absorption because they have a longer post-yield response in comparison to the stretch dominated structures (in compression) which tend to buckle and rupture/fail/collapse quickly post yield (Deshpande 2001). The anelastic behaviour of honeycombs is well described in various experimental and modelling studies (Gibson *et al* 1989, Triantafillou *et al* 1989, Maiti *et al* 1984, Klintworth & Stronge 1988, Papka & Kyriakides 1994, Papka & Kyriakides 1998a&b, Miller *et al* 2010a&b).

Gibson & Ashby later add further complexity to their hexagonal honeycomb model allowing accounting for shear with in the ribs using Timoshenko beam theory developing predictions for the Young's modulus, Poisson's ratio and the shear modulus (Gibson & Ashby 1997). The equations for E_1^* v_{12}^* are shown in Equation 1-9 and Equation 1-10.

$$E_1^* = \left(\frac{t}{l}\right)^3 \frac{\cos\theta}{\left(\frac{h}{l} + \sin\theta\right) \sin^2\theta} \frac{1}{1 + (2.4 + 1.5v_s + \cot^2\theta)(t/l)^2} E_s$$

Equation 1-9

$$v_{12}^* = \frac{\cos^2\theta}{\left(\frac{h}{l} + \sin\theta\right) \sin\theta} \frac{1 + (1.4 + 1.5v_s)(t/l)^2}{1 + (2.4 + 1.5v_s + \cot^2\theta)(t/l)^2}$$

Equation 1-10

The effective elastic shear modulus of certain hexagonal honeycombs was investigated by (Kelsey *et al* 1958) and (Grediac 1993) via both theoretical analysis and experimental studies on hexagonal cell honeycombs. Kelsey *et al* adopted the unit displacement and unit load methods to develop expressions for upper and lower limits for the shear modulus of honeycombs. The work by Kelsey *et al* made the following five assumptions that have been adopted in the majority of work regarding the modelling of honeycombs.

(1) The adhesive provides a perfect bond between the common faces of the foil and also between the foil edges and the sandwich faces, without contributing any additional stiffness or flexibility to the core.

(2) The core is of perfect manufacture so that all cells are of identical size and shape and are symmetrical about longitudinal and transverse centre lines.

(3) The elements of the core are only capable of carrying shear stress in the plane of the individual foil panels, over each of which the shear stress (or strain) is constant.

(4) The thickness t of the foil is small compared with the dimensions l and h .

(5) The effect of the finite radius of the cell corners is negligible. This assumption has been shown to be valid provided $\sin \theta \gg r/l$ and $\cos \theta \gg (r-h)/l$, where r is the corner radius. (Kelsey *et al* 1958).

A series of investigations by Papka and Kyriakides has focused on the in-plane properties of honeycombs. In (Papka and Kyriakides, 1994) the in-plane compressive response of metallic honeycombs is investigated experimentally and numerically. Papka and Kyriakides show the initial linear elastic response of hexagonal honeycombs followed by the extended load plateau as the honeycomb is crushed and finally the densification region as the ribs come into contact with each other. This three stage response can be seen in the experimental and numerical results presented by Papka and Kyriakides in Figure 1.6 along with images of the progressive collapse.

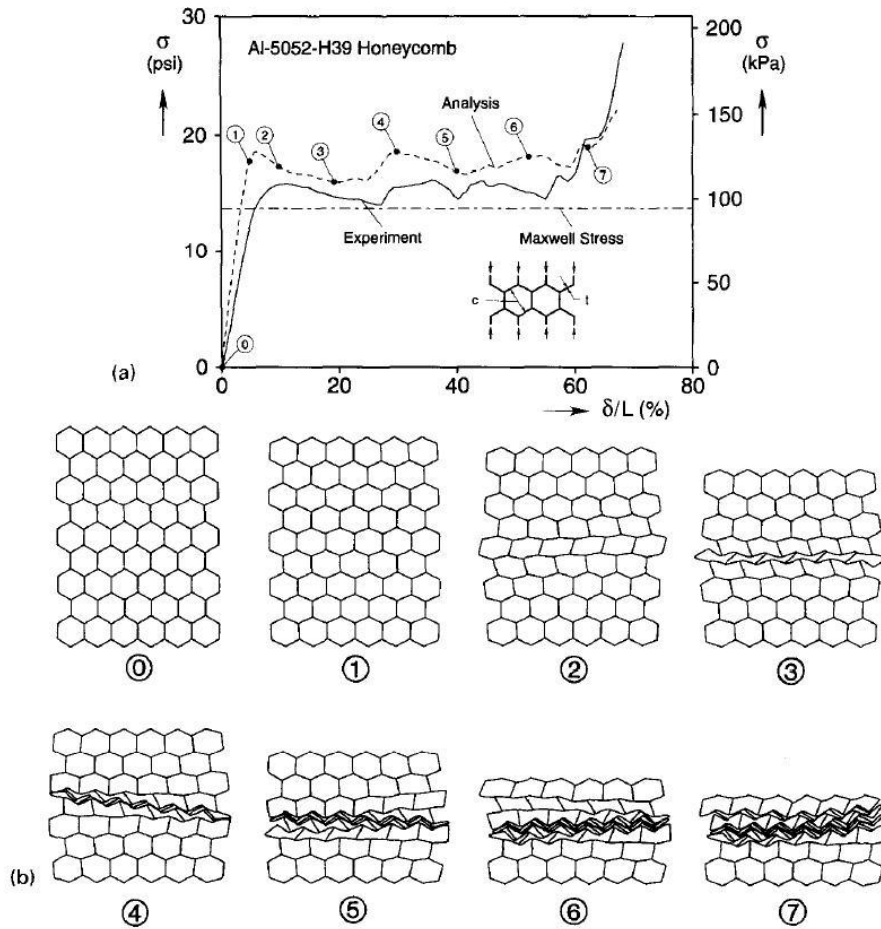


Figure 1.6: (a) Comparison of measured and calculated force-displacement responses of a 9 x 6 cells honey-comb specimen. (b) Sequence of calculated collapse configurations (Papka and Kyriakides, 1994).

The effect of the manufacturing process was also investigated in (Papka and Kyriakides, 1994) via a two stage numerical model where the expansion process was initially modelled followed by a secondary compression load. The expanded and ideal honeycombs were then compared and showed close approximation to each other. The work was revisited again by Papka and Kyriakides in 1998 (Papka and Kyriakides, 1998a) investigating larger arrays. The results confirm those previously presented in the 1994 paper. The study was further extended to polycarbonate honeycombs in (Papka and Kyriakides, 1998b & Chung & Waas 2001). The biaxial crushing of honeycomb was investigated in (Papka and Kyriakides, 1999a&b) experimentally and numerically respectively. The in-plane buckling of honeycombs under bi-axial stress was also investigated by Zhang and Ashby (Zhang and Ashby 1992a) who also found that the

magnitude of the buckling stress is dependent on the relative density of the structure not the size of the unit cell, Zhang and Ashby also noted that the shape of the collapse surface depends on the geometry of the unit cell. Predictably the common failure mode of low relative density honeycombs was found to be via elastic buckling, whilst honeycomb with a higher relative density were more likely to experience plastic yield as the first failure mode. The work undertaken by Zhang and Ashby allowed the model to be adapted for changes in the boundary conditions to model a free restricted or fixed end.

Early work by (Shaw & Sata 1966) looked at the plastic behaviour of cellular materials. Shaw & Sata noted the Luder's-like bands at an angle of approximately 84° in the cellular materials investigated, specifically foam. The foam had a similar response to the honeycomb investigated in (Papka and Kyriakides, 1994) when an initial upper yield point was reached as a row collapsed it was followed by subsequent lower yield points, due to the progressive collapse of adjacent cells. Work by Ashby (Ashby 1983) investigated elastic, plastic creep and fracture mechanical properties for cellular solids specifically naturally occurring cellular solids, idealised as foams and hexagonal honeycombs to describe the deformation mechanisms. The paper shows that the deformation mechanism and material properties are dependent on the constituent material and the cell geometry. The work was further developed by (Klintworth and Stronge 1988) who investigated the deformation laws and Elasto-plastic yield for in-plane crushed honeycombs. Subsequent work by Maiti *et al* (Maiti *et al* 1984) reiterating the points made by Gibson and Ashby's previous work the material properties of cellular materials are highly dependent on the density not the cell size. Maiti *et al* also investigated the fracture toughness of foams also finding that the fracture toughness was dependent on the density rather than the cell size. The initial yield equations of 2D and 3D lattice grid composites were deduced by Fan H *et al* (Fan H *et al* 2008) using the integration method to model the stress strain curves of stretch dominated lattices. The work focused on multiple geometries including triangular and Kagome lattices. Fan H *et al* used the Ramberg-Osgood method to model non-linearities of the constituent material. Fan H *et al* found that the elastic buckling mode was more important for lattices of relative low density.

The prediction of the onset of failure in aluminium honeycombs was investigated by Triantafyllidis and Schraad (Triantafyllidis and Schraad, 1998) analytically and numerically looking closely at the influence of specimen size, geometric microstructural imperfections. Geometric imperfections were broken down into two categories; firstly systematic imperfections during the manufacturing process such as variation in the bonding length between ribs and over and under expansion of cells during the expansion method, secondly random geometric imperfections occurring due to material fabrication. The influence of bond imperfection was shown to have a dramatic effect on the cell behaviour as does the random geometric imperfections.

The effect of defects on the in-plane properties of honeycombs were investigated by (Wang & McDowell 2003) by randomly removing cell walls of periodic triangular and square honeycombs. The work showed that the in-plane properties of some geometries are more dependent on defects than other. For instance Wang & McDowell showed that triangular cell honeycombs experiences a more gradual decrease of properties than square or hexagonal cell honeycombs. Wang & McDowell also showed that the response and extent of decay was also dependant on the relative density of the honeycombs, highlighting the point that the deformation of honeycombs is also dependant on the relative density of the structure. Wang and McDowell went on to further investigate the in-plane stiffness and yield strength of multiple geometries in (Wang & McDowell 2004) paper. Wang and McDowell concluded that the geometry plays an important role in determining the properties of a honeycomb, with significant differences between bending dominated and stretch dominated structures. The effect of changing the relative density is also investigated and attention drawn to the increase of elastic buckling in low relative density structures. Wang and McDowell also agree with previous statements by Gibson and Ashby that the size scale of honeycombs does not determine the response of a honeycomb but the aspect ratio is the dominate factor.

Work investigating the effect of cell height on the in-plane properties of honeycombs when modelling was undertaken by Chen and Ozaki (2009). It was found that the properties were independent of the core height when modelling. This has important implication for future work when modelling honeycombs, as unit depth may be used to

determine the in-plane properties. This means that the size of models can be reduced by decreasing the computational cost when conducting such investigations.

1.2.1.2 Out-of-Plane Properties

The first known study on the out-of-plane properties of honeycombs was undertaken by Kelsey *et al* in (Kelsey *et al* 1958) paper. The paper focuses on the shear modulus of honeycomb cores. Predictions of the upper and lower limits are described using the unit displacement and unit load method. The paper limits itself to the elastic shear response of the aluminium honeycombs investigated. The subject was later addressed by Gibson and Ashby in (Gibson and Ashby 1988), who considered linear elastic properties of honeycombs and the out-of-plane buckling response of honeycombs. The primary deformation mode and crushing stress of axial compressed honeycombs was investigated by (McFarland 1963) via a semi-empirical model. Wierzbicki (Wierzbicki 1983) later added further complexity allowing for both bending and stretch deformation of honeycombs.

The knowledge of the out-of-plane properties of hexagonal honeycombs was further developed by Zhang and Ashby in (Zhang and Ashby 1992b) who investigated the shear and compression of honeycombs and went onto identified buckling, debonding and fracture as possible collapse mechanisms. The terminology used by Zhang and Ashby can be seen in Figure 1.7 along with the out-of-plane buckling of a hexagonal honeycomb under axial compression. Zhang and Ashby used experimental investigation of hexagonal honeycombs to validate analytical predictions. A similar approach was taken by Wang in (Wang 1991) who investigated the elastic properties along with the elastic buckling and plastic yield stress of square and triangular honeycombs.

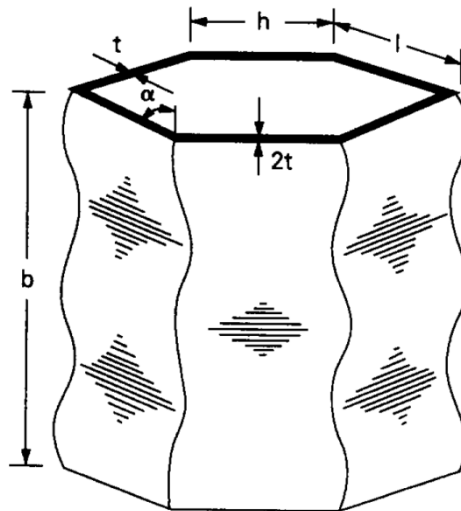


Figure 1.7: Shows the out-of-plane buckling of a hexagonal honeycomb under axial compression and the terminology used in (Zhang and Ashby 1992b).

Much of the early work investigating the out-of-plane properties including elastic buckling and plastic yield are presented in Gibson and Ashby's second edition (Gibson and Ashby 1997). Who use beam mechanics to describe the behaviour of honeycombs. The terminology for the out-of-plane dimensions according to Gibson and Ashby can be seen in Figure 1.8 and are used throughout the presented work.

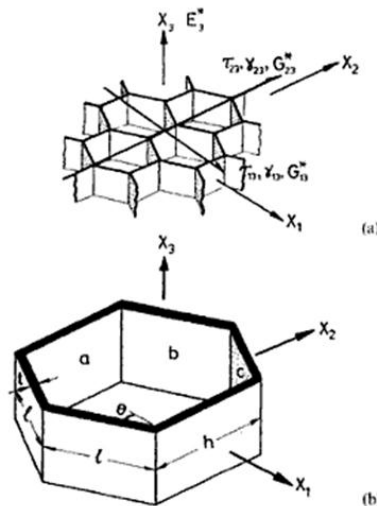


Figure 1.8: Shows the terminology and dimensions used by Gibson and Ashby (Gibson and Ashby 1997). Specifically a) honeycomb carrying loads on the faces normal to X_3 and b) dimensions of a hexagonal honeycomb.

Using beam mechanics Gibson and Ashby defined prediction for the out-of-plane properties of hexagonal honeycombs such as the out-of-plane Young's modulus E_3^* , the buckling stress σ_{el}^* and the plastic collapse stress σ_{pl}^* among others. The out-of-plane Young's modulus for a hexagonal honeycomb can be seen in Equation 1-11.

$$\frac{E_3^*}{E_s} = \left\{ \frac{h/l + 2}{2(h/l + \sin\theta)\cos\theta} \right\} \left(\frac{t}{l} \right)$$

Equation 1-11

Gibson and Ashby (1997) investigated the out-of-plane Euler buckling of a hexagonal honeycomb by considering the buckling of a plate with constraints along the two edges which lie parallel to the loading direction modelling the interaction between adjacent plates. The buckling load is determined by the second moment of area and the width of the plate (l or h). Gibson and Ashby concluded that the elastic buckling stress can be described as in Equation 1-12

$$\sigma_{el3}^* = \frac{2}{(1 - \nu_s^2)} \frac{(l/h + 2)}{(h/l + \sin\theta)\cos\theta} \left(\frac{t}{l} \right)^3 E_s$$

Equation 1-12

In a similar approach Gibson and Ashby predicted the plastic collapse stress as can be seen in Equation 1-13.

$$\sigma_{pl3}^* = \frac{(h/l + 2)}{2\cos\theta(h/l + \sin\theta)} \left(\frac{t}{l} \right)^3 \sigma_{ys}$$

Equation 1-13

Wu and Jiang undertook an experimental investigation of the axial crush of honeycombs under quasi-static and impact loads (Wu and Jiang 1997). The results showed that when subjected to a quasi-static load honeycombs experience a high peak load followed by a progressive plastic buckling region and subsequently plastic folding. Under impact loading investigated honeycombs responded in a similar manner to the quasi-static loading, but experienced higher crush strength, thought to be due to the compacted plastic fold mechanism under dynamic loads a result also seen by Goldsmith

and Sackman (1992) and Goldsmith and Louie (1995). Wu and Jiang concluded that for best use as an energy absorber under both quasi-static and dynamic loads the selection of small cell size to cell height is recommended. There have been several explanations for the increased crush strength under dynamic load, such as micro-inertia proposed in (Deshpande and Fleck 2000) and (Zhao *et al* 2005) along with others. Although other theories have also been put forward, such as that by Zhou and Mayer (Zhou and Mayer 2002) who proposed, trapped air could be the reason. Hong *et al* (Hong *et al* 2008) also investigated the dynamic crush of honeycombs and suggested that the increased crush strength as the impact velocity increases is due to the curvature of the yield surface increases near the pure compression state.

Cote *et al* (2004) investigated the out of plane properties of square honeycombs in particular comparing the compressive response as a function of the relative density. Cote *et al* showed that the peak stress is relatively insensitive to the ratio of the cell size to height and the existence of face sheets. The initial yield surfaces are derived for periodic honeycombs by Wang and McDowell (2005). The effect of elastic buckling has been removed by increasing the relative density to such a point that elastic buckling is demoted as the primary failure mode and promoting plastic yield. Wang and McDowell concluded that the cell geometry determines the yield surface shape of honeycombs of the same relative density via analytical and experimental validations.

Later work by Aktay *et al* (Aktay *et al* 2008) uses several finite element analysis techniques to model the crush behaviour of hexagonal honeycombs. Aktay *et al* uses three types of modelling, a detailed honeycomb micromechanics model, a homogenised material model and a homogenised discrete/finite element model used in a semi-adaptive numerical coupling (SAC) technique. The micro-mechanical model proved effective at modelling crush energy absorption, but was computationally expensive due to the fine mesh requirements. The homogenised model was useful to model the core as part of a sandwich panel, but was ineffective at modelling the crush response. The ability of the SAC model to simulate the extensive compression core crushing failures was more successful as it was also able to model material compaction due to local crushing. Aktay *et al* found that the crush response consisted of three phases for the considered relative densities; elastic buckling, plastic buckling followed by debonding

and fracture at cell interfaces. The micro-mechanical model of honeycomb cells used Belytschko-Tsay-4 node-thin shell elements to model the walls of the honeycomb, whilst the homogenised model uses a solid element that was assigned the anisotropic global properties of the honeycomb. The SAC technique used a similar approach to the homogenised model with solid elements, which were replaced by particles. This results in a progressive collapse of the structure as locally damaged areas are allowed to fail without element elimination and loss of contact forces. The out-of-plane crush response of hexagonal honeycombs can be seen in Figure 1.9, which shows the high initial stiffness of the honeycomb until a peak stress is achieved at which point elastic buckling or plastic yield are experienced. This is followed by a plateau region where progressive buckling and collapse occurs with the formation of folds and subsequent contact until the entire depth of the honeycomb has collapsed at which point densification occurs and is represented by the increased applied load.

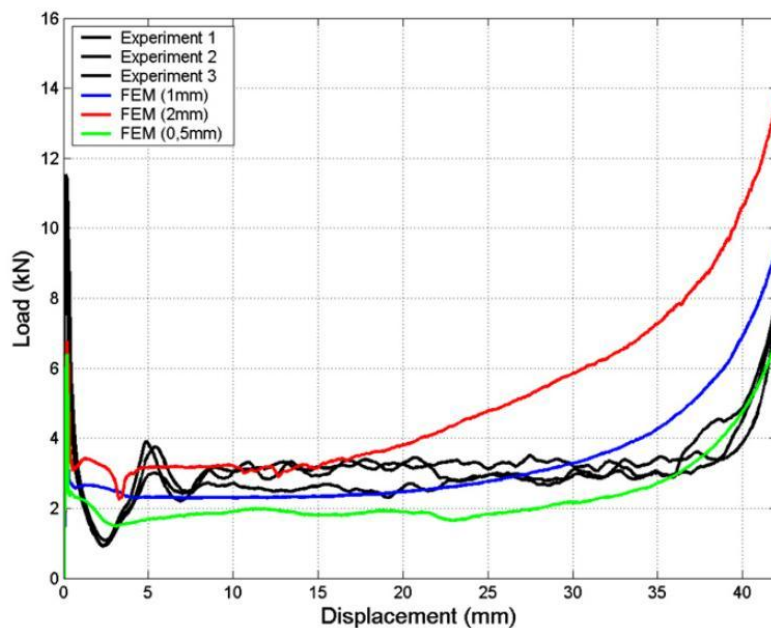


Figure 1.9: Shows the analytical and experimental out-of-plane crush response of hexagonal honeycombs as present in (Aktay *et al* 2008).

The progressive out-of-plane crushing is also investigated by Wilbert *et al* (2011) via numerical methods and validated by experimental tests. The paper investigates the effect of varying the sample size (array) and the representative boundary conditions applied to a unit cell. The paper finds that with the correct boundary conditions a unit

cell can be used to describe the global response of larger arrays, but with reduced computational cost. The models are able to accurately predict elastic buckling with the aid of a perturbation applied to the centre of rib faces. The model also predicts the folding of ribs along with the formation of folds, due to the modelled contact forces.

The use of chiral honeycombs has been investigated in (Scarpa *et al* 2007) using analytical, numerical and experimental analysis focusing on the out-of-plane compressive strength due to elastic buckling. Finite element implicit analysis was conducted using both brick element and shell elements by means of ANSYS 8.1. The geometry used to model the chiral honeycombs consisted of a cylinder and half-length ligaments. This was done using the assumption of symmetric deformation given by the local buckling behaviour of the chiral honeycomb and could be used for conventional hexagonal honeycombs. Scarpa *et al* showed that the introduction of cylinders in chiral honeycombs increased the out-of-plane compressive strength of honeycombs when compared to conventional hexagonal honeycombs of the same relative density. This work was further investigated by Miller *et al* (2010a) who took a similar approach investigating four and six connectivity chiral honeycombs. Miller *et al* reiterated previous work by Scarpa *et al*, finding that chiral honeycombs has a greater density specific buckling load than conventional hexagonal honeycombs. Further work on enhancing the buckling strength of honeycomb core can be seen in (Miller *et al* 2010b). The density specific peak compression stress was investigated for re-entrant hexagonal honeycomb and compared to conventional hexagonal honeycomb. Also investigated was the introduction of ribs and fillets on the compressive strength of the honeycombs. It was found that re-entrant honeycombs had density specific buckling stress 13% larger than the conventional hexagonal honeycomb.

1.2.1.3 Manufacture

There have been many manufacture techniques developed of the years to produce affordable cellular materials (Bitzer 1997). The manufacture a multiple cellular materials were detailed in (Wadley 2006) specifically honeycombs and truss structures. The paper outlines geometries and dimensions for honeycombs and truss structures whilst providing formula for respective relative densities. The paper goes onto describes and illustrates manufacture techniques, such as the expansion method, corrugated

manufacture and a strip and slot method, as seen in Figure 1.10, Figure 1.11 and Figure 1.12 respectively (Wadley 2006). The strip and slot method was successfully used to manufacture square honeycombs in (Cote *et al* 2004).

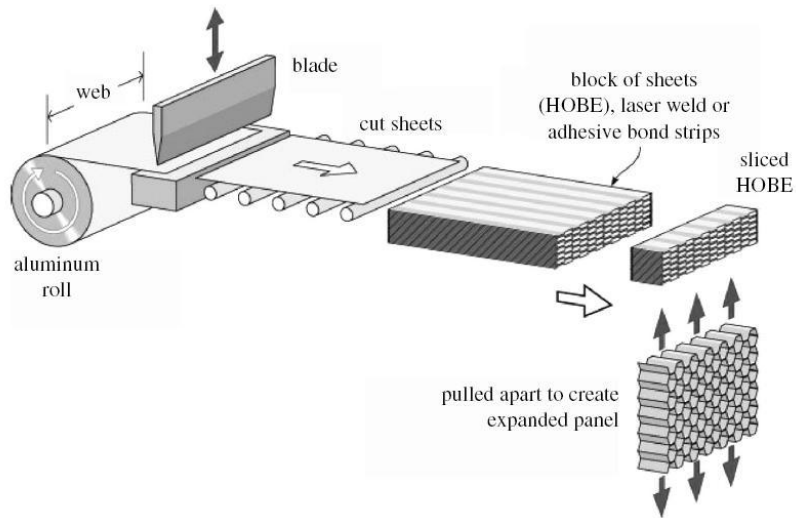


Figure 1.10: Shows the expansion method for manufacturing low density hexagonal honeycombs (Wadley 2006).

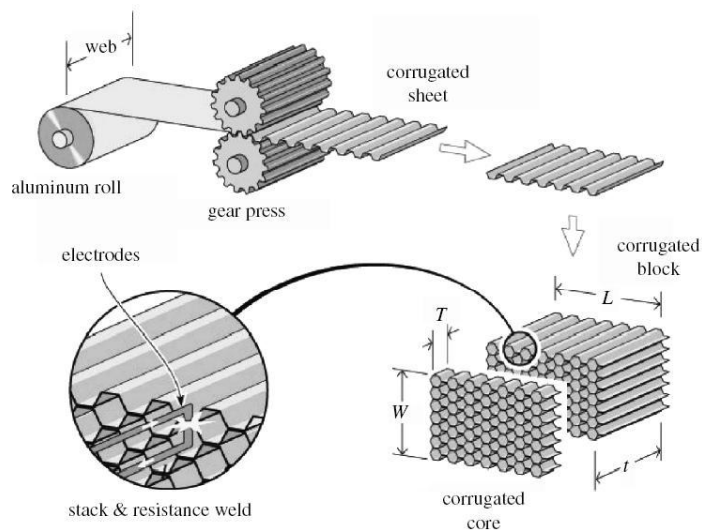


Figure 1.11: Shows the corrugation manufacturing process used to make high relative density honeycombs (Wadley 2006).

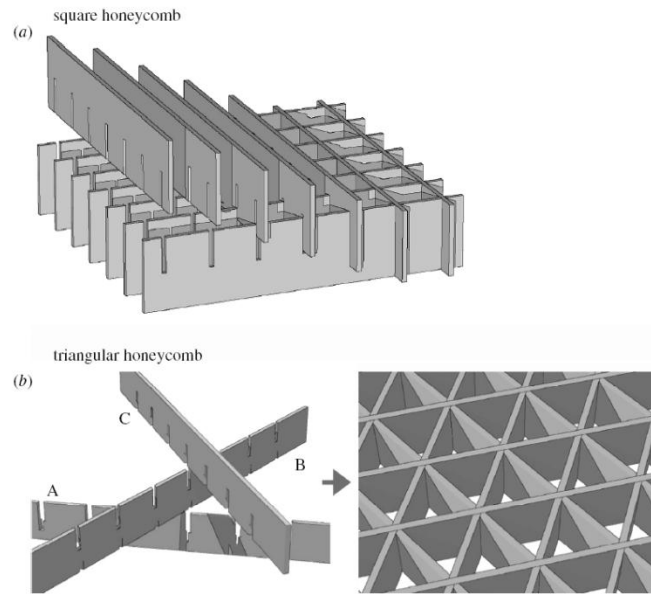


Figure 1.12: Shows a slot and strip method for a) square honeycombs and b) triangular honeycombs (Wadley 2006).

More recently additive layer manufacture has been employed to manufacture small samples for testing and characterisation (Scarpa *et al* 2007 and Miller *et al* 2010a&b),

1.3 Hierarchy

Many natural materials possess excellent compromises between density specific elastic properties and damage tolerance and/or toughness, many of these seem to contain structural hierarchy over multiple length scales either by accident of their manufacture or specifically to aid in the material properties of the structure Hierarchical structures are common in nature (bone, wood, tendons, glass sponge skeletons) (Aizenberg *et al.*, 2005, Buehler, 2006, Fratzl and Weinkamer, 2007, Lakes, 1993, Qing and Mishnaevsky Jr, 2009a&b) and are also used in man-made structures (Lakes 1993 and Fan *et al* 2008). The hierarchical structure of organic materials and biological systems generally plays a vital part in the property, function and its existence (Fratzl and Weinkamer 2007 and Gao 2006).

Pioneering work by Lakes (1993) considered the elastic properties of structures with multiple sets of hierarchy, termed ‘multi-hierarchy structures’, treating a sub-structure as an effective continuum at the super-structure length scale. In other words hierarchical materials contain structural element which themselves have structure. The number of recognisable structural levels is referred to as the hierarchical order and is denoted by (n). A material that is thought of as a continuum has $n = 0$ a material that has a latticework of continuous ribs is said to have $n = 1$ a ‘first order’ hierarchical structure (hierarchy at one length scale, e.g. a conventional honeycomb) is similarly a ‘second order’ hierarchical structure has hierarchy at two length scales $n = 2$. Lakes demonstrated a naturally occurring 5th order hierarchical structure in human compact bone as shown in Figure 1.13 and a manmade hierarchical structure with 3rd order hierarchy in the Eiffel Tower shown in Figure 1.14. Lakes goes on to say that hierarchical material can be used as a “basis of synthesising new microstructures which give rise to enhanced or useful physical properties”.

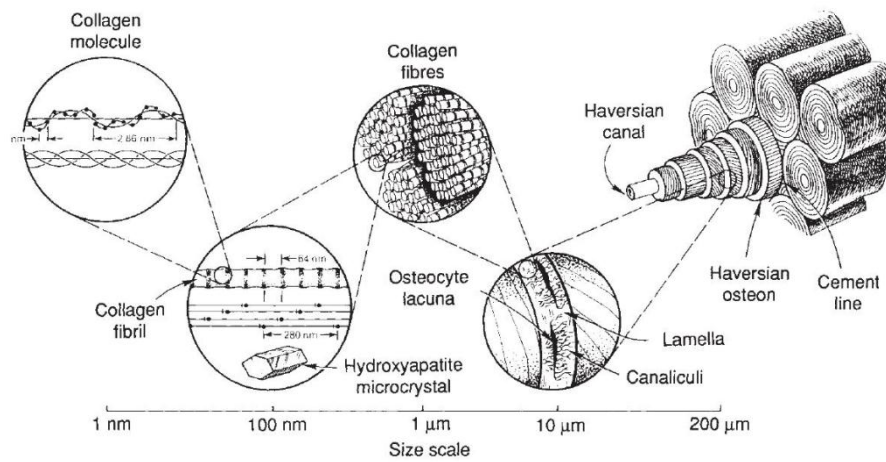


Figure 1.13: Shows hierarchical structure in human compact bone over multiple size scales (Lakes 1993)

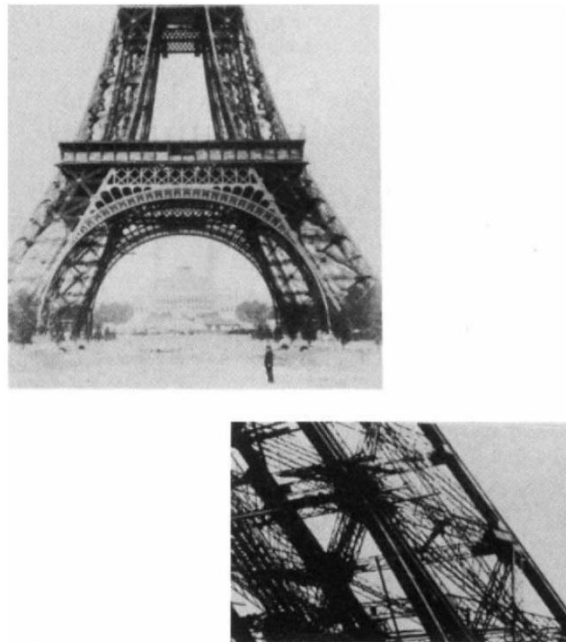


Figure 1.14: Shows the hierarchical structure in the Eiffel tower (Loyrette, 1985) used by Lakes to demonstrate manmade hierarchy (Lakes, 1993).

The use of hierarchical materials enables the ability to choose the material properties, via section shape and micro-structural degrees of freedom of a structure for the desired characteristics (Ashby 1991). For a structure that has only one size scale of cells can be described by the relationship that can be seen in Equation 1-14 as referred to in (Lakes 1993).

$$\frac{E^*}{E_s} = k[\rho_{rel}^*/\rho_s]^r$$

Equation 1-14

Where E^* is the Young's modulus of the cellular material, E_s is the Young's Modulus of the constituent material, ρ_{rel}^* is the relative density of the cellular material, ρ_s is the density of the constituent material. The atomic structure can be ignored due to the continuum description of the ribs (Lakes 1993).

The values of k and r depend on the type of structure. When predicting the properties of a conventional hierarchical material Lakes suggests a different equation in the form of Equation 1-15 (Lakes 1993) developed from Equation 1-14 with the same assumption that the size of the structure making up each rib or wall is much smaller than the rib itself.

$$\frac{E_n}{E_0} = k^n[\rho_{rel}^*/\rho_s]^r$$

Equation 1-15

Lakes noted that for honeycombs deformed out of plane and for foams ($k = 1$), the hierarchical order n does not influence the stiffness, whereas the framework-type structures for which $k < 1$ the stiffness decreases with n . The largest structural element of an object must be negligible in comparison, for the classical continuum view to apply (Lakes 1993). Understanding how hierarchy affects the mechanical properties of a material is necessary when designing structures, since it can guide the synthesis of new materials to be tailored for specific applications. This approach explicitly assumes that the length scale of a sub-structure is fine enough to be negligible when considered with the super-structure. Whilst many examples of this seem to exist in nature, examples in synthetic technology appear to be few. This is mainly because the constraints of current manufacturing techniques make it very difficult to produce sufficiently fine sub-structures. Polymer matrix composites, where the polymer's molecular structure (angstroms to nanometres) and the reinforcing phase (micro-meters to millimetres) can both be tailored, are an obvious synthetic example. To the author's knowledge there has

been no work since to quantify at what point the length scale of a sub-structure can be considered negligible to that of the super-structure.

Parkhouse (Parkhouse, 1984&1987) was the first to perform a quantitative analysis of hierarchical structures, by considering truss structures, honeycombs and tubular geometries to show that hierarchical structures are lighter than elements with simple structure for a given compressive strength. The effects of damage on reliability in homogeneous solids, in structures with one scale size and in those with hierarchical structures where described by (Parkhouse, 1987) who showed that non-hierarchical structure are more dependent on defects and damage.

Since it was recognised that similar geometries are exhibited over multiple length scales in bio materials and the possible benefits recognized (Lakes, 1993 and Parkhouse, 1984&1987), there has been significant investigation into the fractal nature of biomaterials. The apparent mechanical properties and their dependency on size effect were examined in (Carpinteri, 1994 a, b, Carpinteri & Pungo 2005). It was found that considered structures were scale invariant. The strength and stiffness for fractal hierarchical structures were later explored considering geometric and material properties via a simple recursive approach in (Carpinteri *et al* 2009 and Carpinteri & Pungo 2008) the Sierpinski carpet is given as an example for the fractal approach in both papers and is shown in Figure 1.15. This was also developed by the use of rule of mixtures to determine the nominal strength. The self-similarity characteristics of the structure were exploited to develop a condensed fractal approach based on previous work by (Pugno 2006 and Pugno & Carpinteri 2008). The work concluded with a fractal approach that takes into account both geometry and material features, manipulating processes from (Halsey *et al* 1986).

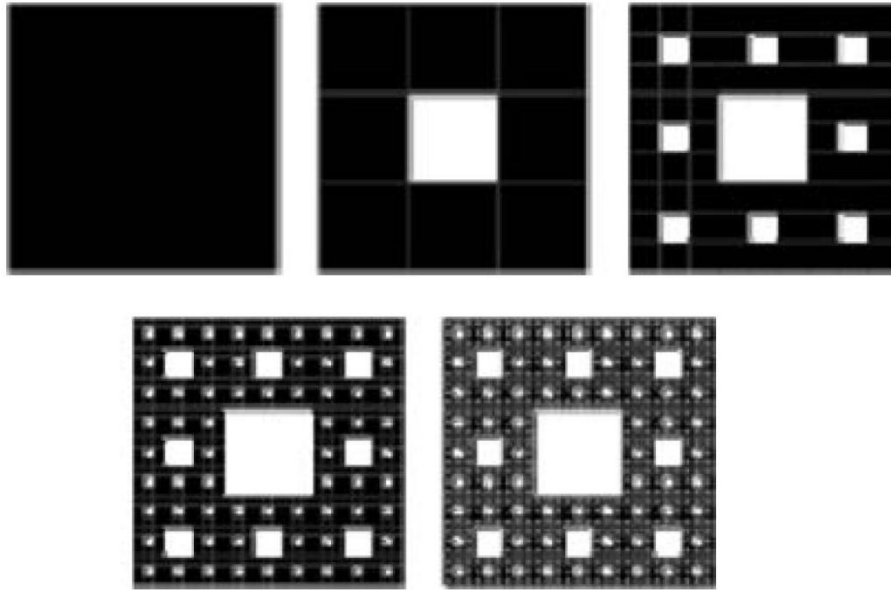


Figure 1.15: Show the Sierpinski carpet as presented in (Carpinteri *et al* 2009 and Carpinteri & Pungo 2008) where at different levels of observation; it corresponds to a deterministic hierarchical bar in which the empty space is the soft matrix, and the complementary zones are the hard.

Lakes states that “most of the gain in strength occurs in the first few level of hierarchy” and that increasing the n levels of hierarchy yields diminishing returns. This is revisited by Murphey & Hinkle (2003) who investigate the performance trends as the hierarchical order number increases. Murphy concludes that subject to bending requirements 2^{nd} order structures are two orders of magnitude lighter and that results are different to column optimisations, hypothesising that this is due to the bending/stretch dominated nature of the structure.

One of the first manufactures examples of hierarchical honeycombs are those developed by Bhat *et al* (1989) who constructed second order structures by manufacturing sandwich panels with a honeycomb core, the ribs of the honeycomb were themselves a sandwich panel. Bhat then conducted an experimental investigation concluding that the 2nd order sandwich panel had a six times greater compressive strength than an equal mass conventional honeycomb sandwich panel. This work was later revisited by Kooistra *et al* (2007), specifically inserting corrugated core into honeycomb ribs to create a 2nd order hierarchical structure as can be seen in Figure 1.16. As hierarchical structures had the same relative densities to conventional versions, ribs were relatively

thicker and as such had larger second moments of area, and because the ribs were predominantly deformed in flexure, exhibited higher density specific elastic modulus. This increased density specific elastic modulus, and in some cases strength along with the number of collapse modes. Kooistra also presented analytical models for the transverse stiffness and strength of 2nd order corrugated cores. The optimal design of second order structure took into account the six collapse modes present due to the introduction of the hierarchy. The maximum compressive and shear strengths for a prescribed effective relative density were also determined. Kooistra determined that 2nd order corrugated cores have significantly higher collapse strengths compared to their equivalent mass first order counterparts for relative densities $\rho_{rel}^* < 0.05$. Kooistra also concluded that increasing the hierarchical order to greater than two can increase the collapse strength only at relative densities $\rho_{rel}^* < 0.005$. In contrast, increasing the level of structural hierarchy yields no enhancements in the stiffness of the corrugated core for stretch dominated structures.

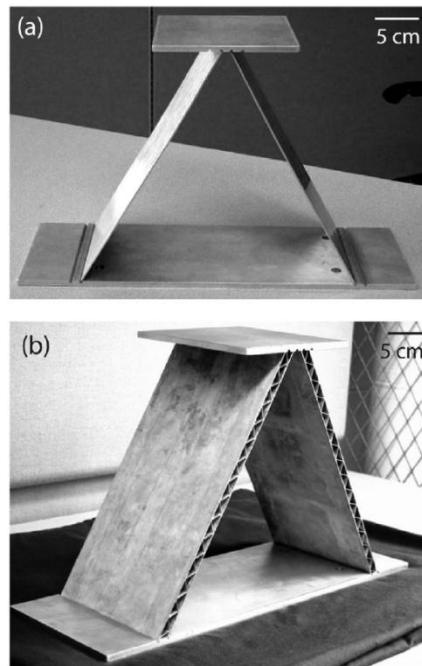


Figure 1.16: Shows photographs of (a) first and (b) second order corrugated cores as manufactured by Kooistra (Kooistra *et al*, 2007).

A similar approach was taken by Fan and co-workers (Fan *et al*, 2008) who examined hierarchical honeycomb ribs formed from skins and cores, i.e. sandwich panels and can

be seen in Figure 1.17. Similar to the work by Kooistra, Fan deduced equations for the stiffness, the buckling strength, the plastic collapse strength, the brittle failure strength and the fracture toughness. Fan concluded that the inclusion of hierarchical walls greatly enhance the mechanical properties of the cellular materials compared to conventional versions of the same relative density. Fan also reported substantial enhancements in the stiffness and the Euler buckling strength at an order of magnitude for the flexural dominated honeycomb structure, but no enhancement to the stretch dominant iso-grid structure. The changes to the stiffness is interesting as Kooistra (Kooistra *et al*, 2007) reported no increase in stiffness as the hierarchical order increased. Fan also noted increases in the plastic collapse strength, the brittle failure strength and the fracture toughness of the hierarchical honeycomb along with hierarchical honeycomb being more damage tolerant to cracks and insensitive to wavy imperfections of cell walls. Fan also suggests the hierarchical honeycombs most important application is energy absorption given the greatly enhanced buckling strength and plastic collapse compared to conventional honeycombs of the same relative density.

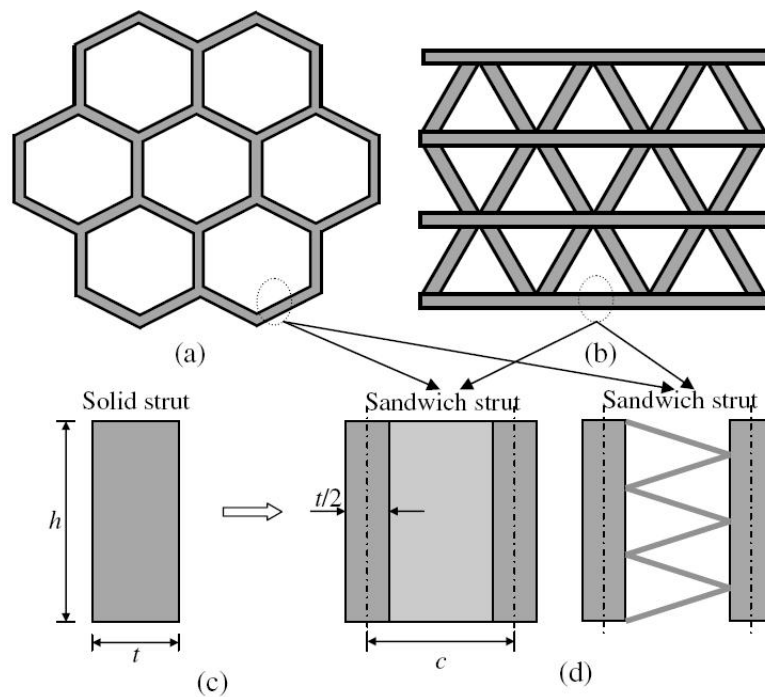


Figure 1.17: Shows Nomenclature for solid and sandwich struts of honeycombs: (a) two-order honeycomb; (b) two-order isogrid; (c) solid strut; and (d) sandwich struts (Fan *et al*, 2008).

A similar approach to Kooistra and Fan to implement hierarchy was adopted by Cote *et al* (2009). Cell walls of a conventional honeycomb were replaced with sandwich plates made from glass fibre / epoxy composite faces and a polymethacrylimide foam core to create a 2nd order hierarchical structure, which can be seen in Figure 1.18. Cote investigated the through thickness properties focusing on three possible collapse mechanisms: elastic buckling of the sandwich walls of the honeycomb, elastic wrinkling, and plastic micro-buckling of the faces of the honeycomb. Cote developed analytical expressions validated by FE models with geometric imperfections. The results showed that hierarchical honeycombs with monolithic composite cores had a higher compressive strength than conventional honeycombs. Cote also stated that the characterization of the imperfections remains a challenging task, which would need to be examined in future work.

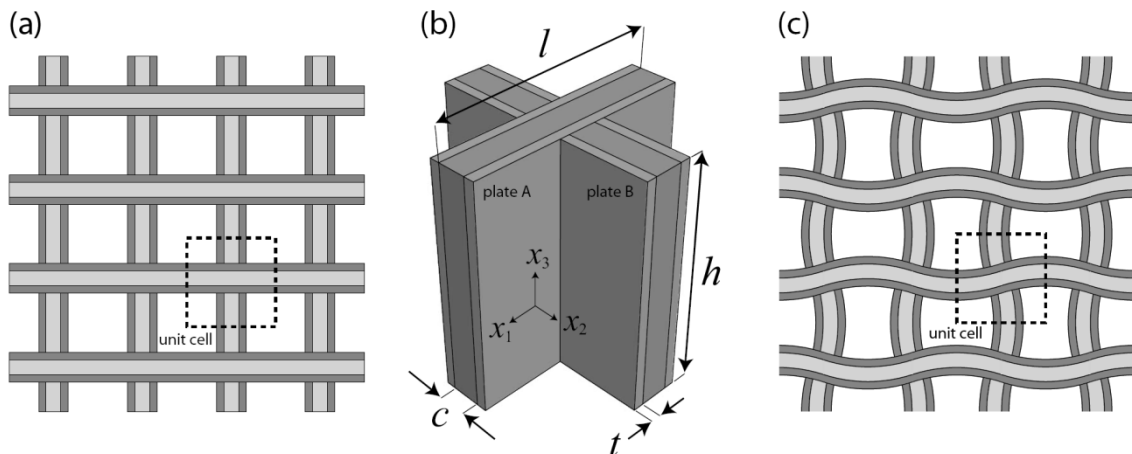


Figure 1.18: Shows (a) Sketch of a square honeycomb core with the cell walls of the core made from a mesoscopic sandwich panels, (b) schematic of the unit cell and geometrical parameters employed in the analytical model and finite element analysis, and (c) torsional-axial buckling mode of square honeycomb core (Cote *et al* 2009).

Another recent investigation of hierarchical honeycombs was undertaken by Ajdari and co-workers (Ajdari *et al* 2012) who took a fractal approach to manufacturing hierarchical honeycombs. This was achieved by replacing every three-edge vertex of a regular hexagonal lattice with a smaller hexagon, which can be seen in Figure 1.19 (Ajdari *et al* 2012). Ajdari combined analytical, numerical and experimental methods to

investigate the mechanical behaviour of two-dimensional hierarchical honeycomb structures. It was found that the dimension ratios for different hierarchical orders controlled the effective elastic modulus and Poisson's ratio of the structure. Ajdari found that a broad range of elastic properties and behaviours can be achieved by tailoring the structural organization, specifically the dimension ratios and that hierarchical structure can exceed that of conventional honeycombs by up 3.5 in terms of stiffness.

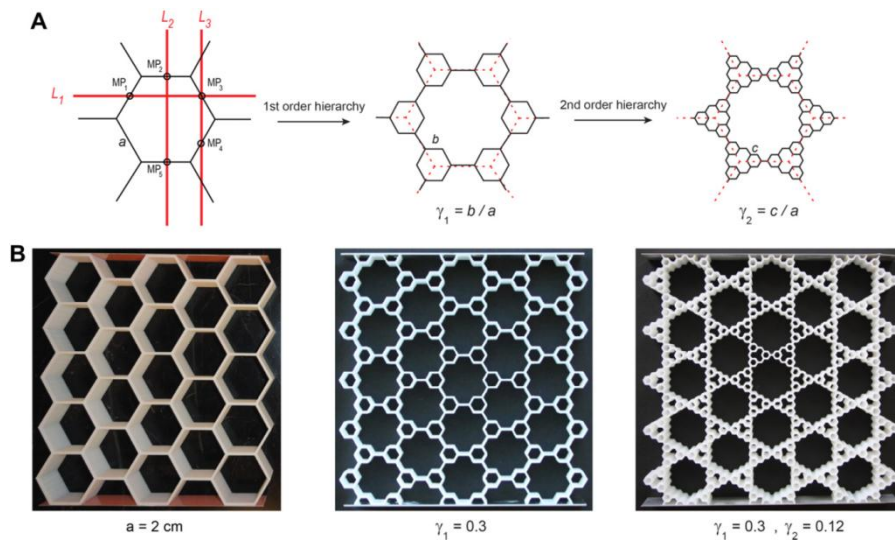


Figure 1.19: Shows Hierarchical honeycombs. (A) Unit cell of the hierarchical honeycombs with regular structure and with 1st and 2nd order hierarchy. (B) Images of honeycombs with $a = 2$ cm fabricated using three-dimensional printing (Ajdari *et al* 2012).

In recent work by (Pugno & Chen 2011) who calculated the in-plane elastic properties of hierarchical nano-honeycombs. Surface effects were taken into account for non-hierarchical honeycombs and via an iterative process derived stiffness-to density ratio at level n for hierarchical structures. This work was extended to 3-D nanofoams in (Chen Q & Pugno N, 2012a) in particular looking at the Young's modulus and plastic strength. As in the previous paper Chen & Pugno incorporate the effects of the surface elasticity and surface residual stress in the linear elastic and plastic analyses. It is shown that there is a link between the cross-sectional dimensions and the influences of the surface effect on Young's modulus and plastic strength. Chen & Pugno furthered their work in (Chen Q & Pugno N, 2012b) by studying the elastic buckling of up to 3rd order hierarchical

honeycombs as shown in Figure 1.20, determining the real local buckling stress along with the progressive failure of the hierarchical structure. Chen & Pugno concluded that the stress/strain law and deformation energy shows that increasing hierarchical order n induces lower energy density but higher specific energy. It was also suggested that the hierarchical structure can be tuned at each hierarchical level to tailor the mechanical behaviour of the structure, which would be attractive for design of a new class of light but effective energy-absorption materials.

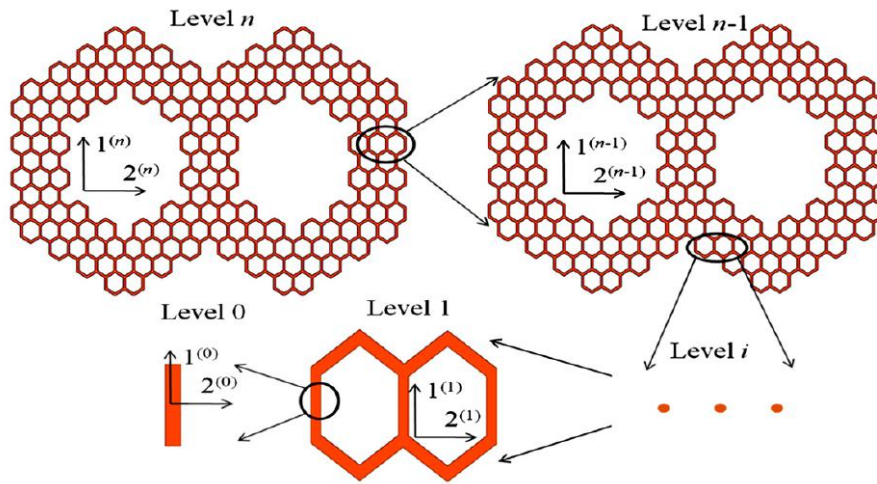


Figure 1.20: Shows level n hierarchical honeycombs as presented in (Chen & Pugno, 2012b).

The elastic properties of nano-porous materials with hierarchical structures, were investigated by Xia *et al* (2011) looking at the dependence on the size scale of the microstructure. Surface tension and surface elasticity were account for in a core-shell model for surface effects with one level of nano-sized open or closed to derive the Young's modulus. The results reveal that surface effects on the elastic response of nano-porous materials become significant when the average width of the ligaments is below 10 nm. This could be used in the design of hierarchically structured nano-porous materials

A new approach to model hierarchical structure is proposed, based both on geometric and material considerations and involving simple recursive formulas (Rodrigues 2002). Rodrigues describes a hierarchical computational procedure for optimizing material distribution as well as the local material properties of mechanical elements. The local

properties are designed using a topology design approach, leading to single scale microstructures, which may be restricted in various ways, based on design and manufacturing criteria. Implementation issues are also discussed and computational results illustrate the nature of the procedure. Coelho (Coelho 2008) work presents an extension of (Rodrigues 2002) work, covering the simultaneous characterisation of the optimal topology of the structure and the optimal design of the cellular material used in its construction. In the study on hierarchy it is suggested that the optimisation model works at two interconnected levels, the global and local levels. The class of cellular materials, defining the material microstructure, is restricted to single scale cellular materials, with the cell geometry locally optimised for the given objective function and constraints. The model uses the asymptotic homogenisation model to obtain the equivalent material properties for the specific local microstructures designed using a SIMP based approach. The effect structural hierarchy has on the damping properties were investigated in (Lakes 2002). The introduction of hierarchy in viscoelastic composites allows the achievement of high concentrations of spherical inclusions, and that it enables simultaneous stiffness and damping.

To the best of the authors' knowledge few studies have considered placing a sub-structure out-side of the rib, or of distributing a significant proportion of the cell's mass outwards from the rib centre in a hierarchical sense other the approach of [Burlayenko and Sadowski 2009] that investigated the effects of filling honeycomb voids with foam. Indeed there has been no systematic exploration of hierarchical honeycombs and their properties, in terms of their geometry across their hierarchical levels.

Chapter 2. Modelling

2.1 Introduction

The aim of this chapter is to determine the benefits, drawbacks and pragmatic limits of Finite Element Analysis [FEA] techniques to determine the global material properties of considered structures. Investigated are the elements that can be used within ABAQUS (ABAQUS, version 6.9. Dassault Systèmes) to model honeycombs along with element size and count by means of convergence studies. Also examined are the effects of boundary conditions used when representing a periodic unit cell and compared to larger tessellated cells in the form of arrays. It was important to understand the pragmatic limits of the software and approach at this early stage, due to the computational demand associated with modelling hierarchy which is determined over multiple length scales. The work presented endeavours to described hierarchy as discrete structures, where previously hierarchy has been modelled using continuum theories computationally and analytically Carpinteri (2009), Lakes (1993). An FEA approach was chosen to investigate the introduction of hierarchy into honeycombs due to the flexibility to study and compare multiple geometries and variables quickly and efficiently.

Modelled is a conventional hexagonal honeycomb as shown in Figure 2.1, which is annotated according to Gibson and Ashby's terminology (Gibson, & Ashby 1997), it can be seen that boundary sharing beams have either half l or half t to represent a repeatable unit cell. Also shown is the effective length of the beam denoted as l' which can be used to give a lower limit for the length of the rib, when loaded in flexure.

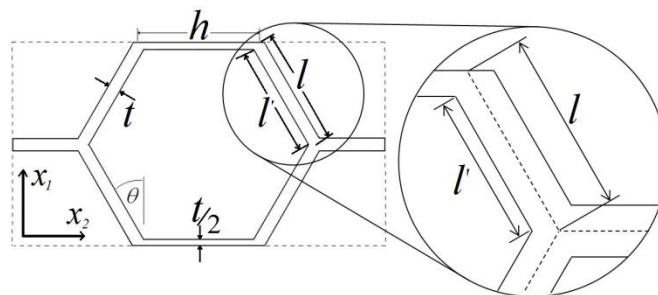


Figure 2.1: Conventional hexagonal honey annotated according to Gibson and Ashby's terminology also shown is the effective length of the beam denoted as l' .

One of the presiding factors over the material properties of honeycombs or cellular materials in general is the relative density ρ_{rel}^* . The relative density ρ_{rel}^* of a hexagonal honeycomb can be found by calculating the volume of the constituent material V_{con} divided by the volume of the cell V_{cell} as described below. The volume of the constituent material within a hexagonal unit cell can be calculated as in Equation 2-1.

$$V_{con} = (t(2h + 4l))d$$

Equation 2-1

Where V_{con} is the volume of the constituent material and terms h , l and t relate to the dimensions of a hexagonal honeycomb as described in Figure 2.1. The term d is the depth of the honeycomb in this case chosen as unit depth and is maintained for all models throughout this study unless otherwise stated. This approach neglects to take into account for overlapping edges that become significant when t is large and is also independent of θ of the honeycomb also described in Figure 2.1. Instead the volume of the constituent material within a hexagonal unit cell can be calculated as in Equation 2-2.

$$V_{con} = \left((2h + 4l)t - t^2 \left(\frac{2}{\cos\theta} - \tan\theta \right) \right) d$$

Equation 2-2

The volume of a hexagonal unit cell can be calculated as in Equation 2-3.

$$V_{cell} = (2l \cos\theta)(2h + 2l\sin\theta)d$$

Equation 2-3

Where V_{cell} is the volume of a hexagonal unit cell, h , l , t , θ and d are as previously described in Figure 2.1. The relative density ρ_{rel}^* of all models was calculated using Equation 2-4.

$$\rho_{rel}^* = \frac{\rho_{cell}}{\rho_{con}} = \frac{V_{con}}{V_{cell}}$$

Equation 2-4

Another presiding factor over the material properties of a honeycomb is the geometry of the structure. In the current study a triangular honeycomb is investigated and can be

seen in Figure 2.2. The relative density ρ_{rel}^* for a triangular honeycomb and how it is determined is shown below.

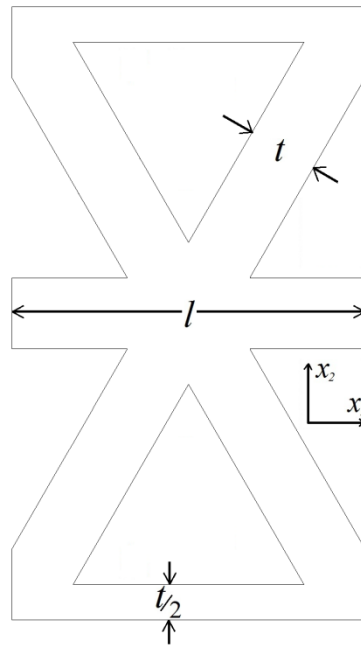


Figure 2.2: Unit cell for a conventional triangular honeycomb annotated according to Gibson and Ashby's terminology.

The relative density ρ_{rel}^* of a triangular honeycomb can be found in a similar way to a hexagonal honeycomb, by calculating the volume of the constituent material V_{con} divided by the volume of the cell V_{cell} . The volume of the constituent material within a triangular unit cell can be calculated as in Equation 2-5.

$$V_{con} = (6lt)d$$

Equation 2-5

Where V_{con} is the volume of the constituent material and terms h , l and t relate to the dimensions of a triangular honeycomb as described in Figure 2.2. The term d is the depth of the honeycomb and assumed as unit depth. Similar to the hexagonal model this approach neglects to take into account for overlapping edges that become significant when t is large. Instead the volume of the constituent material within a triangular unit cell can be calculated as in Equation 2-6.

$$V_{con} = (6t^2 + 5t(l - t\sqrt{3}))d$$

Equation 2-6

The volume of a triangular unit cell can be calculated as in Equation 2-7.

$$V_{cell} = (l^2\sqrt{3})d$$

Equation 2-7

Where V_{cell} is the volume of the triangular unit cell. Therefore the relative density of the triangular unit cell can be calculated using Equation 2-4.

2.2 Method

2.2.1 Wire Elements

Initially *2D planar deformable wire* elements were investigated using ABAQUS to model the in-plane global properties of conventional honeycombs. Hexagonal and triangular honeycombs were modelled over a range of relative densities and results compared to proven analytical Gibson and Ashby (1997). Hexagonal and triangular honeycomb geometries were created in ABAQUS where $l = h = 10$ for hexagonal honeycombs according to Figure 2.1 and $l = 10$ for triangular honeycombs according to Figure 2.2 the thickness t was specified later in the property section. Initially quarter or half models were investigated due to the four or two fold symmetry present in hexagonal and triangular honeycomb respectively, as shown in Figure 2.3 and Figure 2.4 and was further expanded to a full unit cell, 2x2, 3x3, 4x4, and 8x8 arrays.

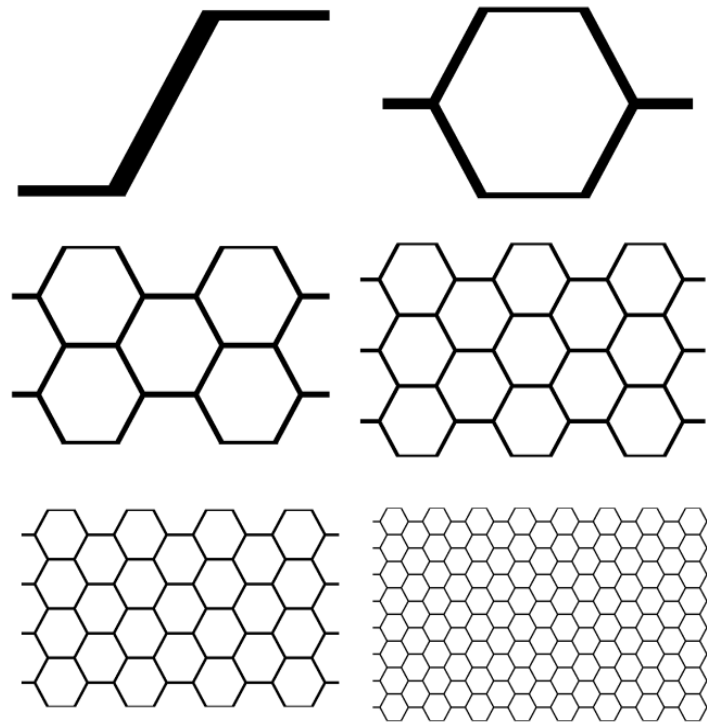


Figure 2.3: Hexagonal honeycombs from a quarter unit cell to an 8x8 array.

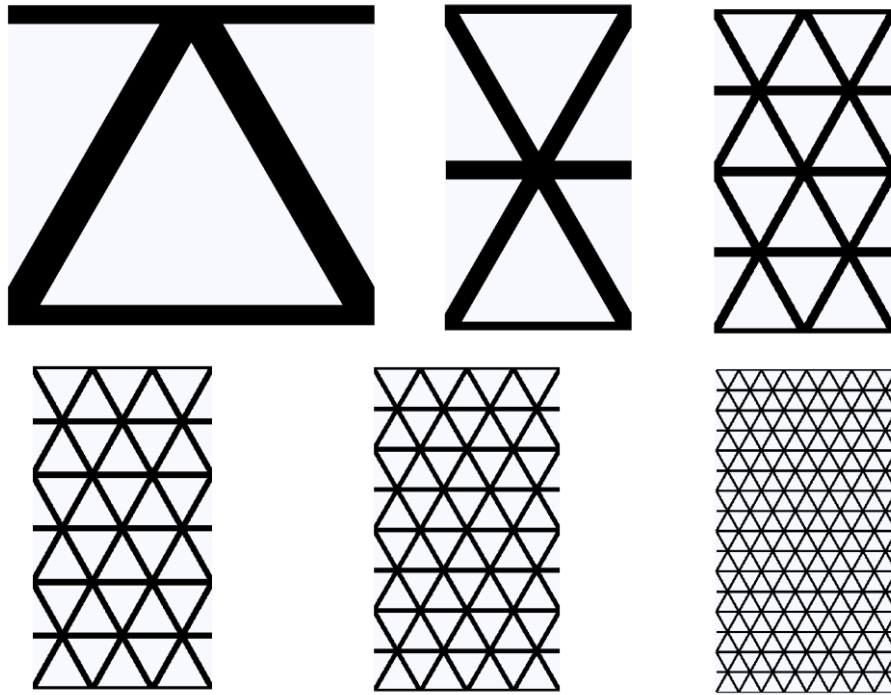


Figure 2.4: Triangular honeycombs from a half unit cell to an 8x8 array.

As it was initially thought that samples could be manufactured via Selective Laser Sintering (SLS) with nylon powder (Duraform 3D systems), which had a set of approximately linear and isotropic elastic constants (specifically $E_s = 1600$ MPa, $G_s = 593$ MPa and $\nu_s = 0.35$) (Miller 2010 & Caulfield 2007), these material properties were used for all cases. Beam profiles were specified for rectangular ribs, two profiles were created for each model i) to represent the thickness t of ribs specified in the model and ii) to represent the thickness of boundary sharing ribs assigned to $t/2$ as shown in Figure 2.1 and Figure 2.2. The depth of each rib was defined as a unit depth for all cases. The thickness t and the unit depth were defined by the dimensions a and b for the cross sectional area as shown in Figure 2.5, where a is the unit depth when the n_1 target vector is specified as 0.0, 0.0, 1.0 (z-direction) for the *Beam Section Orientation*.

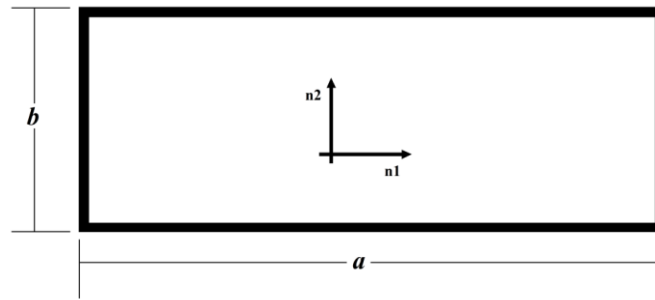


Figure 2.5: Cross sectional area and terminology of profiles used to describe the profile of ribs.

A beam Section was then created where appropriate profiles were chosen along with the material properties of the rib. Ribs were then assigned an appropriate section depending on the required rib thickness t or $t/2$. In the *Step Module* a *Static, General* step was created as a quasi-static linear elastic model was required to determine the in-plane elastic modulus.

The boundary conditions applied to the model can be described as; the upper most edges of the model were displaced axially and uniformly to produce a global 0.1 % strain in the X_1 axis (normal to the h rib). The lower most edge of the model edge was constrained to zero displacement in the X_1 axis but allowed to freely displace in the X_2 axis. One model edge parallel to the X_1 axis was constrained to zero displacement in the X_2 axis, and the other allowed to displace freely but guided in the X_1 axis, i.e. elements on this edge were constrained to remain in an axis parallel to the X_1 axis as shown in Figure 2.6. These boundary conditions simulate uniaxial compression in a honeycomb continuum, as described in (Odegard 2003). To extract data history outputs were created to output the reaction force RF2 on the upper most edge of the model and the uniform displacement U2.

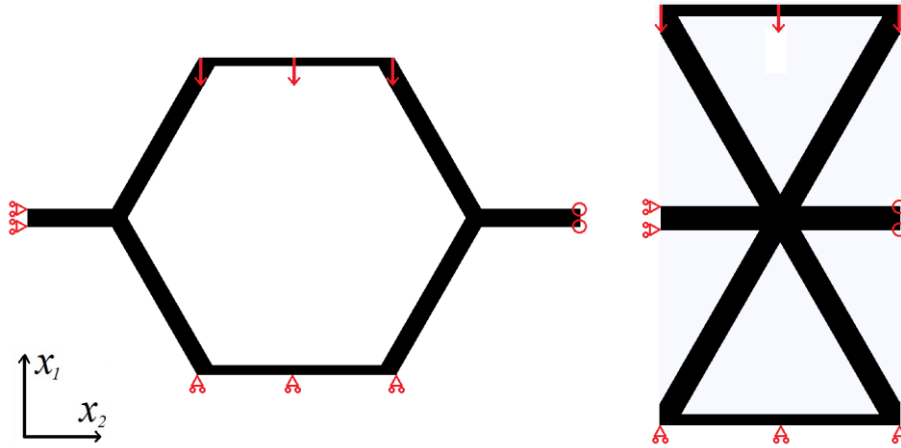


Figure 2.6: Boundary conditions applied to a) hexagonal honeycomb and b) triangular honeycomb

A convergence test was then undertaken for hexagonal quarter cell models for relative densities of $\rho_{rel}^* = 0.0115$ and $\rho_{rel}^* = 0.494$ as in Equation 2-4 (equivalent to a hexagonal honeycomb of dimensions $l = h = 10, t = 0.1$ and $l = h = 10, t = 5$ respectively) and triangular half-cell models for relative densities of $\rho_{rel}^* = 0.0287$ and $\rho_{rel}^* = 0.909$ as in Equation 2-4 (equivalent to a triangular honeycomb of dimensions $l = 10, t = 0.1$ and $l = 10, t = 4$ respectively). The convergence test was implemented by decreasing the *approximate global size* of elements incrementally from 10 to 0.001 within the *Seed Part Instance* options thus increasing the number of element in the model. Example meshes for a hexagonal and a triangular honeycomb are shown in Figure 2.7, which have 20 elements along a single beam. Implicit elements were used due to the linear elastic interest of the problem. The effect of using linear (B21: A 2-node linear beam in a plane) and quadratic (B22: A 3-node quadratic beam in a plane) elements were also compared (Papka & Kyriakides 1994 & 1998 (1)) (Chung & Waas 2001). The Young's modulus E_I^* was calculated by summing the total reaction force on the displaced model edge, divided by the product of projected area (unit depth) and the imposed strain of 0.1%. This process was then repeated for a full cell, 2x2, 3x3, 4x4, and 8x8 arrays.

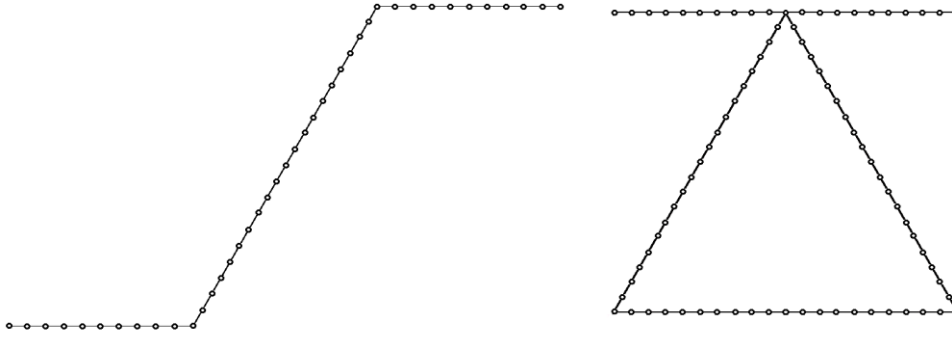


Figure 2.7: a) Shows an example mesh for a quarter cell hexagonal honeycomb with 20 elements along the length of a single beam and b) Shows an example mesh for a half cell triangular honeycomb with 20 elements along the length of a single beam.

2.2.2 Shell Elements

To investigate the feasibility of using *2D Planar deformable shell elements* within ABAQUS to model the in-plane global properties of conventional honeycombs. Hexagonal and triangular honeycombs were model over a range of relative densities and results compared to proven analytical Gibson and Ashby (1997). A hexagonal and triangular honeycomb were created where $l = h = 10$ for a hexagonal honeycomb and $l=10$ for a triangular honeycomb according to Figure 2.1 and Figure 2.2 respectively and the discrete thickness t specified. Initially quarter models were investigated due to the four fold symmetry present in a hexagonal honeycomb and half models for triangular honeycombs as shown in Figure 2.3 and Figure 2.4 respectively this was further expanded to a full unit cell and 2x2, 3x3, 4x4 and 8x8 arrays.

The same material properties were assigned to the shell element models as applied to the beam element models assuming nylon powder (Duraform 3D systems) which had a set of approximately linear and isotropic elastic constants (specifically $E_s = 1600$ MPa, $G_s = 593$ MPa and $\nu_s = 0.35$) (Miller 2010 & Caulfield 2007) the material properties were used for all cases. A section was then created where material properties were chosen and the depth of each rib defined and specified as unit depth as for all cases. A *Static, General* step was created as a quasi-static linear elastic model was required to determine the in-plane elastic modulus. The boundary conditions, extraction of data and post processing were exactly the same as in the *2D planar deformable wire* elements model and can be seen in Figure 2.6.

A convergence test was then undertaken for a hexagonal quarter cell model for relative densities $\rho_{rel}^* = 0.0115$ and $\rho_{rel}^* = 0.494$ as in Equation 2-4 (equivalent to a hexagonal honeycomb of dimensions $l = h = 10, t = 0.1$ and $l = h = 10, t = 5$ respectively) and triangular half-cell models for relative densities of $\rho_{rel}^* = 0.0287$ and $\rho_{rel}^* = 0.9090$ as in Equation 2-4 (equivalent to a triangular honeycomb of dimensions $l = 10, t = 0.1$ and $l = 10, t = 4$ respectively). The convergence test was implemented by decreasing the *Approximate global size* of elements incrementally from 0.5 to 0.005 for hexagonal and triangular models alike when $t=0.1$ and decreasing the *Approximate global size* of elements incrementally from 5 to 0.05 for hexagonal honeycombs and 5 to 0.04 for triangular honeycombs when $t = 5$ and $t = 4$ respectively within the *Seed Part Instance* options thus increasing the number of element in the model. Implicit element were used due to the linear elastic interest of the problem, the element used was (CPS4R: A 4-node bilinear plane stress quadrilateral, reduced integration, hourglass control). This process was then repeated for a full cell, 2x2, 3x3, 4x4, and 8x8 arrays.

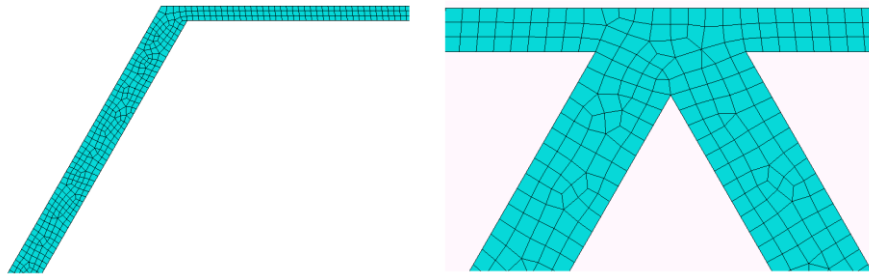


Figure 2.8: Shows an example mesh of a hexagonal and triangular honeycomb with a $\rho_{rel}^* = 0.0115$ and $\rho_{rel}^* = 0.273$ respectively, it can be seen that the average number of elements spanning the rib is approximately 5.

A *quad dominated free technique* was used to mesh the geometry as a structure mesh created relatively high aspect ratio elements, whereas the *free technique* produced relatively even mesh geometries. An example mesh of a hexagonal honeycomb with a $\rho_{rel}^* = 0.0115$ and a triangular honeycomb of $\rho_{rel}^* = 0.273$ are shown in Figure 2.8, it can be seen that the average number of elements spanning the rib is approximately 5.

2.3 Results

Results from the numerical modelling are presented, concerning types of element used along with convergence tests, with respect to element size and count. Also shown is the effect of boundary conditions and sample size for numerical modelling.

2.3.1 Wire Elements

A convergence test for *2D planar deformable wire* elements was undertaken and the results are shown graphically in Figure 2.9 to Figure 2.12 where the in-plane Young's modulus is plotted against the number of elements along each beam for linear (B21) and quadratic (B22) wire elements.

2.3.1.1 Hexagonal

A convergence test for a hexagonal honeycomb is shown in Figure 2.9 for a low relative density $\rho_{rel}^* = 0.0115$ and for a high relative density $\rho_{rel}^* = 0.494$ in Figure 2.10. It can be seen in both Figure 2.9 and Figure 2.10 that the quadratic (B22) elements converge with a fewer element count per rib, converging at approximately 10 elements per beam for both relative densities investigated, whereas the linear (B21) elements converge at approximately 100 elements per rib.

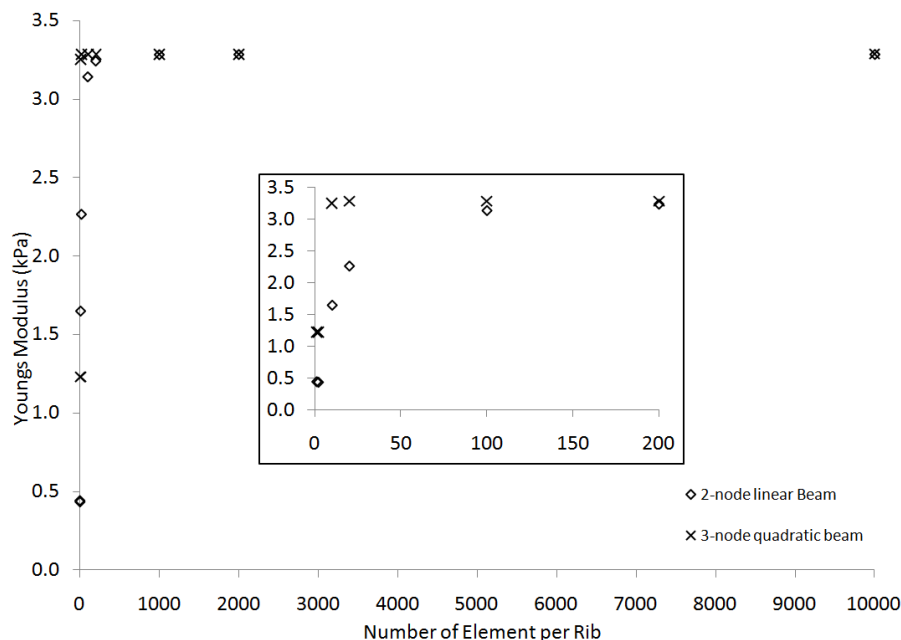


Figure 2.9: Convergence graph for the Young's modulus of a hexagonal honeycomb (quarter cell) against the number of elements along a rib for a relative density $\rho_{rel}^* = 0.0115$ for linear (B21) and quadratic (B22) elements.

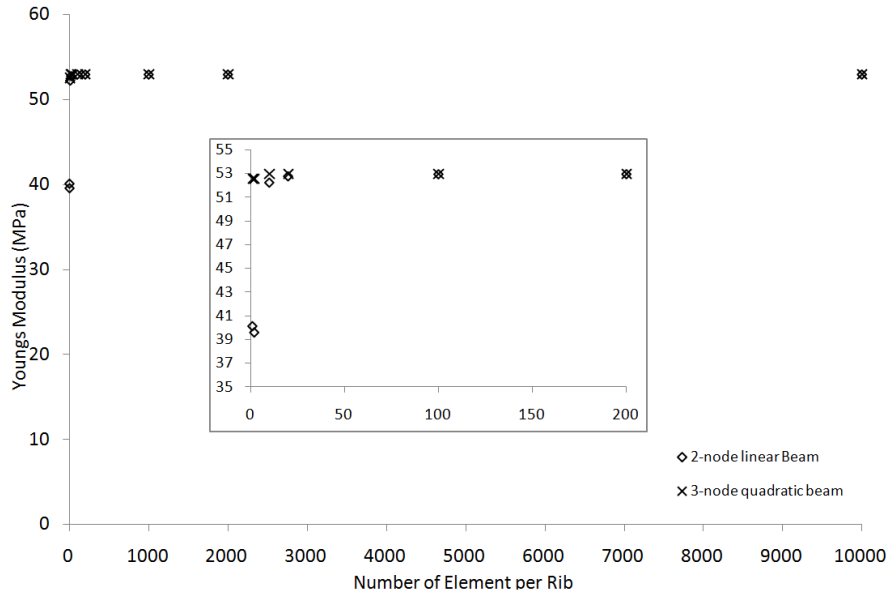


Figure 2.10: Convergence graph for the Young's modulus of a hexagonal honeycomb (quarter cell) against the number of elements along a rib for a relative density $\rho_{rel}^* = 0.494$ for linear (B21) and quadratic (B22) elements.

2.3.1.2 Triangular

A convergence test for a triangular honeycomb is shown in Figure 2.11 for a low relative density $\rho_{rel}^* = 0.0287$ and for a high relative density $\rho_{rel}^* = 0.9090$ in Figure 2.12. It can be seen in both Figure 2.11 and Figure 2.12 that triangular honeycombs are less sensitive to the element size when compare to the response of hexagonal honeycombs, which could be due to the stretch/compression dominated deformation mechanism of the triangular honeycomb opposed to the flexure dominated deformation mechanism of the hexagonal honeycomb.

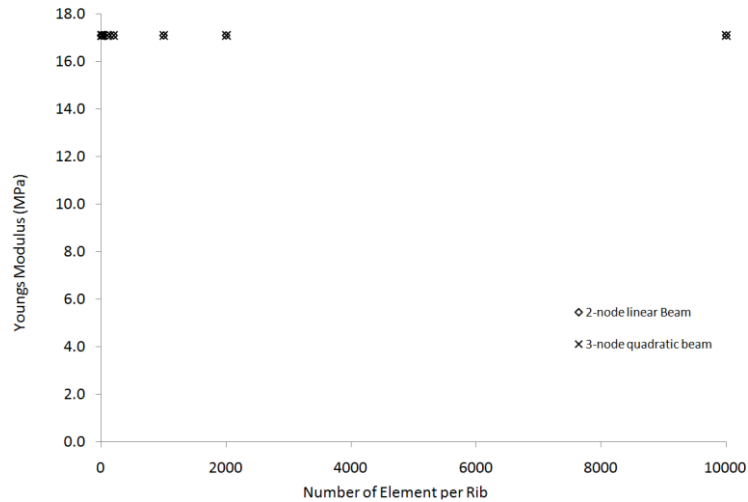


Figure 2.11: Convergence graph for the Young's modulus of a triangular honeycomb (half-cell) against the number of elements along a rib for a relative density $\rho^*_{rel} = 0.0287$ for linear (B21) and quadratic (B22) elements.

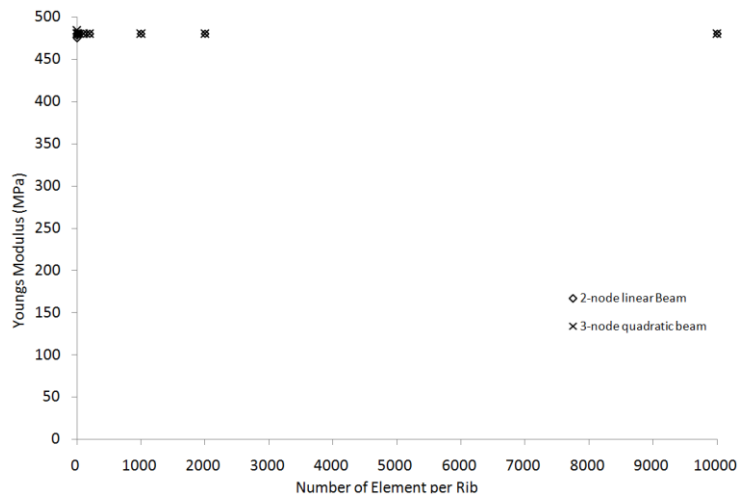


Figure 2.12: Convergence graph for the Young's modulus of a triangular honeycomb (half-cell) against the number of elements along a rib for a relative density $\rho^*_{rel} = 0.909$ for linear (B21) and quadratic (B22) elements.

2.3.2 Boundary Conditions and Sample Size

The results of changing the relative density of hexagonal honeycombs is shown in Figure 2.13 where the Young's modulus is plotted against the relative density ρ^*_{rel} of the unit cell, for a quarter cell, full cell, 2x2, 3x3, 4x4, and 8x8 arrays and compared to Gibson and Ashby's prediction for in-plane Young's modulus as described in Equation

1-4 And allowing for shear in Equation 1-9, which becomes significant for $\rho_{rel}^* > 0.218$, It can be seen in Figure 2.13 where there is a clear separation of the two analytical predictions when $\rho_{rel}^* > 0.218$.

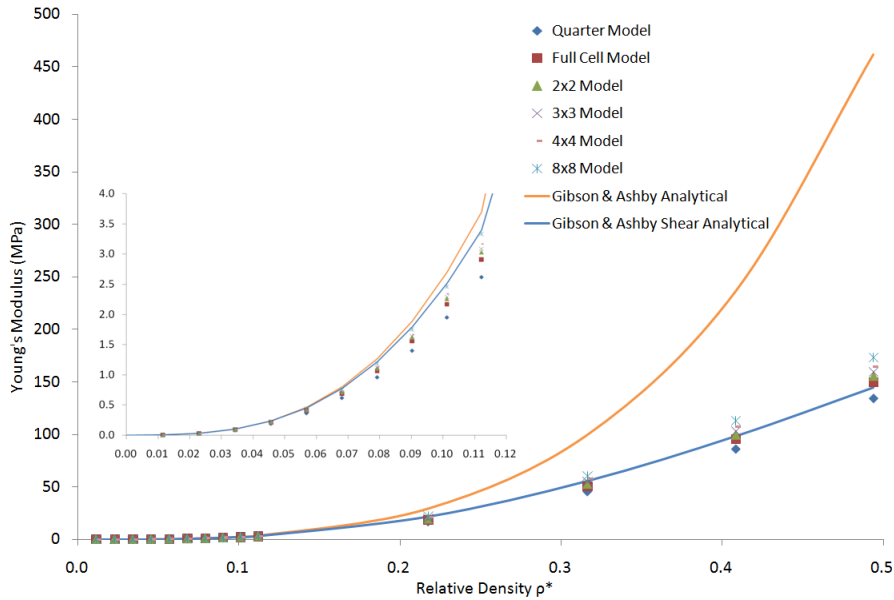


Figure 2.13: Young's modulus against the relative density ρ_{rel}^* of hexagonal honeycombs for a quarter cell, full cell, 2x2, 3x3, 4x4, and 8x8 arrays.

The results of changing the relative density of triangular honeycombs is shown in Figure 2.14 where the Young's Modulus is plotted against the relative density ρ_{rel}^* of the unit cell, for a half cell, full cell, 2x2, 3x3, 4x4, and 8x8 arrays and compared to Gibson and Ashby's prediction for in-plane Young's modulus as described in Equation 1-4 and Equation 1-9

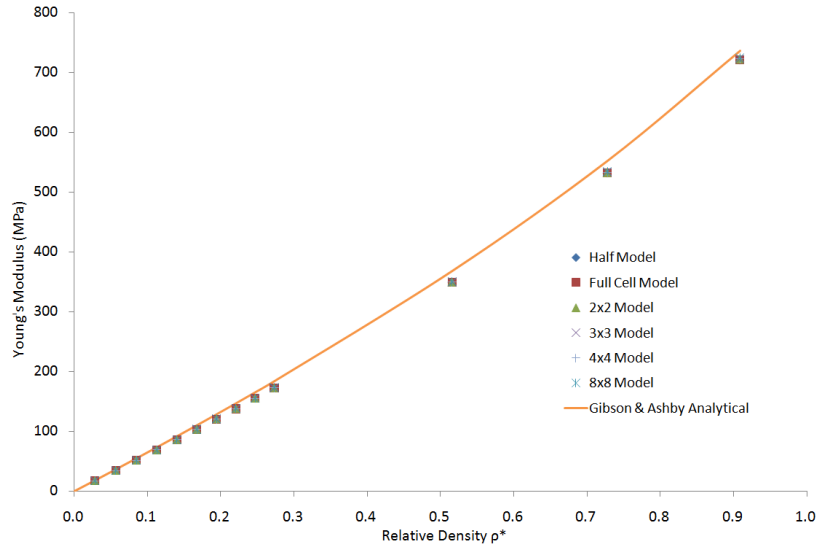


Figure 2.14: Young's modulus against the relative density ρ_{rel}^* of triangular honeycombs for a half cell, full cell, 2x2, 3x3, 4x4, and 8x8 arrays.

2.3.3 Shell Elements

A convergence test for *2D planar deformable shell* elements was undertaken and the results are shown graphically in Figure 2.15 to Figure 2.18 where the In-plane Young's modulus is plotted against the average number of elements spanning each rib for linear (CPS4R) elements.

2.3.3.1 Hexagonal

A convergence test for a hexagonal honeycomb is shown in Figure 2.15 for a low relative density $\rho_{rel}^* = 0.0115$ and for a high relative density $\rho_{rel}^* = 0.494$ in Figure 2.16. It can be seen that there is little change in the in-plane Young's modulus when there is more than an average of 5 elements spanning a rib for both relative densities of $\rho_{rel}^* = 0.0115$ and $\rho_{rel}^* = 0.494$.

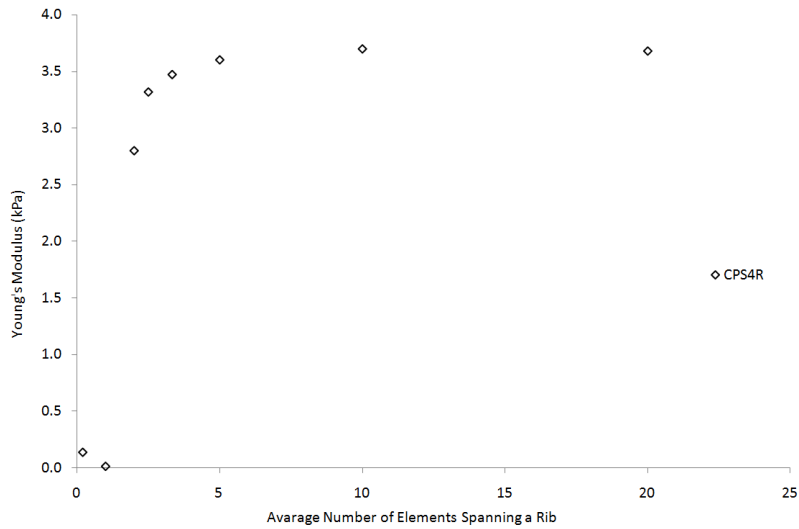


Figure 2.15: Convergence graph for the Young's modulus of a hexagonal honeycomb (quarter cell) against the average number of elements spanning a rib for a relative density $\rho^*_{rel} = 0.0115$, for linear (CPS4R) elements.

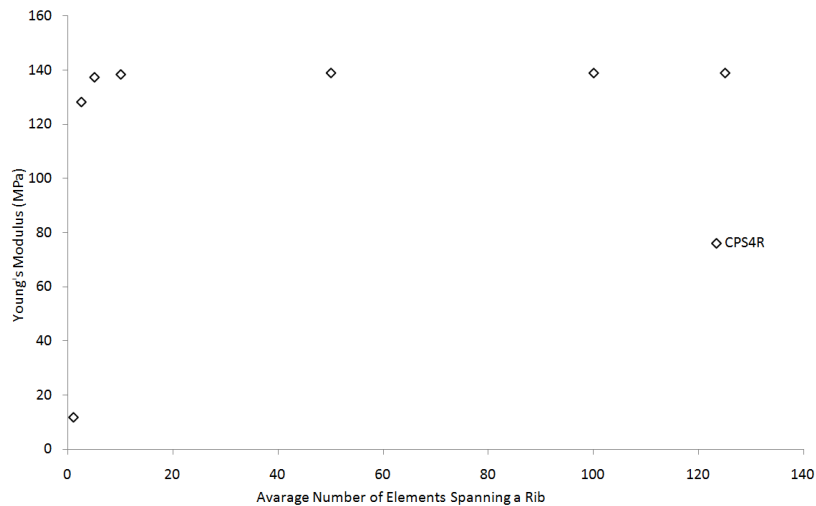


Figure 2.16: Convergence graph for the Young's modulus of a hexagonal honeycomb (quarter cell) against the average number of elements spanning a rib for a relative density $\rho^*_{rel} = 0.494$, for linear (CPS4R) elements.

2.3.3.2 Triangular

A convergence test for a triangular honeycomb is shown in Figure 2.17 for a low relative density $\rho^*_{rel} = 0.0287$ and for a high relative density $\rho^*_{rel} = 0.909$ in Figure 2.18. It can also be seen that there is little change in the in-plane Young's modulus when

there is more than an average of 5 elements spanning a rib for both relative densities of $\rho_{rel}^* = 0.0287$ and $\rho_{rel}^* = 0.909$.

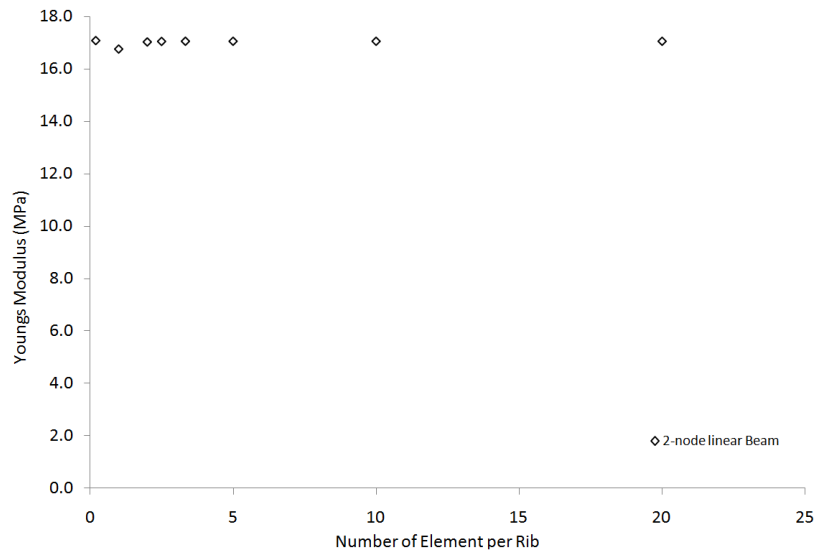


Figure 2.17: Convergence graph for the Young's modulus of a triangular honeycomb (half-cell) against the average number of elements spanning a rib for a relative density $\rho_{rel}^* = 0.0287$, for linear (CPS4R) elements.

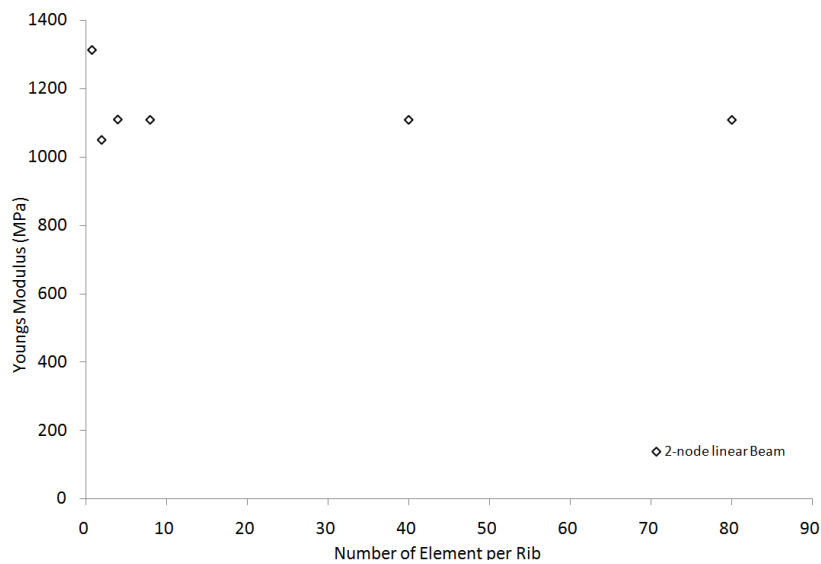


Figure 2.18: Convergence graph for the Young's modulus of a triangular honeycomb (half-cell) against the average number of elements spanning a rib for a relative density $\rho_{rel}^* = 0.909$, for linear (CPS4R) elements.

2.3.4 Boundary Conditions and Sample Size

The results of changing the relative density of hexagonal honeycombs is shown in Figure 2.19 and Figure 2.20 where the Young's Modulus is plotted against the relative density ρ_{rel}^* of the unit cell, for a quarter cell, full cell, and 8x8 array and compared to Gibson and Ashby's prediction for in-plane Young's modulus as described in Equation 1-4 and allowing for Shear in Equation 1-9.

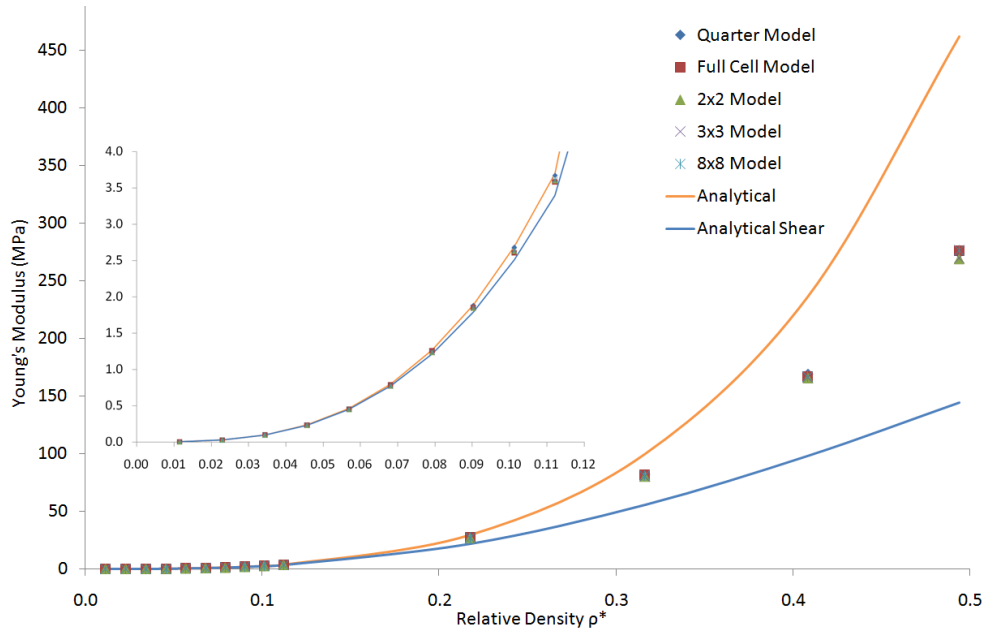


Figure 2.19: Young's modulus against the relative density ρ_{rel}^* of hexagonal honeycombs for a quarter cell, full cell, 2x2, 3x3, 4x4, and 8x8 arrays.

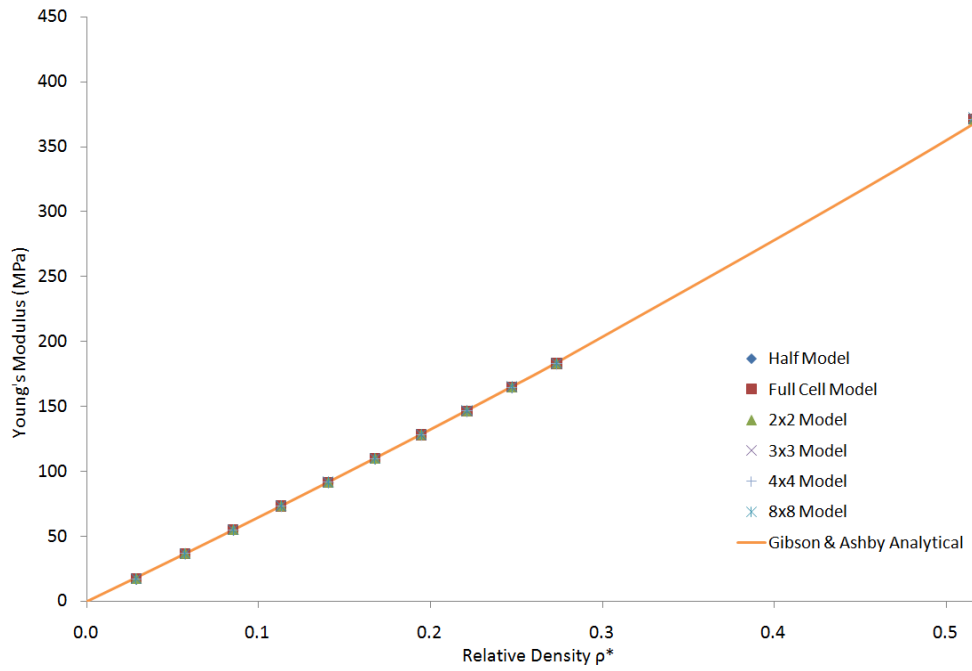


Figure 2.20: Young's modulus against the relative density ρ^*_{rel} of triangular honeycombs for a quarter cell, full cell, 2x2, 3x3, 4x4, and 8x8 arrays.

2.4 Discussion

2.4.1 Wire Elements

It can be seen in the *2D Planar deformable wire element* convergence results from Figure 2.9 to Figure 2.12 that the flexure-dominated hexagonal honeycomb are more sensitive to the element size than that of the stretch/compression dominated triangular honeycomb. This is due to elements when loaded in flexure not fully capturing the curvature of the beam with a coarse mesh, whereas elements in the stretch/compression dominated triangular honeycomb experience an axial displacement and are less dependent on element size to capture the mode of deformation. It can be seen for hexagonal honeycombs in Figure 2.9 and Figure 2.10 that quadratic (B22) elements converge at a lower element count compared to linear (B21) elements specifically quadratic (B22) element converge at about 10 elements per beam and linear (B21) converge at about 100 elements per beam. This is due to the 3 node beam better determining the curvature of the beam.

A comparison of sample size is shown in Figure 2.13 for hexagonal honeycombs of changing relative density ρ_{rel}^* it can be seen that the two analytical predictions show close correlation up to a relative density of approximately $\rho_{rel}^* 0.218$ when shear within the ribs of the honeycomb becomes significant. At this point the analytical that does not allow for shear is an over estimate of the Young's modulus and the model that allows for shear within the rib is more accurate. The 8x8 array results correlate closely with the analytical that allows for shear within the rib along with the 4x4, 3x3, 2x2, unit cell and quarter cell which converge to the 8x8 result. Models predict well the Young's modulus for hexagonal honeycombs of low relative density as there is smaller percentage difference. However the percentage difference increases for higher relative densities. This could be due to problem of modelling low aspect ratio beams. There is a strong correlation between analytical and FEA results for predicting the in-plane Young's modulus of triangular honeycombs using *2D planar deformable wire elements* as shown in Figure 2.14.

2.5 Shell Elements

It can be seen in the *2D Planar deformable shell element* convergence results from Figure 2.15 to Figure 2.18 that the flexure dominated hexagonal honeycomb are more

sensitive to the element size than that of the stretch/compression dominated triangular honeycomb. This can be explained similarly to the wire elements and is due to elements when loaded in flexure not fully capturing the curvature of the beam, whereas elements in the stretch/compression dominated triangular honeycomb experience an axial displacement and are less dependent on element size to capture the mode of deformation. In contrast to wire elements the critical size of element is not dependent on the length of the rib, but the number of elements that span a rib. It can be seen from Figure 2.15 and Figure 2.16 that for a convergence for the in-plane Young's modulus the minimum number of elements spanning a rib is 5.

A comparison of sample size is shown in Figure 2.19 for hexagonal honeycombs of changing relative density ρ_{rel}^* it can be seen that the two analytical predictions and FEA results show close correlation up to a relative density of approximately $\rho_{rel}^* = 0.218$ when shear within the ribs of the honeycomb becomes significant. All FEA results show strong agreement for different sample sizes. There is a strong correlation between the analytical and FEA results for predicting the in-plane Young's modulus of triangular honeycombs using *2D planar deformable shell elements*.

2.6 Conclusion

It has been established that when using beam 2D deformable wire elements to model honeycombs, particularly hexagonal, that quadratic (B22) elements are more favourable and that an element count of at least 10 elements should be along each rib.

It has also been shown that an 8x8 array is more favourable when modelling an in-plane honeycomb but is computationally expensive. A full unit cell is relatively accurate up to a relative density $\rho_{rel}^* < 0.0569$ with a percentage difference less than 10% and is accurate up to a relative density $\rho_{rel}^* < 0.0115$ with a percentage difference less than 2%

Due to the increase in uncertainty over the accuracy of results as the relative density increases, low relative density structure will be investigated. The accuracy of 2D deformable wire elements show good agreement with analytical and 2D deformable shell element for low relative densities $\rho_{rel}^* < 0.11$ and can therefore be used to reduce the computational cost of modelling discrete hierarchy.

Chapter 3. Introducing Hierarchy into Honeycombs

3.1 Introduction

The aim of this chapter is to determine the in-plane elastic effects of introducing hierarchy into a honeycomb structure and comparing the material properties to that of a conventional honeycomb of the exact same relative density ρ_{rel}^* .

Several parameters that describe the nature of hierarchy in honeycombs were defined (see following sub-sections) and sequentially and systematically varied between limits in a series of finite element modelling studies. A two dimensional finite element model was generated for the unit cell of each honeycomb and its in-plane axial elastic modulus determined in compression as described in Chapter 2.

Note that geometric symmetry for the regular hexagonal and triangular honeycombs means in-plane isotropy; likewise the square cell honeycomb will exhibit in-plane orthotropy (Gibson & Ashby 1997). Only second order hierarchy, i.e. a super and one sub-structure were considered, given the primary motivation was to explore pragmatic limits. This is due to the increased complexity of numerical modelling and manufacture when introducing hierarchy. It is also believed that there are diminishing returns as the hierarchical order increases. Previous theoretical studies have considered more hierarchical levels [Lakes 1993], which have shown little additional effect on properties with hierarchy greater than order 3. Relationships between the parameters in question and elastic modulus were established via numerical simulations and compared to analytical results.

Preliminary models were established to check validity of boundary conditions, convergence, numerical accuracy, whilst benchmarking against established analytical models for such honeycombs [Gibson and Ashby 1982, Masters and Evans 1996] as shown in Chapter 2.

3.2 Methods

The following section discusses the manner in which hierarchy was introduced in-plane into a honeycomb along with the parameters and variables that are apparent with the introduction of hierarchy. The section also describes the method that each parameter was investigated by means of computational modelling.

3.2.1 Hierarchical Length Ratio

Hierarchy was initially introduced into a honeycomb by introducing a sub-structure of a different length size into a conventional honeycomb as shown in Figure 3.1 and Figure 3.2 for hexagonal and triangular structures respectively, where the black honeycomb represents the super-structure and the red represents the sub-structure. The super-structure can be described in terms of l_{sup} , h_{sup} , t_{sup} and θ_{sup} and the sub-structure can be described in terms of l_{sub} , h_{sub} , t_{sub} and θ_{sub} as shown in Figure 3.1 and Figure 3.2.

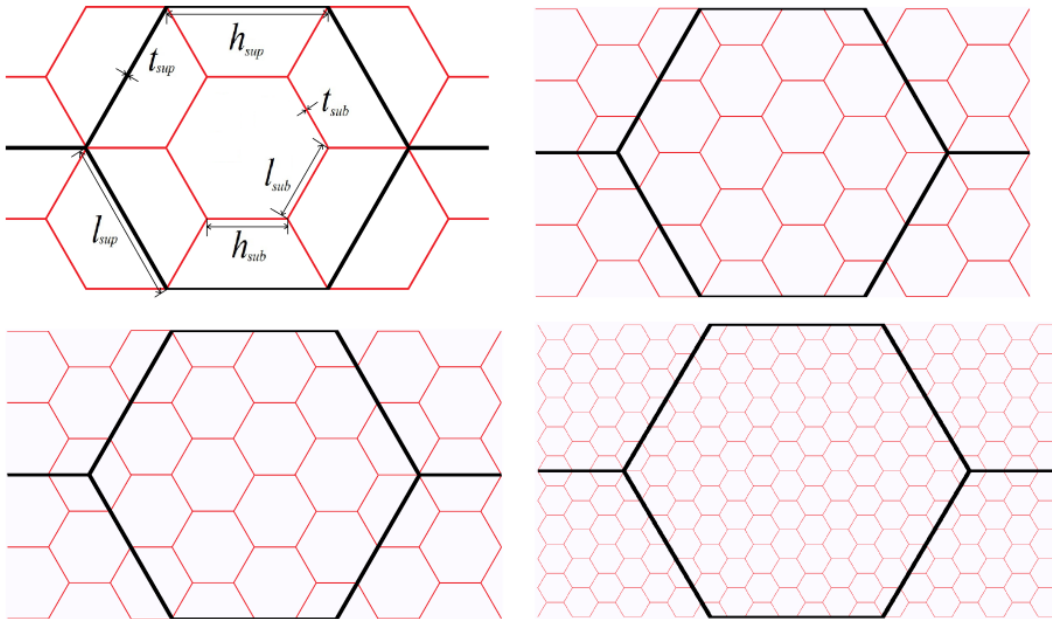


Figure 3.1: Shows the geometry for hierarchical hexagonal honeycombs with different HLR's λ . a) Shows a full cell of a hierarchical hexagonal honeycomb with associated terminology when $\lambda = 0.5$, b) shows a full cell of a hierarchical hexagonal honeycomb when $\lambda = 0.25$, c) similarly when $\lambda = 0.2$ and d) when $\lambda = 0.1$.

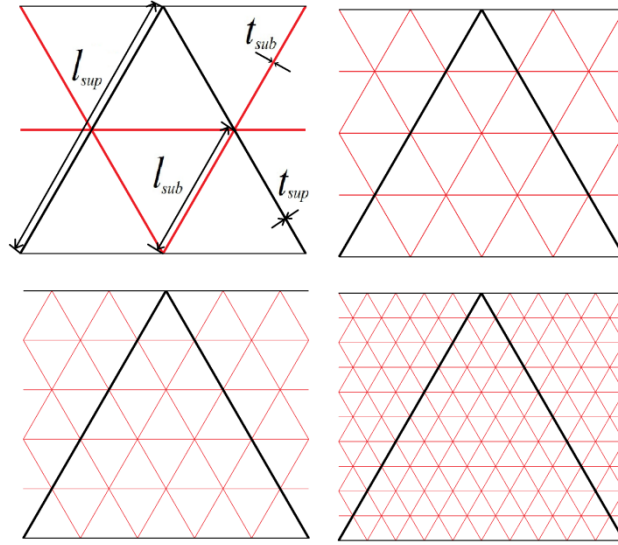


Figure 3.2: Shows the geometry for hierarchical triangular honeycombs with different HLR's λ . a) Shows a full cell of a hierarchical triangular honeycomb with associated terminology when $\lambda = 0.5$, b) shows a full cell of a hierarchical triangular honeycomb when $\lambda = 0.25$, c) similarly when $\lambda = 0.2$ and d) when $\lambda = 0.1$.

It was then necessary to determine at what point the sub-structure could be considered as a continuum to the super-structure as mentioned in Lakes (1993). The issue of treatment of a sub-structure as a continuum was investigated via a series of models in which the relative length of the sub-structure to the super-structure was iteratively decreased. The HLR λ can be used to describe the difference in length scales between the sub and super-structure and is defined by the fraction of a characteristic length of the sub-structure l_{sub} to a similar length of the super-structure l_{sup} , as in Equation 3-1.

$$\lambda = \frac{l_{sub}}{l_{sup}}$$

Equation 3-1

Specifically, hierarchy was introduced and benchmarked against a conventional honeycomb by arbitrarily removing 50% of the mass from a conventional honeycomb and allocating the removed mass to the sub-structure, so the existing geometry of the conventional honeycomb becomes the super-structure. This meant that hierarchical honeycombs could be compared to conventional on an equal density basis. The HLR λ was decreased from 50% to 2.5% of l_{sup} , i.e. the number of sub-structure cells along a

super-structure rib varied from 2 to 40. 2D planar wire models were used to determine the in-plane Young's modulus with boundary conditions and element types and sizes as established in Chapter 2.

The elastic modulus was calculated as the total reaction force divided by the projected area (unit depth), divided by the imposed strain of 0.1% (calculated as the imposed deflection divided by the original cell dimension). In some cases, the sub-structure was considered to occupy all of the free volume/area in the unit cell, and in some cases only a proportion. Results for hierarchical honeycombs were compared to conventional honeycombs of the exact same relative density $\rho_{rel}^* = 0.00577$, which was constant for all models. The unit cell ribs of the hierarchical honeycombs remained as solid beams, as per conventional versions.

The same material properties were assigned to the sub and super-structure ribs as applied to the beam and shell element models in Chapter 2 assuming nylon powder (Duraform 3D systems) which had a set of approximately linear and isotropic elastic constants (specifically $E_s = 1600$ MPa, $G_s = 593$ MPa and $\nu_s = 0.35$) (Miller 2010 & Caulfield 2007) the material properties were used for all cases. The sub and super-structure cells were modelled using 2D Timoshenko beam elements (B22), a 3-node quadratic beam in a plane, using a commercial Finite Element (FE) analysis package ('ABAQUS', Dassault Systèmes) (Papka & Kyriakides 1994 & 1998 (1)) (Chung & Waas 2001). Boundary sharing beams have either half thickness or half-length depending on contact with the boundary, so that the symmetry of the unit cell allowed tessellation into a uniform honeycomb.

The upper most edges of the cell sub and super-structure were displaced uniformly in compression so the cells were at 0.1 % global strain in the X_1 axis as described in (Odegard 2003). The contralateral cell edges were constrained to zero displacement in the X_1 axis but were allowed to freely displace in the X_2 axis. Cell edges parallel to the X_1 axis were constrained to zero displacement in the X_2 axis, akin to being on rollers. A constraint was applied to the elements on the extreme of the contralateral edge so they were free to displace in any direction except that they remained in an axis parallel to the applied strain. These boundary conditions simulate uniaxial compression in a honeycomb continuum and can be seen in Figure 2.6 in Chapter 2.

The sub-structure was modelled as a discrete structure in a manner similar to that for the super-structure. The thickness t_{sub} was varied to ensure consistent mass between models with different values of the length l_{sub} . Integer values of λ , the Hierarchical Length Ratio (HLR), were specified so that the super- and sub-structure unit cells shared ribs. The thicknesses of edge sharing ribs in the sub-structure were $t_{sub}/2$ and $t_{sup}/2$ as per the super-structure. It was possible to use unit cells of the hierarchical structure to model an infinite array, i.e. containing super-and sub-structures, because of the two fold symmetry of the cell.

3.2.2 Co-ordination number

The co-ordination number of the unit cells, i.e. the number of ribs connecting at nodes, in both the sub- and super-structure, was varied. Possible tessellating unit cells could have coordination numbers of; 6 (a triangle), 4 (a square) and 3 (a hexagon) as shown in Figure 3.3.

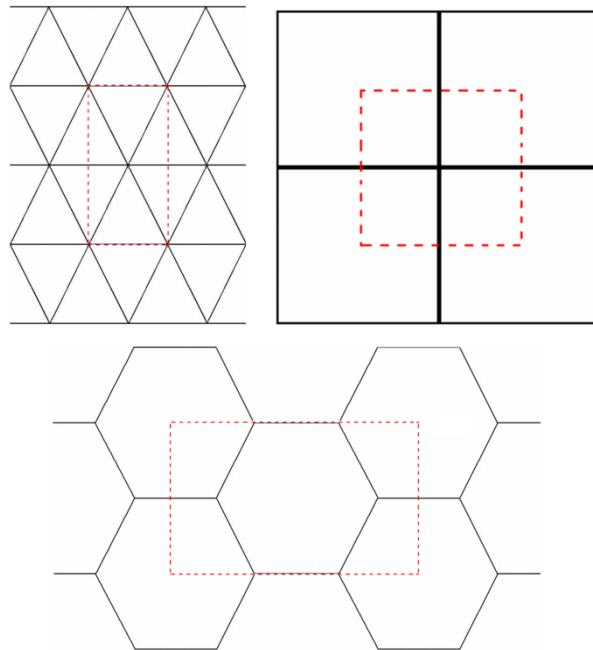


Figure 3.3: Shows 2D honeycombs of different connectivity and co-ordination number. a) A triangular honeycomb with co-ordination number = 6, b) a square honeycomb with co-ordination number = 4 and c) a hexagonal honeycomb with co-ordination number = 3.

The coordination numbers of the sub and super-structure are denoted here as two numbers in sequence respectively, e.g. (3-6) (hexagonal super-structure and triangular sub-structure). All possible combinations of co-ordination numbers were explored; 3-3, (3-4), (3-6), (4-3), (4-4), (4-6), (6-3), (6-4) and (6-6), examples of some of which are shown in Figure 3.4. As in the previous section mass was evenly distributed between the sub and super-structure hence 50% of the mass was in the sub-structure and 50% within the super-structure. 2D planar wire models were used to determine the in-plane Young's modulus with boundary conditions and element types and sizes as described in Chapter 2.

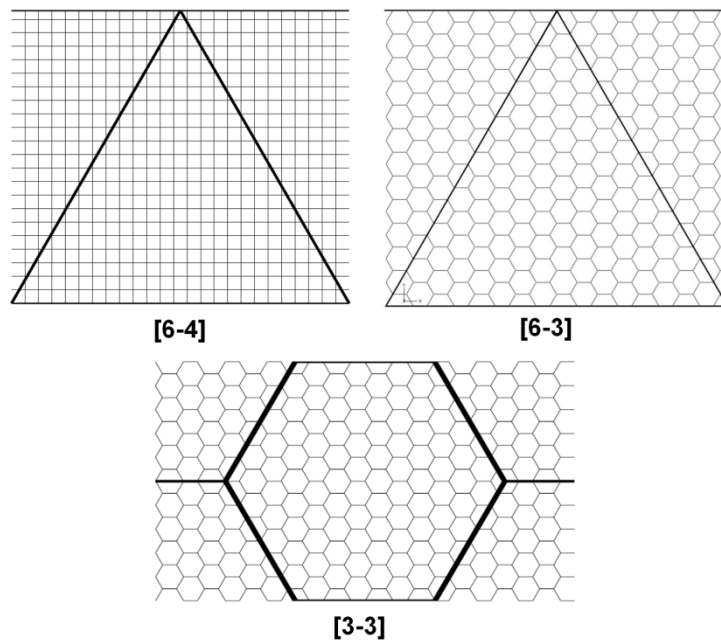


Figure 3.4: Shows the geometry of hierarchical honeycombs with different co-ordination numbers a) 6-4 for a triangular super-structure and square sub-structure, b) 6-3 for a triangular super-structure and hexagonal sub-structure, c) 6-6 for a hexagonal super-structure and hexagonal sub-structure.

3.2.3 Mass Distribution

Initially the proportion of mass distributed between the sub and super-structure was chosen as 50% as in the first two sub-sections. This was further explored by changing the proportion of mass between the sub and super-structure. The mass distribution can therefore be used to describe the volume of mass within the sub-structure compared to

the total mass within the structure and indirectly the super-structure as shown in Equation 3-2.

$$\text{Mass Distribution}(\%) = \frac{V_{sub}}{V_{sub} + V_{sup}} 100$$

Equation 3-2

Where V_{sub} is the volume of material in the sub-structure and V_{sup} is the volume of material in the super-structure, when the sub and super-structure consist of the same constituent material.

The proportion of mass distributed between the sub and super-structure was explored by maintaining l_{sub} and l_{sup} for a given HLR $\lambda = 0.04$ and changing the thickness t_{sub} and t_{sup} proportionally ensuring the relative density ρ_{rel}^* of the cell was maintained constant. This change in thicknesses effectively changed the mass distribution between the sub and super-structure as can be seen in Figure 3.5 which shows two hierarchical honeycombs with a HLR $\lambda = 0.1$ for two different mass distributions of 20% and 80% of mass within the sub-structure. FE models were established using 2D planar wire elements to determine the in-plane Young's modulus with boundary conditions and element types and sizes as previously described in Figure 2.6 in Chapter 2 for hierarchical hexagonal and triangular honeycombs with $\lambda = 0.04$, i.e. a fine sub-structure likely to approximate a continuum. Eleven discrete mass proportions were considered, from 0.0 to 1.0 inclusive, with intervals of 0.1.

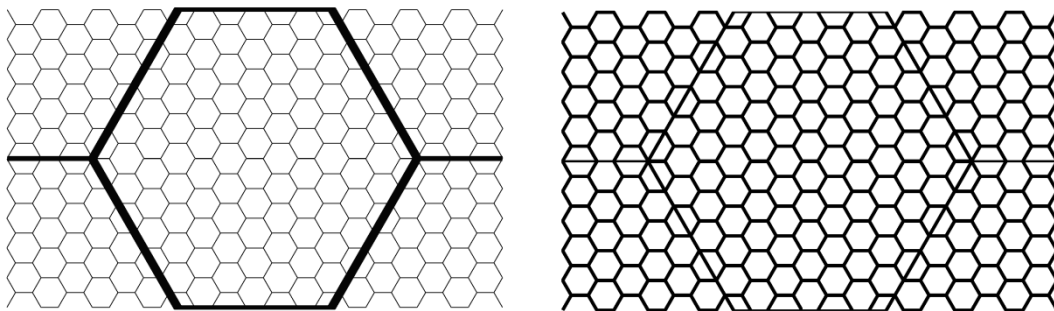


Figure 3.5: Shows how the mass distribution between the sub and super-structure can be change for a hexagonal hierarchical honeycomb when $\lambda = 0.1$ for a) when the 20% of the total mass is within the sub-structure and b) when the 80% of the total mass is within the sub-structure.

3.2.4 Functional Grading

Previous work has focused on the effects of introducing a sub-structure filling the whole of a unit cell as shown in Figure 3.1, Figure 3.2, Figure 3.4 and Figure 3.5. It is possible to conceive of non-uniform distributions of mass in the sub-structure, in contrast to previous sections. This is in effect a kind of functional grading whereby instead of varying in space the volume fraction of an inclusion, the distance the sub-structure extends from the super-structure was varied. To explore the effect of such functional grading of the sub-structure in this manner models were created in which the number of sub-cells from the super-structure were varied as shown in Figure 3.6 and Figure 3.7 where the length l_{sub} remained constant, but t_{sub} was varied to ensure constant density of the unit cell as can be seen with the number of sub-cells extended from the super-structure rib.

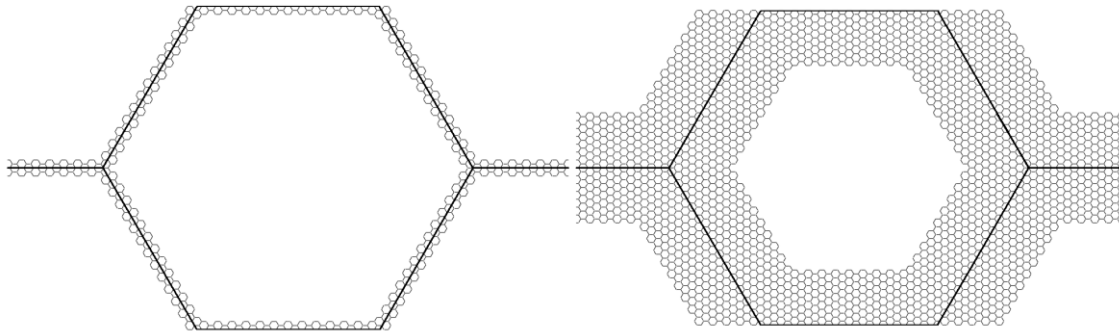


Figure 3.6: Shows hexagonal hierarchical honeycombs where the sub-structure only part fills the area in the centre of the super-structure unit cell.

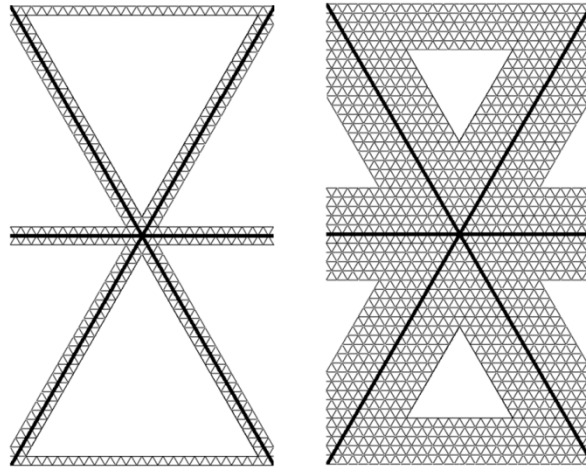


Figure 3.7: Shows triangular hierarchical honeycombs where the sub-structure only part fills the area in the centre of the super-structure unit cell.

Importantly this allowed the removal of sub-structure in certain areas of the cell, that is voids were allowed in the sub-structure, in contrast to the previous sections where super-structure cells' voids were completely filled with sub-structure cells. The two key parameters which described the dimensions of the sub and super structure for a given unit cell size were.

- i) The extent away from the super-structure cell which the sub-structure occupied, and
- ii) The distribution of mass between the sub and super-structure.

The mass distribution was varied from 50%, 75%, 95% and 100%, the latter entirely replacing the super-structure with sub-structure. The hexagonal hierarchical honeycomb was investigated for sub-structure cells spanning the super-structure from 2 – 20 cells and the triangular hierarchical honeycomb was investigated for sub-structure cells spanning the super-structure from 1 – 7 cells both for a HLR of $\lambda = 0.04$. The reason for a different number of triangular sub-cells spanning the super-structure is due to the shape of the triangular cell that is taller and thinner whereas the hexagonal was taken a short and wide. The connectivity of the triangular super-structure also limited the number of sub-cells that span the super-structure before approaching a conventional triangular honeycomb.

3.2.5 Functional Grading and Co-Ordination Number

Previous work described showed that the mass distributions away from 1.0 in the sub-structure proved deleterious to the Young's modulus of hierarchical honeycombs. It is therefore possible to conceive of a hierarchical honeycomb where the mass distribution equals 100% of mass distributed in the sub-structure and the super-structure. Co-ordination number and dimensions are defined by the global geometry of the sub-structure, which has a co-ordination number independent of that of the super-structure. This can be seen in Figure 3.8 for a hierarchical honeycomb with a hexagonal super-structure and a hexagonal sub-structure. Co-ordination numbers investigated were (3-3), (3-6), (6-6) and (6-3) for a range of super-structure aspect ratios as shown in Figure 3.9.

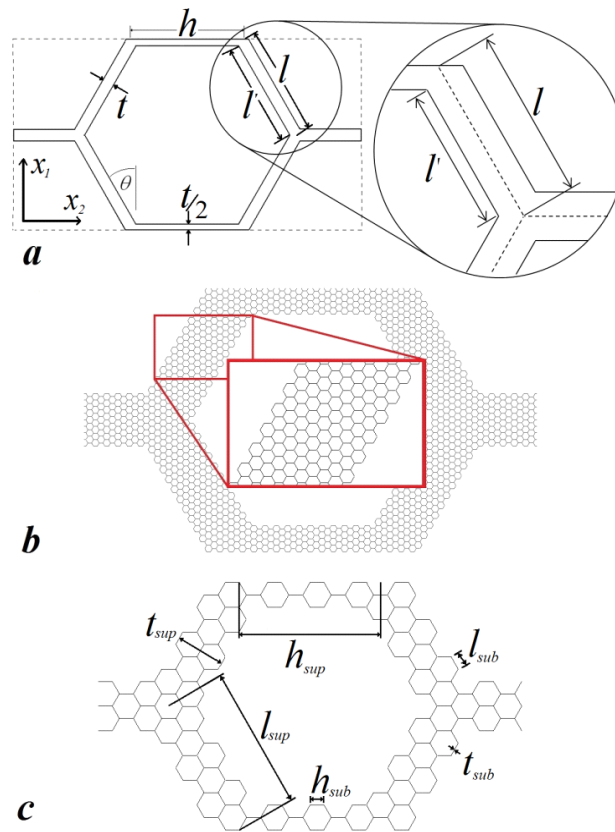


Figure 3.8: a) Shows the cell geometry and parameters for a conventional hexagonal honeycomb unit cell according to Gibson and Ashby's terminology. b) A unit cell of a second order hierarchical honeycombs with a HLR of $\lambda=0.015$ and a super-structure aspect ratio $\alpha_{sup} = 2.88$. c) A unit cell of a second order hierarchical honeycombs with a HLR of $\lambda=0.1$ and a super-structure aspect ratio $\alpha_{sup} = 2.88$, along with annotated terminology.

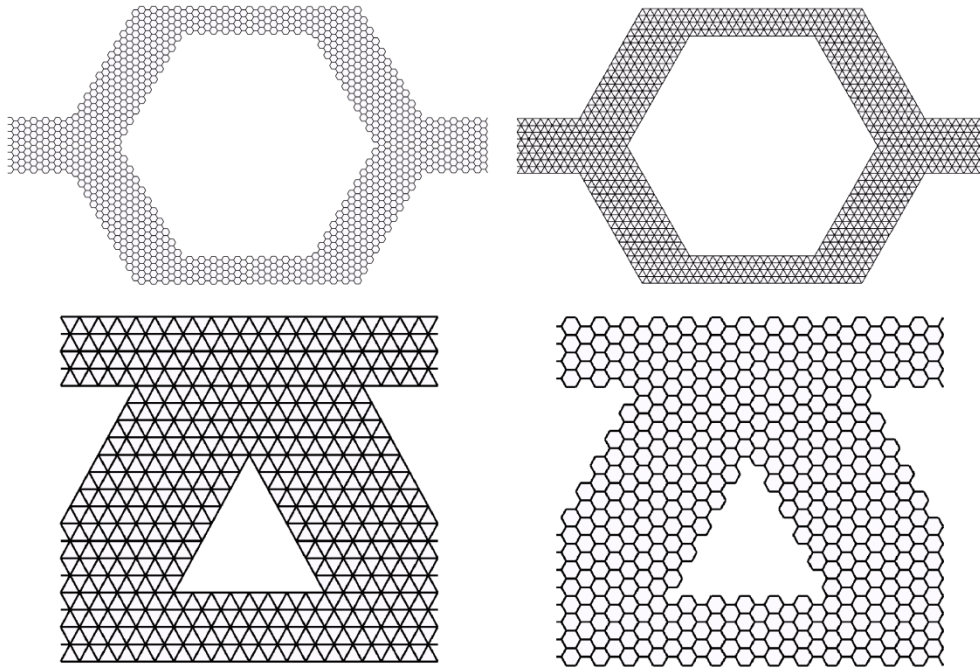


Figure 3.9: Shows hierarchical honeycombs with 100% of the mass within the sub-structure and a super-structure aspect ratio $\alpha_{sup} = 2.88$. a) Hexagonal super-structure hexagonal sub-structure (3-3), b) hexagonal super-structure triangular sub-structure (3-6), c) triangular super-structure triangular sub-structure (6-6) and d) triangular super-structure hexagonal sub-structure (6-3).

The various parameters describing functional grading hierarchical honeycombs are shown in Figure 3.8 and defined in the following. The cells of conventional and hierarchical honeycombs have ribs of length l and h , and thickness t , as shown in Figure 3.8 in both a conventional and hierarchical honeycombs. The aspect ratio of a honeycomb rib is defined as its length divided by its thickness, as shown in Equation 3-3 for conventional honeycombs and Equation 3-4 for the super-structure of hierarchical honeycombs. The parameter values for super- and sub-structure cells are noted by the subscripts sub and sup (referring to sub-and super-structure parameters respectively), and as described in (Taylor 2011).

$$a = \frac{l}{t}$$

Equation 3-3

$$a_{sup} = \frac{l_{sup}}{t_{sup}}$$

Equation 3-4

3.2.6 Functional Grading, Co-ordination Number and HLR

The first step in applying functional grading to hierarchical honeycombs was to determine the length scale of the sub-structure, relative to that of the super-structure, at which it could be considered to be a continuum as in the previously discussed HLR section. The ratio of the lengths in the sub and super-structure is the HLR λ and is defined according to Equation 3-1. The critical value of the HLR at which continuum behaviour was attained was determined by iteratively decreasing the value of λ for three example hierarchical honeycombs of different aspect ratios ($\alpha_{sup} = 11.5$, $\alpha_{sup} = 2.88$ and $\alpha_{sup} = 1.15$) for hexagonal super-structures and ($\alpha_{sup} = 11.5$ and $\alpha_{sup} = 2.88$) for triangular super-structures. Super-structure aspect ratios $\alpha_{sup} = 1.15$ were not investigated for triangular super-structures as at this aspect ratio the more dense triangle structure is effectively a continuum of sub-structure with no second order hierarchy present.

To change λ the lengths l_{sub} , h_{sub} and t_{sub} of the sub-structure were iteratively decreased, while lengths l_{sup} , h_{sup} and t_{sup} remained constant, effectively increasing the number of sub-cells spanning the thickness of the super-structure, as shown in Figure 3.10, Figure 3.11, Figure 3.12 and Figure 3.13 for the four co-ordination numbers investigated in this manner. Square geometries were not investigated due to problems tessellating square arrays with hexagonal and triangular geometries and the inherently poor off-axis properties.

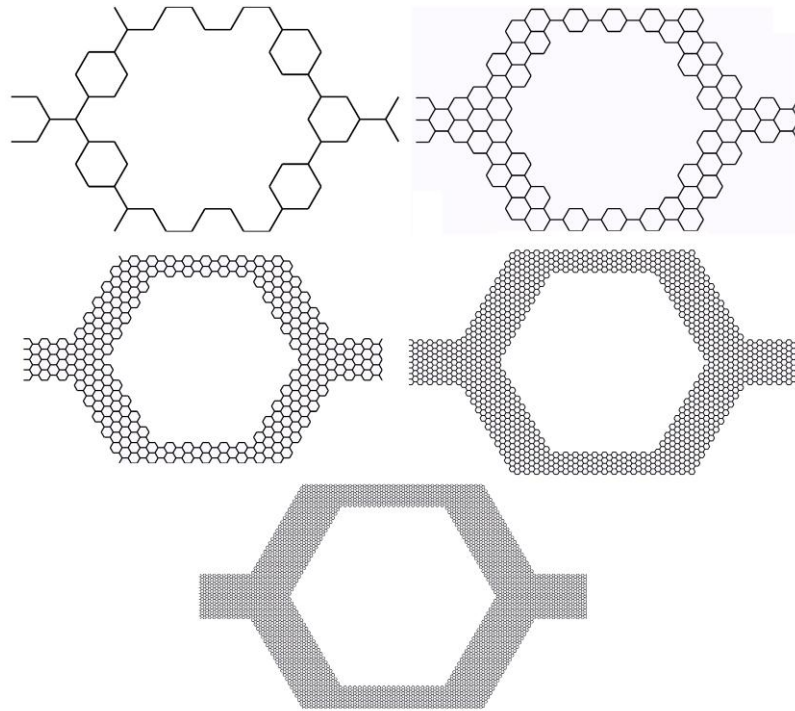


Figure 3.10: Shows how the HLR changes for a (3-3) hierarchical honeycomb with a super-structure aspect ratio $\alpha_{sup} = 2.88$ a) the super-structure is one sub-cell wide when $\lambda = 0.2$, b) the super-structure is two sub-cells wide when $\lambda = 0.1$, c) the super-structure is four sub-cells wide when $\lambda = 0.05$, d) the super-structure is eight sub-cells wide when $\lambda = 0.025$ and e) the super-structure is sixteen sub-cells wide when $\lambda = 0.012$.

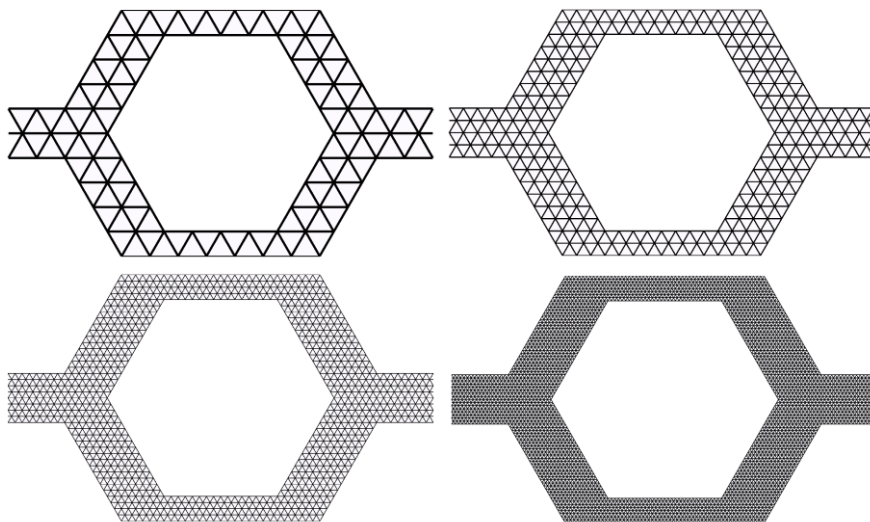


Figure 3.11: Shows how the HLR changes for a (3-6) hierarchical honeycomb with a super-structure aspect ratio $\alpha_{sup} = 2.88$ a) the super-structure is two sub-cells wide when $\lambda = 0.1$, b) the super-structure is four sub-cells wide when $\lambda = 0.05$, c) the super-structure is eight sub-cells wide when $\lambda = 0.025$ and d) the super-structure is sixteen sub-cells wide when $\lambda = 0.012$.

$\lambda = 0.2$, b) the super-structure is four sub-cells wide when $\lambda = 0.1$, c) the super-structure is eight sub-cells wide when $\lambda = 0.05$ and d) the super-structure is sixteen sub-cells wide when $\lambda = 0.025$.

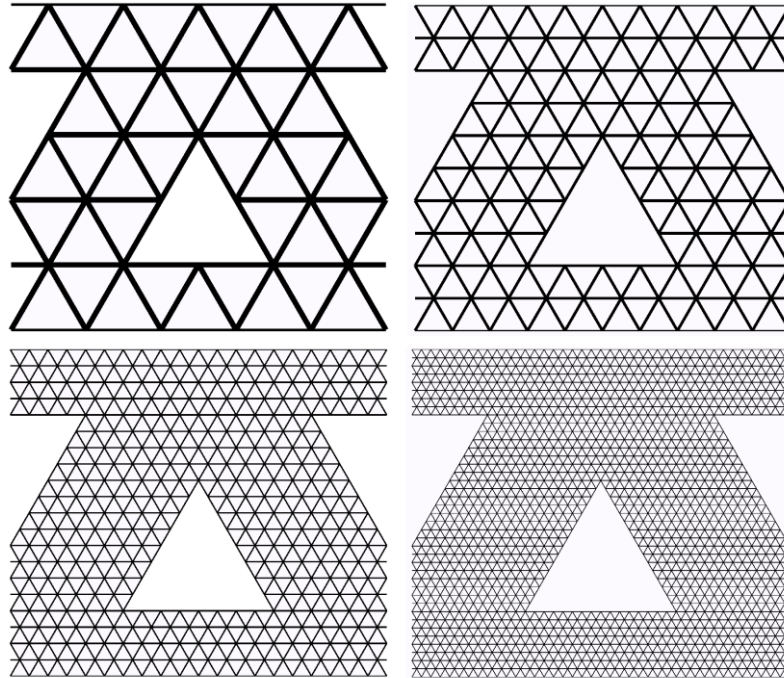


Figure 3.12: Shows how the HLR changes for a (6-6) hierarchical honeycomb with a super-structure aspect ratio $\alpha_{sup} = 2.88$ a) the super-structure is two sub-cells wide when $\lambda = 0.2$, b) the super-structure is four sub-cells wide when $\lambda = 0.1$, c) the super-structure is eight sub-cells wide when $\lambda = 0.05$ and d) the super-structure is sixteen sub-cells wide when $\lambda = 0.025$.

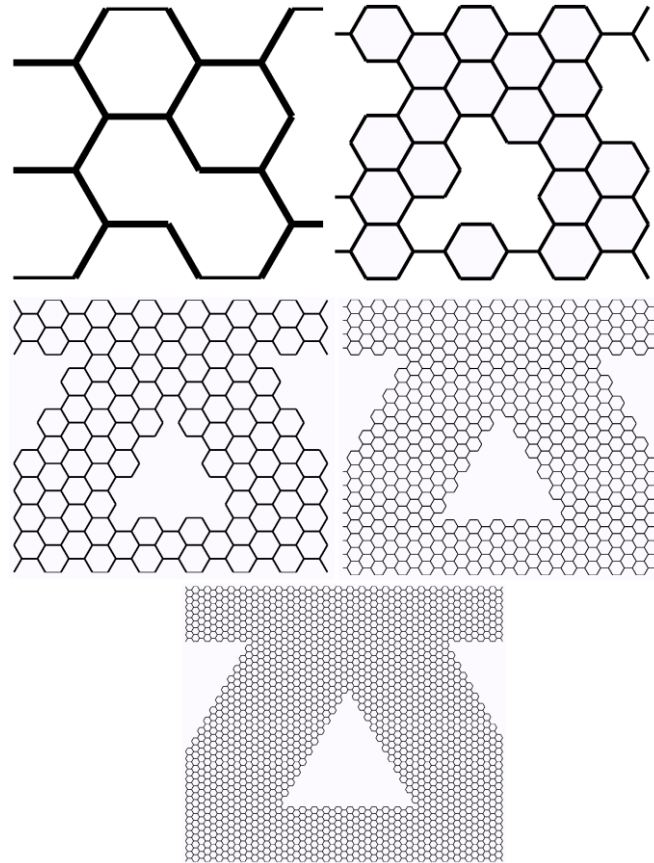


Figure 3.13: Shows how the HLR changes for a (6-3) hierarchical honeycomb with a super-structure aspect ratio $\alpha_{sup} = 2.88$ a) the super-structure is two sub-cells wide when $\lambda = 0.2$, b) the super-structure is four sub-cells wide when $\lambda = 0.1$, c) the super-structure is eight sub-cells wide when $\lambda = 0.05$ and d) the super-structure is sixteen sub-cells wide when $\lambda = 0.025$.

3.2.7 Functional Grading, Co-ordination Number and Change in Aspect Ratio

Once the critical value of λ , and thus the number of sub-cells spanning the super-structure, was determined, it was then possible to investigate further the effect of changing the super-structure aspect ratio as shown in Figure 3.14, Figure 3.15, Figure 3.16, and Figure 3.17. This was achieved by maintain the number of sub-cells spanning the super-structure for the sub-structure to be considered a continuum. It was determined in the previous investigation into the HLR, which found increases in the number of cells spanning the super-structure greater than 8 made little difference on the elastic response of the structure as shown in the results section of this chapter. The effects of changing the super-structure aspect ratio α_{sup} whilst maintaining 8 sub-cells

spanning the super-structure the length l_{sub} was varied ensuring that there were always an integer number of sub-cells along the length l_{sup} it was also necessary to change t_{sub} depending on the length l_{sub} and the number of sub-structure ribs in order to maintain constant mass.

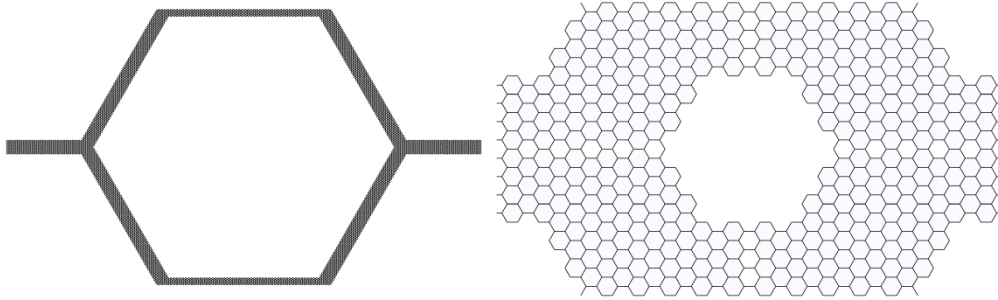


Figure 3.14: Shows how the sub and super-structure dimensions change for a hexagonal super-structure and hexagonal sub-structure hierarchical honeycomb for a) when the super-structure aspect ratio $\alpha_{sup} = 11.5$ and b) when the super-structure aspect ratio $\alpha_{sup} = 1.15$.

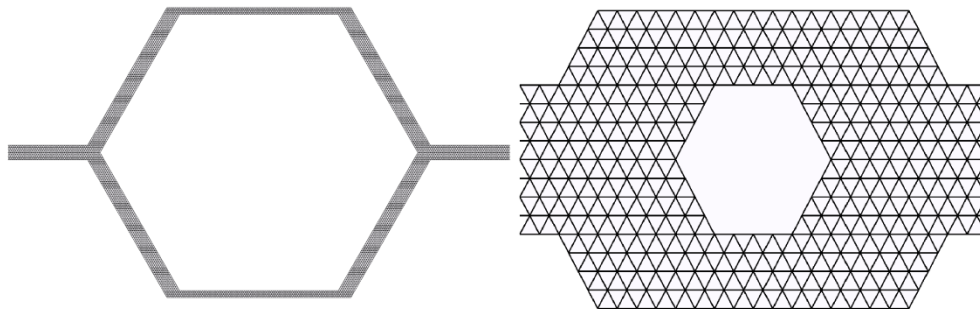


Figure 3.15: Shows how the sub and super-structure dimensions change for a hexagonal super-structure and triangular sub-structure hierarchical honeycomb for a) when the super-structure aspect ratio $\alpha_{sup} = 11.5$ and b) when the super-structure aspect ratio $\alpha_{sup} = 1.15$.

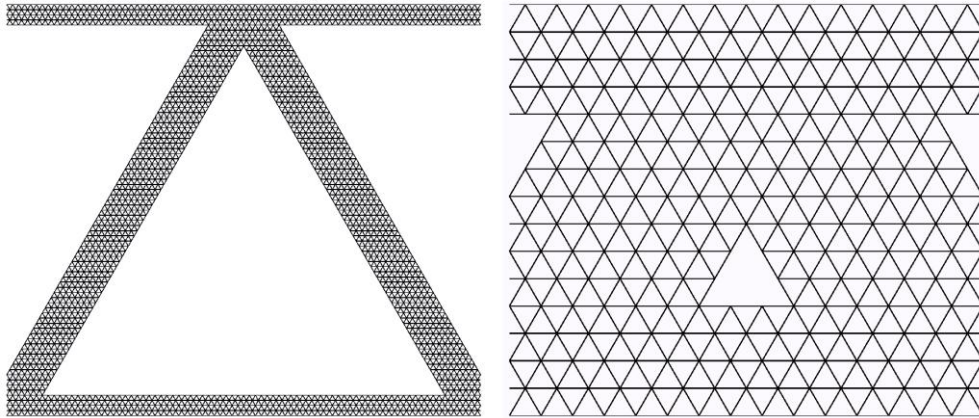


Figure 3.16: Shows how the sub and super-structure dimensions change for a triangular super-structure and triangular sub-structure hierarchical honeycomb for a) when the super-structure aspect ratio $\alpha_{sup} = 11.5$ and b) when the super-structure aspect ratio $\alpha_{sup} = 2.88$.

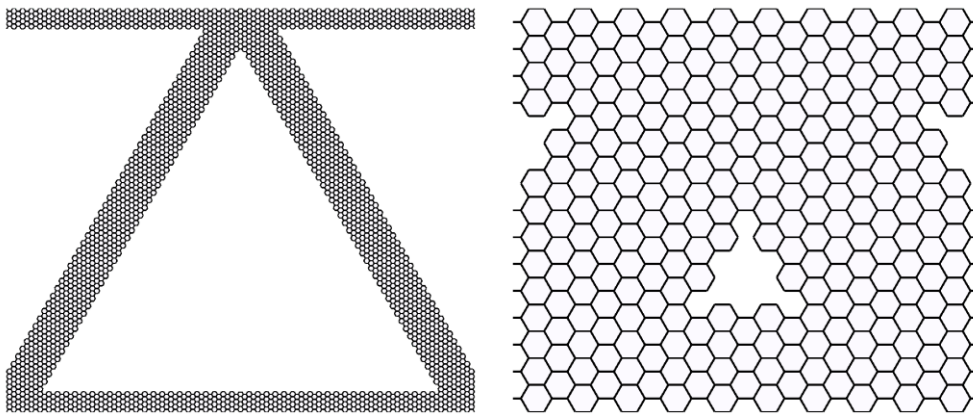


Figure 3.17: Shows how the sub and super-structure dimensions change for a triangular super-structure and hexagonal sub-structure hierarchical honeycomb for a) when the super-structure aspect ratio $\alpha_{sup} = 11.5$ and b) when the super-structure aspect ratio $\alpha_{sup} = 2.88$.

Preliminary models were undertaken investigating the in-plane Poisson's ratio and shear modulus. It was found that the introduction of hierarchy had little effect on the Poisson's ratio from 1 and the structure remained in-plane isotropic. The shear modulus could therefore be calculated from the in-plane Young's modulus using Hook's Law. As such the shear modulus has not been investigated in this study.

3.3 Analytical

3.3.1 Conventional honeycombs

Following the annotation of Gibson and Ashby (1982) honeycombs are given geometric parameters similar to those set out in Figure 3.8a, and extended to a hierarchical honeycomb in Figure 3.8c. Gibson and Ashby (1982) set out the fundamental underpinnings of the behaviour of honeycombs, i.e. as tessellations of unit cell structures formed from beams or plates. Thus using beam mechanics, expressions could be derived for the elastic properties, e.g. the in-plane Young's modulus for a hexagonal honeycomb in Equation 3-5 and the in-plane Young's modulus for a triangular honeycomb in Equation 3-6, for a range of 2D and 3D cellular solids including honeycombs. Note that for hierarchical honeycombs such as shown in Figure 3.8a, the true functional length of the super-structure l rib is unclear, with possible extremes ranging from l to l' .

$$\frac{E_1^*}{E_s} = \left(\frac{t}{l}\right)^3 \frac{\cos\theta}{(h/l + \sin\theta)\sin^2\theta}$$

Equation 3-5

$$\frac{E_1^*}{E_s} = 1.15 \frac{t}{l}$$

Equation 3-6

Where E_s is the Young's modulus of the constituent material. Similar expressions are given for the other Young's and shear moduli and the Poisson's ratios.

Masters and Evans (1996) later refined these models by accounting for other deformation modes, specifically stretching/compression and hinging of ribs. Gibson and Ashby (1997) further developed their hexagonal honeycomb model by including axial (tension/compression) and shear deformation of ribs as shown in Equation 3-7. Shear deformation becomes significant and therefore must be considered analytically in hexagonal honeycombs when the aspect ratio $\alpha < 5$ (or to be conservative $\alpha < 10$), where the aspect ratio α is the length l over thickness t as seen in Equation 3-3 and

Equation 3-4 shear is consider negligible in triangular honeycombs at these low aspect ratios due to the stretch dominated nature of the structure.

$$E_1^* = \left(\frac{t}{l}\right)^3 \frac{\cos\theta}{\left(\left(\frac{h}{l}\right) + \sin\theta\right) \sin^2\theta} \frac{1}{1 + (2.4 + 1.5v_s + \cot^2\theta) \left(\frac{t}{l}\right)^2} E_s$$

Equation 3-7

3.3.2 Hierarchical honeycombs

These equations can be adapted for hierarchical honeycombs. The equations in any of the work on honeycomb models described previously, being based on beam mechanics, are valid for continua and so are independent of size. Thus within hierarchical honeycombs, they can be used to describe the properties of all of the honeycombs individually. It might seem reasonable to assume therefore that a sub-structure honeycomb can be treated as a continuum and its predicted properties used in calculation of the properties of the super-structure. Equation 3-8 is derived for a hexagonal sub-structure honeycomb from those of Ashby and Gibson (1997) and is used as a continuum in Equation 3-9 for a hexagonal super-structure honeycomb, i.e. a hierarchical honeycomb. However, it is not proven whether this assumption of a continuum sub-structure is valid if the size scales of the sub and super-structures are not very different. This issue is addressed later in the HLR results section of the Chapter.

$$E_{1_{sub}}^* = \left(\frac{t_{sub}}{l_{sub}}\right)^3 \frac{\cos\theta}{\left(\left(\frac{h_{sub}}{l_{sub}}\right) + \sin\theta\right) \sin^2\theta} E_s$$

Equation 3-8

$$E_{1_{sup}}^* = \left(\frac{t_{sup}}{l_{sup}}\right)^3 \frac{\cos\theta}{\left(\left(\frac{h_{sup}}{l_{sup}}\right) + \sin\theta\right) \sin^2\theta} E_{1_{sub}}^*$$

Equation 3-9

In the case where ribs have aspect ratios $\alpha < 5$, the beam equation including axial and shear deformation must be used. Versions of Equation 3-8 and Equation 3-9 which allow for axial and shear deformation are given below in Equation 3-10, Equation 3-11

and Equation 3-12, which include the Poisson's ratio ν_{21}^* for a hexagonal honeycomb (adapted from Gibson and Ashby 1997).

$$E_{1sub}^* = \left(\frac{t_{sub}}{l_{sub}}\right)^3 \frac{\cos\theta}{\left(\left(\frac{h_{sub}}{l_{sub}}\right) + \sin\theta\right) \sin^2\theta} \frac{1}{1 + (2.4 + 1.5\nu_s + \cot^2\theta) \left(\frac{t_{sub}}{l_{sub}}\right)^2} E_s$$

Equation 3-10

$$\nu_{21sub}^* = \frac{\sin\theta \left(\frac{h_{sub}}{l_{sub}}\right) + \sin\theta}{\cos^2\theta} \left(\frac{t_{sub}}{l_{sub}}\right)^3 \frac{1 + (2.4 + 1.5\nu_s)(t_{sub}/l_{sub})^2}{1 + \left(2.4 + 1.5\nu_s + \tan^2\theta + \frac{2(h_{sub}/l_{sub})}{\cos^2\theta}\right) \left(\frac{t_{sub}}{l_{sub}}\right)^2}$$

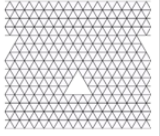
Equation 3-11

$$E_{1sup}^* = \left(\frac{t_{sup}}{l_{sup}}\right)^3 \frac{\cos\theta}{\left(\left(\frac{h_{sup}}{l_{sup}}\right) + \sin\theta\right) \sin^2\theta} \frac{1}{1 + (2.4 + 1.5\nu_{21sub}^* + \cot^2\theta) \left(\frac{t_{sup}}{l_{sup}}\right)^2} E_{1sub}^*$$

Equation 3-12

This approach is not just limited to a hexagonal sub-structure hexagonal super-structure (3-3), but are also valid for other co-ordination numbers such as (3-6), (6-6) and (6-3). Where the sub-structure material properties such as Young's modulus E_{1sub}^* can be defined by the geometry, dimension and constituent material properties of the sub-structure using Gibson and Ashby's predictions and then used as the constituent material properties for the super-structure. It is then possible to determine the material properties of the hierarchical structure using Gibson and Ashby's predictions for the geometry, dimensions and constituent material properties of the super-structure. The analytical equations applied to the sub and super-structure of hierarchical honeycombs is shown in Table 3.1.

Table 3.1: Shows the analytical equations applied to the sub and super-structure of hierarchical honeycombs of co-ordination number (3-3), (3-6), (6-6) and (6-3).

Co-ordination Number	Image	Sub-Structure	Super Structure
(3-3)		$E_{i\ sub}^* = \left(\frac{t_{sub}}{l_{sub}}\right)^3 \frac{\cos\theta}{\left(\left(\frac{h_{sub}}{l_{sub}}\right) + \sin\theta\right) \sin^2\theta} \frac{1}{1 + (2.4 + 1.5v_2 + \cot^2\theta) \left(\frac{t_{sub}}{l_{sub}}\right)^2} E_s$	$E_{i\ sup}^* = \left(\frac{t_{sup}}{l_{sup}}\right)^3 \frac{\cos\theta}{\left(\left(\frac{h_{sup}}{l_{sup}}\right) + \sin\theta\right) \sin^2\theta} \frac{1}{1 + (2.4 + 1.5v_{2\ sub}^* + \cot^2\theta) \left(\frac{t_{sup}}{l_{sup}}\right)^2} E_{i\ sub}^*$
(3-6)		$E_{i\ sub}^* = 1.15 \frac{t_{sub}}{l_{sub}} E_s$	$E_{i\ sup}^* = \left(\frac{t_{sup}}{l_{sup}}\right)^3 \frac{\cos\theta}{\left(\left(\frac{h_{sup}}{l_{sup}}\right) + \sin\theta\right) \sin^2\theta} \frac{1}{1 + (2.4 + 1.5v_{2\ sub}^* + \cot^2\theta) \left(\frac{t_{sup}}{l_{sup}}\right)^2} E_{i\ sub}^*$
(6-6)		$E_{i\ sub}^* = 1.15 \frac{t_{sub}}{l_{sub}} E_s$	$E_{i\ sub}^* = 1.15 \frac{t_{sup}}{l_{sup}} E_{i\ sub}^*$
(6-3)		$E_{i\ sub}^* = \left(\frac{t_{sub}}{l_{sub}}\right)^3 \frac{\cos\theta}{\left(\left(\frac{h_{sub}}{l_{sub}}\right) + \sin\theta\right) \sin^2\theta} \frac{1}{1 + (2.4 + 1.5v_2 + \cot^2\theta) \left(\frac{t_{sub}}{l_{sub}}\right)^2} E_s$	$E_{i\ sub}^* = 1.15 \frac{t_{sup}}{l_{sup}} E_{i\ sub}^*$

3.4 Results

Preliminary models were found to reproduce the patterns seen in established literature very well, for instance the relationship between the rib aspect ratio and elastic modulus. The FE models are accurate for aspect ratios greater than 10 to within 5% of established results [Gibson and Ashby 1997].

3.4.1 Hierarchical Length Ratio

The results investigating the study on HLR in hexagonal honeycombs are summarised in Figure 3.18, which shows the Young's modulus of a hierarchical honeycomb versus the relative length of the sub-structure cell. The Young's modulus is normalised to the modulus of a conventional hexagonal honeycomb of the exact same density but first order hierarchy. It is clear that none of the hierarchical honeycombs are as stiff as the first order conventional honeycomb, in contrast to previous studies [Lakes 1993, Fan 2008, and Kooistra 2007].

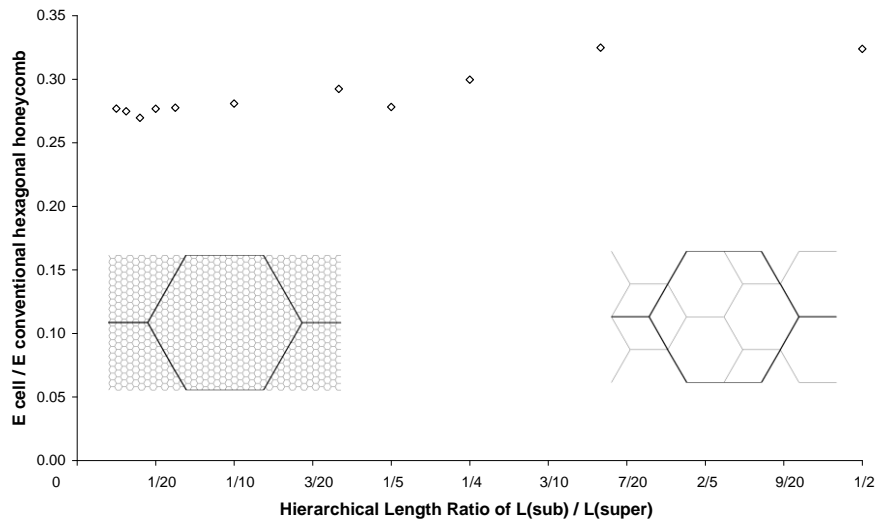


Figure 3.18: The elastic modulus for a hierarchical hexagonal honeycomb normalized to a conventional hexagonal honeycomb of equivalent mass is plotted against the HLR shown.

In contrast to the data for hexagonal honeycombs the triangular based honeycombs are almost unaffected by the relative scale of the sub-structure, as seen in Figure 3.19. Of note is that all of the triangular hierarchical honeycombs were greater than 95% of the elastic modulus of the conventional triangular honeycomb.

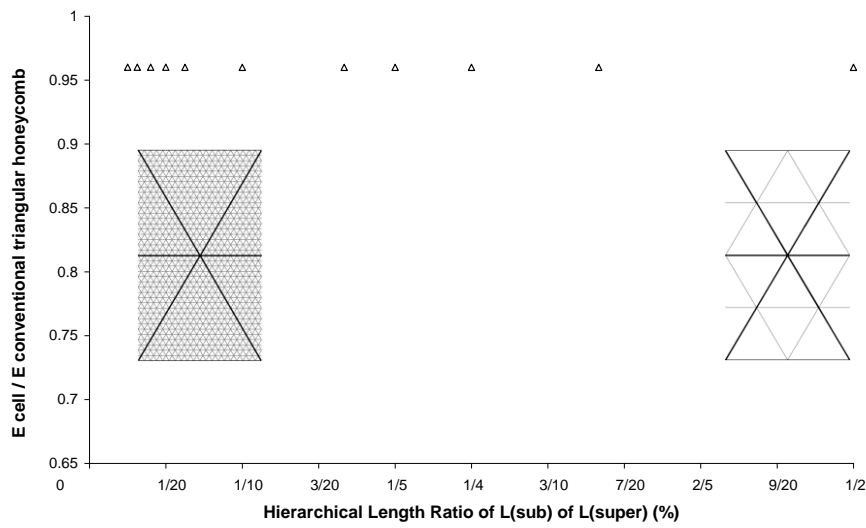


Figure 3.19: The elastic modulus for a hierarchical equilateral triangle honeycomb normalized to a conventional triangular honeycomb of equivalent mass against the HLR.

3.4.2 Co-ordination number

The effects of combining cells of similar and dissimilar coordination number are shown in Figure 3.20. These results are a little more complex but show that, regardless of the super-structure's coordination, stiffness is highest with sub-structures of 4 co-ordination, followed by 6 co-ordination, followed by 3 co-ordination. Honeycombs with 3 coordination cells in either the sub or super-structure tend to have a lower Young's modulus. Seemingly poorer performers such as the 6-6 and 3-3 honeycombs may have benefits in terms of isotropy if this is desirable for a particular application, compared to the other anisotropic honeycombs.

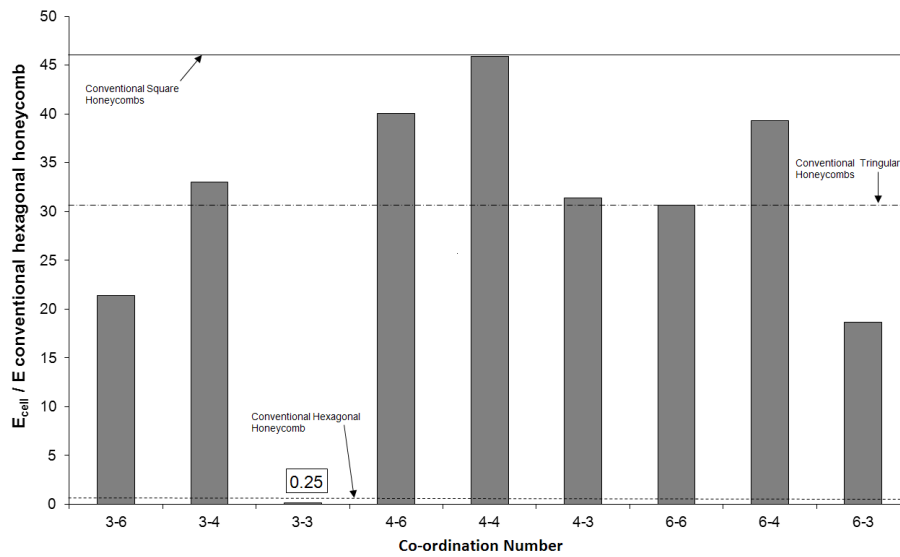


Figure 3.20: Elastic modulus of unit cells normalised to a conventional hexagonal honeycomb of equivalent mass, against the cell co-ordination numbers. The coordination number of a triangle is 6, a square is 4 and a hexagon is 3. It also shows the normalised Young’s modulus for conventional hexagonal, triangular and square honeycombs.

3.4.3 Mass Distribution

The effect of distributing a proportion of mass between the sub and super-structure is reported in Figure 3.21. The effect is much more pronounced in the 3-3 honeycomb than the 6-6. As expected the 6-6 and 3-3 honeycomb with a mass distribution of 100% has a similar elastic modulus to a similar density, coarser, zero order honeycomb, i.e. the honeycomb with mass distribution of 0.0%. This agrees with the literature [Gibson & Ashby 1982, Evans 1991, and Masters & Evans 1996].

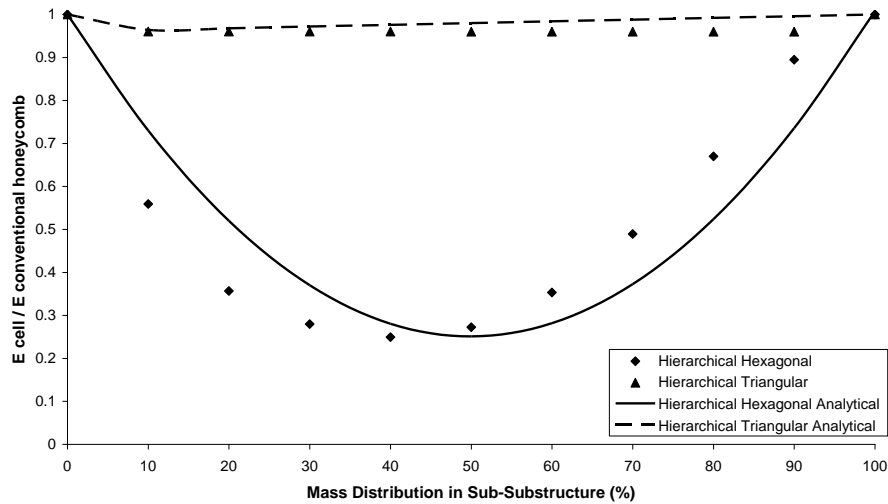


Figure 3.21: Young's modulus normalised to a conventional hexagonal honeycomb of equivalent mass against the mass distribution within the sub-structure.

3.4.4 Functional Grading

Distributing the mass non-uniformly by functional grading the honeycombs, and importantly the proportion of mass between the sub and super-structure, has marked effects upon the elastic modulus of the hierarchical honeycombs, see Figure 3.22. This figure shows for a 3-3 honeycomb that the stiffness is very sensitive to the distance the sub-structure extends outwards from the super-structure rib. Where more than 0.75 of the mass is placed in the sub-structure the honeycomb elastic modulus can exceed the elastic modulus of an equivalent first order honeycomb by up to 1.5, if the mass distribution is optimised. This pattern is almost reversed completely for the 6-6 honeycombs, see Figure 3.23, with the stiffest honeycombs being those with mass evenly distributed away from the super-structure and approaching a conventional triangular honeycomb. The geometry of the 3-3 and 6-6 honeycombs determines they will be isotropic in-plane.

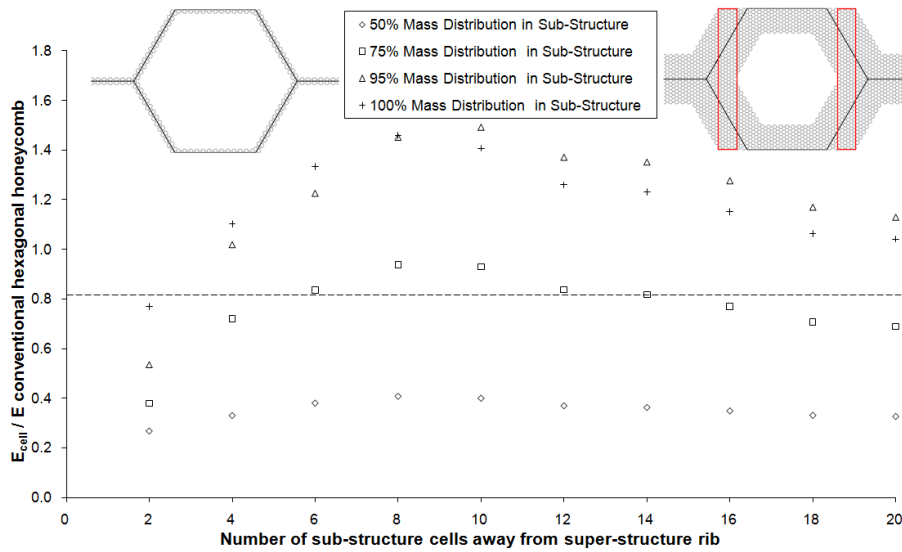


Figure 3.22: The elastic modulus normalised to a conventional hexagonal honeycomb of equivalent mass for hierarchical hexagonal structures with multiple mass distributions against the effective aspect ratio of the super-structure (considering the additional sub-structure thickness). The illustration shows columns of contiguous cells.

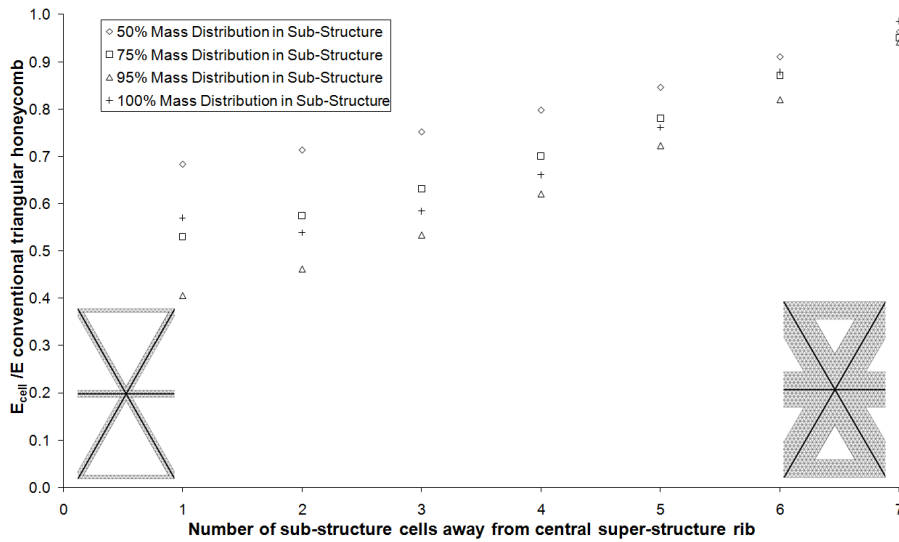


Figure 3.23: The elastic modulus normalised against a conventional triangular honeycomb of equivalent mass for hierarchical equilateral triangular structures for multiple mass distributions against the aspect ratio of the super-structure (considering the additional sub-structure thickness).

3.4.5 Functional Grading and Co-ordination Number HLR

The results of changing the HLR for a functionally graded hierarchical honeycomb where 100% of the mass is with the sub-structure was investigated the results show that varying HLR affects in the in-plane Young's modulus E_I^* . As the number of cells across the super-cell rib increases from low values up to approximately 8, see Figure 3.24 Figure 3.25 Figure 3.26 Figure 3.27 where E_I^* is plotted vs the number of sub-cell rows across the super-structure rib. The in plane modulus E_I^* is normalised to the Young's modulus of a conventional honeycomb of the same relative density. (Note that the analytical model ignores the discrete nature of the sub-structure and so results are not shown here). The HLR λ appears to be unimportant, but the numbers of sub-cells spanning the super-structure see Figure 3.24, Figure 3.25, Figure 3.26 and Figure 3.27. Note, that for $l/t = 1.16$ Figure 3.24 there is a decrease in the substructure's aspect ratio when the number of sub-cells spanning the super-structure is 1 (because the number of ribs must be integral). This results in an anomalously high stiffness.

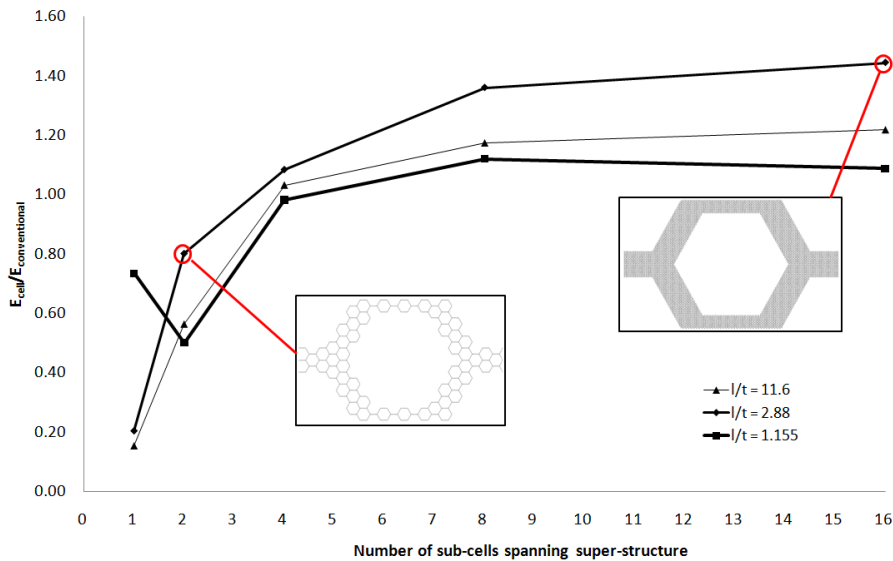


Figure 3.24: The FE predicted Young's modulus of a hexagonal super-structure and a hexagonal sub-structure HHs (normalised with respect to a conventional hexagonal honeycomb of the same relative density) vs the number of sub-cells spanning the super-structure.

The result of changing the HLR for a functionally graded hierarchical honeycomb where 100% of the mass is with the sub-structure has been investigated for a hexagonal

super-structure and a triangular sub-structure in Figure 3.25 the results show a plateau in the in-plane Young's modulus E_I^* when the number of cells across the super-cell reaches approximately 8.

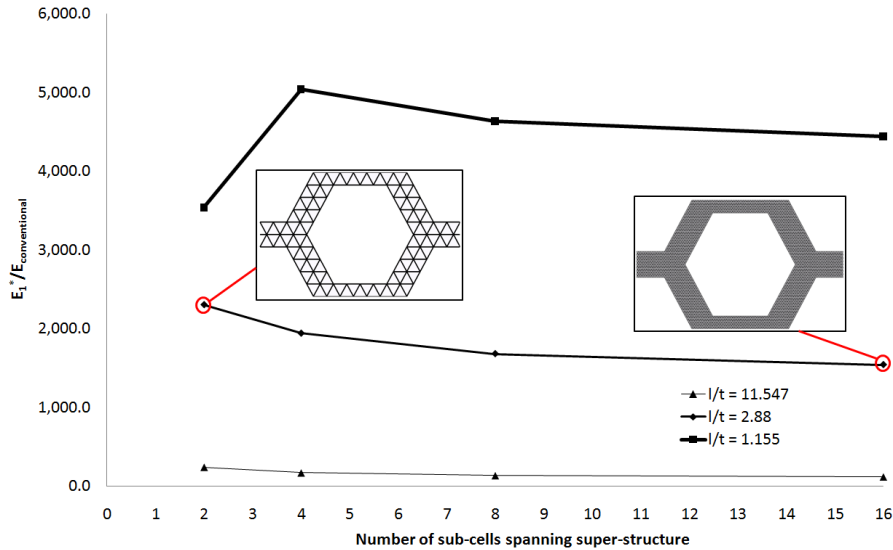


Figure 3.25: The FE predicted Young's modulus of a hexagonal super-structure and a triangular sub-structure HCs (normalised with respect to a conventional hexagonal honeycomb of the same relative density) vs the number of sub-cells spanning the super-structure.

The result of changing the HLR for a functionally graded hierarchical honeycomb where 100% of the mass is with the sub-structure has been investigated for a triangular super-structure and a triangular sub-structure. Figure 3.26 shows a plateau in the in-plane Young's modulus E_I^* when the number of cells across the super-cell reaches approximately 8.

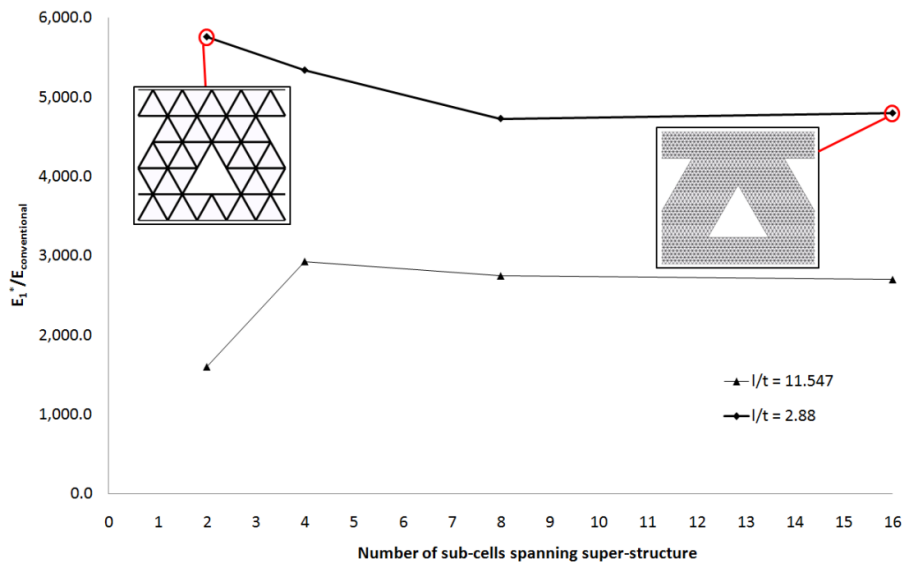


Figure 3.26: The FE predicted Young's modulus of a triangular super-structure and a triangular sub-structure hierarchal honeycomb (normalised with respect to a conventional hexagonal honeycomb of the same relative density) vs the number of sub-cells spanning the super-structure.

The result of changing the HLR for a functionally graded hierarchical honeycomb where 100% of the mass is with the sub-structure was investigated for a triangular super-structure and a hexagonal sub-structure. Figure 3.27 shows a plateau in the in-plane Young's modulus E_1^* as the number of cells across the super-cell reaches approximately 8.

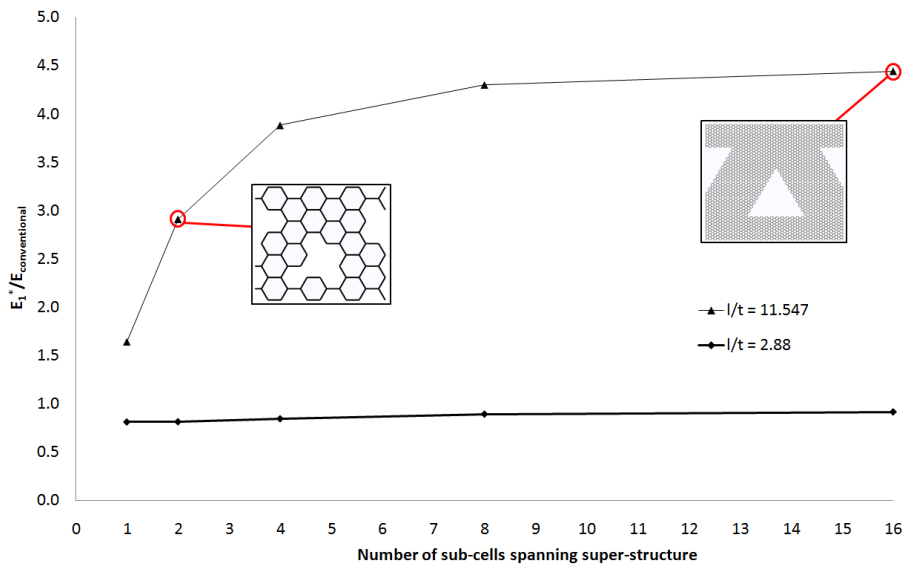


Figure 3.27: The FE predicted Young's modulus of a triangular super-structure and a hexagonal sub-structure HHs (normalised with respect to a conventional hexagonal honeycomb of the same relative density) vs the number of sub-cells spanning the super-structure.

3.4.6 Functional Grading and Co-ordination Number, Change in Aspect Ratio

The Young's modulus is plotted against the super-structure aspect ratio for hierarchical honeycombs with multiple co-ordination numbers of (6-6), (3-6), (6-6) and (6-3) in Figure 3.28, Figure 3.29, Figure 3.30 and Figure 3.31 respectively. FE results are compared to analytical predictions as previously established in Table 3.1. There is a complex relationship between these parameters, with several examples exceeding the stiffness of a conventional honeycomb of the same relative density.

The results for the in-plane Young's modulus for changing the super-structure thickness t_{sup} with a constant super-structure length l_{sup} for hierarchical honeycombs with hexagonal super-structure and a hexagonal sub-structure are shown in Figure 3.28. The analytical model predicts the drop in Young's modulus for high t_{sup} , but does not predict the decrease when t_{sup} is less than 3.

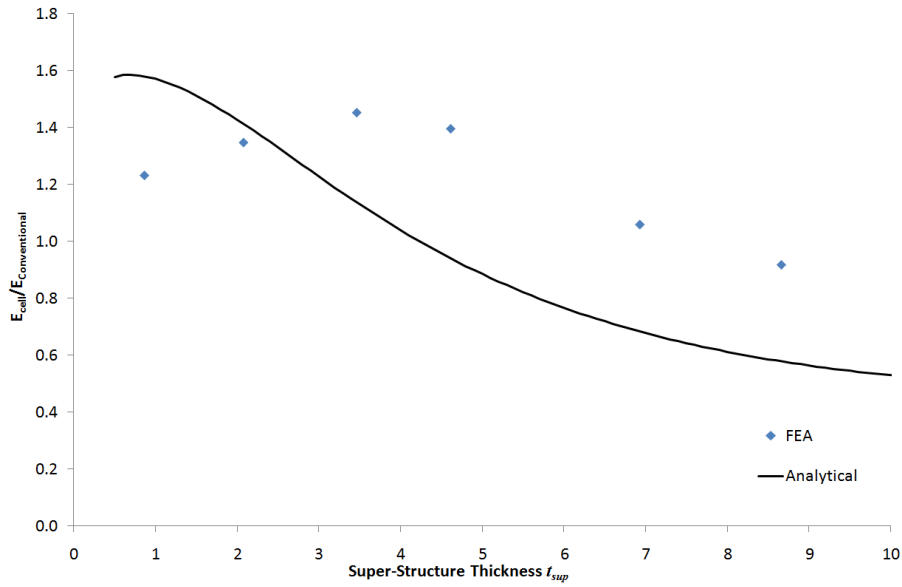


Figure 3.28: Young's moduli vs the super-cell rib thickness t_{sup} for FE models compared to analytical, for a hexagonal super-structure and hexagonal sub-structure (3-3) hierarchical honeycombs (normalised to that of a conventional honeycomb of the same relative density) and a relative density $\rho_{rel}^* = 0.00577$, when $l_{sup} = 10$.

The results for the in-plane Young's modulus for changing the super-structure thickness t_{sup} with a constant super-structure length l_{sup} for hierarchical honeycombs with hexagonal super-structure and a triangular sub-structure are shown in Figure 3.29 the analytical predicts the increase in Young's modulus as t_{sup} , increase but underestimates the modulus for high t_{sup} .

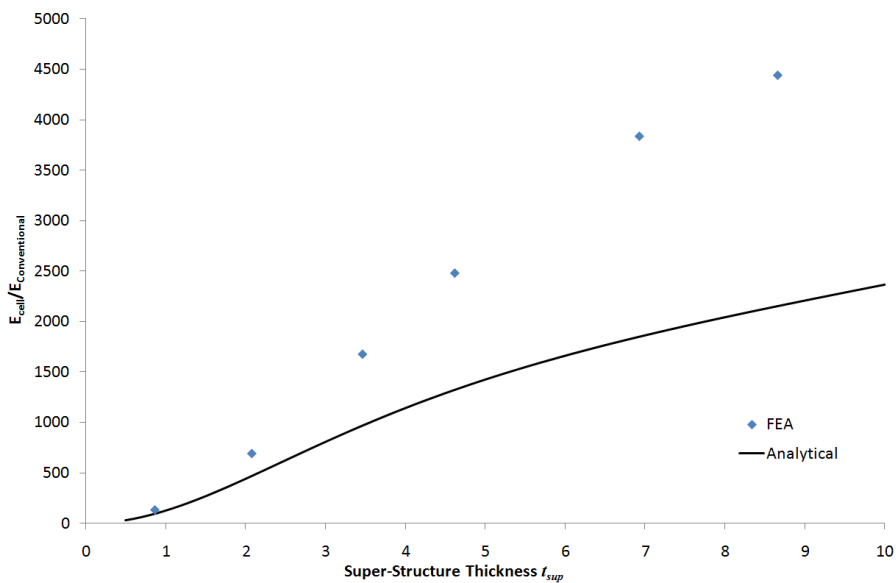


Figure 3.29: Young's moduli vs the super-cell rib thickness t_{sup} for FE models compared to analytical, for a hexagonal super-structure and triangular sub-structure (3-6) hierarchical honeycombs (normalised to that of a conventional honeycomb of the same relative density) and a relative density $\rho_{rel}^* = 0.00577$, when $l_{sup} = 10$.

The results for the in-plane Young's modulus for changing the super-structure thickness t_{sup} with a constant super-structure length l_{sup} for hierarchical honeycombs with triangular super-structure and a triangular sub-structure are shown in Figure 3.30 the analytical predicts the increase in Young's modulus as t_{sup} , increase but underestimates the modulus for high t_{sup} .

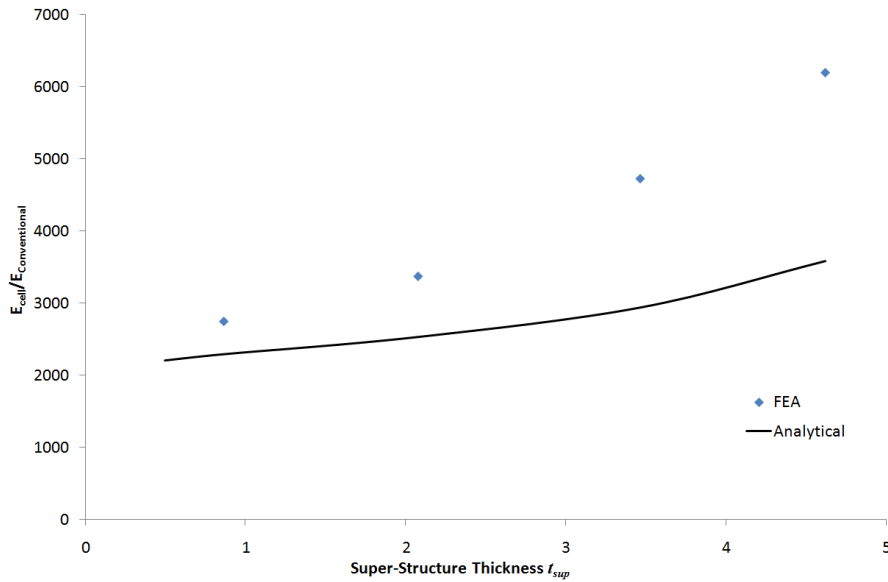


Figure 3.30: Young's moduli vs the super-cell rib thickness t_{sup} for FE models compared to analytical, for a triangular super-structure and triangular sub-structure (6-6) hierarchical honeycombs (normalised to that of a conventional honeycomb of the same relative density) and a relative density $\rho_{rel}^* = 0.00577$, when $l_{sup} = 10$.

The results for the in-plane Young's modulus for changing the super-structure thickness t_{sup} with a constant super-structure length l_{sup} for hierarchical honeycombs with triangular super-structure and a hexagonal sub-structure is shown in Figure 3.31 the analytical accurately predicts the decay in Young's modulus as t_{sup} , increase.

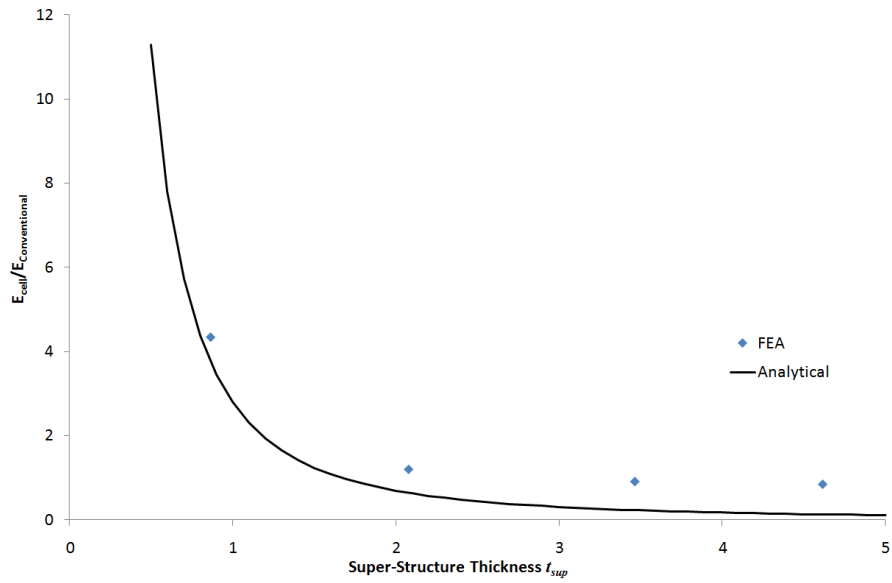


Figure 3.31: Young's moduli vs the super-cell rib thickness t_{sup} for FE models compared to analytical, for a triangular super-structure and hexagonal sub-structure (6-3) hierarchical honeycombs (normalised to that of a conventional honeycomb of the same relative density) and a relative density $\rho_{rel}^* = 0.00577$, when $l_{sup} = 10$.

3.5 Discussion

3.5.1 Hierarchical Length Ratio and Mass Distribution

The most apparent feature of the results for both the hexagonal and triangular honeycombs, Figure 3.18 and Figure 3.19, is the reduction in elastic modulus caused by the distribution of mass from the super-structure to the sub-structure. Predictably the effect is much more marked in the hexagonal honeycomb than the triangular. Since deformation in the hexagonal super-structure unit cell is flexure dominated. Halving its mass and therefore rib thickness would be expected to reduce the flexural elastic modulus of the hexagonal honeycomb ribs, and therefore the cell, by a factor of 8, (the second moment of a beam is dependent upon t_{sup}^3). A similar halving of the mass and thickness t_{sup} in the triangular cell, which deforms primarily in tension, would be expected to reduce the elastic modulus of the cell by a factor of two, since the sectional area is dependent on t_{sup} . Super-structures in which the mass has been halved, by themselves would have a relative elastic modulus of 12.5% in flexure and 50% in compression. Sub-structure honeycombs of similar mass density, geometry and aspect ratio as their super-structure should have similar elastic modulus Gibson and Ashby (1997). Treating the sub and super-structures as phases in a composite and calculating their moduli in isolation via the Gibson and Ashby relations see Equation 3-5 and Equation 3-6, it is possible to predict the in-plane Young's modulus. Doing so would suggest the second order hexagonal honeycomb would have 25% of the elastic modulus of the first order version, and similarly the second order triangular honeycomb would have 100% of the elastic modulus of the first order triangular honeycomb. This explains well the results seen in Figure 3.18, Figure 3.19 and Figure 3.21.

3.5.2 Co-ordination number

The results presented in Figure 3.20 show the effects of changing the hierarchical co-ordination number. Since triangular and square unit cells are inherently stiffer on-axis than hexagonal geometric cells, it is perhaps unsurprising that adding sub-structures formed of either stiffened hexagonal super-structures. The 3-3 honeycomb was the least stiff of all geometries considered, since it is entirely flexure dominated and, as noted previously, is at its minimum elastic modulus with a mass ratio of 0.5. Square cells perform favourably in comparison to other geometries in terms of on-axis elastic

modulus. However, they have a trade off in terms of anisotropy, being markedly less stiff off axis. The deformation mode changes from stretching/compression on-axis to flexure off axis Gibson & Ashby (1997). The issue of in-plane isotropy in these honeycombs has not been examined in detail here, but it is noteworthy that that regular hexagonal and triangular unit cells (the 3-3, 3-6, 6-6 and 6-3 honeycombs) exhibit in-plane isotropy by dint of their geometric symmetry Gibson & Ashby (1997). It is clear that the 4-4 honeycomb, and most likely any combination involving a 4 coordinate cell, will exhibit anisotropy.

3.5.3 Functional Grading

There are two relationships in the data for functionally graded honeycombs, Figure 3.22 and Figure 3.23, that are worthy of note. The first is that for all mass fractions there is a dependency of the elastic modulus on the distance the sub-structure extends away from the super-structure, reaching a maximum for 3-3 honeycombs when the number of cells away from the central rib is 4 or 5. The elastic modulus of these honeycombs is affected by two phenomena i) the decreasing aspect ratio of the sub-structure cell ribs with increasing spread away from the super-structure rib, and ii) the width of contiguous sub-structure in axial tension/compression (the region bordered by the red box in Figure 3.22). The former arises because the elastic modulus of a beam in flexure is markedly dependent upon the $(t/l)^3$ term [Gibson and Ashby 1997], and the latter because regions of sub-structure forming contiguous on-axis columns are effectively loaded in tension/compression rather than shear or flexure. Summation of these two phenomena results in the curve seen in Figure 3.22. The second relationship of note in the functionally graded honeycombs is the relationship between the mass fraction distributed into the sub-structure and the elastic modulus of the honeycomb, most notably in the hexagonal honeycombs, see Figure 3.22. This is a reflection of the trend seen in Figure 3.21 where uneven distribution of mass between sub and super-structures is preferential to an even distribution.

The most stiff second order hierarchical sub-structures are those in which most, if not all, of the mass is concentrated into the sub-structure, and in which the sub-structure itself is graded, i.e. does not occupy the entire unit cell volume. In these cases, a new unit cell is effectively formed from the finer sub-structure honeycomb. These findings

have implications for the manufacture and use of hierarchical honeycombs in applications, most notably that implementation of a second order hierarchy must be done carefully. These results concur with that of (Fan *et al* 2008).

3.5.4 Functional Grading and Co-ordination Number HLR

A critical number of sub-cells can be defined as that at which the sub-structure behaves effectively as a continuum in the super-structure, lying between 4 and 8 in Figure 3.24. This can be explained by the geometry of the structure where the aspect ratio α_{sub} of the sub-structure converges between 4 and 8 cells (i.e. the change in α_{sub} is greater between 1 and 2 sub-cells spanning the super-structure than change in α_{sub} between 8 and 16 spanning the super-structure). The increased Young's modulus for low super-structure aspect ratio functionally graded hierarchical honeycombs with only 1 sub-cell across the super-structure arises because these structures have few redundant beams meaning all load carrying beams are low aspect ratio α_{sub} . This explanation is also true for other hierarchical co-ordination numbers shown in Figure 3.25, Figure 3.26 and Figure 3.27.

3.5.5 Functional Grading and Co-ordination Number, Change in Aspect Ratio

There is a complex relationship between the co-ordination number and the super-structure aspect ratio, with several examples exceeding the stiffness of the same relative density conventional honeycomb.

The results in Figure 3.28 show a trade-off between the flexural stiffness (EI product) of the hexagonal sub and super-structure as the cell's stiffness is dominated by a $(t/l)^3$ term which means that changes in rib thickness have profound effects upon elastic properties. The analytical and FE models agree in terms of the pattern of the change in in-plane Young's modulus, if not in absolute values. If the analytical was extended to a super-structure thickness $t_{sup} = 0$ then the Young's modulus would also approach 0. However at such low thicknesses the super-structure ribs are so dense they are better described as solid material described by the constituent material properties not the material properties of the sub-structure. The results in Figure 3.29 for a hexagonal super-structure and a triangular sub-structure show an increase in Young's modulus as t_{sup} increases. This is due to the super-structure being dominated by a $(t/l)^3$ term, which is not counteracted by a subsequent decrease in the sub-structure thickness t_{sub} , as the sub-structure properties are dominated by a (t/l) term. The results in Figure 3.30 for a

triangular super-structure and a triangular sub-structure show an increase in Young's modulus as t_{sup} increases due to changes in the geometry in the sub-structure where more mass is in direct compression the results tend to an optimum result of a conventional triangular honeycomb. The results in Figure 3.31 for a triangular super-structure and a hexagonal sub-structure show the opposite of what is happening in Figure 3.28. It shows an exponential increase in Young's modulus as t_{sup} decrease. This is due to the super-structure properties being dominated by a (t/l) term that is not counteracted by a subsequent increase in the sub-structure thickness t_{sub} which determines the sub-structure properties that are dominated by a $(t/l)^3$ term.

A probable reason for the discrepancies between the numerical and analytical results is that the analytical model fails to predict local stress concentrations that occur in sub-structure cells close to super-structure nodes. Another reason that also explains the discrepancies is that when sub-structure ribs are removed (compared to a conventional array) to allow for the super-structure geometry, the local deformation mechanism may change. This also explains the larger discrepancies in co-ordination numbers that have a triangular sub-structures that would otherwise be stretch dominated, but are bending dominated due to the change in local connectivity. This would also explain the increased deviation at greater super-structure thicknesses as the analytical underestimates the in-plane Young's modulus. There is also the fact that even though an effort has been made to establish when a continuum can be assumed it is still an assumption that is made in the analytical predictions.

The work in this chapter has highlighted the implications of introducing hierarch into honeycombs and the variables that determine the response of a hierarchical unit cell that can be used to describe a continuum. It has also recognised the difference between the stretch dominated triangular honeycomb and the bending dominated hexagonal honeycomb. The work has shown at what length scale or rather what point the sub-structure can be described as a continuum to the super-structure a question proposed in (Lakes 1993). This has really implications when considering the feasibility of manufacturing hierarchical materials and size scale involved along with hierarchical order numbers considered. The work combining co-ordination numbers and subsequently stretch and bending dominated structures (Deshpande 2001) has also

shown the possibility of combine the two to tailor material properties. This has been shown for the elastic regime but could hold potential benefits in the non-linear plastic regime. It has also been shown that is possible to increase the in-plane Young's modulus of a conventional hexagonal honeycomb via the introduction of hierarchy and subsequent optimisation by up to 175% which could result is a decrease in the density of the honeycomb whilst maintaining in-plane stiffness, which is often desirable in the transport and construction industries.

3.6 Conclusions

The aim of this work was to understand how the in-plane elastic properties of honeycombs were affected by hierarchy, and then to find if elastic modulus could be maintained or improved on an equal density basis. It is clear that honeycombs are sensitive to hierarchical sub-structures, particularly the fraction of mass shared between the super- and sub-structures. The introduction of an additional level of hierarchy without reducing performance is difficult. However it is possible by functional grading such hierarchies to improve the in-plane modulus, in this case by up to 175% compared to a similar density first order hierarchy (conventional) hexagonal honeycomb. This was achieved by using a hexagonal sub and super-structure alone and orders of magnitude greater with the introduction of triangular structures. An exhaustive exploration of functional grading of hierarchy was not within the remit of this work but it seems to hold potential for further improvement of performance.

The transition in the super-cell rib from behaviour of a discrete structure to that of a continuum was established as being a function of the number of sub-cells spanning the super-structure rather than a function of HLR λ . The transition number of cells was found to be approximately 8. This finding was used in all subsequent models involving hierarchy in this nature. This result helps to indicate the feasibility of hierarchy in honeycombs, by which the advantages of hierarchy are achievable over realistic length scales.

Chapter 4. In-Plane Change in The Sub-Structure Poisson's Ratio

4.1 Introduction

As the previous chapter highlighted it is possible to insert an additional level of hierarchy into a conventional 1st order honeycomb to create a 2nd order hierarchical honeycomb that can result in deleterious effects on the global material properties specifically the in-plane Young's modulus, it was however possible to exceed the in-plane Young's modulus of a conventional honeycomb on an equal density basis by careful optimisation. The idea of inserting an additional level of hierarchy into a honeycomb has been further developed to include a sub-structure of a different Poisson's ratio to that of the sub-structure by means of introducing re-entrant honeycombs and changing the internal angle θ_{sub} .

The term Auxetic derived from the Greek *auxetos* meaning "that which may be increased" coined by (Evans *et al* 1991) is used to describe a class of material that contracts normal to a compressive force and expands normal to a tensional force, meaning the material has a negative Poisson's ratio as illustrated in Figure 4.1.

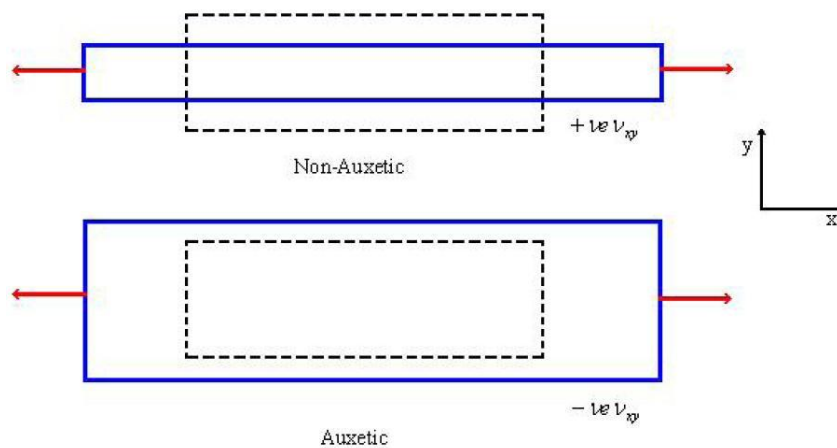


Figure 4.1: Comparison of a auxetic and a conventional material under tension

Iron pyrite is one of the earliest recorded materials to experience a negative Poisson's ratio of -0.14285 in (Love 1892). Single crystal iron pyrite is naturally occurring, but the first person to manufacture a negative Poisson's ratio was (Lakes 1987) who made a

re-entrant foam structure to create a negative Poisson's Ratio of -0.7. Honeycomb cells with various values of Poisson's ratios, including negative values, are well known (Lakes 1987, Lakes 1993 (2) Evans 1991, Masters & Evans 1996, Prall & Lakes 1996, Evans & Alderson 2000, Miller *et al* 2009 & 2010 and Taylor *et al* 2011).

It was thought that if hierarchy was introduced as in the previous chapter where the sub-structure filled all the void of the super-structure and each level of hierarchy had opposing Poisson's ratio, that there would be an increase in the in-plane Young's modulus. Specifically the super-structure of the hierarchical honeycomb is hexagonal where $l = h$ and $\theta_{sup} = 30^\circ$ with a Positive Poisson's Ratio (PPR) $\nu_{sup} = 1$ and the sub-structure has a Negative Poisson's Ratio (NPR) by means of a re-entrant hexagonal honeycomb when $\theta_{sub} < 0^\circ$ as shown in Figure 4.2. It can be seen that for an axial compression in the X_1 direction there is a transverse displacement in the X_2 direction determined by the Poisson's ratio of the structure as shown by the red and black arrows representing the sub and super-structure respectively. It can also be seen that the sub and super structure displacements oppose each other in the transverse direction, which could have an effect on the deformation mechanism.

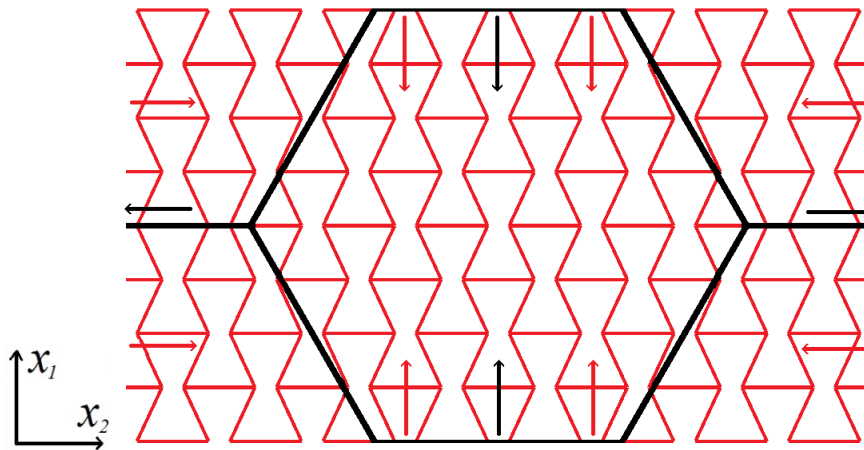


Figure 4.2: A hierarchical honeycomb with a NPR sub-structure. The super-structure is shown in red along with arrows representing the effects of in-plane compression. The sub-structure is shown in black with arrows showing the direction of displacement due to in-plane compression.

Honeycomb cells with various values of Poisson's ratios, including negative values, are well known (Lakes 1987, Lakes 1993 (2) Evans 1991, Masters & Evans 1996, Prall & Lakes 1996, Evans & Alderson 2000, Miller *et al* 2009 & 2010 and Taylor *et al* 2011).

4.2 Method

The following section discusses the implementation of NPR sub-structures in hierarchical honeycombs. It was a very similar process to that described in the previous chapter. Initially investigated was the effect of the HLR followed by the effect of changes in θ_{sub} then an investigation into the anisotropic behaviour of NPR sub-structure hierarchical honeycombs and changes in the h_{sub}/l_{sub} ratio. The section describes the method that each parameter was investigated by means of computational modelling.

4.2.1 Hierarchical Length Ratio

Firstly the effect of introducing a NPR sub-structure was investigated in a similar manner to introducing hierarchy as in the previous chapter by exploring if the HLR between the sub and super-structure has an effect (Lakes 1993 (1)). This was investigated by decreasing the length l_{sub} and h_{sub} and changing t_{sub} to ensure constant relative density. Unfortunately it was not as easy to introduce a NPR sub-structure as a conventional hexagonal or triangular structure as it was necessary to have an integer number of sub-cells within the unit cell for it to remain repeatable. This was difficult as not only was the size of the sub-cells different to the super-cell, but also the shape of the sub-cell due to the nature of re-entrant honeycombs. This was overcome by determining the length l_{sub} by the angle θ_{sub} and number of cells in the X_1 direction and then allowing $l_{sub} \neq h_{sub}$ and determining h_{sub} by the length l_{sub} , angle θ_{sub} and number of cells in the X_2 direction. The effect of decreasing the HLR for hierarchical honeycombs with a NPR sub-structure was investigated for 3 re-entrant honeycombs when $\theta_{sub} = -5$, $\theta_{sub} = -10$ and $\theta_{sub} = -25$ for an arbitrary mass distribution between the sub and super-structure of 0.5 as shown in Figure 4.3, Figure 4.4 and Figure 4.5.

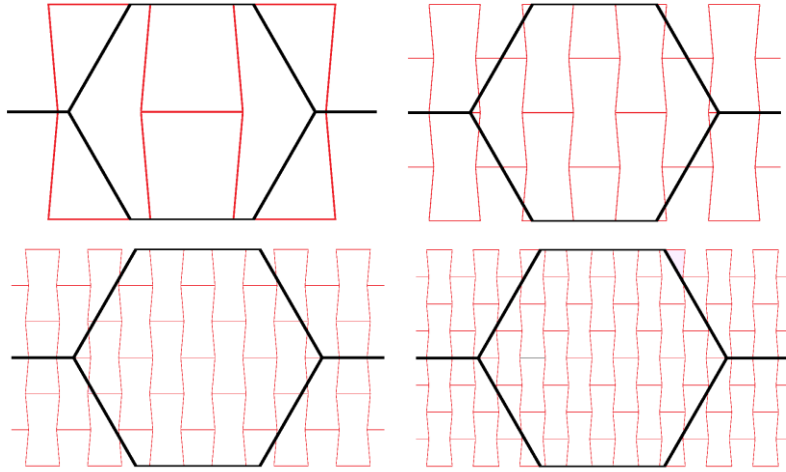


Figure 4.3: Shows how the HLR of the hierarchical honeycomb with a NPR substructure changes when $\theta_{sub} = -5$.

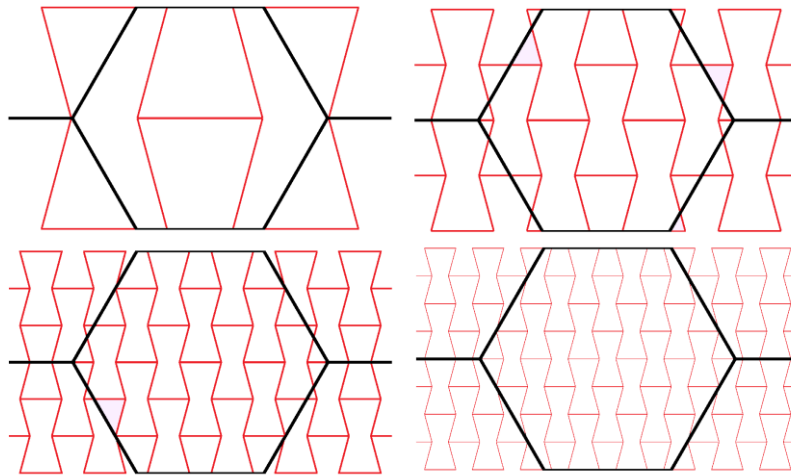


Figure 4.4: Shows how the HLR of the hierarchical honeycomb with a NPR substructure changes when $\theta_{sub} = -15$.

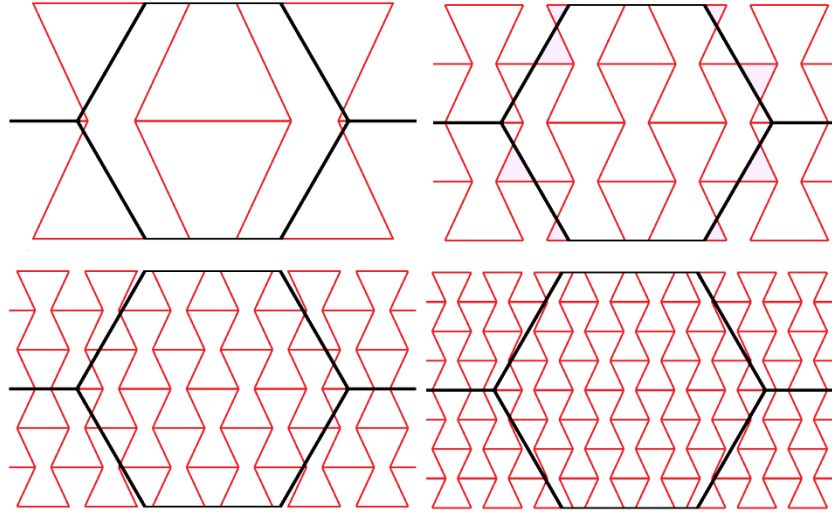


Figure 4.5: Shows how the HLR of the hierarchical honeycomb with a NPR sub-structure changes when $\theta_{sub} = -25$.

4.2.2 Investigating Change in θ_{sub}

The effect of the changing the Poisson's ratio of the sub-structure was explored by creating a number of models of a 3-3 honeycomb, where the internal angle θ_{sub} of the sub-structure was varied from -27.5° to $+30^\circ$ (at an angle of -30° the inverted ribs touch when $l_{sub}=h_{sub}$) with 2.5° intervals. A sub-structure with negative values of θ_{sub} has a NPR (Gibson and Ashby 1982, Masters and Evans 1996). Models were established similarly to those in the previous section, where the geometry of the super-structure was maintained when $l_{sup} = h_{sup} = 10$ and $t_{sup} = 0.25$ it was necessary to change l_{sub} and h_{sub} due to the change in θ_{sub} to ensure an integer number of sub-cells spanned the super-cell in the X_1 and X_2 axis. Since the density of the honeycomb increases as θ_{sub} decreases, it was also necessary to alter t_{sub} to ensure constant relative density for mass distributions between the sub and super-structure of 50% and 75% in the sub-structure (Taylor *et al* 2011). All the hierarchical honeycombs with NPR sub-structures investigated have an equivalent relative density to a conventional honeycomb of $l = h = 10$ and $t = 0.5$ relative density $\rho_{rel}^* = 0.0577$. The anisotropy of including a re-entrant sub-structure was determined by calculating the Young's modulus in the X_1 and X_2 directions along with the shear modulus and Poisson's ratio of hierarchical honeycombs and using tensor rotations to determine the off axis properties. The change in Young's modulus was then plotted as a polar plot for off axis properties (Taylor *et al* 2011).

4.2.3 Investigating Change in h/l

The effect of changing the ratio of h_{sub}/l_{sub} was investigated by changing the number of sub-cells spanning the unit cell in the X_2 direction to the number of cells in the X_1 direction. Increasing the h_{sub}/l_{sub} ratio would have the effect of increasing the thickness of re-entrant beams that are undergoing bending during shear and compression. It was thought that this change could decrease the extent of anisotropy present in hierarchical honeycombs with a re-entrant sub-structure. Polar plots were produced for a sub-structures with internal angles of $\theta_{sub} = -5^\circ$, $\theta_{sub} = -10^\circ$ and $\theta_{sub} = -30^\circ$ for mass distributions of 25% and 50% in the sub-structure, investigating h_{sub}/l_{sub} ratios of 1, 2 and 3 as shown in Figure 4.6, Figure 4.7 and Figure 4.8 when $\theta_{sub} = -10^\circ$. Ratios for h_{sub}/l_{sub} of 2 and 3 were investigated when $\theta_{sub} = -30^\circ$, $h/l = 1$ was not considered as re-entrant beams coincide forming a triangular sub-structure. Internal angles of $\theta_{sub} = -5^\circ$, $\theta_{sub} = -10^\circ$ and $\theta_{sub} = -30^\circ$ where chosen as $\theta_{sub} = -5^\circ$ and $\theta_{sub} = -10^\circ$ showed favourable responses with respect to in-plane Young's modulus and $\theta_{sub} = -30^\circ$ was an extreme value that performed poorly in comparison. Polar plots were created in a similar manner to those in the previous section by calculating the Young's modulus in the X_1 and X_2 directions along with the shear modulus and Poisson's ratio of hierarchical honeycombs and using tensor rotations to determine the off axis properties.

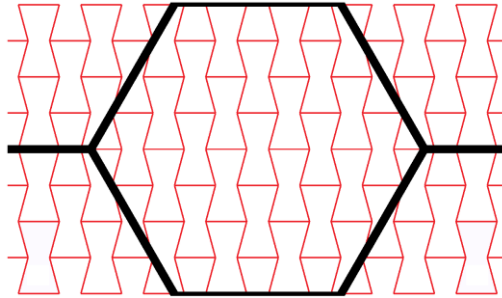


Figure 4.6: Shows a hierarchical honeycomb with a re-entrant sub-structure with an internal angle $\theta_{sub} = -10^\circ$ with an h/l ratio approximately equal to 1.

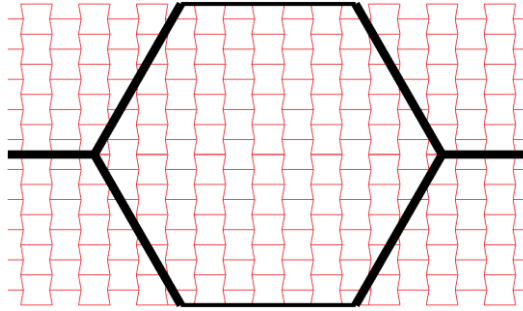


Figure 4.7: Shows a hierarchical honeycomb with a re-entrant sub-structure with an internal angle $\theta_{sub} = -10^\circ$ with an h/l ratio approximately equal to 2.

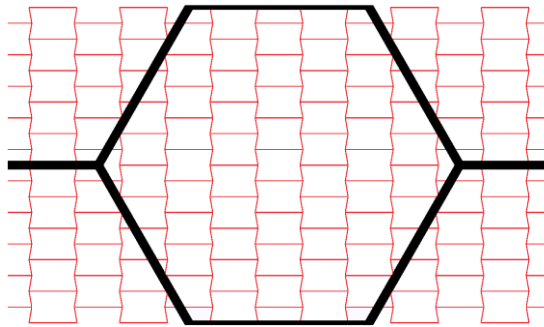


Figure 4.8: Shows a hierarchical honeycomb with a re-entrant sub-structure with an internal angle $\theta_{sub} = -10^\circ$ with an h/l ratio approximately equal to 3.

4.3 Analytical

It is possible to think of a hierarchical honeycomb as two constitutive parts made from the sub and super-structure for which the material properties are known (Gibson and Ashby 1982, Masters and Evans 1996) The in-plane Young's modulus of the sub and super-structure can be determined by using Equation 4-1 and Equation 4-2 respectively. It is then possible to use the Voigt rule of mixtures as in Equation 4-3 to determine the in-plane Young's modulus for the unit cell as done for the mass distribution section in the previous chapter. This approach assumes that the deformation behaviours are independent and purely bending dominated ignoring stretching and compression within the structure.

$$E_{1sub}^* = \left(\frac{t_{sub}}{l_{sub}}\right)^3 \frac{\cos\theta}{\left(\left(\frac{h_{sub}}{l_{sub}}\right) + \sin\theta\right) \sin^2\theta} \frac{1}{1 + (2.4 + 1.5\nu_s + \cot^2\theta) \left(\frac{t_{sub}}{l_{sub}}\right)^2} E_s$$

Equation 4-1

$$E_{1sup}^* = \left(\frac{t_{sup}}{l_{sup}}\right)^3 \frac{\cos\theta}{\left(\left(\frac{h_{sup}}{l_{sup}}\right) + \sin\theta\right) \sin^2\theta} \frac{1}{1 + (2.4 + 1.5\nu_s + \cot^2\theta) \left(\frac{t_{sup}}{l_{sup}}\right)^2} E_s$$

Equation 4-2

$$E_c = E_a f + E_b (1 - f)$$

Equation 4-3

Where E_c is the Young's modulus of the composite material E_a and E_b represent the Young's modulus of the constituent materials and f is a volume fraction.

It is known that the sub and super-structure are bending dominated independently as shown in Equation 4-1 and Equation 4-2 and described in (Gibson and Ashby 1982, Masters and Evans 1996). It is thought at certain opposing Poisson's ratios for instance a PPR super-structure and NPR sub-structure the rotations of the sub and super-structure due to the bending of ribs oppose each other negating bending. The ribs of the sub and super-structure can be considered as stretch dominated. It is possible to consider sub and super-structure ribs as columns within the honeycomb that are in

compression or tension to calculate an upper limit considering that ribs are purely stretch dominated.

In the results section it is shown that the in-plane Young's modulus of hierarchical honeycombs with a NPR sub-structure are independent of the hierarchical length ratio. It is therefore possible to consider the simplest hierarchical honeycomb where the HLR is approximately 1. To simplify the problem further a quarter cell can be examined which, excluding horizontal beams parallel to the X_2 axis, consists of two sub-structure ribs of length l_{sub} and thickness t_{sub} depending on the internal angle θ_{sub} and one super-structure rib of length t_{sup} and l_{sup} all thickness depend on the relative density of the cell and the mass distribution between the sub and super-structure. It is possible for given internal angles θ_{sub} , θ_{sub} , lengths l_{sub} , l_{sup} thickness t_{sub} , t_{sup} , and constituent material E_s to calculate an upper limit purely considering compression of ribs. A uniform displacement δx can then be applied to the top of the ribs in the X_1 axis with a zero displacement at the bottom. The axial displacement of the sub and super-structure ribs can be described as in Equation 4-4 and Equation 4-5 respectively.

$$\Delta l_{sub} = \delta x \cos \theta_{sub}$$

Equation 4-4

$$\Delta l_{sup} = \delta x \cos \theta_{sup}$$

Equation 4-5

The axial reaction force of each rib can then be calculated for the sub and super-structure ribs as in Equation 4-6 and Equation 4-7 respectively.

$$Q = E_s \frac{\delta x \cos \theta_{sub}}{l_{sub}} t_{sub} d$$

Equation 4-6

$$P = E_s \frac{\delta x \cos \theta_{sup}}{l_{sup}} t_{sup} d$$

Equation 4-7

The total X_1 reaction force can then be calculated using Equation 4-8.

$$F_{Total} = 2Q\cos\theta_{sub} + P\cos\theta_{sup}$$

Equation 4-8

The total cross sectional area of the quarter cell is calculated in Equation 4-9.

$$A_{Total} = (l_{sup}\sin\theta_{sup} + h_{sup})d$$

Equation 4-9

When $l_{sup} = h_{sup}$, $\theta_{sup} = 30^\circ$ and d can be considered as unit depth this can be written as in Equation 4-10.

$$A_{Total} = 1.5l_{sup}d$$

Equation 4-10

The result for the Young's modulus E_1^* for a hierarchical honeycomb with a NPR sub-structure is presented in Equation 4-11.

$$E_1^* = \frac{E_s \cos\theta_{sup}}{(\sin\theta_{sup} + 1)} \left(\frac{2 \cos^2\theta_{sub} t_{sub}}{l_{sub}} + \frac{\cos^2\theta_{sup} t_{sup}}{l_{sup}} \right)$$

Equation 4-11

This can be used as an upper limit for hierarchical honeycombs purely allowing for compression of ribs.

4.4 Results

4.4.1 Hierarchical Length Ratio

The results investigating the effect of the hierarchical length ratio in hierarchical hexagonal honeycombs with a NPR sub-structure are summarised in Figure 4.9. The figure presents the Young's modulus of a hierarchical honeycomb with NPR sub-structure normalised to a conventional hexagonal honeycomb of the exact same relative density but first order hierarchy against the HLR between the sub and super-structure. It is clear that the HLR of the hierarchical honeycombs has little if any effect on the in-plane Young's modulus of hierarchical hexagonal honeycombs when changing the sub structure Poisson's ratio. The results presented in Figure 4.9 also show that the introduction of hierarchy and changing the sub-structure Poisson's ratio has a great effect on the in-plane Young's modulus, increasing the modulus by a multiple of up to approximately 75 when $\theta_{sub} = -5^\circ$.

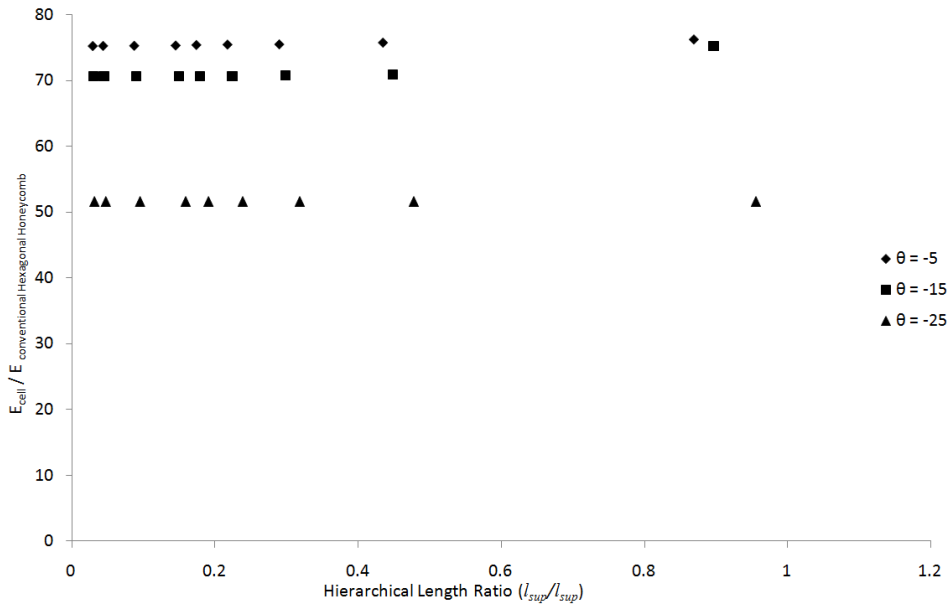


Figure 4.9: Young's modulus of a hierarchical honeycomb with NPR sub-structure normalised to a conventional hexagonal honeycomb of the exact same relative density against the HLR between the sub and super-structure for sub-structure angles $\theta_{sub} = -5^\circ$, $\theta_{sub} = -10^\circ$ and $\theta_{sub} = -25^\circ$.

4.4.2 Investigating Change in θ_{sub}

The internal angle of the sub-structure, and thus its Poisson's ratio, has a strong and complex relationship with the elastic modulus of the honeycomb, see Figure 4.10 and Figure 4.11, which shows the Young's modulus normalised to that of a conventional hexagonal honeycomb against the internal angle of the sub-structure for 50% and 75% mass distributions in the sub-structure respectively. Also shown is the analytical results allowing for bending as a lower limit Equation 4-3 and stretching as an upper limit Equation 4-11. It can be seen that the bending dominated analytical result asymptotes when $\theta_{sub} = 0$, this is due to the sub-structure effectively forming a column which is not allowed for in the analytical (Gibson and Ashby 1982) at which point the stretch dominated analytical is representative to the mode of deformation. As could be expected from the analytical, the FEA shows that the on-axis elastic modulus is high when $\theta_{sub} = 0$, i.e. the sub-structure cell is rectangular, but is surprisingly higher when $\theta_{sub} = -10$ for a 50% mass distribution and $\theta_{sub} = -7.5$ for a 75% mass distribution, a result not seen before in first order honeycombs (Gibson and Ashby 1982, Masters & Evans 1996)

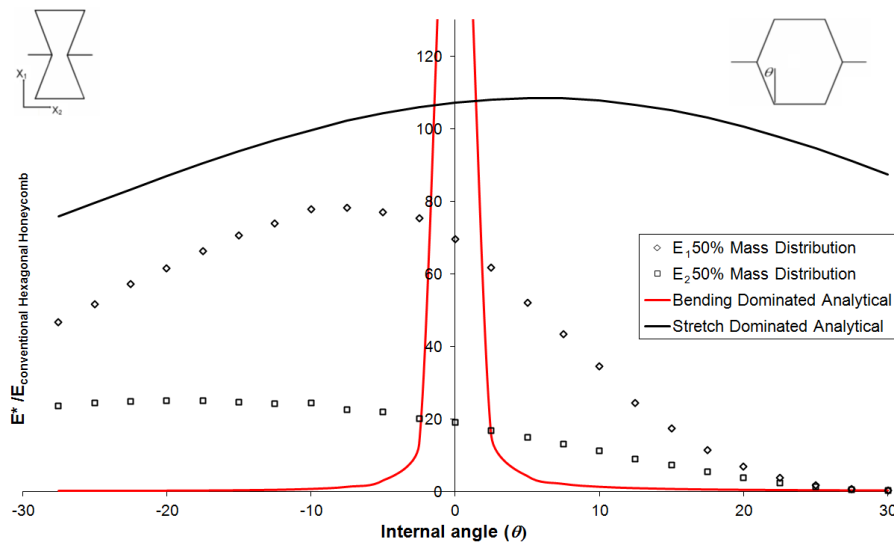


Figure 4.10: Young's modulus E_1 and E_2 (referring to the X_1 and X_2 axis) normalized to that of a conventional hexagonal honeycomb against the internal angle of the sub-structure. Also shown is the lower limit, bending dominated analytical proposed in Equation 4-3 along with the upper limit stretch dominated analytical proposed in Equation 4-11 for a mass distribution of 50% in the sub-structure. For all cases the super-structure internal angle $\theta_{sup} = 30^\circ$.

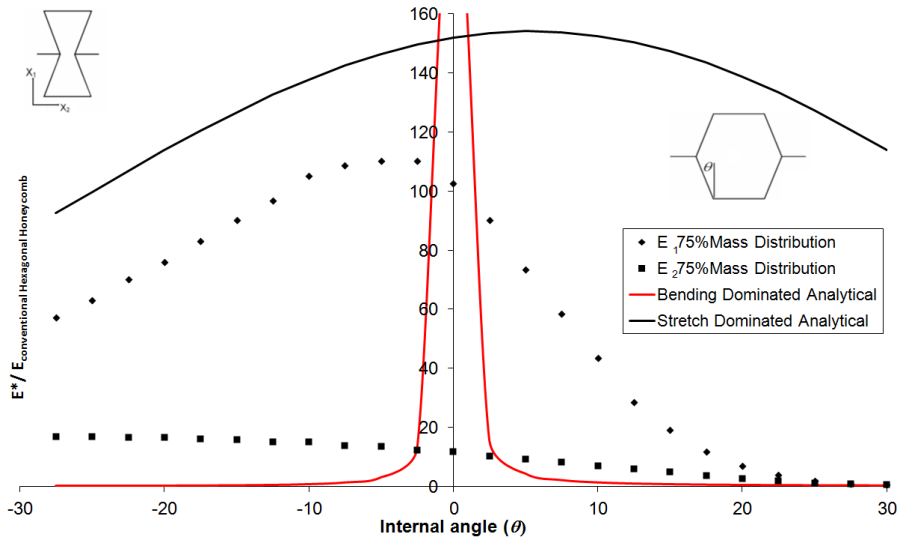


Figure 4.11: Young's modulus E_1 and E_2 (referring to the X_1 and X_2 axis) normalized to that of a conventional hexagonal honeycomb against the internal angle of the sub-structure. Also shown is the lower limit bending dominated analytical proposed in Equation 4-3 along with the upper limit stretch dominated analytical proposed in Equation 4-11 for a mass distribution of 75% in the sub-structure. For all cases the super-structure internal angle $\theta_{sup} = 30^\circ$.

The off-axis in-plane modulus is shown in Figure 4.12 for the hierarchical honeycombs plotted in Figure 4.10 and Figure 4.11 for mass distribution of 50% and 75% when the internal angle of the sub-structure $\theta_{sub} = -10$, which has a NPR sub-structure and a PPR super-structures. Polar plots were generated by determining the Young's modulus E_1 and E_2 along with the shear modulus G_{12} and G_{21} and the Poisson's ratio's ν_{12} and ν_{21} of the hierarchical honeycomb and using tensor rotations to calculate the off axis properties. It is clear that on-axis the modulus (the blue and red lines) can be many multiples of the conventional first order hierarchy honeycomb (the solid black line), but that this is reversed for most off-axis loading. Adjusting the mass distribution between super- and sub-structure eliminates some of this drop off in stiffness, but not all. It is worthy of note that the structure is fully anisotropic, since E_1 does not equal E_2 .

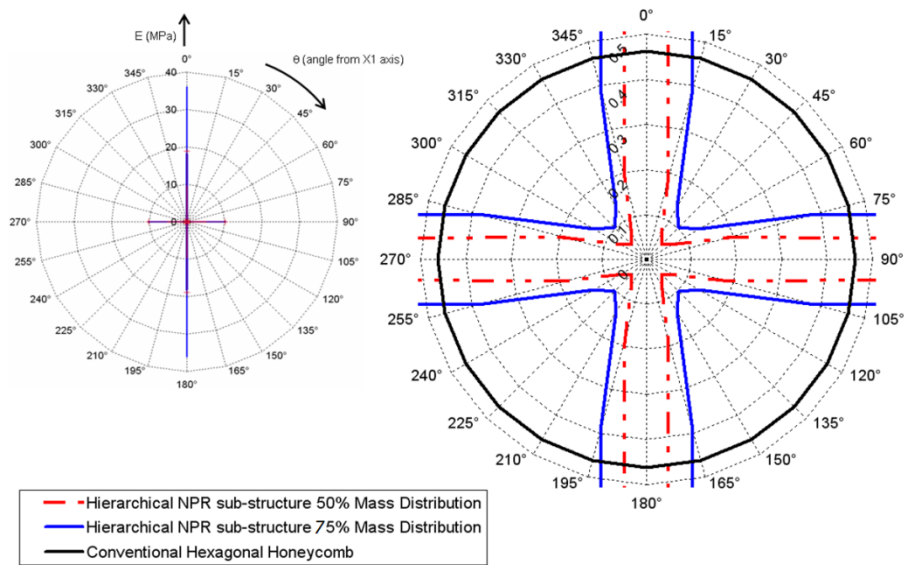


Figure 4.12: The anisotropy present in re-entrant hierarchical structures shown by a polar plot of the Young's modulus vs loading angle for two hierarchical honeycombs with a NPR sub-structures ($\theta_{sub} = -10^\circ$), with mass distributions of 50% and 75%. A conventional hexagonal honeycomb is shown for comparison in black.

4.4.3 Investigating Change in h/l

The result of changing the h/l ratio is reported in Figure 4.13, Figure 4.14 and Figure 4.15. It can be clearly seen that changes in the h_{sub}/l_{sub} ratio have little or no effect on the off axis properties, but does have a limited effect on the on axis properties with $h_{sub}/l_{sub} = 1$ resulting in greater in-plane modulus than $h_{sub}/l_{sub} = 2$, which in turn has a great in-plane modulus than $h_{sub}/l_{sub} = 3$. As in Figure 4.12 it can be seen that a change in the mass distribution between the sub and super-structure has some effect on the extent of isotropy, but not enough to exceed a conventional hexagonal honeycomb at an angle of 45° .

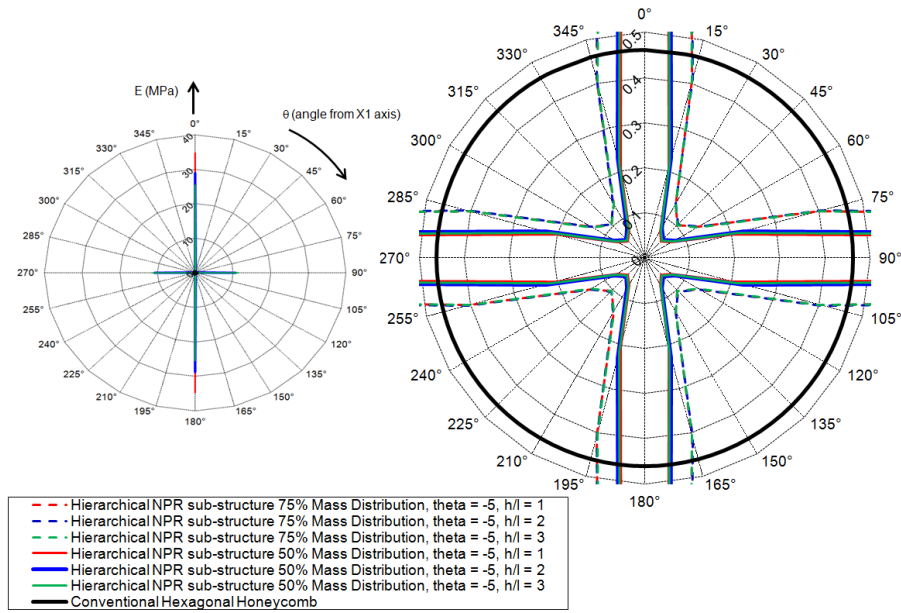


Figure 4.13: Polar plot of Young's modulus for on axis and off axis properties for h_{sub}/l_{sub} ratios of 1, 2 and 3 for the sub-structure along with the effects of changing the mass distribution from 50% to 75% in the sub-structure for hierarchical honeycombs with a NPR sub-structures ($\theta_{sub} = -5^\circ$). A conventional hexagonal honeycomb is shown for comparison in black.

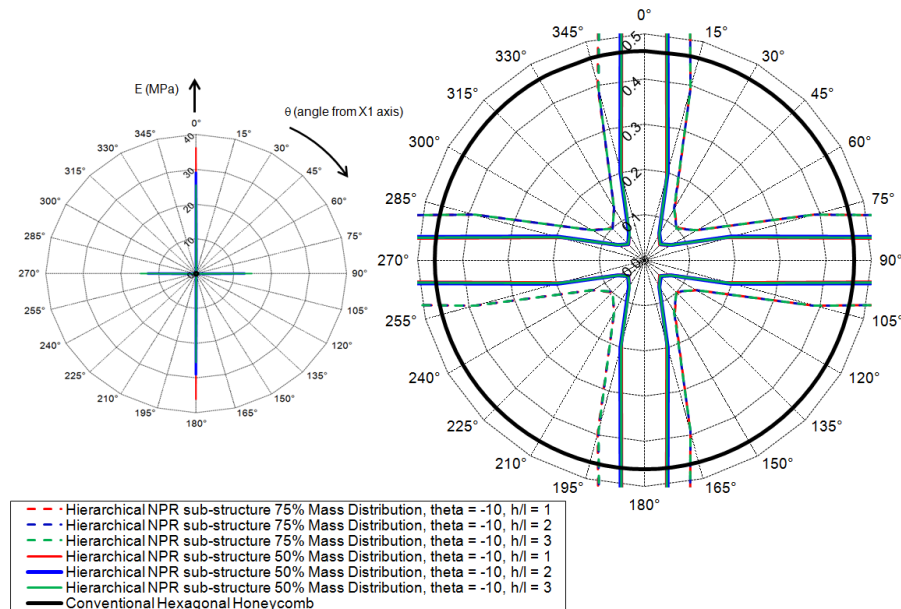


Figure 4.14: Polar plot of Young's modulus for on axis and off axis properties for h_{sub}/l_{sub} ratios of 1, 2 and 3 for the sub-structure along with the effects of changing the mass distribution from 50% to 75% in the sub-structure for hierarchical honeycombs with a NPR sub-structures ($\theta_{sub} = -10^\circ$). A conventional hexagonal honeycomb is shown for comparison in black.

with a NPR sub-structures ($\theta_{sub} = -10^\circ$). A conventional hexagonal honeycomb is shown for comparison in black.

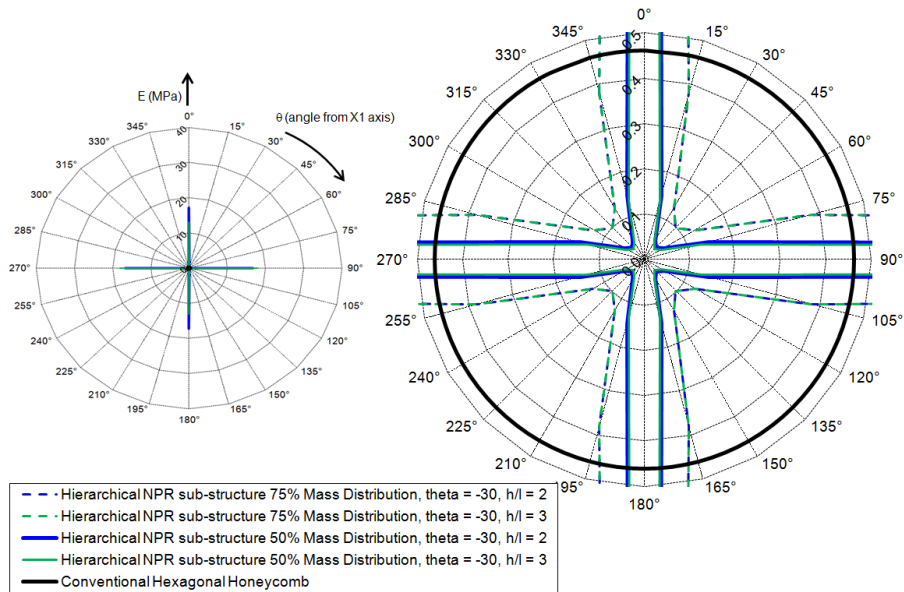


Figure 4.15: Polar plot of Young's modulus for on axis and off axis properties for h_{sub}/l_{sub} ratios of 1 and 2 for the sub-structure along with the effects of changing the mass distribution from 50% to 75% in the sub-structure for hierarchical honeycombs with a NPR sub-structures ($\theta_{sub} = -30^\circ$). A conventional hexagonal honeycomb is shown for comparison in black.

4.5 Discussion

The relationship of the Poisson's ratios of the sub-structure with the elastic modulus of the honeycomb is intriguing. It has been shown in Figure 4.9 that the HLR between the sub and super-structure has little effect on Young's modulus of the hierarchical unit cell. The change in the internal angle of the sub-structure and subsequently the sub-structures Poisson's ratio does however have a marked effect on the properties of the hierarchical honeycomb. Notably, many cases with NPR sub-structures and PPR super-structures had higher elastic moduli than cases where both sub- and super-structures had similar Poisson's ratios, see Figure 4.10 and Figure 4.11. The modulus was maximal where $\theta_{sub} = -10^\circ$ in Figure 4.10 when the mass distribution is 50% in the substructure and $\theta_{sub} = -5^\circ$ in Figure 4.11 when the mass distribution is 75% in the sub-structure. Indeed these moduli are higher than the Voigt bound via rule of mixtures averaging purely allowing for bending also shown in the figures. This underestimation for the upper bound is due to its limitation to isotropic elastic constituent materials, which re-entrant or non-uniform hexagonal honeycombs are not. The bound estimation also neglects significant Poisson's ratio effects that are present in the NPR hierarchical structures such as the opposing kinematics of the sub and super-structure, for instance where the Poisson's ratios $\nu_{12} = 1$ at $\theta_{sup} = 30^\circ$ in the super-structure and $\nu_{12} = -6.76$ at $\theta_{sub} = -10^\circ$ in the sub-structure for the 50% mass distribution, and $\nu_{12} = -12.4$ at $\theta_{sub} = -5^\circ$ in the sub-structure for the 75% mass distribution. The effects of Poisson's ratios on upper and lower bounds have been studied recently (Liu 2009), in work which showed that it is possible to exceed the Voigt bound estimation if the interaction of constituent materials' Poisson's ratios is accounted for, but it is also possible to exceed the Young's modulus of stiffest constituent material.

Exploring this issue further, a comparison can be made between the following two cases shown in Figure 4.10 and Figure 4.11, i) the sub-structure has $\theta_{sub} = -10^\circ$ and ii) $\theta_{sub} = +10^\circ$. These honeycombs have the same super-structures (both with $\theta_{sup} = 30^\circ$). The sub-structure with $\theta_{sub} = -10^\circ$ is less stiff than the $\theta_{sub} = +10^\circ$ sub-structure because the aspect ratio (t_{sub}/l_{sub}) of the ribs in the former's unit cell is smaller in order to retain similar density to the $\theta_{sub} = +10^\circ$ cell ($t_{sub}/l_{sub} = 0.0238$ and 0.3386 respectively). Since the NPR ($\theta_{sub} = -10^\circ$) sub-structure is less stiff it might be reasonable to expect that the hierarchical honeycomb with the NPR substructure would be less stiff than the

honeycomb with the PPR sub-structure ($\theta_{sub} = +10^\circ$), but this is not the case, see Figure 4.10 and Figure 4.11. So it is clear that treating these hierarchical honeycombs as composites must be done with caution since the interaction between super- and sub-structure can result in relatively larger moduli. Furthermore, there is an unexpected shift in the maximum stiffness away from $\theta_{sub} = 0^\circ$, see Figure 4.10 and Figure 4.11. For any hexagonal honeycomb, including the sub-structure honeycombs, the axial elastic modulus is known to be maximal as $\theta_{sub} \rightarrow 0^\circ$ (Gibson and Ashby 1982, Evans 1991, Masters and Evans 1996). Yet in these second order hierarchical honeycombs this maximum modulus values are for those with sub-structure with NPR values. Again, this indicates the complex interaction between super- and sub-structure.

As shown in previous work on honeycombs (Gibson and Ashby 1982, Masters and Evans 1996) hexagonal honeycombs are bending dominated. However when PPR super-structure and NPR sub-structure are combined in hierarchical honeycombs as presented here there is a change in the deformation response away from pure bending of beams to include a stretch dominated behaviour, this effect is maximal when the rotation of ribs due to bending oppose each other negating flexure due to bending causing the stretching dominance. This effect is maximal at the peak of the curves shown in the FEA results presented in Figure 4.10 and Figure 4.11. This response is reiterated in the peak Young's modulus occurring at a lower negative internal angle of $\theta_{sub} = -5^\circ$ when the mass distribution is 75% in the sub-structure compared to $\theta_{sub} = -10^\circ$ when the mass distribution is 50%. This is due to the sub-structure having a more dominate effect as the mass distribution increases, resulting in a lower internal angle of the sub-structure to oppose the rotation due to bending of the super-structure. The analytical proposed in this chapter Equation 4-11 provides an upper limit purely taking into account the stretch dominated behaviour of sub and super-structure ribs and is also plotted in Figure 4.10 and Figure 4.11.

Considering off-axis properties, the modulus at a loading angle of E_2 (90degs) also increased as the internal cell angle $\theta_{sub} \rightarrow -20$, but not as markedly as E_1 (0degs). The maximal off-axis modulus similarly increased as the sub-structure cells became NPR ($\theta_{sub} < 0$) but less markedly, see Figure 4.10 and Figure 4.11. Findings of this nature concerning NPR sub-structures have not been seen before. The off-axis behaviour of the

in-plane modulus is shown more completely in Figure 4.12, highlighting the strong anisotropy present in this honeycombs ($\theta_{sub} = -10^\circ$). The first order (conventional) honeycomb is isotropic with a Young's modulus of 0.461 MPa, whereas the second order hierarchical honeycomb peaks at 36.1 MPa loaded at 0° and is minimal at 0.048 when loaded at $\pm 45^\circ$

The effect of changing the h_{sub}/l_{sub} ratio of the sub-structure on the anisotropy of hierarchical honeycombs with a NPR sub-structure is shown in Figure 4.13, Figure 4.14 and Figure 4.15. It can be seen that there is little change on the off axis properties despite the increase in sub-structure rib thickness for the cost of reducing the number of cells. There is however a change in the X_1 and X_2 Young's modulus as the h_{sub}/l_{sub} ratio changes, which is to be expected as higher values increase the Young's modulus in the X_2 axis and lower values promoting the X_1 properties. It can also be seen that the mass distribution has an effect on the extent of anisotropy as lower mass distributions increases the off axis properties and decrease the X_1 and X_2 Young's modulus. This is due to a higher proportion of mass in the super-structure tending towards the isotropic behaviour of the regular hexagonal honeycomb.

It has been shown that the inclusion of NPR sub-structures to a PPR super-structure can increase the on axis in-plane Young's Modulus of hierarchical honeycombs. However this results is a highly anisotropic structure with a minimum Young's modulus at 45° of axis. The fact that the HLR has little effect on the response of the hierarchical honeycomb has implications to the manufacture in that there are no restrictions between the length scales of the sub and super-structure. NPR sub-structure hierarchical honeycombs could be used in applications where specific loading conditions are known utilising the increased on axis Young's modulus. However given the increase complexity of manufacturing NPR sub-structure hierarchical honeycombs, a more attractive alternative might be a conventional triangular honeycomb, which has a greater in-plane Young's modulus than a conventional hexagonal honeycomb and is also in-plane isotropic.

4.6 Conclusion

The effect of introducing a NPR sub-structure has the effect of markedly increasing the on axis properties at the expense of increasing the anisotropy present in the hierarchical honeycomb. This type of hierarchical honeycomb could be utilised when there is a known and constant direction of loading. The results show that it is not necessary for there to be a difference in length scale between the sub and super-structure when introducing a NPR sub-structure. This has important implication when considering the feasibility of manufacturing hierarchical structure.

Chapter 5. In-Plane Functionally Graded Hierarchical Honeycombs

5.1 Introduction

The excellent density specific mechanical properties of honeycombs make them desirable as light weight structures and particularly as cores in sandwich panels. Honeycombs are widely used in industries where these properties are in demand, e.g. aerospace (Bitzer 1997, Gibson and Ashby 1997) Reducing the density of honeycombs without sacrifice to their mechanical performance is advantageous. Honeycombs are often able to retain functionality after impact due to the progressive collapse inherent with their in-plane bending dominated structure (Gibson *et al* 1989, Triantafillou *et al* 1989, Deqiang and Weihong 2009).

There has been lots of interest in the functional grading of materials such as composites in recent years (Birman and Byrd 2007), and whilst there are a few studies of functional grading of honeycombs, in the main this has been for thermal or electrical properties (Seepersad *et al* 2004, Xia *et al* 2002). Mechanical properties were investigated by Ajdari *et al* (2009) concluding that the elastic modulus was sensitive to the density gradient across the domain. Other work on functional grading in honeycombs has focussed on impact energy absorption, Ajdari *et al* (2011). Similarly, little work has been undertaken on hierarchy in honeycombs (Lakes 1993, Kooistra 2007, Fan 2008, Taylor 2011) but this has shown that improvements in elastic properties on a density specific basis are possible with careful design. The authors are not aware of any work combining functional grading and hierarchy for honeycombs in synthetic materials, although both phenomena are known to occur simultaneously in many natural materials (Fratzl 2007, Fratzl and Weinkamer 2007, Silva *et al* 2006). Many of these natural materials possess excellent density specific elastic and other properties (Fratzl 2007, Fratzl and Weinkamer 2007 and Gao 2006).

Materials that have a gradual change in either the volume fraction or physical properties of constituent materials within a composite are often described as being functionally graded. Functional grading of materials in general is now in a fairly mature state, with

manufacturing methods for functionally graded composites and modelling methods to predict their properties now developed (Birman and Byrd 2007, Markworth *et al*, 1995, Miyamoto *et al*, 1999, Noda, N, 1999). Work focusing on the elastic properties of functionally graded honeycombs is limited, with studies by Ajdari *et al* (2009), Lira and Scarpa (2010) and Taylor *et al* (2011), demonstrating how global elastic properties of honeycombs are indeed sensitive to the various parameters associated with functional grading. There has been more work undertaken on failure, dynamic and impact properties of functionally graded honeycombs demonstrating improved performance *vs* ungraded honeycombs (Ajdari *et al* 2011, Kirugulige 2005, Apetre *et al* 2006, Wang *et al* 2009). Whilst there is good evidence for beneficial effects of functional grading in terms of failure and damage processes in honeycombs, little work has been done to establish if there is a penalty in elastic performance for functional grading, with some indications from Ajdari *et al* (2009) and Lira and Scarpa (2010) that there are indeed such penalties in some cases.

Hierarchy has been the subject of much investigation in natural and other materials (Fratzl 2007, Fratzl and Weinkamer 2007) but little effort has been given to fundamental understanding of elastic properties and hierarchy. Hierarchical structures can be given a hierarchy order number which describes the number of distinct size scales at which there is architecture; a conventional honeycomb has an order number of one. The primary works on elastic properties and hierarchy are the work of Gibson and Ashby (1982) and Lakes (1993). Gibson and Ashby (1992) showed that the elastic properties of a honeycomb were not dependent upon absolute size of the cells, but rather the aspect ratio of the cell ribs. Coarser or finer honeycombs would therefore have the same properties as long as the cell rib aspect ratio was unchanged. This underlay the independence of elastic properties of honeycombs to their hierarchical order in Lakes (1993). Recently the present authors (Taylor *et al* 2011) have shown that hierarchy in hexagonal honeycombs usually does lead to large changes in elastic properties, because i) for constant relative density the aspect ratio of cell ribs does change with hierarchical order numbers greater than one, ii) mixed shear and flexure deformation modes can make some cell ribs more compliant than their aspect ratio would predict.

Kooistra (2007) and Fan (2008) have both developed case studies of hierarchical sandwich panel cores with improved performance over existing non-hierarchical (conventional) configurations. The work herein explores how in-plane mechanical properties of honeycombs are changed by functional grading of a hierarchical structure.

5.2 Methods

The in plane elastic properties of functionally graded hierarchical honeycomb was calculated via numerical models which considered each unit cell as a discrete structure, and made no assumptions about sub-cells as continua and via analytical models which assumed that sub-cells could be considered as continua. In this sense the numerical models provided validation for the analytical models.

5.2.1 Finite Element Model

The various parameters describing honeycombs, functional grading and hierarchy are shown in Figure 3.8 and defined in the following. The cells of conventional and hierarchical honeycomb honeycombs have ribs of length l and h , and thickness t , as shown in Figure 3.8 in both a conventional and hierarchical honeycomb. The aspect ratio of a honeycomb rib is defined as its length divided by its thickness, as shown in Equation 5-1 The parameter values for super- and sub-structure cells are noted by the subscripts $_{sub}$ and $_{sup}$ (referring to sub-and super-structure parameters respectively), and as described in (Taylor 2011).

$$a = \frac{l}{t}$$

Equation 5-1

The first step in applying functional grading to the honeycombs was to determine the length scale of the sub-structure, relative to that of the super-structure, at which it could be considered to be a continuum. This was determined in Chapter 3 where it was found that when the number of sub-cells spanning the super-structure is greater than 8 the sub-structure can be considered as a continuum to the super-structure. The ratio of the lengths in the sub-and super-structure is the Hierarchical Length Ratio (HLR) λ and is defined according to Equation 5-2. The critical value of the HLR at which continuum behaviour was attained was determined by iteratively decreasing the value of λ for three example hierarchical honeycombs of different aspect ratios ($\alpha_{sup} = 11.547$, $\alpha_{sup} = 2.88$ and $\alpha_{sup} = 1.155$).

$$\lambda = \frac{l_{sub}}{l_{sup}}$$

Equation 5-2

To change λ the lengths l_{sub} , h_{sub} and t_{sub} of the sub-structure were iteratively decreased, while lengths l_{sup} , h_{sup} and t_{sup} remained constant, effectively increasing the number of sub-cells spanning the thickness of the super-structure, as shown in Figure 3.8. Once the critical value of λ , and thus the number of sub-cells spanning the super-structure, was determined, it was then possible to investigate non-uniform distributions of mass in the sub-structure.

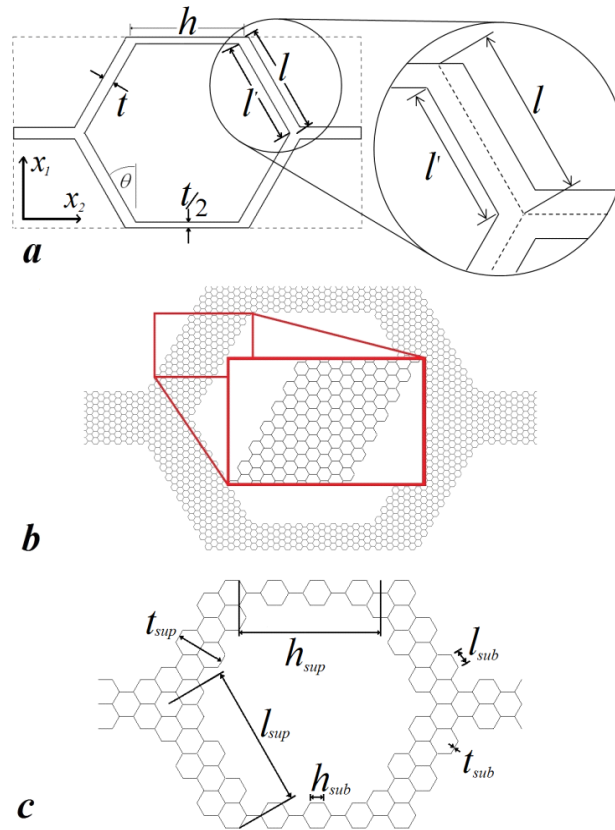


Figure 5.1: 1a Cell geometry and parameters for a conventional hexagonal honeycomb unit cell according to Gibson and Ashby's terminology. 1b: A unit cell of a second order hierarchical honeycomb with a hierarchical length ratio of $\lambda=0.015$ and a super-structure aspect ratio $\alpha_{sup}=2.88$. 1c: A unit cell of a second order hierarchical honeycomb with a hierarchical length ratio of $\lambda=0.1$ and a super-structure aspect ratio $\alpha_{sup}=2.88$, along with annotated terminology.

Functional grading was applied by gradually varying the thickness of sub-structure ribs t_{sub} in rows of sub-cells as a function of the row's position through the thickness of the super-structure rib, see Figure 5.2. There were two ways in which to implement this variation, i) by changing t_{sub} and maintaining l_{sub} , and ii) changing l_{sub} and maintaining t_{sub} . A change in t_{sub} was chosen since in this manner it was possible for sub-cells to tessellate but not possible if l_{sub} was varied. The various distributions of t_{sub} produced different distributions of mass throughout the unit cell, as shown in Figure 5.2. It is important to note that the total mass of each unit cell was maintained, as was the total cell area, ensuring similar relative density between different distributions. Mass distributions were defined by a string of percentages of total rib thickness for four rows of sub-cells making up half a super-structure rib, see Figure 5.2 and Figure 5.3. Hence, a uniform distribution would be denoted as (25/25/25/25), i.e. the percentage of total rib thickness for regions 1, 2 3 and 4 are 25% each. Twelve other non-uniform distributions were also considered, listed in Table 5.1. These 13 distributions were considered for unit cells with a relative density of $\rho_{rel}^* = 0.00577$ which is equivalent to a conventional hexagonal honeycomb when $l=h=10$ and $t=0.05$ other densities also investigated were $\rho_{rel}^* = 0.011547$, $\rho_{rel}^* = 0.017321$ and $\rho_{rel}^* = 0.023094$, making 52 discrete functionally graded hierarchical honeycombs.

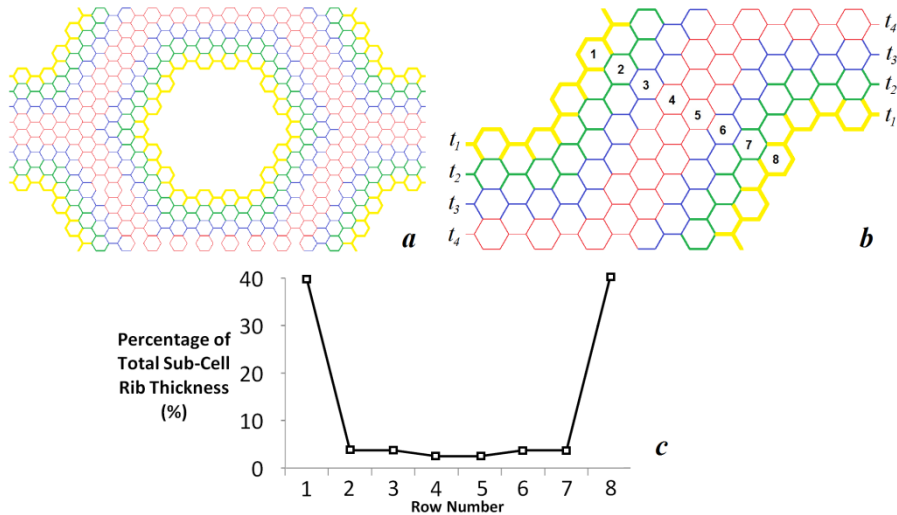


Figure 5.2: A hierarchical unit cell with a distribution of sub-cell rib thicknesses around the super-cell's regions. a) Shows a full unit cell with the same rib thickness distribution as Figure 2b. This super-cell has 4 regions, i.e. $i = 4$. b) A quarter unit cell in which the sub-cell ribs are coloured according to thickness, t_i , in this case decreasing from the

edges inwards. Each of the 4 regions shown here have ribs of thickness t_1 , t_2 , t_3 or t_4 . Cells form rows normal to the rib thickness, and these are shown numbered 1 – 8. c) Shows how the percentage rib thickness changes across the super-structure rib for a (80/7.5/7.5/5) mass distribution.

Rib	Thickness %												
	25	40	50	50	60	70	80	10	10	15	5	5	5
t_1	25	30	25	20	20	15	7.5	20	15	15	15	10	7.5
t_2	25	20	15	15	15	10	7.5	30	25	20	20	15	7.5
t_3	25	10	10	15	5	5	5	40	50	50	60	70	80

Table 5.1: Shows the distributions studied as a percentage of rib thickness for each region.

Two dimensional finite element models were generated for each unique unit cell, and its in-plane axial Young's modulus calculated. A set of linear isotropic elastic constants were chosen as the constitutive material and used for all cases (specifically $E_s = 1600$ MPa, $G_s = 593$ MPa and $\nu_s = 0.35$) (Miller 2010 & Caulfield 2007). The sub and super-cells were modelled using a minimum of 20 2D Timoshenko beam elements (B22: a 3-node quadratic beam) per cell rib (as established in Chapter 2) using a commercial Finite Element (FE) analysis package (ABAQUS, version 6.9. Dassault Systèmes). Boundary sharing ribs had either half thickness or half-lengths, so that the symmetry of the model allowed tessellation of the quarter cell into a full cell and on into a uniform honeycomb. The upper most edges of the model were displaced axially and uniformly to produce a global 0.1 % strain in the X_1 axis (normal to the h rib), as described by Odegard (2003). The contralateral model edge was constrained to zero displacement in the X_1 axis but allowed to freely displace in the X_2 axis. One model edge parallel to the X_1 axis was constrained to zero displacement in the X_2 axis, and the other allowed to displace freely but guided in the X_1 axis, (i.e. elements on this edge were constrained to remain in an axis parallel to the X_1 axis). These boundary conditions simulate uniaxial compression in a honeycomb continuum Odegard (2003). It was possible to use a unit cell to model the hierarchical continua, i.e. containing sub and super-structures.

The Young's modulus E_I^* was calculated by summing the total reaction force on the displaced model edge, divided by the product of projected area (unit depth) and the

imposed strain of 0.1%. Honeycombs of only second order of hierarchy, i.e. a sub and one super-structure, were considered though further levels are have been considered [Lakes 1993]. This was in part for the sake of computational ease and in part a reflection of pragmatic likely manufacturing limits.

5.3 Analytical models

5.3.1 Conventional honeycombs

Extending on work from Chapter 3 it is possible to produce analytical models that predict the response of functionally graded hierarchical honeycombs. Recapping work from Chapter 3 and following the annotation of Gibson and Ashby (1982) honeycombs are given geometric parameters similar to those set out in Figure 3.8a, and extended to a hierarchical honeycomb in Figure 3.8c. Gibson and Ashby (1982) set out the fundamental underpinnings of the behaviour of honeycombs, i.e. as tessellations of unit cell structures formed from beams or plates. Thus using beam mechanics, expressions could be derived for the elastic properties, e.g. the in-plane Young's modulus in Equation 3-5, for a range of 2D and 3D cellular solids including honeycombs. Note that for hierarchical honeycombs such as shown in Figure 3.8a, the true functional length of the super-structure l rib is unclear, with possible extremes ranging from l to l' .

$$\frac{E_1^*}{E_s} = \left(\frac{t}{l}\right)^3 \frac{\cos\theta}{(h/l + \sin\theta)\sin^2\theta}$$

Equation 5-3

Where E_s is the Young's modulus of the constituent material. Similar expressions are given for the other Young's and shear moduli and the Poisson's ratios.

Masters and Evans (1996) later refined these models by accounting for other deformation modes, specifically stretching/compression and hinging of ribs. Gibson and Ashby (1997) further developed their honeycomb model by including axial (tension/compression) and shear deformation of ribs as shown in Equation 5-1. Shear deformation becomes significant when the aspect ratio $\alpha < 5$ (or to be conservative $\alpha < 10$), where the aspect ratio α is the length l over thickness t as seen in Equation 5-1.

$$E_1^* = \left(\frac{t}{l}\right)^3 \frac{\cos\theta}{\left(\left(\frac{h}{l}\right) + \sin\theta\right)\sin^2\theta} \frac{1}{1 + (2.4 + 1.5\nu_s + \cot^2\theta)\left(\frac{t}{l}\right)^2} E_s$$

Equation 5-4

5.3.2 Hierarchical honeycombs

These equations can be adapted for hierarchical honeycombs. The equations in any of the work on honeycomb models described previously, being based on beam mechanics, are valid for continua and so are independent of size. They can be used to describe a honeycomb of any size scale, thus within hierarchical honeycombs, they can be used to describe the properties of all of the honeycombs individually. It might seem reasonable to assume therefore that a sub-structure honeycomb can be treated as a continuum and its predicted properties used in calculation of the properties of the super-structure. Equation 3-8 is derived for a sub-structure honeycomb from those of Ashby and Gibson (1997) and is used as a continuum in Equation 3-9 for a super-structure honeycomb, i.e. a hierarchical honeycomb. However, it is not proven whether this assumption of a continuum sub-structure is valid if the size scales of the sub and super-structures are not very different. This issue is addressed later in the work.

$$E_{1_{sub}}^* = \left(\frac{t_{sub}}{l_{sub}}\right)^3 \frac{\cos\theta}{\left(\left(\frac{h_{sub}}{l_{sub}}\right) + \sin\theta\right) \sin^2\theta} E_s$$

Equation 5-5

$$E_{1_{sup}}^* = \left(\frac{t_{sup}}{l_{sup}}\right)^3 \frac{\cos\theta}{\left(\left(\frac{h_{sup}}{l_{sup}}\right) + \sin\theta\right) \sin^2\theta} E_{1_{sub}}^*$$

Equation 5-6

In the case where ribs have aspect ratios $\alpha < 5$, the beam equation including axial and shear deformation must be used. Versions of Equation 3-8 and Equation 3-9 which allow for axial and shear deformation are given below in Equation 3-10, Equation 3-11 and Equation 3-12 (adapted from Gibson and Ashby 1997).

$$E_{1_{sub}}^* = \left(\frac{t_{sub}}{l_{sub}}\right)^3 \frac{\cos\theta}{\left(\left(\frac{h_{sub}}{l_{sub}}\right) + \sin\theta\right) \sin^2\theta} \frac{1}{1 + (2.4 + 1.5v_s + \cot^2\theta) \left(\frac{t_{sub}}{l_{sub}}\right)^2} E_s$$

Equation 5-7

$$v_{21_{sub}}^* = \frac{\sin\theta \left(\frac{h_{sub}}{l_{sub}}\right) + \sin\theta}{\cos^2\theta} \left(\frac{t_{sub}}{l_{sub}}\right)^3 \frac{1 + (2.4 + 1.5v_s)(t_{sub}/l_{sub})^2}{1 + \left(2.4 + 1.5v_s + \tan^2\theta + \frac{2(h_{sub}/l_{sub})}{\cos^2\theta}\right) \left(\frac{t_{sup}}{l_{sub}}\right)}$$

Equation 5-8

$$E_{1sup}^* = \left(\frac{t_{sup}}{l_{sup}}\right)^3 \frac{\cos\theta}{\left(\left(\frac{h_{sup}}{l_{sup}}\right) + \sin\theta\right) \sin^2\theta} \frac{1}{1 + (2.4 + 1.5\nu_s + \cot^2\theta) \left(\frac{t_{sup}}{l_{sup}}\right)^2} E_{1sub}^*$$

Equation 5-9

5.3.3 Functionally graded hierarchical honeycombs

This work can be further developed to model a functionally graded hierarchical honeycomb where the thicknesses of sub-structure ribs, t_i , vary between the i regions in the super-structure, see Figure 5.2. This is only one of the myriad of ways in which functional grading could be brought about in such honeycombs. Figure 5.2 shows a functionally graded hierarchical honeycomb with four distinct regions of rib thickness (represented as line colour).

The distribution of sub-structure rib thickness, and how this changes across the super-structure rib, is shown in Figure 5.2a and in more detail in 2b. This distribution of sub-structure rib thickness (as a percentage of the sum of sub-structure rib thicknesses) is shown graphically in Figure 5.2c, in this case for a mass distribution of (80/7.5/7.5/5). The row numbers in Figure 5.2c are those shown spanning the super-structure rib thickness in Figure 2a.

Uniform distribution of mass within the sub-structure can be modelled by using Equation 3-9 or Equation 3-12 depending on the chosen values of α . The distribution of mass throughout the super-structure ribs effectively changes the second moment of area of the super-structure rib, considering the properties of the sub-structure regions (with thicknesses of t_1 , t_2 , t_3 or t_4) as continua. Doing so, it is possible to calculate the second moment of area and thus Young's modulus of the super-structure rib using the transform section method (Gere 2001). A section of a super-structure rib is shown in Figure 5.3, demonstrating how the cross-section is formed from rows of sub-cells. The innermost row thickness, h_1 , can be calculated from the architecture of the sub-structure as $h_1 = 4l_{sub} \cos \theta$ for the case shown in Figure 5.2, and similarly for further layers.

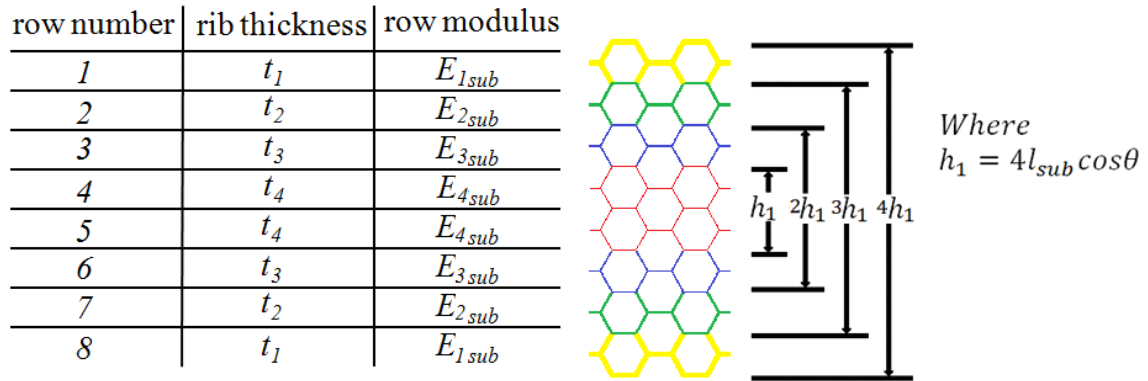


Figure 5.3: The properties of the sub-cells in a super-structure rib, as shown in and the layers' structural parameters. The columns of sub-cells shown represent the thickness of one super-cell rib.

The transform section method produces an effective value for the second moment of area, I , of a composite beam formed from several layers. It does this by considering layers within the beam, of uniform elastic properties but non-uniform layer widths, to describe an equivalent composite beam in which layers have non-uniform elastic properties but uniform cross section (Gere 2001). The width of the equivalent layers are dependent upon the ratio of the Young's modulus of the individual layers to a specified layer, in this case the innermost region (1), specifically n_{1i} in Equation 5-10, Equation 5-11 and Equation 5-12.

$$n_{12} = \frac{E_{sub1}}{E_{sub2}} \quad \text{Equation 5-10}$$

$$n_{13} = \frac{E_{sub1}}{E_{sub3}} \quad \text{Equation 5-11}$$

$$n_{14} = \frac{E_{sub1}}{E_{sub4}} \quad \text{Equation 5-12}$$

The second moment of area of the whole beam can then be calculated in the usual manner for a beam of one material but non-uniform cross section. The second moment of area, I , for a functionally graded hierarchical rib composed of i regions of different beam thickness, see Figure can be described as in the generic Equation 5-13 and is simplified for the case presented in this work in Equation 5-14.

$$\begin{aligned}
I_x = & d \left(\frac{h_1^3}{12} + 2 \left(\frac{n_{12} \left(\frac{h_2-h_1}{2} \right)^3}{12} + \left(n_{12} \frac{h_2-h_1}{2} \right) \left(\frac{h_2+h_1}{4} \right)^2 \right) + \right. \\
& 2 \left(\frac{n_{13} \left(\frac{h_3-h_2}{2} \right)^3}{12} + \left(n_{13} \frac{h_3-h_2}{2} \right) \left(\frac{h_3+h_2}{4} \right)^2 \right) + \dots + \\
& \left. 2 \left(\frac{n_{1(i-1)} \left(\frac{h_{(i-1)}-h_{(i-2)}}{2} \right)^3}{12} + \left(n_{1i} \frac{h_{(i-1)}-h_{(i-2)}}{2} \right) \left(\frac{h_{(i-1)}+h_{(i-2)}}{4} \right)^2 \right) + 2 \left(\frac{n_{1i} \left(\frac{h_i-h_{(i-1)}}{2} \right)^3}{12} + \right. \right. \\
& \left. \left. \left(n_{1i} \frac{h_i-h_{(i-1)}}{2} \right) \left(\frac{h_i+h_{(i-1)}}{4} \right)^2 \right) \right)
\end{aligned}$$

Equation 5-13

Which for this example gives.

$$I_x = \frac{dh_1^3}{12} (1 + 7n_{12} + 19n_{13} + 37n_{14})$$

Equation 5-14

This value of second moment of area, I , can then be used in the calculation of the in-plane elastic properties of a functionally graded hierarchical honeycomb in the normal manner, i.e. using the set of equations given in Gibson and Ashby, for example the in plane Young's modulus E_1 , Equation 5-15.

$$E_{1sup}^* = \frac{\sigma}{\varepsilon} = \left(\frac{h_1^3}{l_{sup}^3} \right) \frac{(1 + 7n_{12} + 19n_{13} + 37n_{14}) \cos \theta}{(h_{sup}/l_{sup} + \sin \theta) \sin^2 \theta} E_{1sub}^*$$

Equation 5-15

Equation 5-15 is valid for slender beams only but can be adapted to account for combined flexure and shear, i.e. a Timoshenko beam Gibson and Ashby (1997), as in Equation 5-16. For slender beams Equation 5-15 and Equation 5-16 give similar results, therefore in this work Equation 5-16 is always used.

$$\begin{aligned}
& E_{1sup}^* \\
& = \left(\frac{h_1^3}{l_{sup}^3} \right) \frac{(1 + 7n_{12} + 19n_{13} + 37n_{14}) \cos \theta}{(h_{sup}/l_{sup} + \sin \theta) \sin^2 \theta} \frac{1}{1 + (2.4 + 1.5v_{21sub}^* + \cot^2 \theta) \left(\frac{t_{sup}}{l_{sup}} \right)^2} E_{1sub}^*
\end{aligned}$$

Equation 5-16

These models are applied to a similar range of parameter values as for the FE modelling, and specifically to investigate i) the mass distributions, ii) effects of shear within the sub- and super-structure ribs, iii) the true effective length of the super-cell rib and iv) the super-structure aspect ratio, which is known to affect the elastic properties of hierarchical honeycombs [Taylor *et al* 2011].

5.4 Results

Results from the numerical modelling, concerning the critical length scale and the functional grading of the sub-structure are presented first, followed by the analytical modelling and a comparison with numerical modelling results.

5.4.1 FE models

For reasons of clarity, three example mass distributions are shown together in Figure 5.4, specifically (5/10/15/70), (50/20/15/15), and a uniform (25/25/25/25) (as per Figure 5.2), and are ranked according to normalised Young's modulus, with the I beam equivalent distribution being the stiffest.

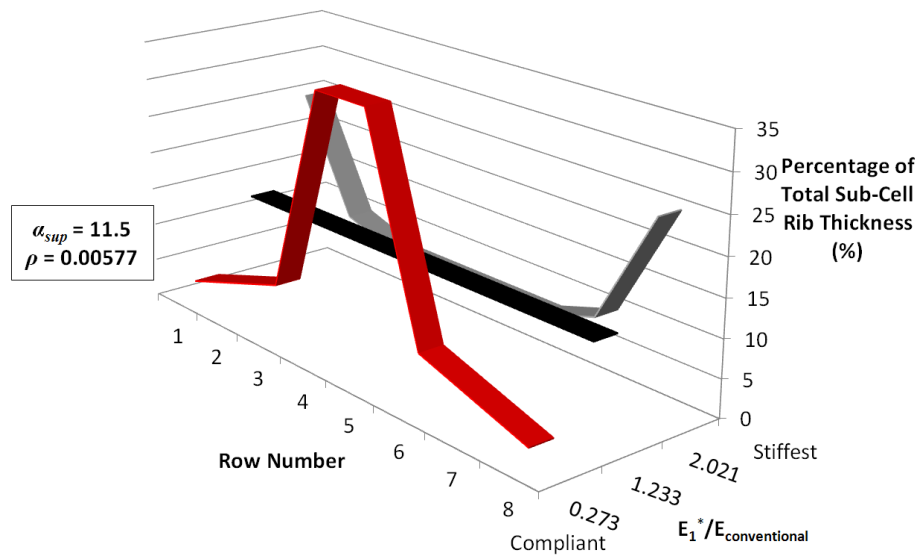


Figure 5.4: Mass distribution across the super-structure rib thickness, plotting the percentage thickness of total sub-cell rib thicknesses *vs* the sub-cell row number. The distributions are ranked by the normalised Young's modulus, i.e. normalised to the conventional honeycomb of similar relative density. The super-structure aspect ratio $\alpha_{sup} = 11.5$. The most compliant of the three distributions was the 'n' shape (5/10/15/70), the uniform distribution (25/25/25/25) next stiffest, and the 'u' shape (50/20/15/15) the stiffest.

Results for all the distributions are given in Figure 5.5 and similarly compare the normalised Young's modulus and mass distributions, in this case all of the same relative density but for 3 different super-structure aspect ratios. The distributions are ranked in order of Young's modulus. These functionally graded hierarchical honeycombs have 8

sub-cells spanning the super-structure rib. The graphs show the in-plane Young's moduli are markedly sensitive to the mass distribution within the sub-cells. The more extreme distributions tend to be less stiff. The uniform distribution is stiffest for low aspect ratio super-structures but not for high aspect ratio super-structures, for instance comparing Figure 5.5a and Figure 5.5b with Figure 5.5c in the latter of which three non-uniform distributions are stiffer than the uniform configuration. The best performing functionally graded honeycombs outperform conventional 1st order (conventional) honeycombs; see Figure 5.5b and Figure 5.5c, being 45% and 100% stiffer respectively.

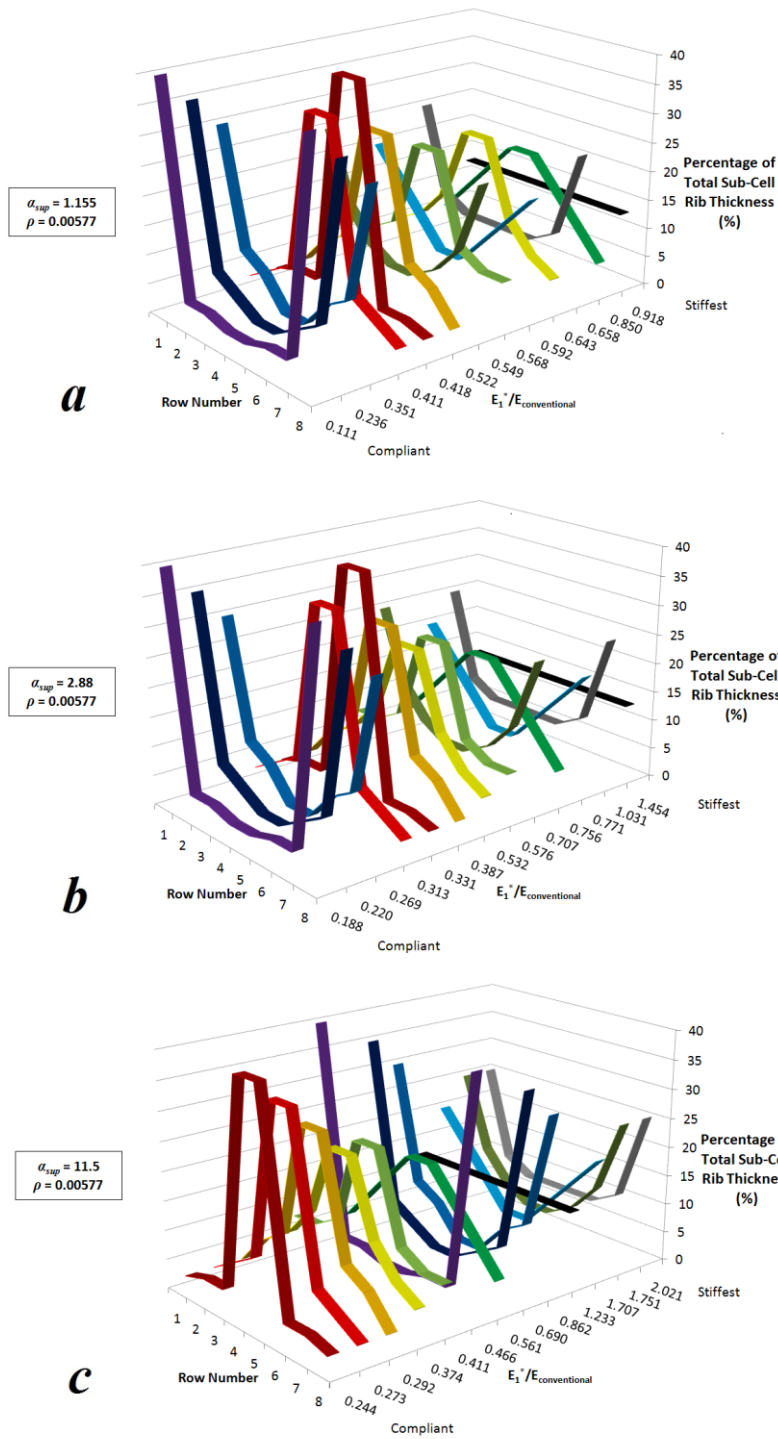


Figure 5.5: The row number of the sub-cells across the super-structure, and the percentage thickness of the sub-cell rib, are shown vs the Young's modulus of the functionally graded hierarchical honeycomb (normalised to that of a conventional honeycomb of similar relative density). For a: super-structure aspect ratio $\alpha_{sup} = 1.16$, b:

Super-structure aspect ratio $\alpha_{sup} = 2.88$ and c: Super-structure aspect ratio $\alpha_{sup} = 11.5$. All model have a relative density $\rho_{rel}^* = 0.00577$.

The effect of relative density is shown in Figure 5.6, in which the super-structure aspect ratio is similar to that of Figure 5.5c but the relative density is higher ($\rho_{rel}^* = 0.0231$ and $\rho_{rel}^* = 0.00577$ respectively). There is a positive relationship between relative density and in-plane Young's modulus as would be expected and there is no change in order of stiffness between mass distributions as relative density changes.

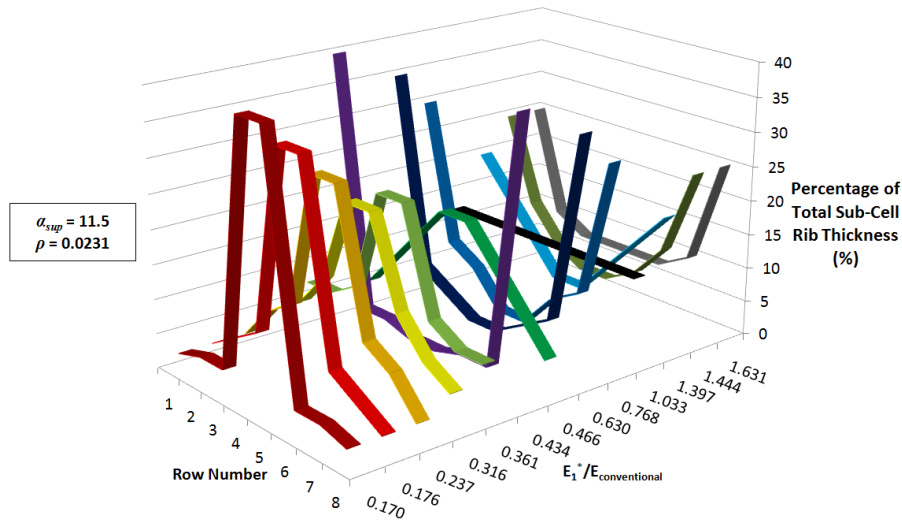


Figure 5.6: The row number of the sub-cells across the super-structure and the percentage thickness of the sub-cell rib, are shown vs the Young's modulus of the functionally graded hierarchical honeycomb (normalised to that of a conventional honeycomb of similar relative density) for a super-structure aspect ratio $\alpha_{sup} = 11.6$ (as in Figure 5.5) and a relative density $\rho_{rel}^* = 0.0231$. (equivalent to a conventional honeycomb with $l=h= 10$ and $t= 0.2$)

The effect of changing the relative density for a range of super structure aspect ratios can be seen by comparing Figure 5.7, Figure 5.8 and Figure 5.9 which plot E_1^* for the various mass distributions at specific aspect ratios but at relative densities of $\rho_{rel}^* = 0.00577$, $\rho_{rel}^* = 0.0116$, $\rho_{rel}^* = 0.0173$ and $\rho_{rel}^* = 0.0231$. For ease of comparison E_1^* for a 1st order honeycomb is also shown in these figures.

The results for changing the relative density of a hierarchical structure with a super-structure aspect ratio $\alpha_{sup} = 2.88$ can be seen in Figure 5.7. Whilst many distributions fall

lower than the conventional hexagonal honeycomb, two have a greater or comparative in-plane Young's Modulus 25,25,25,25 (uniform distribution) and 50,20,15,15.

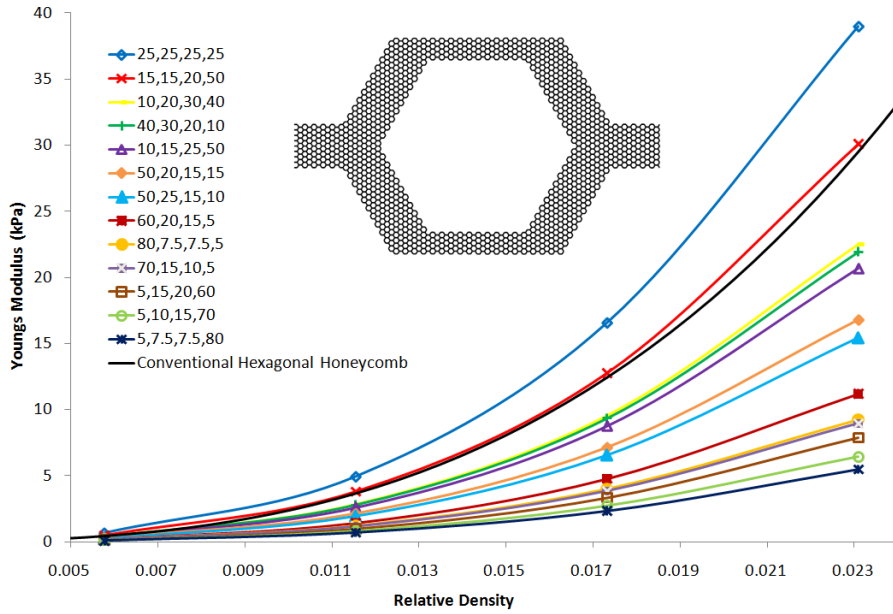


Figure 5.7: Multiple functionally graded hierarchical structures with a hierarchical aspect ratio of $\alpha_{sup} = 2.88$ for different relative densities compared to a conventional hexagonal honeycomb.

The results for changing the relative density of a hierarchical structure with a super-structure aspect ratio $\alpha_{sup} = 1.16$ can be seen in Figure 5.8. All distributions fall lower than the conventional hexagonal honeycomb, but a 25,25,25,25 uniform distribution is comparable.

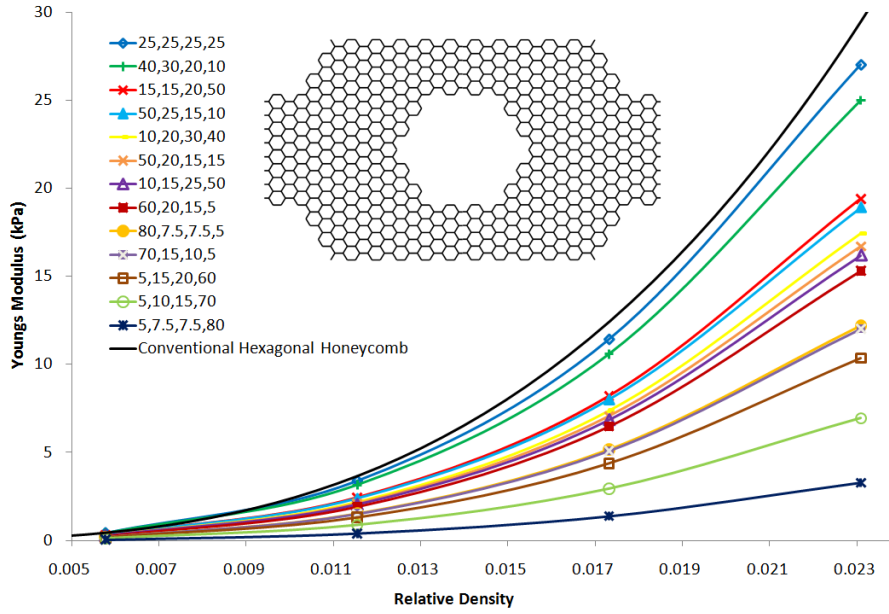


Figure 5.8: Multiple functionally graded hierarchical structures with a hierarchical aspect ratio of $\alpha_{sup} = 1.15$ for different relative densities compared to a conventional hexagonal honeycomb.

The results for changing the relative density of a hierarchical structure with a superstructure aspect ratio $\alpha_{sup} = 11.6$ can be seen in Figure 5.9. Whilst many distributions fall lower than the conventional hexagonal honeycomb, 4 exceed it; of note is the 50,20,15,15 distribution which exceeds the conventional hexagonal honeycomb by approximately 63%.

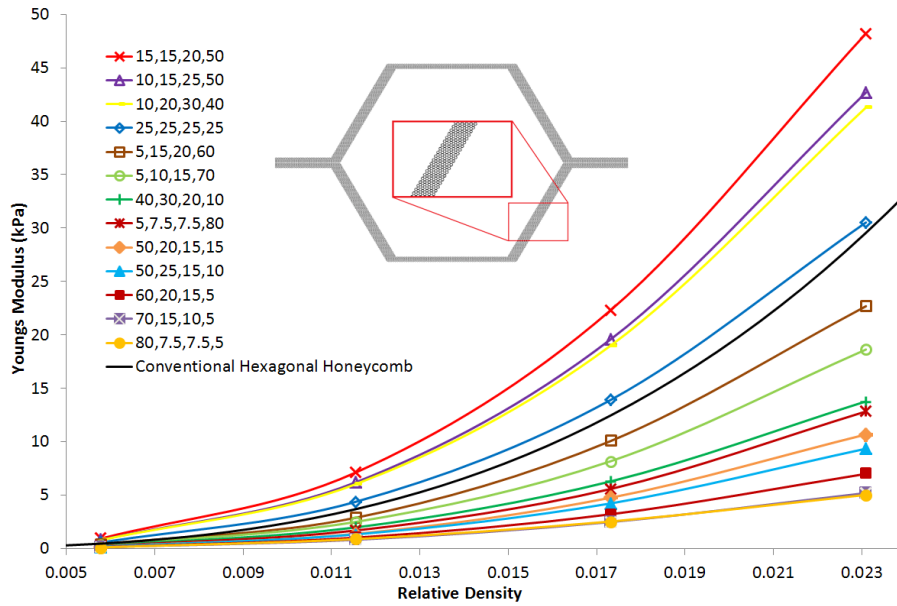


Figure 5.9: Multiple functionally graded hierarchical structures with a hierarchical aspect ratio of $\alpha_{sup} = 11.6$ for different relative densities compared to a conventional hexagonal honeycomb.

5.4.2 Analytical models

From the FE modelling it was clear there were a small number of functionally graded hierarchical honeycomb structures that consistently showed greater or comparable in-plane Young's modulus vs conventional honeycombs, specifically the uniform (25/25/25/25) and three gentle 'U' shaped distributions (e.g. 50/20/15/15), see Figure 5.5c. Several distributions were explored further, and particularly the effect of the super-structure thickness (and thus aspect ratio).

The analytical model predictions, specifically from Equation 5-16 for a uniform distribution (25/25/25/25) are compared with FE model results in Figure 5.10 for a range of super-structure thicknesses and a relative density of $\rho_{rel}^* = 0.00577$. There is a complex relationship between these parameters, with several examples exceeding the stiffness of a similar density conventional honeycomb. Also shown in Figure 5.10 is the effect of the uncertainty over the true effective length of the super-structure's l_{sup} rib. The analytical and FE models agree in terms of the pattern of the change in in-plane Young's modulus, if not in absolute values.

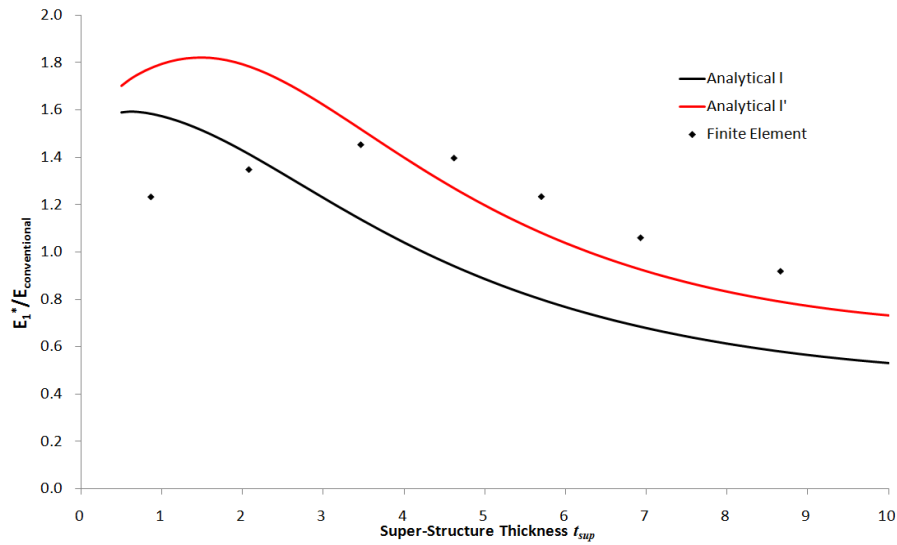


Figure 5.10: The FE and analytical model of Young's moduli vs the super-cell rib thickness t_{sup} , for a functionally graded hierarchical honeycomb with a uniform distribution of mass (normalised to that of a conventional honeycomb of similar relative density) and a relative density $\rho_{rel}^* = 0.00577$, when $l_{sup} = 10$. The model predictions for the shorter effective rib length l' are also shown.

The aspect ratio of the super-structure defines, for a given relative density, the aspect ratio of the sub-cell ribs, and therefore their flexural stiffness. Considering the super-structure rib as a continuum, the aspect ratio should also define the extent of shear deformation. Figure 5.11 illustrates the extent of shear in the sub-cells forming the super-structure rib, in this case a relatively high aspect ratio super-structure.

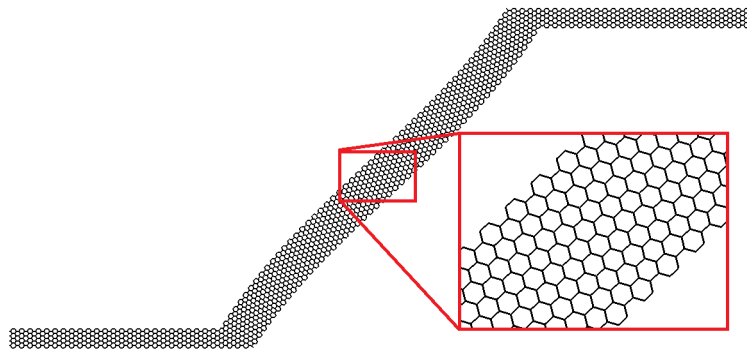


Figure 5.11: The deformed FE mesh of a hierarchical honeycomb with a uniform, (25/25/25/25) distribution for a super-structure aspect ratio $\alpha_{sup} = 11.6$ and a relative density $\rho_{rel}^* = 0.00577$. The deformation scale factor is 10.

Similarly, the in-plane Young's moduli of the best of the gentle 'U' distributions (50/20/15/15), which exceeded stiffness values of both the 1st order (conventional) honeycomb and the uniform distribution functionally graded hierarchical honeycomb, is shown in Figure 5.12. Both analytical and FE model predictions are shown, and disagree strongly. The deformed mesh of the FE model is shown in Figure 5.13 and there is considerable shear deformation in the centre of the rib.

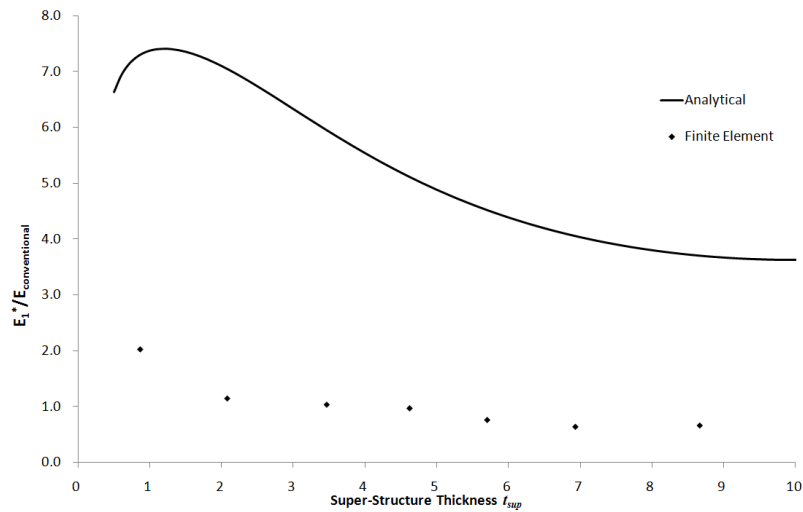


Figure 5.12: The FE and analytical model predictions of in-plane Young's modulus vs t_{sup} for a functionally graded hierarchical honeycomb (normalised to that of a conventional honeycomb of similar relative density) with a 50/20/15/15 mass distribution and a relative density $\rho_{rel}^* = 0.00577$, when $l_{sup} = 10$.

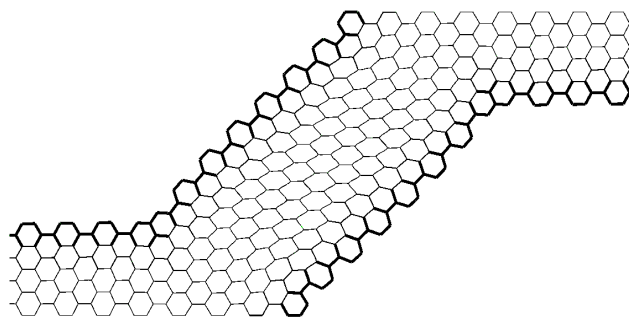


Figure 5.13: Deformation of a functionally graded hierarchical honeycomb with a (50/20/15/15) distribution, a super-structure aspect ratio $\alpha_{sup} = 2.17$ and a relative density

$\rho_{rel}^* = 0.00577$. It can be seen that the centre of the super-structure ribs are shearing and elastically buckling. A deformation factor of 10 has been applied to this image.

The stiffest distribution predicted by Equation 5-16 of the analytical model, i.e. an extreme ‘U’ distribution (80/7.5/7.5/5), was conversely predicted to be very compliant by the corresponding FE model, as shown in Figure 5.14. The analytical model is not capable of capturing the deformation modes in the functionally graded rib seen in the FE model; see Figure 5.15 where there is extensive shear deformation around the rib’s centre axis.

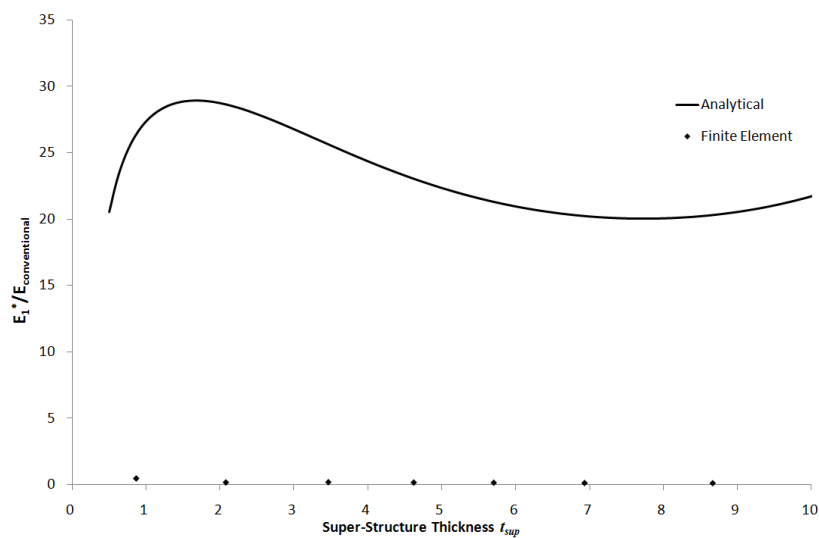


Figure 5.14: The FE and analytical model prediction of in-plane Young’s modulus vs t_{sup} for a functionally graded hierarchical honeycomb (normalised to that of a conventional honeycomb of similar relative density) with an 80/7.5/7.5/5 distribution of the sub-structure and a relative density $\rho_{rel}^* = 0.00577$, when $l_{sup} = 10$.

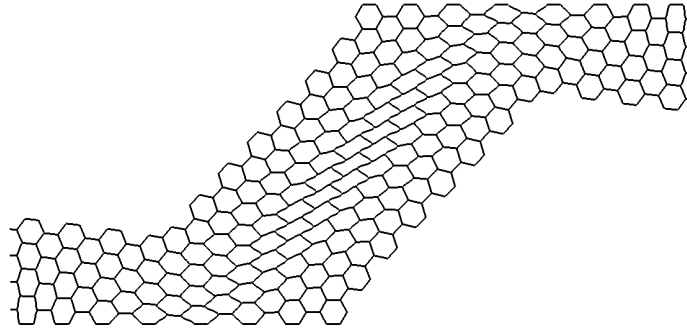


Figure 5.15: Deformation of a functionally graded hierarchical honeycomb with a (80/7.5/7.5/5) distribution, a super-structure aspect ratio $\alpha_{sup}= 2.17$ and a relative density $\rho_{rel}^*=0.005774$. It can be seen that the centre of the super-structure ribs are shearing and elastically buckling. A deformation factor of 10 has been applied to this image.

Super-structures with higher aspect ratios exhibit markedly less shear and lie closer to the predictions of the analytical model, especially when the mass is uniformly distributed in the sub-structure as can be seen in Figure 5.11.

5.5 Discussion

It is possible for the stiffness of hierarchical honeycombs to exceed that of a 1st order honeycomb with either a uniform or some non-uniform mass distributions, see Figure 5.5a and Figure 5.5c. In this study it was possible to exceed the stiffness by factors up to 2, though further improvements could be possible. This enhancement was only possible with super-structures with aspect ratios of at least of 2.88, and arises because the super-cell ribs of the functionally graded hierarchical honeycombs have larger flexural stiffness's (i.e. the product of E and I). Relative density has no effect upon performance *vs* a 1st order honeycomb, at least within the range studied here as shown in Figure 5.6, Figure 5.7, Figure 5.8 and Figure 5.9 where distribution maintain the same sequence despite the change in relative density.

The difference in performance between the uniform and non-uniform distributions is interesting since it points to the fundamental problem in hierarchy in flexure dominated structures. That is the flexural stiffness (EI product) and therefore a hexagonal cell's stiffness is dominated by a $(t/l)^3$ term, which means that changes in rib thickness have profound effects upon elastic properties. The non-uniform distributions perform very badly at low super-structure aspect ratios because of significant shear deformation taking place in the centre of the super-structure ribs, since their shear stiffness has been reduced by redistribution of mass. It is only when super-structure ribs become relatively slender that the excessive shear deformation is less apparent, the extra mass in the edges of the super-cell ribs enhances flexural stiffness.

For similar reasons the more extreme distributions (e.g. 80/7.5/7.5/5) perform very badly within the range of aspect ratios considered here. The analytical models cannot capture the shearing within the super-cell ribs because use of the section transform method requires the shear strain to be uniform across the rib thickness, which is not so for the non-uniform distributions. The correction for the true effective length of the super-cell rib in the analytical model appears to work well, with a better fit to the FE data for low aspect ratio (high t_{sup}) ribs, see Figure 5.10

Functional grading would no doubt incur a penalty in terms of manufacturing speeds and costs, and so would only be introduced if the performance benefit outweighed these penalties. The results herein indicate that hierarchy and functional grading of

honeycombs can be beneficial, but that extra stiffness only arises with hierarchy alone (uniform distribution) when the super-structure's aspect ratio is larger than approximately 1 as can be seen in Figure 5.10, and for functionally graded hierarchical honeycomb (non-uniform distribution) at aspect ratios of approximately 11 or more. It seems possible that a uniform mass distribution would be easier to manufacture than a non-uniform distribution, and if so the optimal super-structure aspect ratio is between 3 and 5. The analytical model similarly demonstrates a peak in stiffness at middling aspect ratios due to trade-off between minimal shear deformation in the sub and super-structures.

5.6 Conclusions

The aim of this investigation was to understand how the in-plane elastic properties of honeycombs were affected by functionally graded or hierarchical honeycombs, and to find if the Young's modulus could be improved on an equal density basis with respect to a conventional (first order) honeycomb.

It is clear that the distribution of mass (specifically sub-cell rib thicknesses) within the super-structure has a strong effect on the Young's modulus, see Figure 5.5. The aspect ratio of the super-structure, α_{sup} , determines which mass distribution is most favourable, since the aspect ratio determines the extent of shear deformation within the super-structure. It is for this reason that the more extreme mass distributions performed less well *vs* the uniform or more gentle distributions, see Figure 5.5 that the analytical models failed to predict well, see Figure 5.10 and Figure 5.12. There are three distinct regimes in the stiffness of honeycombs, i) for very low aspect ratio hierarchical honeycombs, $\alpha_{sup} < 1.2$, a first order (conventional) honeycomb is stiffest, ii) for low aspect ratio hierarchical honeycombs, $1.2 < \alpha_{sup} < 10$, a uniform mass distribution hierarchical honeycomb is stiffer than a conventional honeycomb by 45%, and iii) for higher aspect ratios, $\alpha_{sup} > 10$, some functionally graded hierarchical honeycomb mass distributions are stiffer than conventional honeycombs by 100%.

There are pragmatic manufacturing limits regarding hierarchical honeycombs of uniform or functionally graded configurations. It is likely that functionally graded hierarchical honeycombs would prove very difficult or impossible to manufacture via conventional methods such as the expansion method Gibson and Ashby (1997), and would rely on alternative techniques such as additive layer manufacture. It is possible that hierarchical honeycombs with uniform mass distributions could be manufactured by adapting conventional methods such as the expansion method with subsequent selective cell removal.

Chapter 6. In-Plane Plasticity and Non-Linear Response

6.1 Introduction

Honeycombs are popular for sandwich core and energy absorbing applications. The work undertaken here investigates the elastic-plastic response of hierarchical honeycombs that have a functionally graded sub-structure and a NPR sub-structure. It is thought that the introduction of functionally graded and NPR sub-structures by the implementation of hierarchy will increase the elastic stiffness and energy absorption properties of the honeycombs, prior to the onset of plastic yield of the constituent material. It thought that for low relative density structures the introduction of functional grading hierarchical honeycombs could delay elastic buckling where it would otherwise be the first mode of failure. The stress strain response has been investigated along with the elastic strain energy and plastic strain energy of hierarchical honeycombs, looking at the failure of sub or super-structure ribs. The elastic regime along with the onset of plasticity has been investigated for hierarchical honeycombs and compared to the response of conventional triangular and hexagonal honeycombs.

The aim of this chapter is to investigate the elastic response, considering the onset of elastic buckling as well as the onset of plasticity of hierarchical honeycombs which have been previously investigated in the elastic regime. These hierarchical honeycombs have shown potential increases in favourable properties such as Young's modulus and the potential to delay the onset of elastic buckling and plastic yield. The onset of plasticity in many applications is often considered failure of the structure and is avoided. Whilst the in-plane properties are the focus of this chapter the out-of-plane properties have been investigated in the following chapter.

6.2 Method

The in-plane plastic response of functionally graded and NPR hierarchical honeycombs was calculated via numerical models which considered each unit cell as a discrete structure, and made no assumptions about sub-cells as continua.

6.2.1 Functionally Graded

Models previously described for functionally graded hierarchical honeycombs for which simulations were undertaken in the elastic regime only, were extended to the plastic regime by introducing non-linear geometry and non-linear material properties. Specifically, functionally graded hierarchical structures where 100% of the mass was distributed within the sub-structure were investigated. It is important to note that the super-structure parameters are independent of that of the sub-structure, unless a specific relative density is specified at which point there is a connection between the super-structure aspect ratio and the sub-structure aspect ratio. The super-structure geometry is defined by the global sub-structure geometry as the sub-structure is effectively the constituent material of the super-structure. The sub-structures co-ordination number is independent from that of the super-structure, both of which can be varied for a range of geometries. Co-ordination numbers investigated were (3-3), (3-6), (6-6) and (6-3) for a range of super-structure aspect ratios, specifically for hexagonal super-structures $\alpha = 11.5$, $\alpha = 4.8$, $\alpha = 2.88$, $\alpha = 2.16$, $\alpha = 1.44$ and $\alpha = 1.15$ the extremes of which are shown in Figure 6.1, Figure 6.2 and specifically for triangular super-structures $\alpha = 11.5$, $\alpha = 4.8$, $\alpha = 2.88$ and $\alpha = 2.16$ the extremes of which are shown in Figure 6.3 and Figure 6.4. The two lower aspect ratio super-structures are not included for the triangular super-structure as due to the geometry of the triangular honeycomb the structure would simply be a conventional honeycomb array. Initially models with a relative density of $\rho_{rel}^* = 0.00577$ were investigated, but at such low relative densities elastic buckling was pervasive and dominant, so a higher relative density of $\rho_{rel}^* = 0.0577$ was also investigated to explore the onset of local plasticity and the changes in relative density. A single mass distribution of 100% was investigated for functionally graded structures as it is clearly the most advantageous distribution in terms of the initial elastic response. Models were established in a similar way to those previously described in Chapter 3

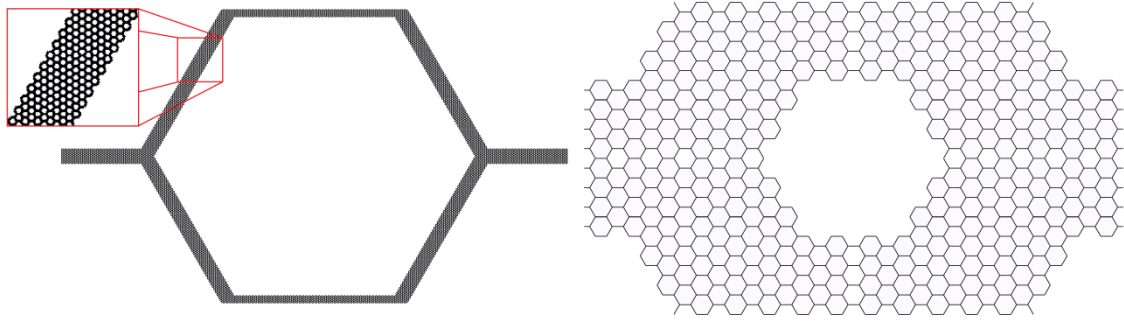


Figure 6.1: Shows how the sub and super-structure dimensions change for a hexagonal super-structure and hexagonal sub-structure hierarchical honeycomb for a) when the super-structure aspect ratio $\alpha_{sup} = 11.5$ and b) when the super-structure aspect ratio $\alpha_{sup} = 1.15$.

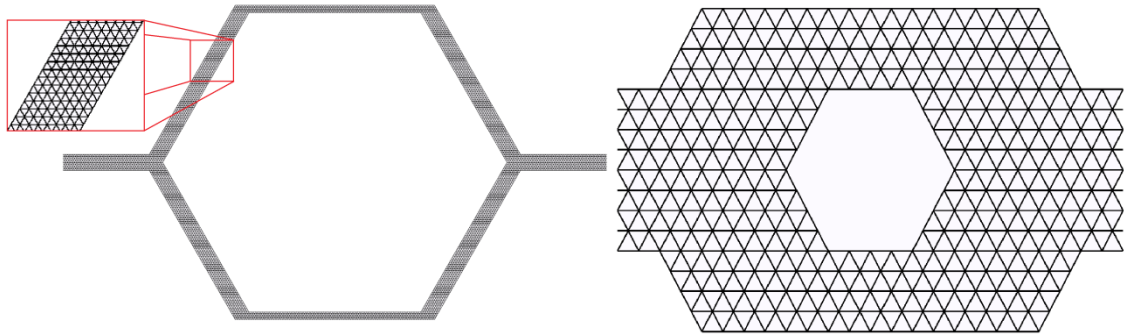


Figure 6.2: Shows how the sub and super-structure dimensions change for a hexagonal super-structure and triangular sub-structure hierarchical honeycomb for a) when the super-structure aspect ratio $\alpha_{sup} = 11.5$ and b) when the super-structure aspect ratio $\alpha_{sup} = 1.15$.

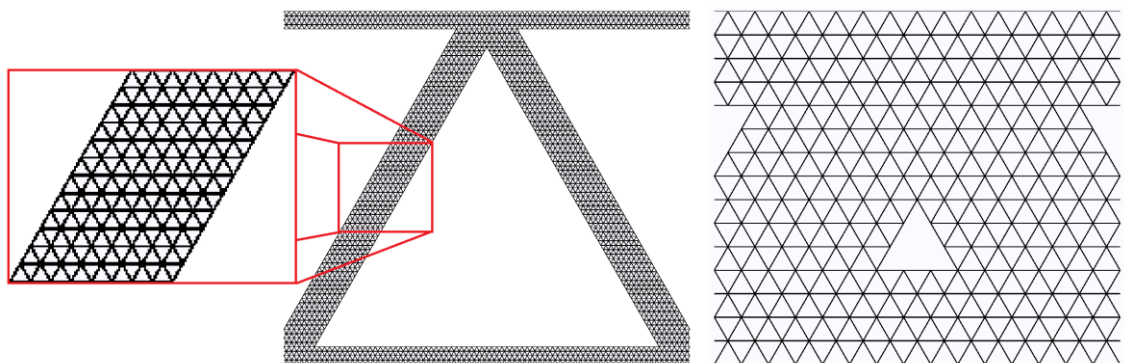


Figure 6.3: Shows how the sub and super-structure dimensions change for a triangular super-structure and triangular sub-structure hierarchical honeycomb for a) when the

super-structure aspect ratio $\alpha_{sup} = 11.5$ and b) when the super-structure aspect ratio $\alpha_{sup} = 2.16$.

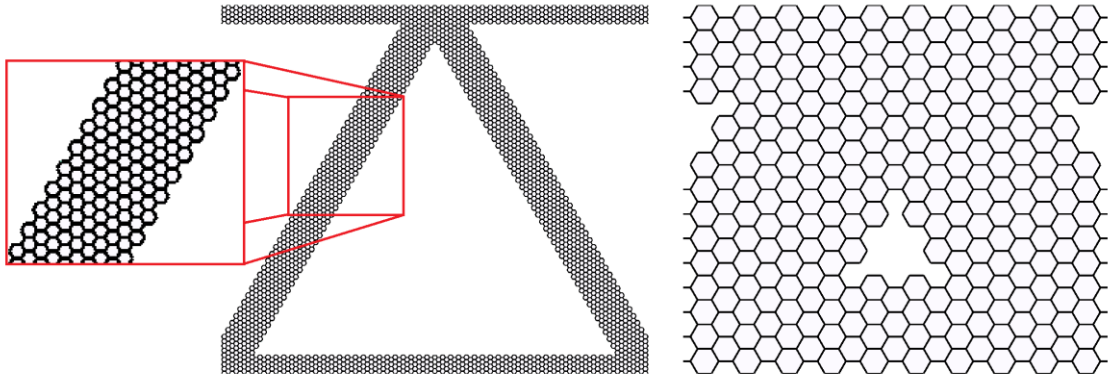


Figure 6.4: Shows how the sub and super-structure dimensions change for a triangular super-structure and hexagonal sub-structure hierarchical honeycomb for a) when the super-structure aspect ratio $\alpha_{sup} = 11.5$ and b) when the super-structure aspect ratio $\alpha_{sup} = 2.16$.

6.2.2 NPR

Models previously described for NPR sub-structures, for which simulations were undertaken in the elastic regime only, were extended to the plastic regime by introducing non-linear geometry and non-linear material properties. NPR sub-structures were investigated for a range of mass distributions. Hierarchical honeycombs with a NPR sub-structure were also investigated for a range of internal angles from -2.5 to -27.5 for a range of mass distributions of 25%, 50% and 75%. A range of mass distributions were investigated for NPR sub-structure models as it has a definite effect in the response of the structures. Models were established in a similar way to those previously described in Chapter 4.

6.2.3 Finite Element Model

Two dimensional finite element models were generated for each unique unit cell. The cells were the same as those developed in Chapters 3 & 4. The constitutive material is initially elastic and then exhibits plastic behaviour, to model this a set of linear isotropic elastic constants were chosen consistent with previous elastic models and used for all cases (specifically $E_s = 1600$ MPa, $G_s = 593$ MPa and $\nu_s = 0.35$) (Miller 2010 & Caulfield 2007) the non-linear material behaviour was specified as elasto-plastic

response. The nonlinear material behaviour was modelled by strain increments and assumed to consist of an elastic part and an inelastic part similar to that proposed (Chung & Waas 2001) (Papka & Kyriakides 1998). The plastic material properties were defined as a yield stress $\sigma_{yield} = 44\text{MPa}$ corresponding to a plastic strain $\varepsilon_{pl} = 0$. Non-linear geometry was specified along with the selection of internal energy E_I and plastic strain energy E_p (Plastic deformation energy) as a history output request to report the energy absorption for the whole model. The output for E_I can be described as in Equation 6-1.

$$E_I = E_S + E_P$$

Equation 6-1

Where E_s = Recoverable strain energy and E_p = Energy absorbed by plastic deformation. This equation is simplified as dissipated energy through creep, electrostatic and other effects can be ignored in this simplified model.

The step used was specified as '*Static, Riks*' which uses the load magnitude as an additional unknown and solves simultaneously for loads and displacements. The '*Static Riks*' step is used due to the issues involved with buckling or collapse behaviour of geometrically non-linear static problems, where the load-displacement response shows a negative stiffness resulting in the structure releasing strain energy to remain in equilibrium similarly to (Shariati & Rokhi 2008, Waas 2002 and Kim & Lee 2002). The Riks method allows static equilibrium states during the unstable phase of the response and is used to predict unstable, geometrically nonlinear collapse of a structure including the nonlinear material behaviour. The strain applied to the model was increased from 0.1% in the elastic regime to 50% to investigate the plastic regime, but due to use of '*Static Riks*' it was not possible to specify the exact strain on the model as an arc length is used to define the progress of the model not a force or a displacement. The sub and super-cells were modelled using a minimum of 20 2D Timoshenko beam elements (B22: a 3-node quadratic beam) per cell rib (Papka & Kyriakides 1998) (Chung & Waas 2001) using a commercial Finite Element (FE) analysis package (ABAQUS, version 6.9. Dassault Systèmes). Boundary sharing ribs had either half thickness or half-lengths, so that the symmetry of the model allowed tessellation of the cell which can be used to

model a honeycomb the boundary conditions were the same as those applied to previous models investigated in Chapters 3 & 4 which are consistent with (Odegard 2004).

As previously described history outputs were created to extract data from the models. Specifically the reaction force on the displaced face along with the displacement for each increment also requested was the internal energy and plastic strain energy. The reaction force normal to the displaced face and the displacement were used to create the stress strain graph as the projected area was known along with the original height of the model. The internal energy was plotted directly against the strain and the plastic strain energy divided by the internal energy also plotted against the strain. These graphs can subsequently be used to determine if the structure is undergoing elastic buckling or plastic yield. For example if a stress strain graph shows a non-linear response at certain strain, the graph could be compared to the plastic strain energy graph. If there is plastic strain energy at the same strain then the structure has plastically yielded however if there is no plastic strain energy at the strain then the structure has elastically buckled.

Whilst the inclusion of non-linear geometry and material properties were incorporated into the model, this was the extent of the model. As the aim of the study is to compare the non-linear elastic response and plastic yield of hierarchical honeycombs to conventional honeycombs, the response up to the yield of the material is considered accurate and is validated in the later experimental chapter. However some models show large strains and a large post yield response with no sign of further fracture or failure, this is a limitation of the model. No attempt to predict the possible areas of fracture have been made depending on the initial onset of plasticity as due to the complex nature of the structures stress concentrations could be move post yield. It is also true to say that imperfections that may occur due to manufacture and the onset of fracture were ignored as they were not within the scope of the study. FE models are validated in Chapter 8, which directly compare models used to investigate the elastic and plastic regime to experimental results.

The (6-6) hierarchical honeycomb was further investigated with the material properties of 52100 bearing steel and aluminium AA356.0 at a relative density of $\rho_{rel}^* = 0.00577$. The material properties of 52100 bearing steel was defined as $E_{st} = 205.0\text{GPa}$ and $\sigma_{yst} = 1.01\text{GPa}$ as specified in (Gupta *et al* 1993) and for aluminium AA356.0 $E_{al} = 72\text{GPa}$,

$G_{al} = 179\text{MPa}$ and $\sigma_{yal} = 164\text{MPa}$ as specified in (Hatch 1984). This was done to investigate the effect of changing the ratio between the Young's modulus and the plastic yield stress that can be achieved by changing the material properties. Specifically examining the onset of plastic yield and elastic buckling. The (6-6) hierarchical honeycomb was chosen as it was the most prone to elastic buckling due to the boundary conditions and higher aspect ratio of sub-structure ribs

6.3 Results

6.3.1 Stress Strain and Internal Energy for $\rho_{rel}^* = 0.00577$

The stress strain response due to in-plane compression simulations using FE are shown for four hierarchical honeycombs of co-ordination number (3-3), (3-6), (6-6) and (6-3) for a relative density of $\rho_{rel}^* = 0.00577$. Each co-ordination number is then further investigated for the effect of changing the super-structure aspect ratio; the results are then compared to the response of hexagonal and triangular conventional honeycombs of the same relative density. Along with the stress strain results, the internal energy (Total strain energy) absorbed by each hierarchical honeycomb is also plotted against strain. The results are then repeated for a relative density of $\rho_{rel}^* = 0.0577$ and include graphs of plastic dissipation energy / internal energy to determine when and to what extent plasticity occurs in each hierarchical honeycomb and compared to conventional honeycombs. The plastic dissipation energy / internal energy are not shown for hierarchical honeycombs of $\rho_{rel}^* = 0.00577$ as no or little plastic strain energy was absorbed by the hierarchical honeycombs investigated. The plastic dissipation energy / internal energy graph was used to determine at what strain a structure experienced plastic strain energy.

6.3.1.1 Hexagonal Super-Structure Hexagonal Sub-Structure (3–3)

The stress strain response of a hexagonal super-structure and hexagonal sub-structure (3–3) hierarchical honeycomb allowing for geometrical and material non-linearities is shown in Figure 6.5. As expected the conventional triangular honeycomb is stiffest in the elastic regime compared to the hierarchical and conventional hexagonal honeycombs. This is due to the loading conditions of hexagonal honeycombs which initially deform due to elastic bending of ribs, whereas the triangular honeycomb is stretch dominated.

It can be seen that there are several hierarchical honeycombs that are stiffer than the conventional hexagonal honeycomb, this concurs with the Young's modulus calculated for the elastic regime in Chapter 3 with current results being identical to those previously presented. The internal energy absorbed by the hierarchical and conventional honeycombs is shown in Figure 6.6, there is little surprise in the results following the stress strain graph in Figure 6.5 but the graph highlights the increased energy absorption

of the conventional triangular honeycomb, whilst hierarchical honeycombs energy absorption performance depends on the super-structure aspect ratio where some are favourable such as when $\alpha_{sup}= 11.5$ and $\alpha_{sup}= 4.80$ when compared to a conventional hexagonal honeycomb whilst $\alpha_{sup}= 1.15$ and $\alpha_{sup}= 1.44$ are not.

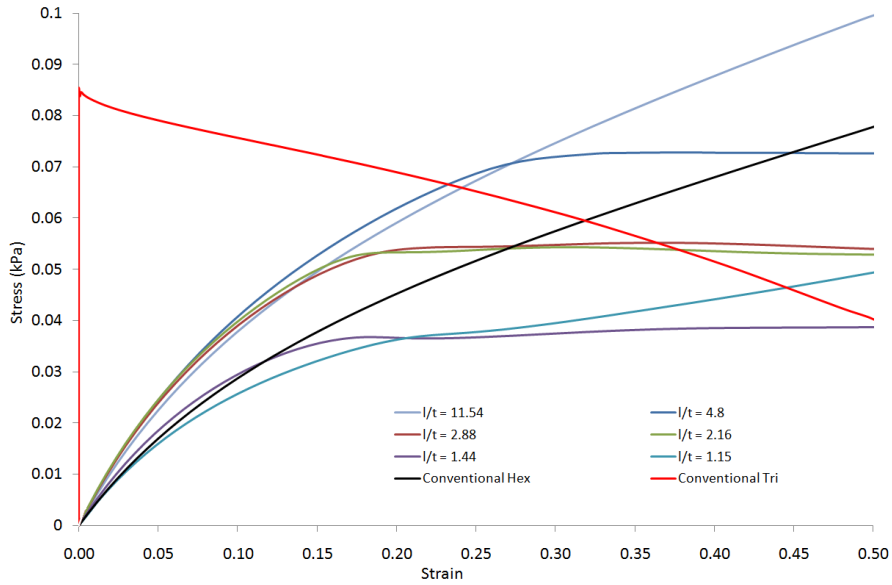


Figure 6.5: Stress Strain response of hierarchical honeycombs with a hexagonal super-structure and a hexagonal sub-structure for multiple super-structure aspect ratios and compared to a conventional triangular and hexagonal conventional honeycomb for a relative density $\rho_{rel}^* = 0.00577$.

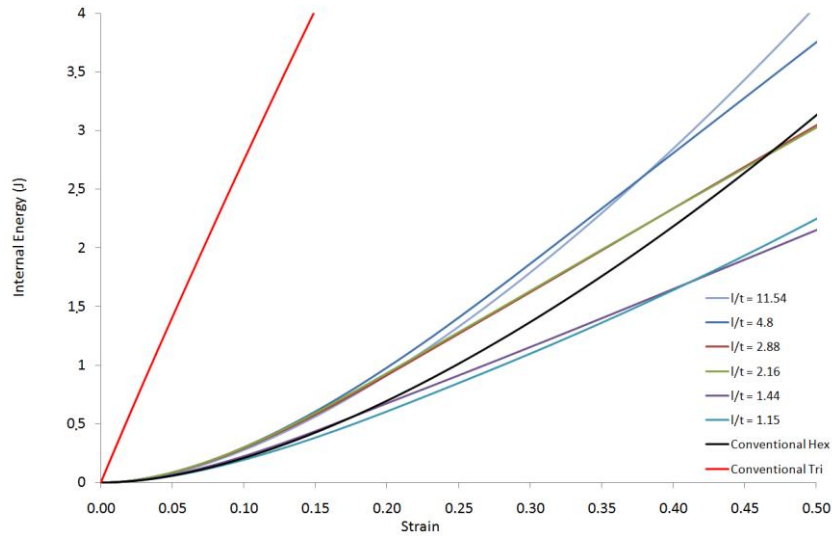


Figure 6.6: Internal energy absorbed by models against applied strain for hierarchical honeycombs with a hexagonal super-structure and a hexagonal sub-structure for multiple super-structure aspect ratios and compared to a conventional triangular and hexagonal conventional honeycomb for a relative density $\rho_{rel}^* = 0.00577$.

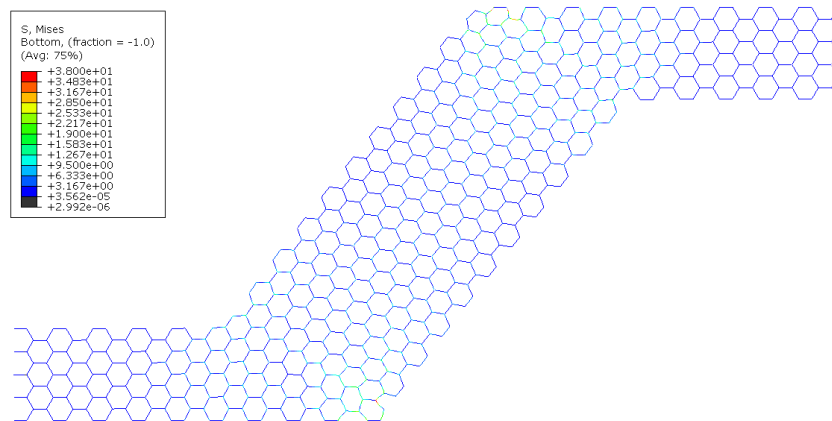


Figure 6.7: Deformation plot of a (3-3) hierarchical honeycomb with a super-structure aspect ratio $\alpha_{sup} = 2.88$.

6.3.1.2 Hexagonal Super-Structure Triangular Sub-Structure (3-6)

The stress strain response of a hexagonal super-structure triangular sub-structure (3-6) honeycomb is shown in Figure 6.8. The purely stretch dominated conventional triangular honeycomb is elastically stiffest and the bending dominated conventional hexagonal honeycomb is the most compliant, whilst the hierarchical honeycombs are a compromise between the two. The lower super-structure aspect ratio deformations

appear to be more stretch dominated with a higher elastic stiffness and the early onset of elastic buckling and the higher super-structure aspect ratio deformation appears to be more bending dominated with a lower elastic stiffness but with a delayed and more progressive elastic buckling. This can be seen as higher aspect ratios tend to the conventional hexagonal and lower aspect ratios tend to the conventional triangular honeycomb. Similarly to the (3-3) co-ordination hierarchical honeycombs the (3-6) hierarchical honeycombs initially deform due to elastic bending of ribs, this is due to the bending dominated super-structure creating rotations for the bending dominated sub-structure at super-structure nodes. It is again important to note that the initial Young's modulus determine in the elastic regime is consistent with previous results in Chapter 3.

The internal energy absorbed by the hierarchical and conventional honeycombs is shown in Figure 6.9, as expected it shows the greater energy absorption of the conventional triangular honeycomb, whilst hierarchical honeycombs energy absorption performance depends on the super-structure aspect ratio. The higher aspect ratio super-structures tend towards the conventional hexagonal honeycomb response and the lower aspect ratio super-structures tend towards the conventional triangular.

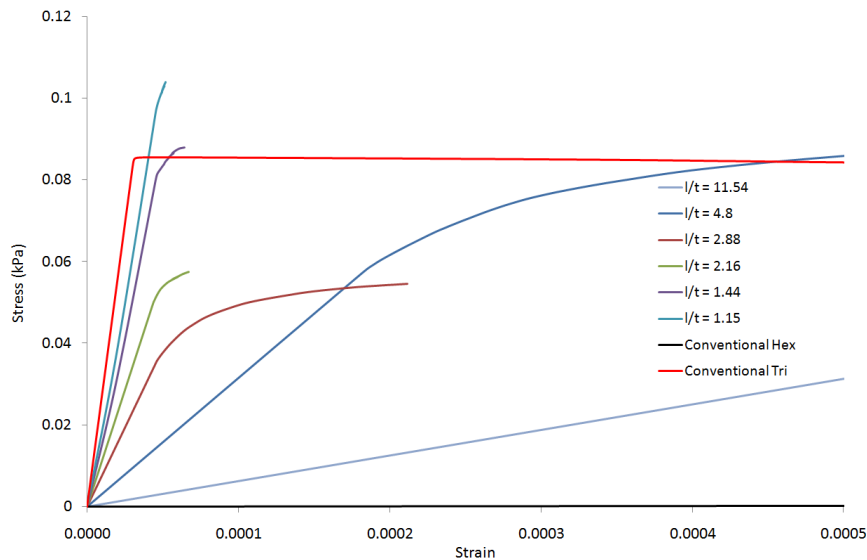


Figure 6.8: Stress Strain response of hierarchical honeycombs with a hexagonal super-structure and a triangular sub-structure for multiple super-structure aspect ratios and compared to a conventional triangular and hexagonal conventional honeycomb for a relative density $\rho_{rel}^* = 0.00577$.

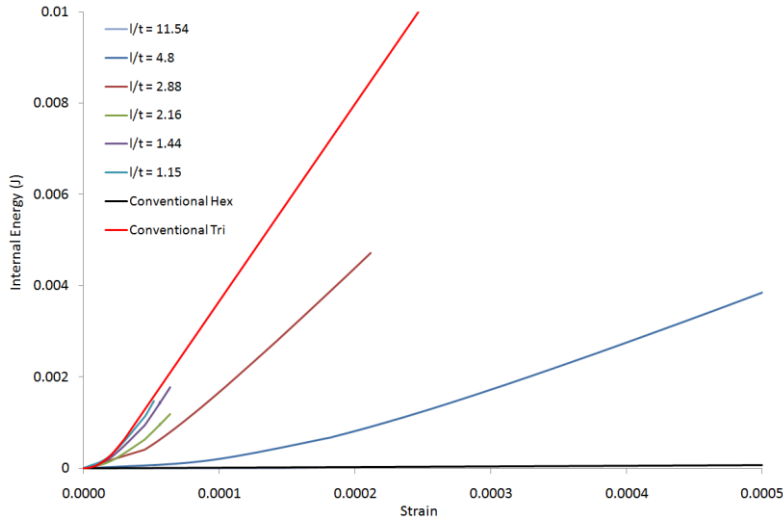


Figure 6.9: Internal energy absorbed by models against applied strain for hierarchical honeycombs with a hexagonal super-structure and a triangular sub-structure for multiple super-structure aspect ratios and compared to a conventional triangular and hexagonal conventional honeycomb for a relative density $\rho_{rel}^* = 0.00577$.

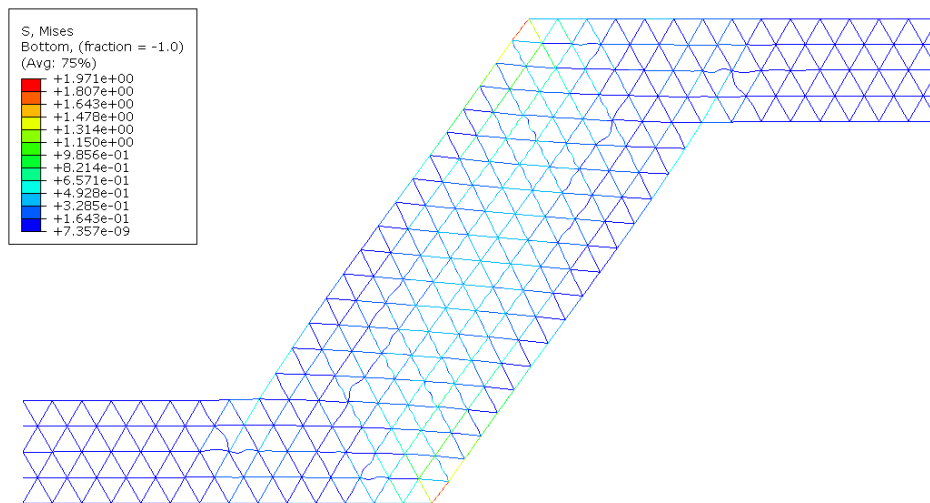


Figure 6.10: Deformation plot of a (3-6) hierarchical honeycomb with a super-structure aspect ratio $\alpha_{sup} = 2.88$.

6.3.1.3 Triangular Super-Structure Triangular Sub-Structure (6-6)

The stress strain response of a triangular super-structure triangular sub-structure (6-6) honeycomb is shown in Figure 6.11. The stretch dominated hierarchical and conventional triangular honeycomb are orders of magnitudes elastically stiffer than the more compliant bending dominated conventional hexagonal honeycomb. It can be seen

that low super-structure aspect ratio hierarchical honeycombs are stiffest with $\alpha_{sup}= 2.16$ being comparable to the conventional triangular honeycomb. However the high super-structure aspect ratio hierarchical honeycombs elastically buckle at a higher stress and strain resulting in greater energy absorption prior to elastic buckling as shown in Figure 6.12. Elastic buckling is defined at the strain at which the stress strain curve diverges from the initial linear elastic region of the graph. This is differentiated from plastic yield of the constituent material due to zero plastic strain energy present in the whole model at the same strain.

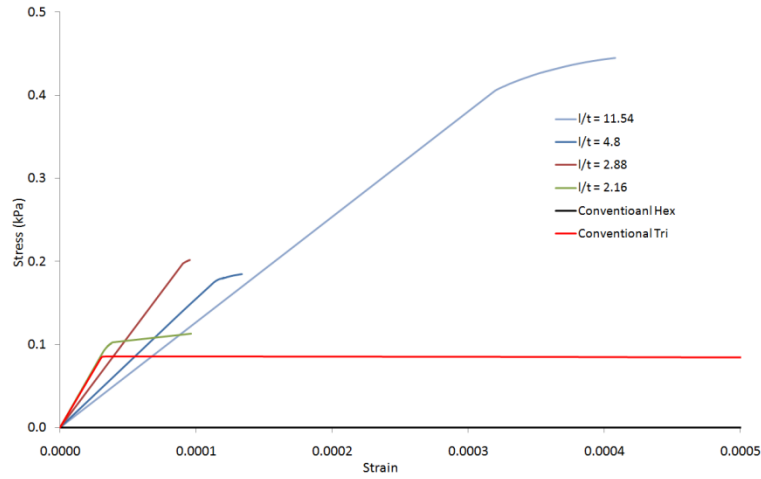


Figure 6.11: Stress Strain response of hierarchical honeycombs with a triangular super-structure and a triangular sub-structure for multiple super-structure aspect ratios and compared to a conventional triangular and hexagonal conventional honeycomb for a relative density $\rho_{rel}^* = 0.00577$.

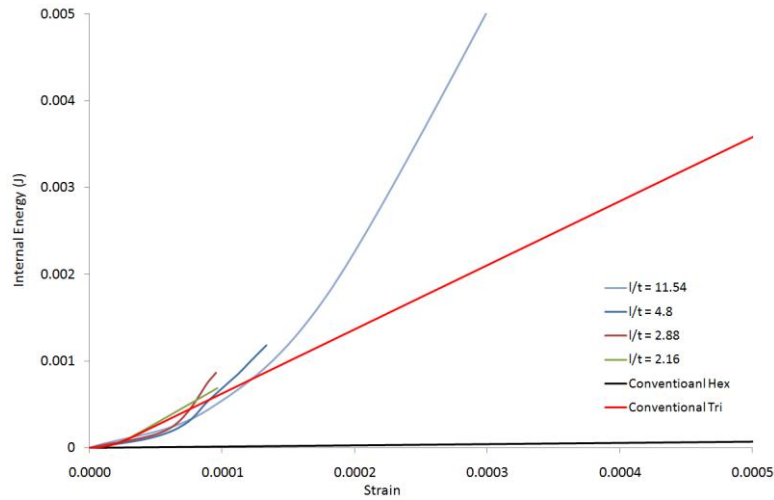


Figure 6.12: Internal energy absorbed by models against applied strain for hierarchical honeycombs with a triangular super-structure and a triangular sub-structure for multiple super-structure aspect ratios and compared to a conventional triangular and hexagonal conventional honeycomb for a relative density $\rho_{rel}^* = 0.00577$.

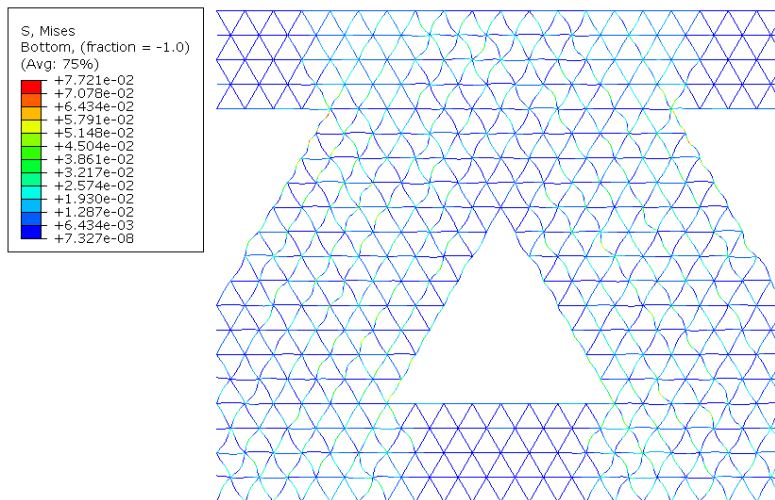


Figure 6.13: Deformation plot of a (6-6) hierarchical honeycomb with a super-structure aspect ratio $\alpha_{sup} = 2.88$.

6.3.1.4 Triangular Super-Structure hexagonal Sub-Structure (6–3)

The stress strain response of a triangular super-structure hexagonal sub-structure (6–3) honeycomb is shown in Figure 6.14. The majority of hierarchical honeycombs are more

compliant than the conventional hexagonal honeycomb and as a result have poor internal energy absorption prior to the onset of elastic buckling as shown in Figure 6.15. However one hierarchical honeycomb does considerably outperform the conventional hexagonal honeycomb when $\alpha_{sup}= 11.5$ and even has a greater internal energy absorption than a conventional triangular honeycomb for strains greater than 14%.

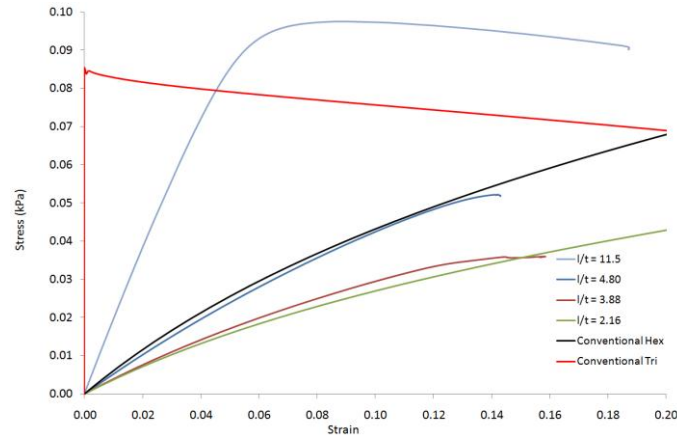


Figure 6.14: Stress Strain response of hierarchical honeycombs with a triangular super-structure and a hexagonal sub-structure for multiple super-structure aspect ratios and compared to a conventional triangular and hexagonal conventional honeycomb for a relative density $\rho_{rel}^* = 0.00577$.

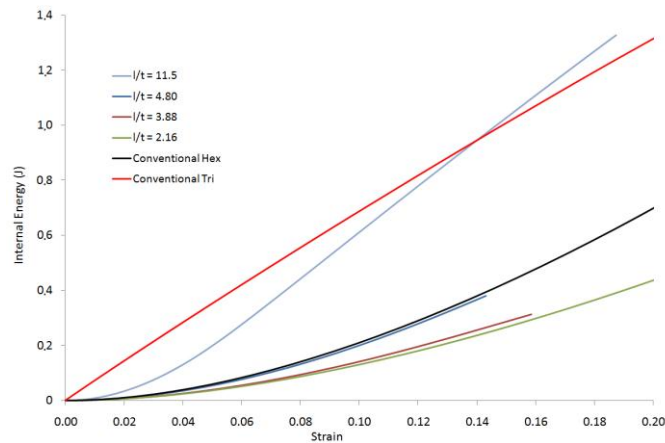


Figure 6.15: Internal energy absorbed by models against applied strain for hierarchical honeycombs with a triangular super-structure and a hexagonal sub-structure for multiple

super-structure aspect ratios and compared to a conventional triangular and hexagonal conventional honeycomb for a relative density $\rho_{rel}^* = 0.00577$.

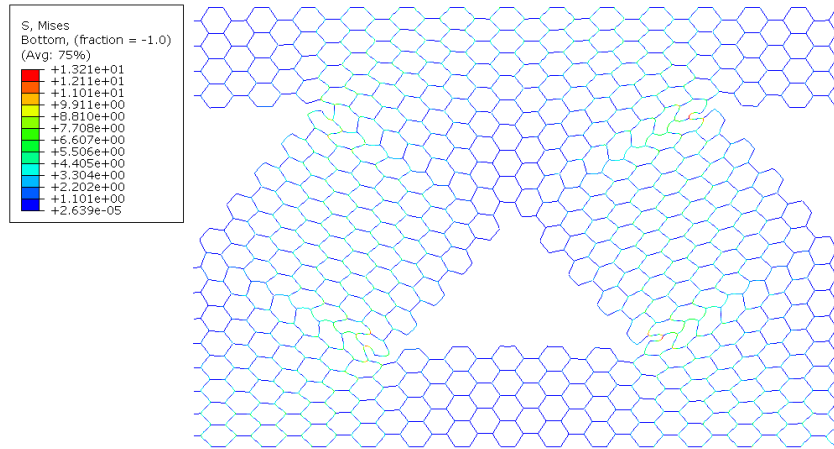


Figure 6.16: Deformation plot of a (6-3) hierarchical honeycomb with a super-structure aspect ratio $\alpha_{sup} = 2.88$.

Due to the very low relative density $\rho_{rel}^* = 0.00577$ honeycombs, the sub and super-structure beams underwent elastic bending or buckled depending on the beams loading conditions due to the inclusion of non-linear geometry, but did not experience any plastic deformation despite the inclusion of non-linear material properties.

6.3.2 Stress, Strain and Internal Energy for $\rho_{rel}^* = 0.0577$

To be able to investigate the onset of plasticity in hierarchical honeycombs the relative density was increased to model hierarchical honeycombs with a relative density of $\rho_{rel}^* = 0.0577$.

6.3.2.1 Hexagonal Super-Structure Hexagonal Sub-Structure (3–3)

The stress strain response of a hexagonal super-structure hexagonal sub-structure (3–3) honeycomb is shown in Figure 6.17. As in the previous section the conventional triangular honeycomb is elastically stiffer than the other structures and elastically buckles prior to the onset of plastic deformation. This can be deduced due to the fact that the stress strain response shows non-linearity at a strain of approximately $\epsilon = 0.003$ but does not show any plastic deformation energy until a strain of approximately $\epsilon = 0.01$. It can be seen that there are several hierarchical honeycombs that are stiffer than the conventional hexagonal honeycomb but they all experience plastic yield at a much

lower strain than the conventional honeycomb. The non-linear response of the conventional and triangular honeycombs is consistent with the response predictions outlined by (Wang and McDowell 2004) depending on the parameters and the constituent material properties.

The internal energy absorbed by the hierarchical and conventional honeycombs is shown in Figure 6.18; the results are consistent with what would be expected from Figure 6.17 which highlights the increased energy absorption of the conventional triangular honeycomb, whilst hierarchical honeycombs energy absorption performance depends on the super-structure aspect ratio, where some are favourable such as when $\alpha_{sup} = 11.5$ and $\alpha_{sup} = 4.80$ when compared to a conventional hexagonal honeycomb, and others $\alpha_{sup} = 1.15$ and $\alpha_{sup} = 1.44$ are not. The fraction of plastic energy absorption to internal energy is shown in Figure 6.19 it can be seen that the onset of plasticity occurs at a lower strain in a conventional triangular honeycomb and at the greatest strain in a conventional hexagonal honeycomb at approximately $\epsilon = 0.1$ with hierarchical honeycombs positioned between the two which showing plastic yield occurring between strains of approximately $0.03 < \epsilon < 0.05$.

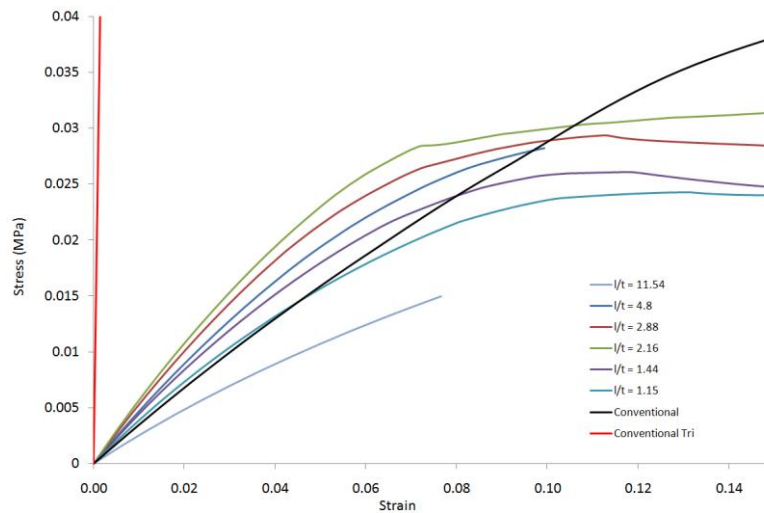


Figure 6.17: Stress Strain response of hierarchical honeycombs with a hexagonal super-structure and a hexagonal sub-structure for multiple super-structure aspect ratios and compared to a conventional triangular and hexagonal conventional honeycomb for a relative density $\rho_{rel}^* = 0.0577$.

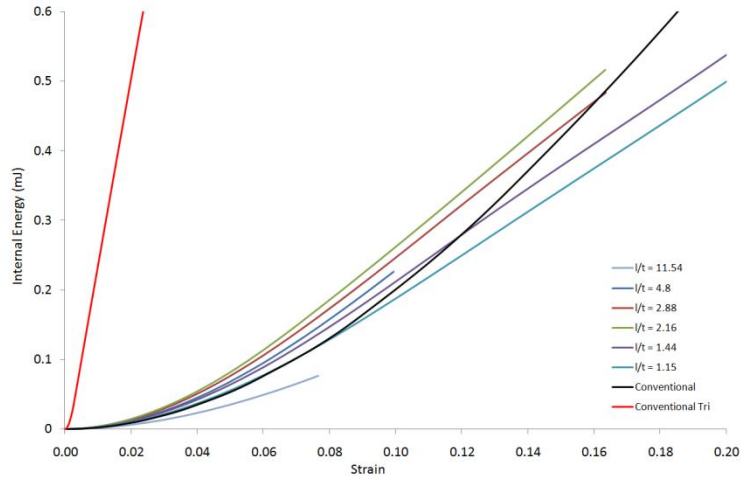


Figure 6.18: Internal energy absorbed by models against applied strain for hierarchical honeycombs with a hexagonal super-structure and a hexagonal sub-structure for multiple super-structure aspect ratios and compared to a conventional triangular and hexagonal conventional honeycomb for a relative density $\rho_{rel}^* = 0.0577$.

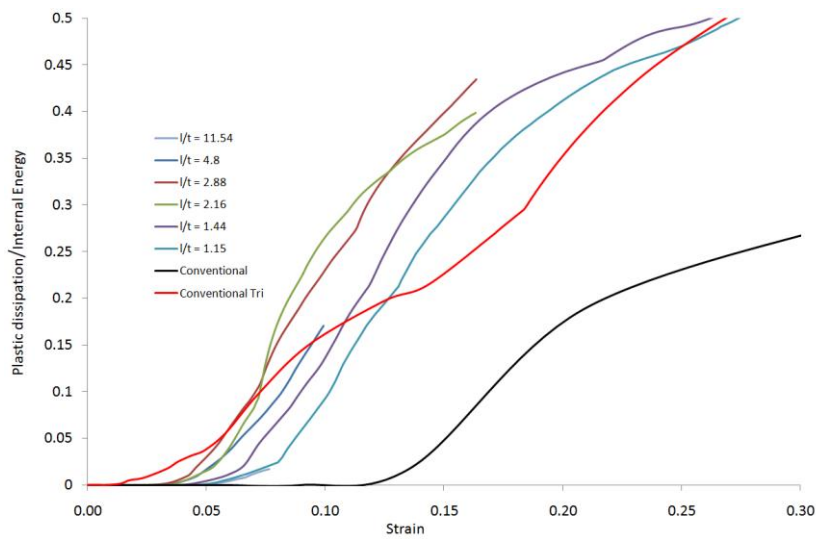


Figure 6.19: Shows the extent of plastic energy absorption as a fraction of internal energy absorbed by the structure against applied strain for hierarchical honeycombs with a hexagonal super-structure and a hexagonal sub-structure for multiple super-structure aspect ratios and compared to a conventional triangular and hexagonal honeycomb for a relative density $\rho_{rel}^* = 0.0577$.

6.3.2.2 Hexagonal Super-Structure Triangular Sub-Structure (3–6)

The stress strain response of a hexagonal super-structure triangular sub-structure (3–6) honeycomb is shown in Figure 6.20. The purely stretch dominated conventional triangular honeycomb is elastically stiffest and the bending dominated conventional hexagonal honeycomb is the most compliant whilst the hierarchical honeycombs are a compromise between the two. As when $\rho = 0.00577$ the lower super-structure aspect ratios appear to be more stretch dominated and higher super-structure aspect ratios are more bending dominated. This can be seen as higher aspect ratios tend to the conventional hexagonal honeycomb and the lower aspect ratios tend to the conventional triangular honeycomb.

The internal energy absorbed by the hierarchical and conventional honeycombs is shown in Figure 6.21, as expected it shows the higher energy absorption of the conventional triangular honeycomb, whilst hierarchical honeycombs energy absorption performance depends on the super-structure aspect ratio. The onset of plasticity can be determined by the of fraction plastic energy absorption to internal energy plotted in Figure 6.22 when the plastic energy absorption energy is greater than zero. It can be seen that plastic deformation occurs at lower strains in the hierarchical honeycombs, then in the conventional triangular honeycomb at approximately $\varepsilon = 0.01$ followed by the hierarchical honeycomb when $\alpha_{sup} = 11.5$ at approximately $\varepsilon = 0.045$ then the conventional hexagonal honeycomb at a much higher strain of approximately $\varepsilon = 0.1$.

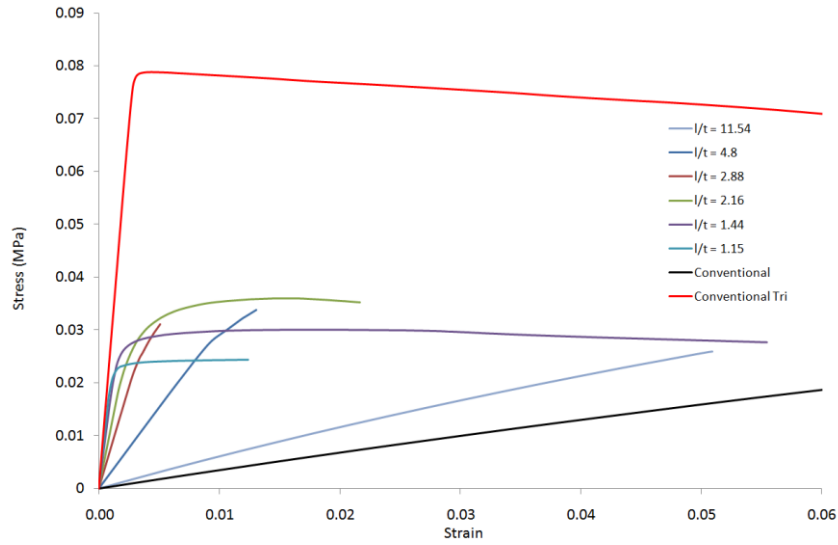


Figure 6.20: Stress Strain response of hierarchical honeycombs with a hexagonal super-structure and a triangular sub-structure for multiple super-structure aspect ratios and compared to a conventional triangular and hexagonal conventional honeycomb for a relative density $\rho_{rel}^* = 0.0577$.

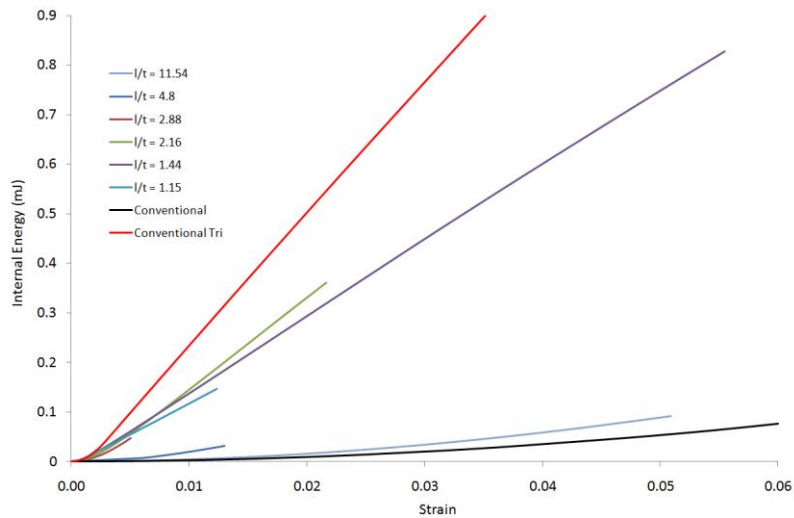


Figure 6.21: Internal energy absorbed by models against applied strain for hierarchical honeycombs with a triangular super-structure and a triangular sub-structure for multiple super-structure aspect ratios and compared to a conventional triangular and hexagonal conventional honeycomb for a relative density $\rho_{rel}^* = 0.0577$.

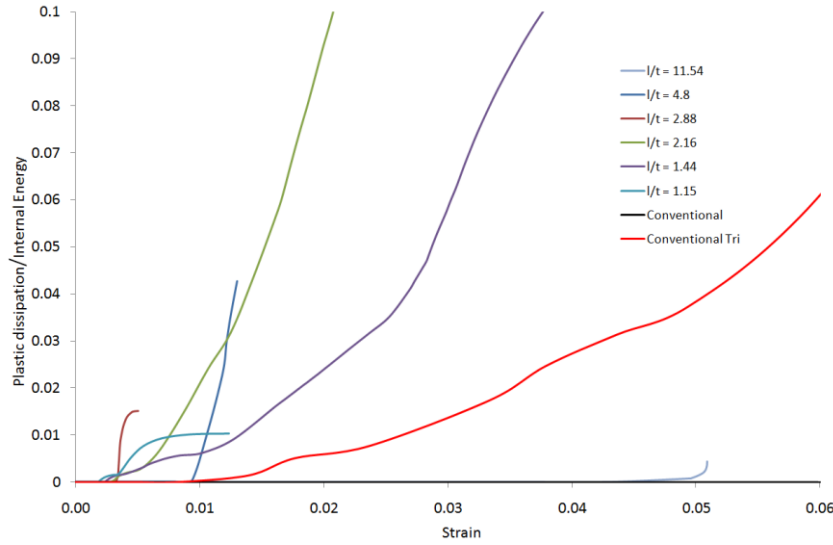


Figure 6.22: Shows the extent of plastic energy absorption as a fraction of internal energy absorbed by the structure against applied strain for hierarchical honeycombs with a hexagonal super-structure and a triangular sub-structure for multiple super-structure aspect ratios and compared to a conventional triangular and hexagonal honeycomb for a relative density $\rho_{rel}^* = 0.0577$.

6.3.2.3 Triangular Super-Structure Triangular Sub-Structure (6–6)

The stress strain response of a triangular super-structure triangular sub-structure (6–6) honeycomb is shown in Figure 6.23. As when $\rho = 0.00577$ the stretch dominated hierarchical and conventional triangular honeycomb are orders of magnitudes stiffer than the more compliant bending dominated conventional hexagonal honeycomb. It can be seen that the lower the super-structure aspect ratio the elastically stiffer the hierarchical honeycomb with $\alpha_{sup} = 2.16$ being comparable to the conventional triangular honeycomb in terms of elastic stiffness. The hierarchical honeycombs with lower super-structure aspect ratios of $\alpha = 2.16$, $\alpha = 2.88$ and $\alpha = 4.80$ elastically buckle at a lower stress and strain resulting in lower energy absorption prior to buckling as shown in Figure 6.24. However it can be seen that as the super-structure aspect ratio increases so does the stress and strain at which buckling occurs. This is highlighted when the super-structure aspect ratio is $\alpha = 11.5$ when the structure elastically buckles at a higher stress and strain than the conventional triangular honeycomb, which ultimately leads to greater energy absorption for strains greater than approximately $\varepsilon = 0.011$ in the hierarchical honeycomb. A plot of plastic energy absorption against internal energy has not been

presented as the stretch dominated nature of the structures resulted in no plastic deformation within considered models.

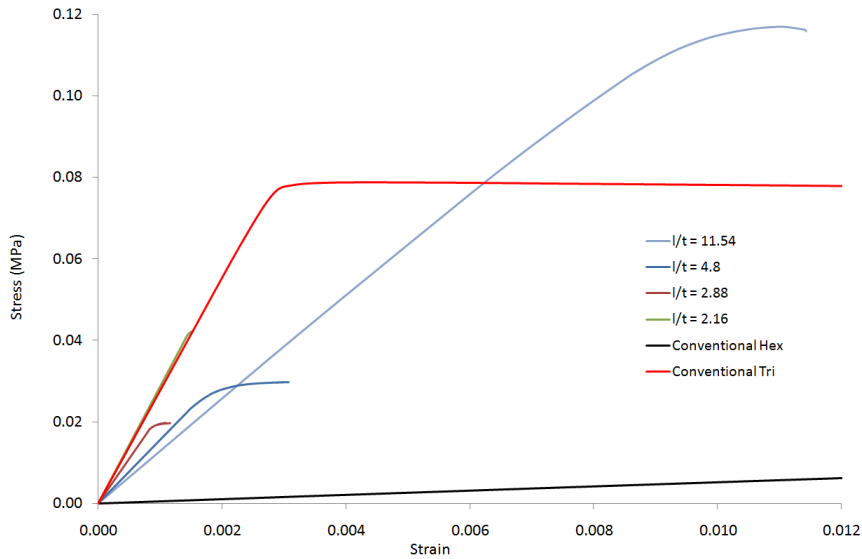


Figure 6.23: Stress Strain response of hierarchical honeycombs with a triangular super-structure and a triangular sub-structure for multiple super-structure aspect ratios and compared to a conventional triangular and hexagonal conventional honeycomb for a relative density $\rho_{rel}^* = 0.0577$.

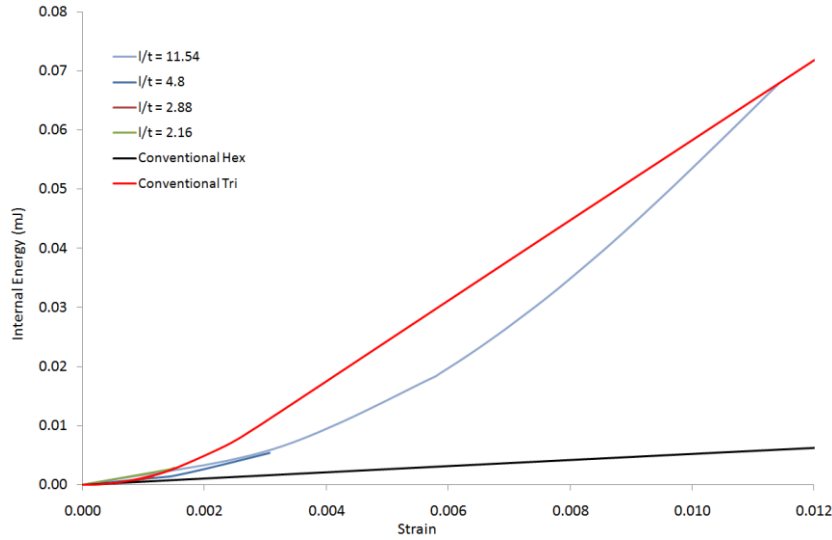


Figure 6.24: Internal energy absorbed by models against applied strain for hierarchical honeycombs with a triangular super-structure and a triangular sub-structure for multiple super-structure aspect ratios and compared to a conventional triangular and hexagonal conventional honeycomb for a relative density $\rho_{rel}^* = 0.0577$.

6.3.2.4 Triangular Super-Structure Hexagonal Sub-Structure (6–3)

The stress strain response of a triangular super-structure hexagonal sub-structure (6–3) honeycomb is shown in Figure 6.25. The majority of hierarchical honeycombs are more compliant than the convention hexagonal honeycomb and as a result have poor internal energy absorption as shown in Figure 6.26. However one hierarchical honeycomb does considerably outperform the conventional hexagonal honeycomb when $\alpha_{sup} = 11.5$ having a considerably higher elastic stiffness and great energy absorption for strains less than $\varepsilon = 0.06$. It can be seen that the onset plastic deformation in the hierarchical honeycombs occurs at lower strain than a conventional hexagonal honeycomb, but at a higher strain than the conventional triangular honeycomb as shown in Figure 6.27.

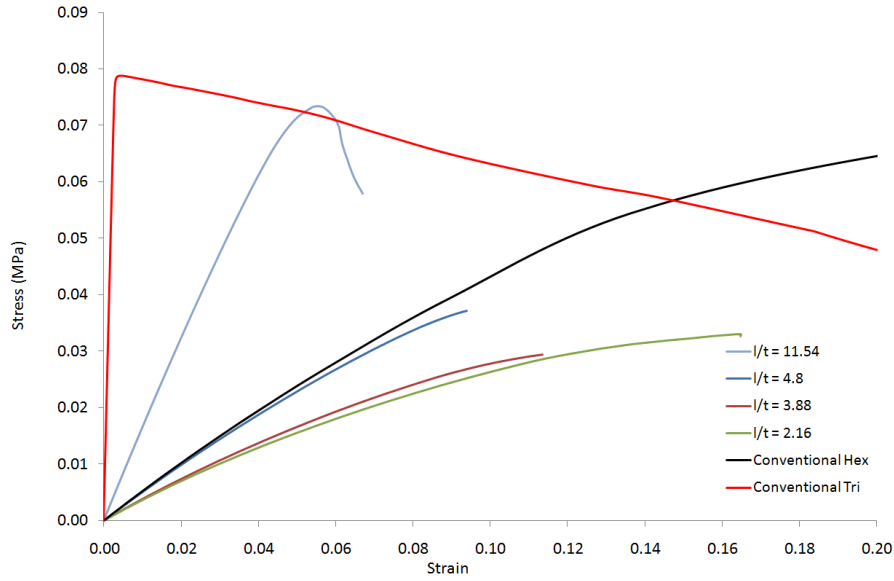


Figure 6.25: Stress Strain response of hierarchical honeycombs with a triangular super-structure and a hexagonal sub-structure for multiple super-structure aspect ratios and compared to a conventional triangular and hexagonal conventional honeycomb for a relative density $\rho_{rel}^* = 0.0577$.

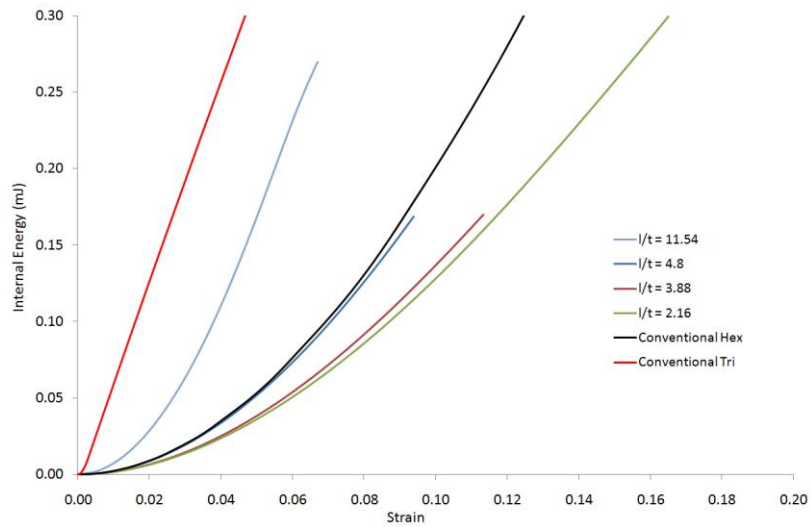


Figure 6.26: Internal energy absorbed by models against applied strain for hierarchical honeycombs with a triangular super-structure and a hexagonal sub-structure for multiple super-structure aspect ratios and compared to a conventional triangular and hexagonal conventional honeycomb for a relative density $\rho_{rel}^* = 0.0577$.

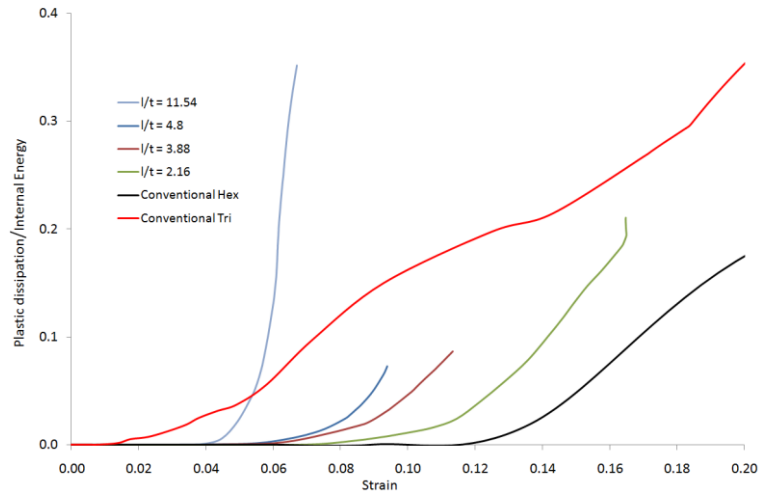


Figure 6.27: Shows the extent of plastic energy absorption as a fraction of internal energy absorbed by the structure against applied strain for hierarchical honeycombs with a triangular super-structure and a hexagonal sub-structure for multiple super-structure aspect ratios and compared to a conventional triangular and hexagonal honeycomb for a relative density $\rho_{rel}^* = 0.0577$.

6.3.3 Triangular Super-Structure Triangular Sub-Structure Aluminium and Steel (6–6)

The stress strain response of (6-6) hierarchical honeycombs with a relative density of $\rho_{rel}^* = 0.00577$ is shown in Figure 6.28 and Figure 6.29 for bearing steel and aluminium AA356.0 respectively. It can be seen that the material response are very similar apart from the increased stress in the steel models, this is expected due to the increased Young's modulus of the material. There is no plastic energy dissipation there for the non-linear response of the stress strain graph is due to elastic buckling of sub-structure ribs.

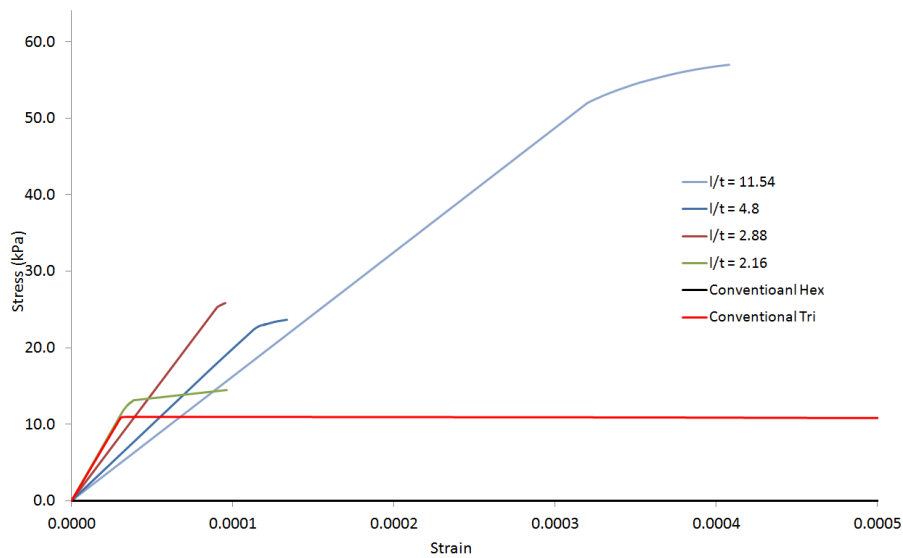


Figure 6.28: Stress Strain response of 52100 bearing steel hierarchical honeycombs with a triangular super-structure and a triangular sub-structure for multiple super-structure aspect ratios and compared to a conventional triangular and hexagonal conventional honeycomb for a relative density $\rho_{rel}^* = 0.00577$.

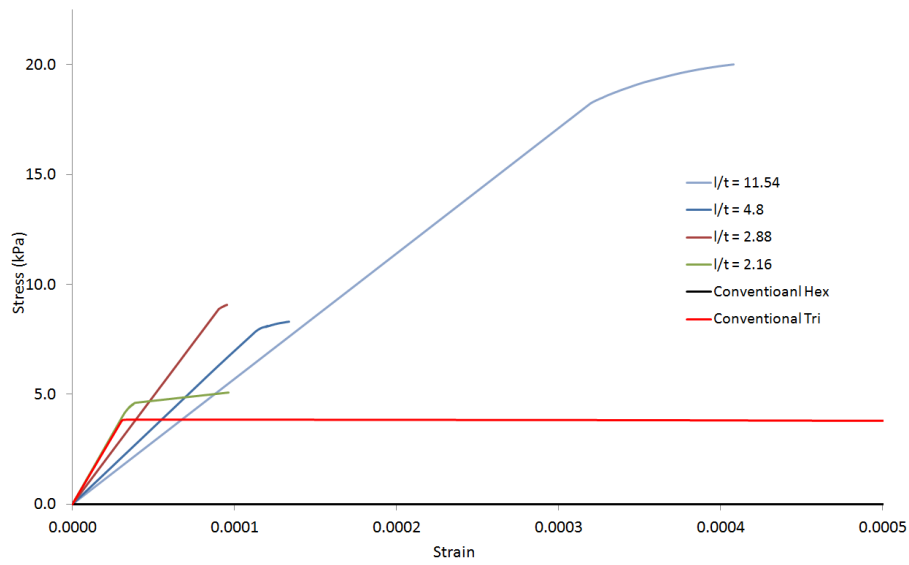


Figure 6.29: Stress Strain response of aluminium AA356.0 hierarchical honeycombs with a triangular super-structure and a triangular sub-structure for multiple super-structure aspect ratios and compared to a conventional triangular and hexagonal conventional honeycomb for a relative density $\rho_{rel}^* = 0.00577$.

6.3.4 Negative Poisson's Ratio Sub-Structure

The result presented in Figure 6.30 to Figure 6.32 show the stress strain response of hierarchical honeycombs with a NPR for mass distributions of 25%, 50% and 75%. Also shown is the stress strain response of a conventional hexagonal honeycomb of the same relative density as a benchmark. There is no plasticity present in the responses shown and changes in the gradient of the stress strain graph are due to elastic buckling of sub-structure ribs. The relationship between the sub and super-structure is complex and it is not possible to predict the buckling stress of individual hierarchical honeycombs. It can be seen that whilst the initial Young's modulus is greater when the mass distribution is 75% the gradient of the plateau post elastic buckling of the sub-structure is much lower than when the mass distribution is 25%. It is important to note that the Young's modulus of the elastic regime correlates with that determined in Chapter 4 for the change in θ_{sub} and the change in mass distribution.

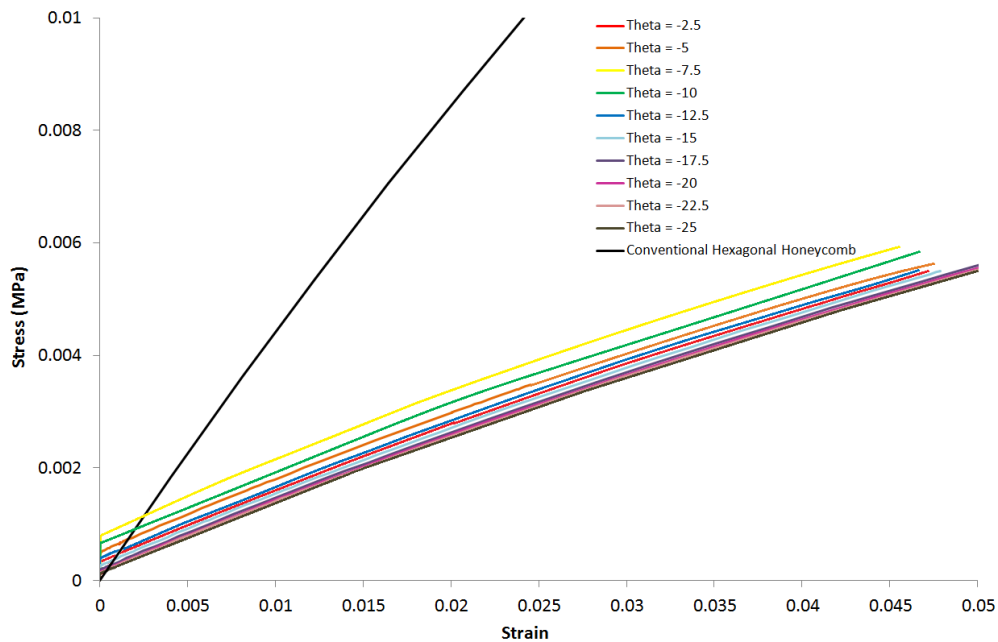


Figure 6.30: Stress strain response of NPR sub-structures with a mass distribution of 25% for internal sub-structure angles of -2.5 to -25.

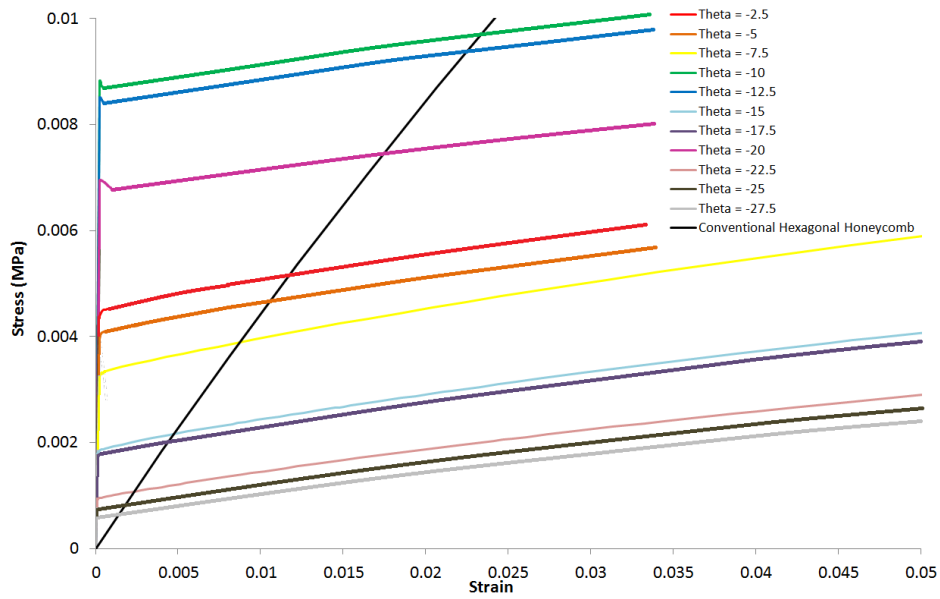


Figure 6.31: Stress strain response of NPR sub-structures with a mass distribution of 50% for internal sub-structure angles of -2.5 to -27.5.

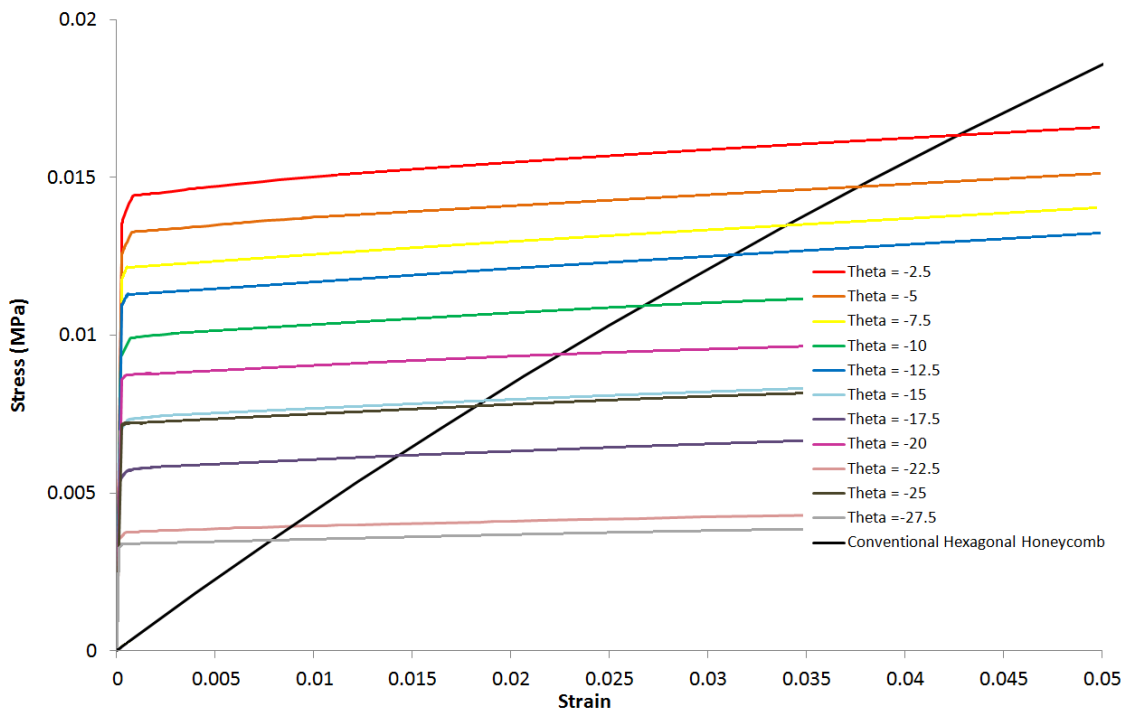


Figure 6.32: Stress strain response of NPR sub-structures with a mass distribution of 75% for internal sub-structure angles of -2.5 to -27.5.

The result reported in Figure 6.33 to Figure 6.35 show the internal energy against strain for hierarchical honeycombs with a NPR for mass distributions of 25%, 50% and 75%. Also shown is the internal energy of a conventional hexagonal honeycomb of the same relative density as a benchmark. It can be seen that the internal energy corresponds to the area under the stress strain plots in Figure 6.30 to Figure 6.32 as expected. The internal energy against strain graphs highlights the effect of changing the mass distribution. When the mass distribution is 25% there is little advantage of a NPR sub-structure and non at strains greater than approximately 0.002. However when the mass distribution is 75% there is a substantial gain in internal energy, up to strains of approximately 4%.

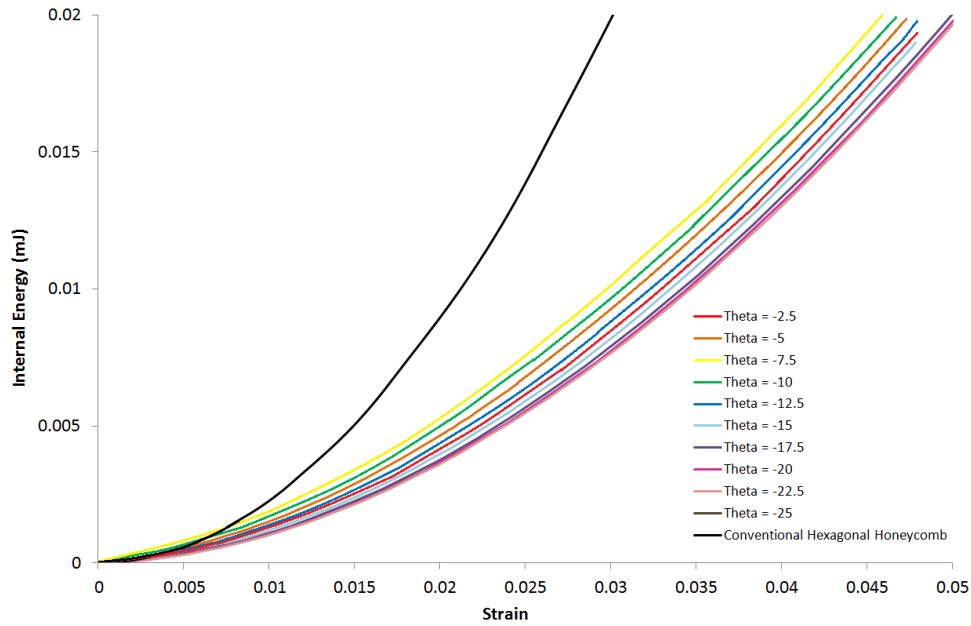


Figure 6.33: Internal energy against strain for NPR sub-structures with a mass distribution of 25% for internal sub-structure angles of -2.5 to -25.

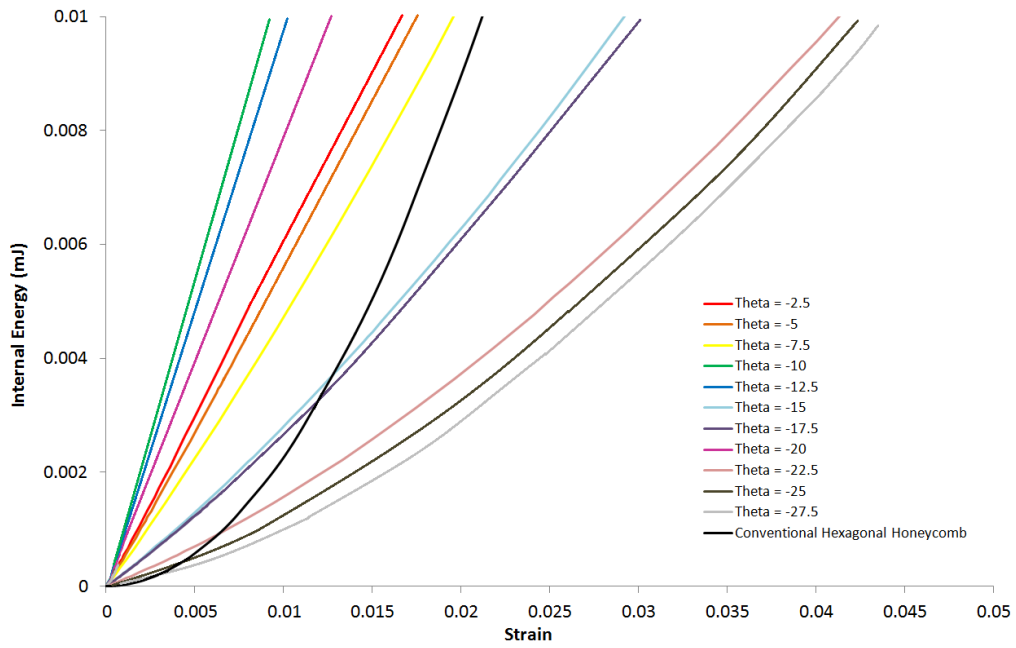


Figure 6.34: Internal energy against strain for NPR sub-structures with a mass distribution of 50% for internal sub-structure angles of -2.5 to -27.5.

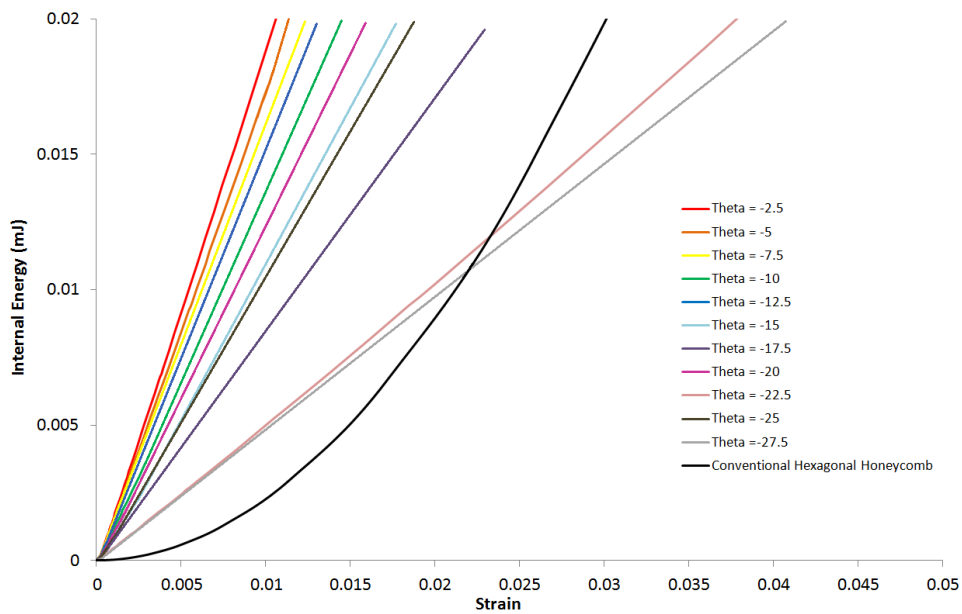


Figure 6.35: Internal energy against strain for NPR sub-structures with a mass distribution of 75% for internal sub-structure angles of -2.5 to -27.5.

6.4 Discussion

6.4.1 Functional Grading for Co-ordination Numbers for $\rho_{rel}^* = 0.00577$

For low relative density honeycombs, when the first mode of failure is elastic bending or elastic buckling of ribs, it is possible for hierarchical honeycombs to increase the buckling stress due to an increase in the second moment of area of ribs. The onset of elastic buckling can be seen by the non-linear response of the stress strain graph given that there is no plastic dissipation energy in the model.

6.4.1.1 Hexagonal Super-Structure Hexagonal Sub-Structure (3–3)

The contrasts in the responses of the bending dominated conventional hexagonal honeycomb and the stretch dominated conventional triangular honeycomb can be seen in Figure 6.5 where a conventional triangular honeycomb is elastically stiffer than the hexagonal honeycomb and elastically buckles at a lower strain due to its higher aspect ratio ribs for the same relative density (Gibson & Ashby 1997). Figure 6.5 also shows the stress strain response of hierarchical honeycombs with a hexagonal sub and super-structure, it can be seen that the bending dominated hierarchical honeycombs are much more compliant than the conventional triangular honeycomb. In this way they are more comparable to the conventional hexagonal honeycomb, with elastic stiffness depending on the super structure aspect ratio, as was examined in Chapter 3. It is explained by a trade off in the global material properties of the sub and super-structure. The hierarchical honeycombs also elastically bend at similar strains to the conventional hexagonal honeycomb, but with variations also dependent on the super-structure aspect ratio. This is due to changes in the sub-structure aspect ratio and subsequently the second moment of area of sub-structure ribs being determined by the super-structure aspect ratio. The response of the stress strain graph is reflected in Figure 6.6 where the internal energy is plotted against the strain, as expected the internal energy absorbed by the triangular honeycomb far exceeds that of the conventional hexagonal and hierarchical honeycombs. Comparing the conventional hexagonal to hierarchical honeycombs there are favourable super-structure aspect ratios that increase the energy absorption of the structure that can be explained by the trade off in the global material properties of the sub and super-structure (Taylor *et al* 2011).

The stress strain response in Figure 6.5 shows a clear plateau region for the hierarchical honeycombs that is not due to plastic yield of the constituent material as there is no plastic deformation present in the models. This however can be explained by the formation of stress concentration as shown in Figure 6.7 at the super-structure nodes causing the global ‘material properties’ to be determined by the parameters of the sub-structure, which have a localised stress increase. Hierarchical honeycombs that are more resistant to the stress concentration are those with a higher super-structure aspect ratio because they have a lower sub-structure aspect ratio that is elastically much stiffer (Gibson & Ashby 1997). This change in aspect ratio can be seen in Table 6.1 and highlights the change in sub-structure parameters due to variations in the super-structure geometry. This can be compared to the aspect ratio of a conventional hexagonal honeycomb of the same density which would have an aspect ratio of $\alpha = 200$ and a conventional triangular honeycomb of $\alpha = 600$.

Super-structure aspect ratio α_{sup}	11.5	4.80	2.88	2.16	1.44	1.15
Sub-structure aspect ratio α_{sub}	20.0	46.1	74.1	94.3	130	157

Table 6.1: Shows the change in sub-structure aspect ratio dependent on the super-structure aspect ratio for a (3-3) hierarchical honeycomb.

An advantage of hierarchical honeycombs with (3-3) co-ordination numbers is that their sub-structure consists of hexagonal cells, meaning this structure could be manufactured in the same way as conventional hexagonal honeycombs by the adhesion and expansion method followed by a secondary process of selectively removing cells to form the super-structure. This technique allows for a lower aspect ratio of sub-structure ribs which are only dependent on the super-structure aspect ratio for a given relative density. The advantages of this manufacturing technique are important considering that the excellent conventional triangular honeycombs face significant manufacturing problems.

This study shows that it is possible to exceed the conventional hexagonal honeycomb in both elastic stiffness and elastic strain energy absorption on an equal density basis, but it is not possible to exceed elastic stiffness or elastic strain energy absorption of a

conventional triangular honeycomb at such a low relative density. There is however an argument to use the (3-3) hierarchical honeycombs over a conventional triangular honeycomb. As previously described the manufacture of the hierarchical honeycombs could quite easily be achieved via the use of conventional manufacturing methods, whereas the construction of triangular honeycombs is still problematic. Also the triangular honeycomb performance is due to its stretch dominated nature, which could be affected by the bending process of constituent materials to form the honeycomb array.

6.4.1.2 Hexagonal Super-Structure Triangular Sub-Structure (3–6)

It can be seen in Figure 6.8 that the initial stiffness of hierarchical honeycombs with a hexagonal super-structure and triangular sub structure increases as the super-structure aspect ratio decreases. The hierarchical honeycombs show a clear trade-off between the bending dominated hexagonal honeycomb and the stretch dominated triangular honeycomb. For lower aspect ratio super-structures the hierarchical honeycombs approach the conventional triangular honeycomb, due to the majority of the structure being determined by the stretch dominated sub-structure. The opposite is true for higher aspect ratio super-structures where the structure is determined by the bending dominated super-structure. This is also represented by the elastic buckling of the hierarchical honeycombs where, again, bending dominated high aspect ratio structures are more comparable to the hexagonal honeycomb and low aspect ratio super-structures are more comparable to the triangular honeycomb. This can also be explained by the changes in the sub-structure aspect ratio that are dependent on the super-structure aspect ratio. Hierarchical honeycombs that have a sub-structure with a lower aspect ratio will have a greater resistance to elastic buckling, as sub-structure ribs have a greater second moment of area (Gibson & Ashby 1997). Table 6.2 shows how the sub-structure aspect ratio changes with that of the super-structure, highlighting why super-structures with a higher aspect ratio buckle at a higher strain. This can be compared to the aspect ratio of a conventional hexagonal honeycomb of the same density which would have an aspect ratio of $\alpha = 200$ and a conventional triangular honeycomb of $\alpha = 600$.

Super-structure aspect ratio α_{sub}	11.5	4.80	2.88	2.16	1.44	1.15
Sub-structure aspect ratio α_{sub}	15.2	142	224	287	396	467

Table 6.2: Shows the change in sub-structure aspect ratio dependent on the super-structure aspect ratio for a (3-6) hierarchical honeycomb.

The elastic strain energy stored in the honeycombs is shown in Figure 6.9 and is as expected considering their stress strain responses. The point is again highlighted that high aspect ratio super-structures tend to a hexagonal honeycomb and low aspect ratio super-structure to a triangular honeycomb. This type of hierarchy with a (3-6) co-ordination shows that it is possible to tailor structures global properties to those desired for specific applications by allowing compromises between stretching and bending dominated structures. This could be utilised for applications where a certain constituent material is required for manufacture and adapting the hierarchical structure to meet the desired properties. Another application could be changing the aspect ratio of the super-structure across a domain resulting in a change in the material properties of the structure in localised areas in term functional grading. This could be used to achieve performance such as those investigated by (Ajdari *et al* 2011).

6.4.1.3 *Triangular Super-Structure Triangular Sub-Structure (6-6)*

It can be seen in Figure 6.11 that the elastic stiffness of hierarchical honeycombs with a triangular sub and super-structure increases as the super-structure aspect ratio decreases as the structures tend to a conventional triangular honeycomb as previously shown in Chapter 3. It can also be seen that elastic buckling occurs at higher strains as the super-structures aspect ratio increases this is due to aspect ratio of sub-structure ribs being dependent on the super-structure aspect ratio and decreases in the sub-structure aspect ratio increases the second moment of area and subsequently delays the onset of elastic buckling. This change in sub-structure aspect ratio is shown in Table 6.3.

Super-structure aspect ratio α_{sub}	11.5	4.80	2.88	2.16
Sub-structure aspect ratio α_{sub}	173	375	540	590

Table 6.3: Shows the change in sub-structure aspect ratio dependent on the super-structure aspect ratio for a (3-6) hierarchical honeycomb.

It can be seen in Figure 6.12 that for low strains that the internal energy absorption of conventional triangular is greatest, but for strains higher than 0.00008 there is a greater energy absorptions in hierarchical honeycombs, of note is the performance of the hierarchical honeycomb when $\alpha_{sup} = 11.5$ where for higher strains the energy absorption greatly exceeds that of a conventional triangular honeycomb despite the conventional triangular honeycomb being elastically stiffer. This is due to the delay in elastic buckling of sub-ribs as the second moment of area is greater for sub-structure ribs which is a result of the inclusion of hierarchy in this nature.

This type of hierarchical honeycomb could be used in high performance applications where low density materials are required. Even though the elastic stiffness is lower than that of a conventional triangular honeycomb the fact that buckling is markedly delayed and that the elastic strain energy is also greatly increased could make the (6-6) hierarchical honeycomb a much more attractive structure than the conventional triangular honeycomb.

6.4.1.4 Triangular Super-Structure Hexagonal Sub-Structure (6-3)

It can be seen in Figure 6.14 that the elastic stiffness of hierarchical honeycombs with a triangular super-structure and a hexagonal sub-structure are more comparable to conventional hexagonal honeycomb similar to the (3-3) hierarchical honeycomb due to the bending dominated sub-structure. The elastic regime response can be explained as in Chapter 3. The majority of hierarchical honeycombs are more compliant than the conventional hexagonal honeycomb, but the hierarchical honeycomb with a super-structure aspect ratio $\alpha_{sup} = 11.5$ shows a clear trade-off between the two conventional honeycombs. When $\alpha_{sup} = 11.5$ the hierarchical honeycomb even has a greater energy absorption for strains greater than 0.144 compared to the conventional triangular honeycomb due to the delay in elastic buckling of ribs as shown in Figure 6.15.

As in the (3-3) hierarchical honeycomb the advantage of hierarchical honeycombs with a (6-3) co-ordination number is that the sub-structure consists of hexagonal cells so the structure could be manufactured as per conventional honeycombs of adhesion and expansion method followed by a secondary process of selectively removing cells to form the super-structure.

6.4.2 Functional Grading for Co-ordination Numbers for $\rho_{rel}^* = 0.0577$

For low relative density honeycombs elastic buckling was the first mode of failure, whereas for higher relative densities the onset of plasticity could be the first mode of failure. To determine at what point a model experienced plastic yield the plastic dissipation energy divide by internal energy was plotted against the applied strain.

6.4.2.1 Hexagonal Super-Structure Hexagonal Sub-Structure (3–3)

As when the relative density $\rho_{rel}^* = 0.00577$ there is contrast in the response of the bending dominated conventional hexagonal honeycomb and the stretch dominated conventional triangular honeycomb which can be seen in Figure 6.17 for relative density $\rho_{rel}^* = 0.0577$. The conventional triangular honeycomb is elastically stiff whereas the hexagonal honeycomb is relatively compliant. When viewed along with Figure 6.18 and Figure 6.19 it can be seen that a triangular honeycomb does not experience plastic dissipation energy until a strain of approximately $\varepsilon = 0.01$ (Figure 6.19), but clearly shows non-linearity at a strain of approximately $\varepsilon = 0.003$ (Figure 6.17). This is due to the high aspect ratio of the rib $\alpha = 60$, meaning a low second moment of area resulting in elastic buckling being the first mode of failure. The second moment of area of ribs for triangular honeycombs will be higher than those of a hexagonal honeycomb for a given relative density due to ribs being thinner as triangular honeycombs have a smaller unit cell for a given length l than a hexagonal honeycomb to maintain the same relative density

As in the previously investigated (3-3) hierarchical honeycomb at a relative density of $\rho_{rel}^* = 0.00577$ the (3-3) hierarchical honeycombs at a relative density of $\rho_{rel}^* = 0.0577$ are still comparable to the bending dominated hexagonal honeycomb, but the first mode of failure is through plastically yielding of sub-structure ribs opposed to elastic buckling. Failure occurs at strains from $0.04 < \varepsilon < 0.05$ for hierarchical honeycombs, this can be compared to a hexagonal honeycomb which experiences plasticity at a strain

of approximately $\varepsilon \approx 0.1$. This is due to changes in the sub-structure aspect ratio and subsequently the second moment of area of sub-structure ribs being determined by the super-structure aspect ratio. The response of the stress strain graph is also reflected in Figure 6.18 where the internal energy is plotted against the strain as expected the internal energy absorbed by the triangular honeycomb far exceeds that of the conventional hexagonal and hierarchical honeycombs. Comparing the conventional hexagonal to hierarchical honeycombs there are favourable super-structure aspect ratios that increase the energy absorption of the structure and can also be explained by the trade off in the global material properties of the sub and super-structure.

The hierarchical (3-3) honeycomb with a relative density $\rho_{rel}^* = 0.0577$ shares the same manufacturing advantage of the same hierarchical honeycomb at a relative density $\rho_{rel}^* = 0.00577$. That it could be manufactured from conventional honeycomb manufacturing methods followed by a secondary selective removal process. The advantages of this manufacturing technique are important considering that the excellent conventional triangular honeycombs face significant manufacturing problems.

This study shows that it is possible to exceed the conventional hexagonal honeycomb in both elastic stiffness and elastic strain energy absorption on an equal density basis, but it is not possible to exceed elastic stiffness or elastic strain energy absorption of a conventional triangular honeycomb at a relative density $\rho_{rel}^* = 0.0577$. The argument to use a hierarchical (3-3) honeycomb opposed to a conventional triangular honeycomb is the same as that for a hierarchical (3-3) honeycomb with a relative density $\rho_{rel}^* = 0.00577$

6.4.2.2 Hexagonal Super-Structure Triangular Sub-Structure (3–6)

It can be seen in Figure 6.20 that the elastic stiffness of hierarchical honeycombs with a hexagonal super-structure and triangular sub-structure increases as the super-structure aspect ratio decreases as the structures tends to a conventional triangular honeycomb as previously explained in Chapter 3. Similarly to when the relative density $\rho_{rel}^* = 0.00577$ the hierarchical honeycombs show a clear trade-off between the bending dominated hexagonal honeycomb and the stretch dominated triangular honeycomb. For low aspect ratio super-structures the hierarchical honeycombs approach the conventional triangular due to the majority of the structure being determined by the stretch dominated sub-

structure. The opposite is true for high aspect ratio super-structure where the structure is determined by the bending dominated super-structure. The onset of plasticity in hierarchical honeycombs occurs at a lower strain than conventional honeycombs determined from Figure 6.22; this is due to stress concentrations in sub-structure ribs at super-structure nodes (Where super-structure ribs connect). As expected the internal energy of structures is greatest for a conventional triangular honeycomb then low aspect ratio hierarchical honeycomb to high aspect ratio followed by conventional hexagonal honeycombs and is shown in Figure 6.21.

Similarly to a relative density $\rho_{rel}^* = 0.00577$ it is possible to some degree to tailor structures global properties to those desired for specific applications by allowing compromises between stretch and bending dominated structures for a (3-6) honeycomb by changing the super-structure aspect ratio.

6.4.2.3 Triangular Super-Structure Triangular Sub-Structure (6–6)

It can be seen in Figure 6.23 that the elastic stiffness of hierarchical honeycombs with a triangular sub and super-structure increases as the super-structure aspect ratio decreases as the structures tends to a conventional triangular honeycomb as previously shown in Chapter 3. Unlike other hierarchical honeycombs with a relative density $\rho_{rel}^* = 0.00577$ (6-6) honeycombs still experience elastic buckling as the first failure mode, similar to the conventional triangular honeycomb. This is due to the same reason as the conventional triangular honeycomb and is because the second moment of area of ribs for triangular honeycomb is lower than those of a hexagonal honeycomb for a given relative density. This is due to thinner ribs, as triangular honeycombs have a smaller unit cell for a given length l than a hexagonal honeycomb to maintain the exact same density and as a result are more prone to elastic buckling. Similarly to when the relative density $\rho_{rel}^* = 0.00577$ it can be seen that elastic buckling occurs at higher strains as the super-structures aspect ratio increases this is due to aspect ratio of sub-structure ribs being dependent on the super-structure aspect ratio and decreases in the sub-structure aspect ratio increases the second moment of area and subsequently delays the onset of elastic buckling. Figure 6.24 shows that for low strains a conventional triangular honeycomb has the greatest internal energy absorption, but for strains greater than approximately 0.011 the internal energy of a hierarchical honeycomb with a super-

structure aspect ratio $\alpha_{sup} = 11.5$ is greater. This is due to the delay in elastic buckling of ribs as the second moment of area is greater for sub-structure ribs which is a result of the inclusion of hierarchy in this nature. An advantage of implementing (6-6) hierarchy in high end applications has been explored in the previous section investigating relative densities $\rho_{rel}^* = 0.00577$.

6.4.2.4 Triangular Super-Structure Hexagonal Sub-Structure (6-3)

Similarly to the previously investigated (6-3) hierarchical honeycomb Figure 6.25 shows that the elastic stiffness of hierarchical honeycombs with a triangular super-structure and a hexagonal sub-structure are more compliant than a conventional hexagonal honeycomb, but when the super-structure aspect ratio $\alpha_{sup} = 11.5$ there is a marked increase in the initial stiffness which is explained in Chapter 3 in terms of sub-structure global material properties have a large effect as the constituent material for the super-structure. Hierarchical honeycombs experience the onset of plasticity at a strain between $0.04 < \varepsilon < 0.07$ depending on the super-structure aspect ratio as shown in Figure 6.27. When $\alpha_{sup} = 11.5$ a clear trade-off between the two conventional honeycombs can be seen and is reflected in the internal energy of the structure as shown in Figure 6.26.

As with previous hierarchical honeycomb that are composed of a hexagonal sub-structure the (6-3) hierarchical honeycomb has the advantage of being produced via a modified conventional manufacturing method.

6.4.2.5 Triangular Super-Structure Triangular Sub-Structure Aluminium and Steel (6-6)

The effect of changing material properties can be seen by comparing Figure 6.11, Figure 6.28 and Figure 6.29 for nylon, steel and aluminium respectively with a relative density of $\rho_{rel}^* = 0.00577$. There is no change in the form of the graphs for the hierarchical honeycombs only the magnitude of the stress which is proportional to the difference in the materials properties of the constituent material, as expected.

6.4.3 Poisson's Ratio Sub-Structure

As Shown in Chapter 4 hierarchical honeycombs with a NPR sub-structure have a greater elastic modulus than that of a conventional hexagonal honeycomb, but are highly anisotropic. This result is reiterated in this section, but also investigates the effect of elastic buckling and the onset of plasticity in ribs. The relationship between the sub- and super-structure is complex, whilst there is a definite trend to the initial Young's modulus of hierarchical honeycombs with a NPR sub-structure as shown in Chapter 4 there is no definite trend at what point the sub-structure will elastically buckle. Although generally structures with a greater Young's modulus have a high buckling stress as shown in Figure 6.30 to Figure 6.32, and is thought to be due to the sub and super-structures rotation due to bending counteracting each other increasing the stretch domination of the structure, which could also delay elastic buckling of ribs. However this is not always the case and some structures buckle at a greater or lower stress than those of a similar internal angle or NPR. This is thought to be due to the complex interaction between the sub and super-structure which can promote localised buckling of ribs at or close to where the sub and super-structure meet. It can be seen that the initial Young's modulus is greater when the mass distribution is 75% compared to 25% and 50% consistent with previous results as the sub-structure is dominate. There is also an increase in the buckling stress of the sub-structure at a mass distribution of 75% due to an increase in the second moment of area of ribs. It can also be seen that the post buckling response gradient of the stress strain graph is greater when the mass distribution is 25% when compared to mass distributions of 50% and 75%. The increased gradient is due to response being dominated by the super-structure, which remains functional post sub-structure buckling. The property of the super-structure is determined by its aspect ratio and is stiffest at lower aspect ratio's as is the case when the mass distribution is 25%.

The most apparent feature of the results presented is the difference between the stretch dominated triangular honeycomb and the bending dominated hexagonal honeycomb. This is also reflected in the response of hierarchical honeycombs that show a clear trade of between the two different types of structure by combining co-ordination numbers in sub and super-structure. It is possible with the use of hierarchy to tailor a cellular materials response, by changing variables such as the co-ordination number and super-

structure aspect ratio to give material properties that would otherwise be unobtainable for conventional honeycombs for a given density. This gives designers the freedom to choose from a wide range of characteristics of materials for a given application, where previously a change in material property was only viable through a change in constituent material or the density.

6.5 Conclusion

The results show that the introduction of hierarchy into honeycombs can have the effect of delaying the onset of elastic buckling, which is most prominent for low relative density structures, but is less apparent in higher relative density structure due to the onset of plasticity becoming the first mode of failure. It is important to note that this is not the case for all hierarchical honeycombs and in some case the material properties of conventional honeycomb are favourable.

Hierarchical honeycombs have the advantage of having the ability to be tailored to the required demands of a certain application if know for a give relative density by changing parameters such as the co-ordination number, mass distribution and the aspect ratio of the super-structure for functionally graded hierarchical honeycombs or the internal angle or mass distribution for NPR sub-structure hierarchical honeycombs.

Chapter 7. Out-of-Plane Plasticity and Non-Linear Response

7.1 Introduction

Honeycombs are commonly used in sandwich core and energy absorbing applications. The work undertaken in this chapter investigates the out-of-plane elastic response and the onset of plasticity of hierarchical honeycombs that have a functionally graded super-structure where the super-structure aspect ratio α_{sup} changes, as in Chapter 3. The stress strain response has been investigated along with the energy absorption of hierarchical honeycombs, examining particularly the onset of elastic buckling and plastic collapse of honeycombs as criteria for failure of sub and super-structure ribs. The onset of plasticity and elastic buckling was examined for hierarchical honeycombs and compared to the response of conventional hexagonal honeycombs of the same relative density. It was thought that the decrease in the sub-structure aspect ratio due to the introduction of hierarchy delays the onset of elastic buckling in a similar manner to decreasing the aspect ratio of conventional honeycombs (Gibson and Ashby 1997). Hexagonal honeycombs of the same relative density were used as a bench mark, as due to the geometry they are more resistant to the onset of elastic buckling as they have a lower aspect ratio when compared to other geometries such as triangles and squares of the same relative density.

The effect of introducing hierarchy into honeycombs was only investigated out-of-plane for functionally graded hierarchical honeycombs with 100% mass distribution within the sub-structure. This type of hierarchy was the chosen as it propose the optimum benefit to the structure in delaying the onset of elastic buckling, due to the decrease aspect ratio of sub-structure ribs. For the same reason only hexagonal sub and super structures (3-3) were investigated since due to the connectivity hexagonal honeycombs already have a lower aspect ratio when compared to triangular or square honeycomb of the same relative density. When loading a honeycomb out-of-plane it is effectively a series of columns in compression and the ribs are all stretch dominated, there is little that can be done to change the plastic collapse stress of the cell without changing the relative density of the cell or the constituent material properties.

The aim of this chapter is to investigate the out-of-plane elastic and plastic response of hierarchical honeycombs that have been previously investigated in-plane and have shown potential increases in favourable properties such as Young's modulus, delayed elastic buckling and plasticity. It is expected that with the introduction of hierarchy it will be possible to increase the elastic buckling of a honeycomb beyond the stress at which plastic collapse occurs.

7.2 Method

The out-of-plane elastic and plastic response of functionally graded hierarchical honeycomb was simulated via numerical models which considered each unit cell as a discrete structure, and made no assumptions about sub-cells as continua as in previous works (Carpinteri *et al.*2009).

7.2.1 Elastic Models, Functional Grading and HLR

The first step of investigating the effect of hierarchy on the out-of-plane properties of honeycombs was to determine the length scale of the sub-structure, relative to that of the super-structure, at which it could be considered to be a continuum as in Chapter 3. This was investigated to determine the effect of the changing HLR and if multiple HLRs had to be investigated when further investigating out-of-plane properties in hierarchy honeycombs. It was also important to understand the implications when considering the possible manufacture of hierarchical honeycombs. The ratio of the lengths in the sub and super-structure is the hierarchical length ratio (HLR) λ and is defined according to Equation 3-1 Chapter 3. The critical value of the HLR at which continuum behaviour was attained was determined by iteratively decreasing the value of λ for three example hierarchical honeycombs of different hexagonal super-structure aspect ratios ($\alpha_{sup} = 11.5$, $\alpha_{sup} = 2.88$ and $\alpha_{sup} = 1.15$). As Shown in Figure 7.1, Figure 7.2 and Figure 7.3. To change λ the lengths l_{sub} , h_{sub} and t_{sub} of the sub-structure were iteratively decreased on an equal density basis, while lengths l_{sup} , h_{sup} and t_{sup} remained constant, effectively increasing the number of sub-cells spanning the thickness of the super-structure, as shown in Figure 7.1, Figure 7.2 and Figure 7.3.

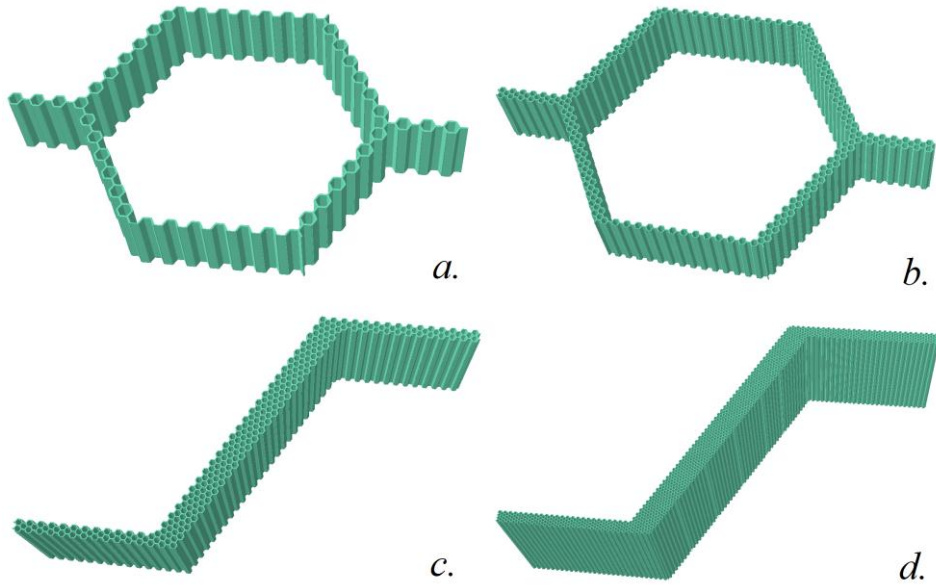


Figure 7.1: Shows how the HLR changes for a (3-3) hierarchical honeycomb with a super-structure aspect ratio $\alpha_{sup} = 11.5$ a) the super-structure is one sub-cell wide when $\lambda = 0.05$, b) the super-structure is two sub-cells wide when $\lambda = 0.025$, c) the super-structure is four sub-cells wide when $\lambda = 0.0125$ and d) the super-structure is eight sub-cells wide when $\lambda = 0.00625$. Quarter cells are shown in c and d so it is simpler to identify the sub-structure.

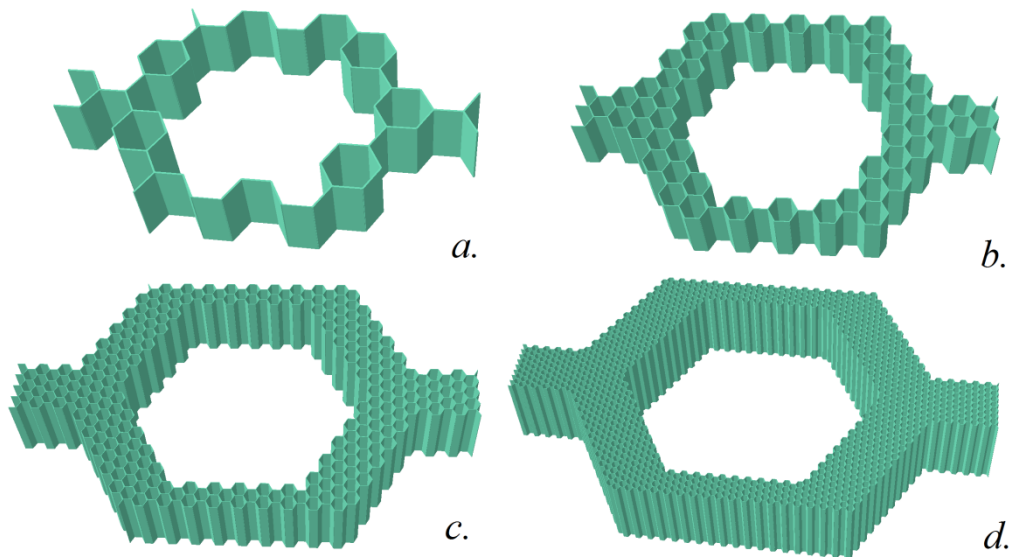


Figure 7.2: Shows how the HLR changes for a (3-3) hierarchical honeycomb with a super-structure aspect ratio $\alpha_{sup} = 2.88$ a) the super-structure is one sub-cell wide when $\lambda = 0.05$, b) the super-structure is two sub-cells wide when $\lambda = 0.025$, c) the super-structure is four sub-cells wide when $\lambda = 0.0125$ and d) the super-structure is eight sub-cells wide when $\lambda = 0.00625$.

=0.2, b) the super-structure is two sub-cells wide when $\lambda = 0.1$, c) the super-structure is four sub-cells wide when $\lambda = 0.05$ and d) the super-structure is eight sub-cells wide when $\lambda = 0.025$.

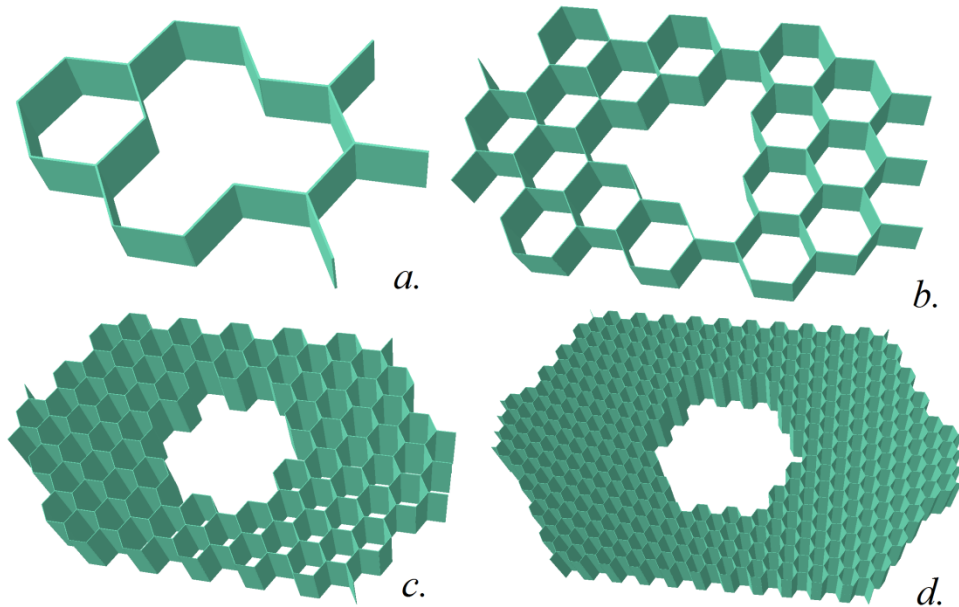


Figure 7.3: Shows how the HLR changes for a (3-3) hierarchical honeycomb with a super-structure aspect ratio $\alpha_{sup} = 1.15$ a) the super-structure is one sub-cell wide when $\lambda = 0.5$, b) the super-structure is two sub-cells wide when $\lambda = 0.25$, c) the super-structure is four sub-cells wide when $\lambda = 0.125$ and d) the super-structure is eight sub-cells wide when $\lambda = 0.0625$.

The relative density of all hierarchical honeycombs investigated was $\rho^* = 0.0577$ which were then compared to conventional hexagonal honeycombs of the same relative density.

7.2.2 Functional Grading and Change in Aspect Ratio

Once the critical value of λ , and thus the number of sub-cells spanning the super-structure was determined, where there is little or no change in the material response. The study was then developed to further investigate the effect of changing the super structure aspect ratio as shown in Figure 7.4. It was shown that the out-of-plane Young's modulus is independent of the HLR and the number of sub-cells spanning the super-structure as presented later in the results section. It was therefore possible to

maintain the number of sub-cells spanning the super-structure for the sub-structure to be considered a continuum to one sub-cell for simplicity. Changing the super-structure aspect ratio α_{sup} whilst maintaining one sub-cell spanning the super-structure was achieved by varying the length l_{sub} , ensuring that there were always an integer number of sub-cells along the length l_{sup} . It was also necessary to change t_{sub} depending on the length l_{sub} and the number of sub-structure ribs in order to maintain a constant relative density. Super-structure aspect ratios investigated were $\alpha_{sup} = 11.5$, $\alpha_{sup} = 5.77$, $\alpha_{sup} = 2.88$, $\alpha_{sup} = 1.73$ and $\alpha_{sup} = 1.15$ as shown in Figure 7.4 a-e.

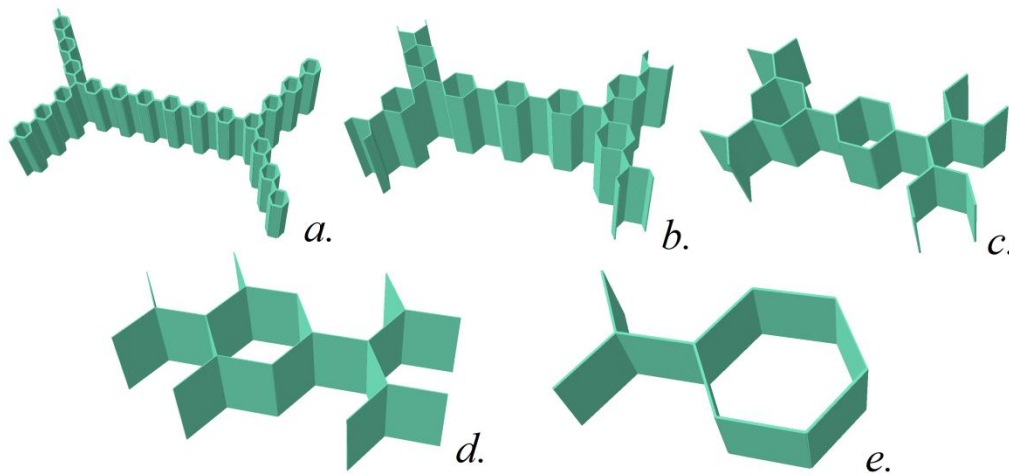


Figure 7.4: Shows how the sub and super-structure dimensions change for a hexagonal super-structure and hexagonal sub-structure hierarchical honeycomb for a) when the super-structure aspect ratio $\alpha_{sup} = 11.5$, b) when the super-structure aspect ratio $\alpha_{sup} = 5.77$, c) when the super-structure aspect ratio $\alpha_{sup} = 2.88$, d) when the super-structure aspect ratio $\alpha_{sup} = 1.73$ and e) when the super-structure aspect ratio $\alpha_{sup} = 1.15$

Models of functionally graded hierarchical structures were developed by producing a 3D part in the finite element software ABAQUS and selecting a deformable shell created via extrusion, the geometry was specified via a 2D sketch. Sketches were created depending on the sub and super-structure dimensions prior to a subsequent extrusion process to a specified value. A set of linear and isotropic elastic constants were defined and used for all cases (specifically $E_s = 1600$ MPa, $G_s = 593$ MPa and $\nu_s = 0.35$). Ribs were then assigned an appropriate section and a rib thickness specified. The rib thickness was dependent on the relative density of the hierarchical honeycomb, the super-structure aspect ratio and the HLR. A *Static, General* step was created as a quasi-

static linear elastic model was required to determine the in-plane Young's modulus for elastic models. The relative density of hierarchical honeycombs investigated was $\rho^*=0.0577$ which were compared to conventional hexagonal honeycombs of the exact same relative density.

The model used to determine the out-of-plane properties of a hierarchical honeycomb was a half unit cell as shown in Figure 7.5, which shows a 2D plan view of a hexagonal honeycomb array along with a unit and half unit cell highlighted. The unit cell used to model the out-of-plane elastic response is consistent with the unit cell used in (Wilbert *et al* 2011) to model the out-of-plane buckling of aluminium conventional hexagonal honeycombs and showed that the half unit cell with the correct boundary conditions replicated well the response of larger honeycomb arrays.

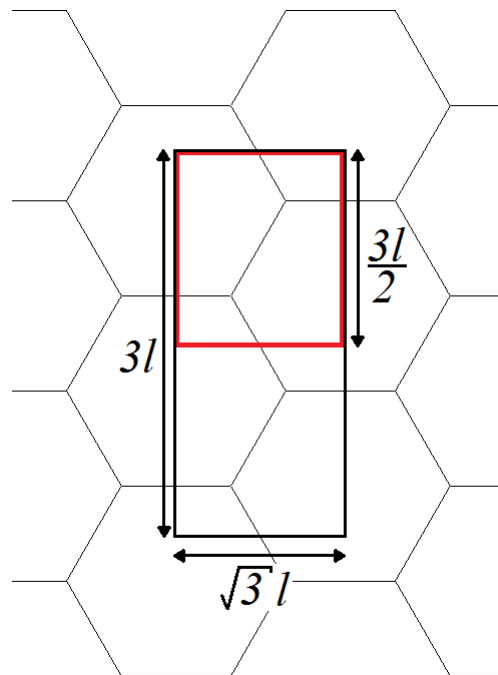


Figure 7.5: 2D plan view of a hexagonal honeycomb array along with a highlighting repeatable unit cell in black and half a repeatable unit cell in red. The global dimensions of the unit cell are also shown.

Boundary conditions applied to the model were comparable to those of a sandwich panel in that the bottom face of the model was restrained to zero displacement in the X,

Y and Z axis along with zero rotation around the X, Y and Z axis effectively encasted. The top face of the model had similar boundary conditions as the bottom but a uniform displacement was applied negatively in the Z axis applying a strain of 0.1% normal to the face, putting the model in compression (Wilbert *et al* 2011). These boundary conditions can be seen in Figure 7.6, for simplicity a conventional honeycomb is shown, but boundary conditions are exactly the same as those applied to hierarchical honeycombs.

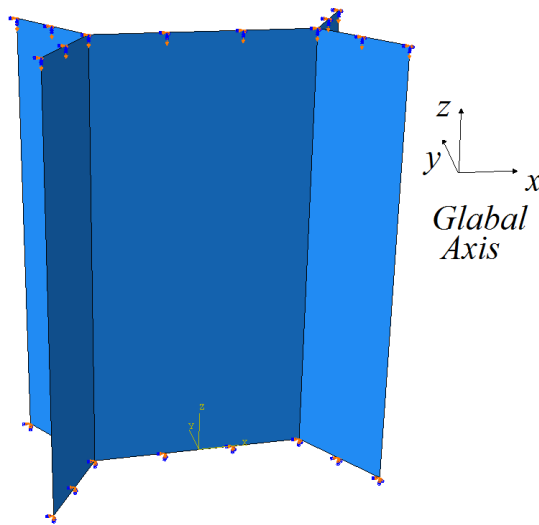


Figure 7.6: Boundary conditions applied to the top and bottom face of a conventional honeycomb.

Boundary conditions applied to the side of the structure where applied by an interaction coupling a node to its counterpart node on the contralateral edge. To apply such interactions two new datum's were created where the X, Y plane of the datum were parallel to the face of the associated rib, as can be seen in Figure 7.7. Nodes were then coupled through displacements in the X, Y and Z axis along with rotations around the X, Y and Z axis according to the edges relative datum. The interaction was applied to each individual node along the rib edge to the corresponding node on the contralateral edge as can be seen in Figure 7.7, for simplicity a conventional honeycomb is shown, but boundary conditions are the same as those applied to hierarchical honeycombs. The boundary conditions shown in Figure 7.6 and Figure 7.7 for a conventional hexagonal honeycomb which are the same as to those presented in (Wilbert *et al* 2011).

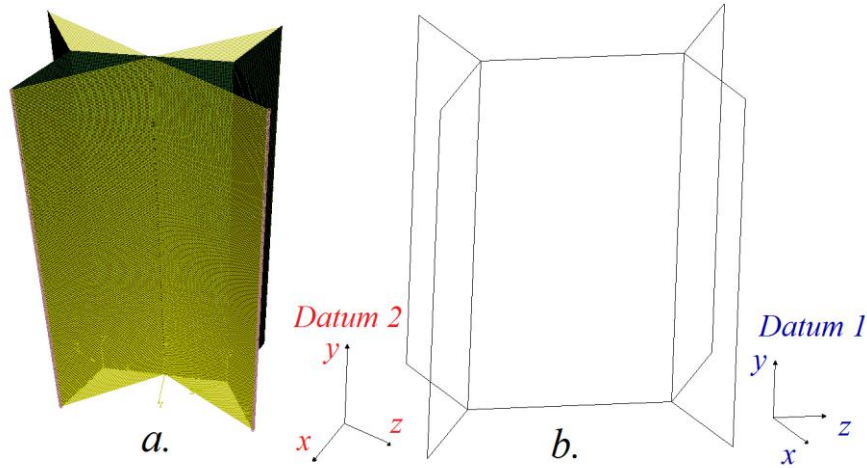


Figure 7.7: a) Shows how the boundary conditions were applied to the vertical edges of a conventional hexagonal honeycomb for the considered unit cell. b) Shows the datum's 1 and 2 that were used to apply the boundary condition to the unit cell.

The total reaction force on the displaced face was recorded for the final increment of the model. This was achieved by selecting a set of the face to be displaced and requesting the displacement and reaction force from the face. This reported the reaction force for all nodes from the previously described set in the direction of the applied displacement for the last increment. The projected area of the cell is known from the geometry of the cell so the global stress can be calculated. A known displacement was applied as a boundary condition and the original height of the model is known from the geometry of the cell, it was therefore possible to calculate the global strain in the model.

7.2.3 Plastic Models

Plasticity models were undertaken in similar manner to the out-of-plane elastic models. The same super-structure aspect ratios of $\alpha_{sup} = 11.5$, $\alpha_{sup} = 5.77$, $\alpha_{sup} = 2.88$, $\alpha_{sup} = 1.73$ and $\alpha_{sup} = 1.15$ were investigated as shown in Figure 7.4. Plasticity models had the same boundary conditions applied as elastic models, but the applied strain was increased to 20% and non-linear geometry and material properties were applied. The non-linear behaviour for plasticity models was specified as an elasto-plastic response of the material and was defined with a yield stress $\sigma_{yield} = 44\text{MPa}$ along with a plastic strain $\varepsilon_{pl} = 0$ for the corresponding stress. This means that the constituent material will behave elastically until it reaches a stress $\sigma_{yield} = 44\text{MPa}$ at which point plastic deformation

occurs and there is no local increase stress as the strain increases (An elasto-plastic material).

For plasticity models a *Static Riks* was used due to the issues involved with buckling or collapse behaviour of geometrically nonlinear static problems where the load-displacement response shows a negative stiffness resulting in the structure releasing strain energy to remain in equilibrium. The Riks method allows static equilibrium states during the unstable phase of the response and is used to predict unstable, geometrically nonlinear collapse of a structure including the nonlinear material behaviour.

Non-linear geometry was specified for plasticity models along with the selection of E_1 (Total strain energy) and E_p (Energy dissipated by rate-independent and rate-dependent plastic deformation) in the *History Output Manager* to report the energy absorption of the model. The output for total strain energy can be described as in Equation 7-1.

$$E_1 = E_s + E_p$$

Equation 7-1

Where E_s = Recoverable strain energy and E_p = Energy absorbed by plastic deformation. This equation is simplified as dissipated energy through creep, electrostatic and other effects can be ignored in this simplified model. The total reaction force on the displaced face was recorded for each increment of the model similar to the elastic model, but reporting data for all increments. A similar process was repeated for a single node on the displaced face and the displacement in the direction of the applied displacement recorded for each increment.

7.3 Analytical

7.3.1 Linear-Elastic Deformation of Conventional honeycombs

Following the annotation of Gibson and Ashby (1997), honeycombs are given geometric parameters the same as those set out in Figure 1.4 and extended to a hierarchical honeycomb in Figure 3.8 Chapter 3. Gibson and Ashby (1997) set out the fundamental underpinnings of the behaviour of honeycombs, i.e. as tessellations of unit cell structures formed from beams or plates. Thus using beam mechanics, expressions could be derived for the elastic properties, e.g. the out-of-plane Young's modulus for a hexagonal honeycomb in Equation 7-2.

$$\frac{E_3^*}{E_s} = \left\{ \frac{h/l + 2}{2(h/l + \sin\theta)\cos\theta} \right\} \left(\frac{t}{l} \right)$$

Equation 7-2

Where E_s is the Young's modulus of the constituent material. Similar expressions are given for the other Young's and shear moduli and the Poisson's ratios.

7.3.2 Linear-Elastic Deformation of Hierarchical honeycombs

These equations can be adapted for hierarchical honeycombs. The equations in any of the work on honeycomb models described previously, being based on beam mechanics, are valid for continua and so are independent of size. Thus within hierarchical honeycombs, they can be used to describe the properties of all of the honeycombs individually. It might seem reasonable to assume therefore, that a sub-structure honeycomb can be treated as a continuum and its predicted properties used in the calculation of the properties of the super-structure. This is shown in Equation 7-3 that is derived for a hexagonal sub-structure honeycomb from those of Ashby and Gibson (1997) and is used as a continuum in Equation 7-4 for a hexagonal super-structure honeycomb, i.e. a hierarchical honeycomb. However, it is not proven whether this assumption of a continuum sub-structure is valid if the size scales of the sub and super-structures are not very different. This issue is addressed later in the Chapter.

$$E_{3sub}^* = \left\{ \frac{h_{sub}/l_{sub} + 2}{2(h_{sub}/l_{sub} + \sin\theta_{sub})\cos\theta_{sub}} \right\} \left(\frac{t_{sub}}{l_{sub}} \right) E_s$$

Equation 7-3

$$E_{3sup}^* = \left\{ \frac{h_{sup}/l_{sup} + 2}{2(h_{sup}/l_{sup} + \sin\theta_{sup})\cos\theta_{sup}} \right\} \left(\frac{t_{sup}}{l_{sup}} \right) E_{3sub}^*$$

Equation 7-4

7.3.3 Non-Linear-Elasticity: Elastic Buckling

Gibson and Ashby (1997) investigated the out-of-plane Euler buckling of a honeycomb by considering the buckling of a plate with constraints along the two edges which lie parallel to the loading direction modelling the interaction between adjacent plates. The buckling load is determined by the second moment of area and the width of the plate (l or h). Gibson and Ashby concluded that the elastic buckling stress can be described as in Equation 7-5

$$\sigma_{el3}^* = \frac{2}{(1 - \nu_s^2)} \frac{(l/h + 2)}{(h/l + \sin\theta)\cos\theta} \left(\frac{t}{l} \right)^3 E_s$$

Equation 7-5

This can be applied to the buckling stress of the sub-structure with appropriate subscripts as shown in Equation 7-6.

$$\sigma_{el3sub}^* = \frac{2}{(1 - \nu_s^2)} \frac{(l_{sub}/h_{sub} + 2)}{(h_{sub}/l_{sub} + \sin\theta_{sub})\cos\theta_{sub}} \left(\frac{t_{sub}}{l_{sub}} \right)^3 E_s$$

Equation 7-6

This buckling stress for the sub-structure can then be used to predict the global buckling stress of the super-structure cell assuming its collapse triggers global collapse. This can be done by taking the ratio of the cross sectional area of the super-structure A_{sup} of the total cross sectional area of the cell A_{cell} each shown in Equation 7-7 and Equation 7-8 respectively. The buckling stress of the super-structure cell can be defined as in Equation 7-9.

$$A_{sup} = \left((2h_{sup} + 4l_{sup})t - t^2 \left(\frac{2}{\cos\theta_{sup}} - \tan\theta_{sup} \right) \right)$$

Equation 7-7

$$A_{cell} = (2l_{sup} \cos\theta_{sup})(2h_{sup} + 2l_{sup}\sin\theta_{sup})$$

Equation 7-8

$$\sigma_{el3sup}^* = \frac{\sigma_{el3sub}^* A_{sup}}{A_{cell}}$$

Equation 7-9

A similar equation could be derived for the elastic buckling of the super-structure considering the sub-structure as a continuum of the super-structure, but the sub-structure will buckle or plastically yield before the super-structure. The super-structure could buckle at a lower stress than the sub-structure, but the sub-structure would have such a low relative density the constituent material of the super-structure would be better described as a continuum with isolated pores.

7.3.4 Plastic Collapse

Gibson and Ashby (1997) investigated the out-of-plane plastic collapse strength of honeycombs by considering the axial yielding of a plate with constraints along the two edges which lie parallel to the loading direction modelling the interaction between adjacent plates. The plastic collapse stress is determined by the second moment of area and the width of the plate (l or h). Gibson and Ashby concluded that the plastic collapse stress can be described as in Equation 7-10.

$$\sigma_{pl3}^* = \frac{(h/l + 2)}{2\cos\theta(h/l + \sin\theta)} \frac{t^3}{l} \sigma_{ys}$$

Equation 7-10

This can subsequently be used to determine the plastic collapse stress of the sub-structure by inserting the sub-structure geometry opposed to those of the conventional hexagonal honeycomb as shown in Equation 7-11.

$$\sigma_{pl_3sub}^* = \frac{(h_{sub}/l_{sub} + 2)}{2\cos\theta_{sub}(h_{sub}/l_{sub} + \sin\theta_{sub})} \frac{t_{sub}}{l_{sub}} \sigma_{ys}$$

Equation 7-11

The plastic collapse stress for the sub-structure can be used to estimate the global plastic collapse stress of the super-structure cell. This can be done in the same way as for the elastic buckling stress by taking the ratio of the cross sectional area of the super-structure A_{sup} of the total cross sectional area of the cell A_{cell} as shown in Equation 7-7 and Equation 7-8 respectively. The plastic collapse stress of the super-structure cell can then be defined as in Equation 7-12.

$$\sigma_{pl_3sup}^* = \frac{\sigma_{pl_3sub}^* A_{sup}}{A_{cell}}$$

Equation 7-12

7.4 Results

7.4.1 Elastic Regime, Functional Grading and HLR

The results of changing the HLR for a functionally graded hierarchical honeycomb where 100% of the mass is within the sub-structure was investigated, the results show that varying the HLR has little or no effect on the out-of-plane Young's modulus E_3^* for super-structure aspect ratios of ($\alpha_{sup} = 11.5$, $\alpha_{sup} = 2.88$ and $\alpha_{sup} = 1.15$). The out-of-plane Young's modulus E_3^* of a hierarchical honeycomb with a functionally graded sub-structure normalised to a conventional hexagonal honeycomb of the same relative density is plotted against the HLR, see Figure 7.8. It can be seen that the as the number of cells across the super-cell rib increases from 1 up to 8, changing the HLR there is no change in the Young's modulus E_3^* . It is clear that the HLR of the hierarchical honeycombs has little if any effect on the out-of-plane Young's modulus of hierarchical hexagonal honeycombs with a functionally graded sub structure. It also indicates that the introduction of a functionally graded sub-structure in term of changing the super-structure aspect ratio α_{sup} has a little effect on the out-of-plane Young's modulus when compared to a conventional hexagonal honeycomb.

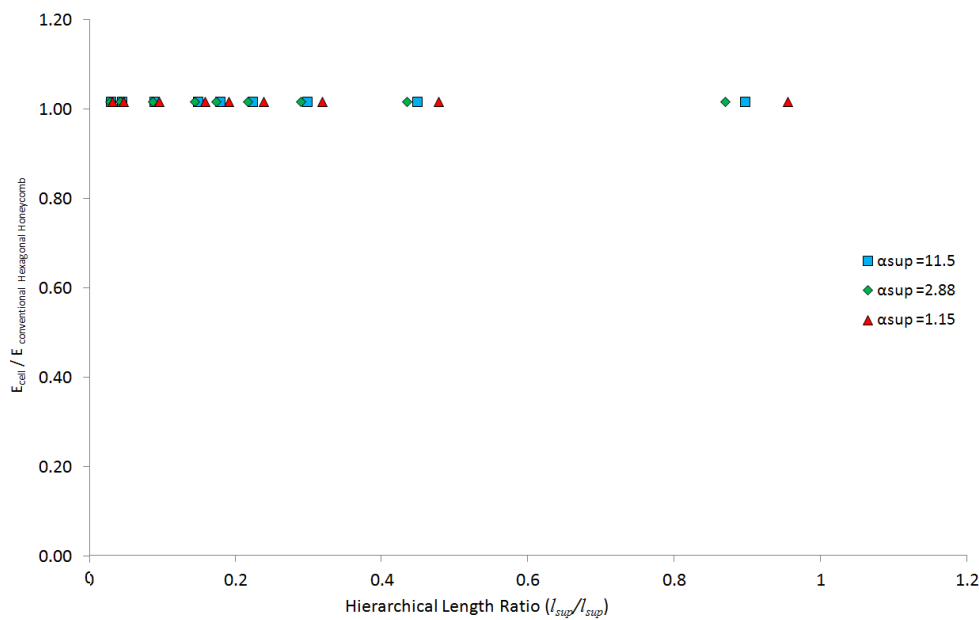


Figure 7.8: Out-of-plane Young's modulus of hierarchical honeycombs normalised to a conventional hexagonal honeycomb of the same relative density against the HLR

between the sub and super-structure for super-structure aspect ratios of ($\alpha_{sup} = 11.5$, $\alpha_{sup} = 2.88$ and $\alpha_{sup} = 1.15$).

7.4.2 Functional Grading and Change in Aspect Ratio

The results of the out-of-plane Young's modulus normalised by that of a conventional hexagonal honeycomb were plotted against the super-structure thickness t_{sup} presented in Figure 7.9. For functionally graded hierarchical honeycomb where 100% of the mass is within the sub-structure for aspect ratios of ($\alpha_{sup} = 11.5$, $\alpha_{sup} = 5.77$, $\alpha_{sup} = 2.88$, $\alpha_{sup} = 1.73$, $\alpha_{sup} = 1.44$, and $\alpha_{sup} = 1.15$). As expected, it can be seen that there is little difference in the elastic response of functionally graded hierarchical honeycombs to that of conventional hexagonal honeycombs, as the out-of-plane models are essentially columns in compression.

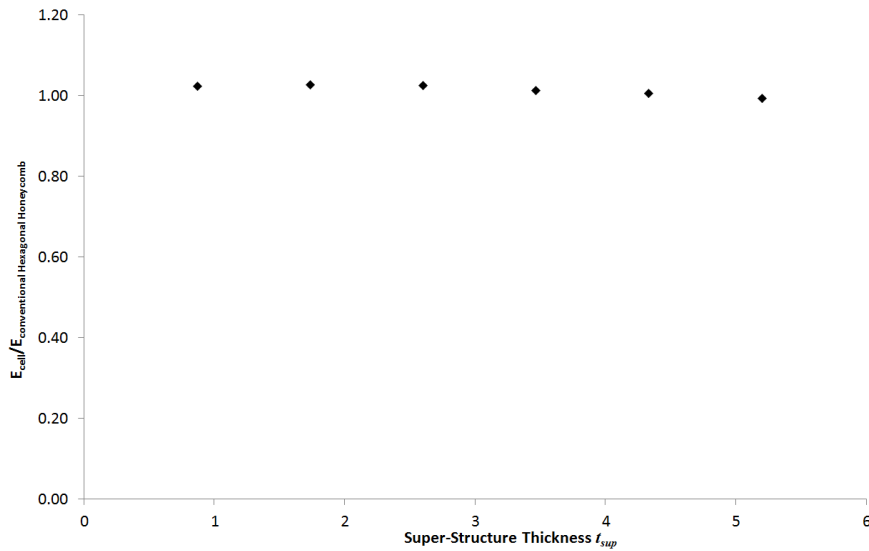


Figure 7.9: Young's modulus of a functionally graded hierarchical honeycomb normalised to a conventional hexagonal honeycomb against the super-structure thickness t_{sup} .

7.4.3 Plastic Regime

The results of the stress strain response due to out-of-plane compression simulations using FE are shown for functionally graded hierarchical honeycombs with a relative density of $\rho^* = 0.0577$. The effects of changing the super-structure aspect ratio of functionally graded hierarchical honeycombs are compared to the response of hexagonal conventional honeycombs of the same relative density. Along with the stress strain results, the internal energy absorbed by each hierarchical honeycomb is plotted against strain; also included is a graph of *Plastic Dissipation Energy / Internal Energy* to determine when and to what extent plasticity occurs in each hierarchical honeycomb and compared to conventional hexagonal honeycombs.

7.4.3.1 Stress Strain Response and Internal Energy for a Relative Density = 0.0577

The out-of-plane stress strain response for the non-linear geometry and elasto-plastic model of functionally graded hierarchical honeycombs compared to conventional hexagonal is presented in Figure 7.10. As expected the initial Young's modulus of the functionally graded hierarchical honeycombs are similar to that of a conventional hexagonal honeycomb concurring with the elastic models presented earlier in this chapter. It can clearly be seen that the conventional hexagonal honeycombs either elastically buckle or plastically yield at a lower stress than functionally graded hierarchical honeycombs, this agrees with the analytical results described in Equation 7-9. The first out-of-plane failure mode of the considered honeycombs can be determined by comparing the stress strain response to *Plastic Dissipation Energy / Internal Energy* against the global strain as shown in Figure 7.11. It is then possible to determine at what strain the stress strain graph is no longer linear and compare this to the strain at which plastic energy is dissipated in the model.

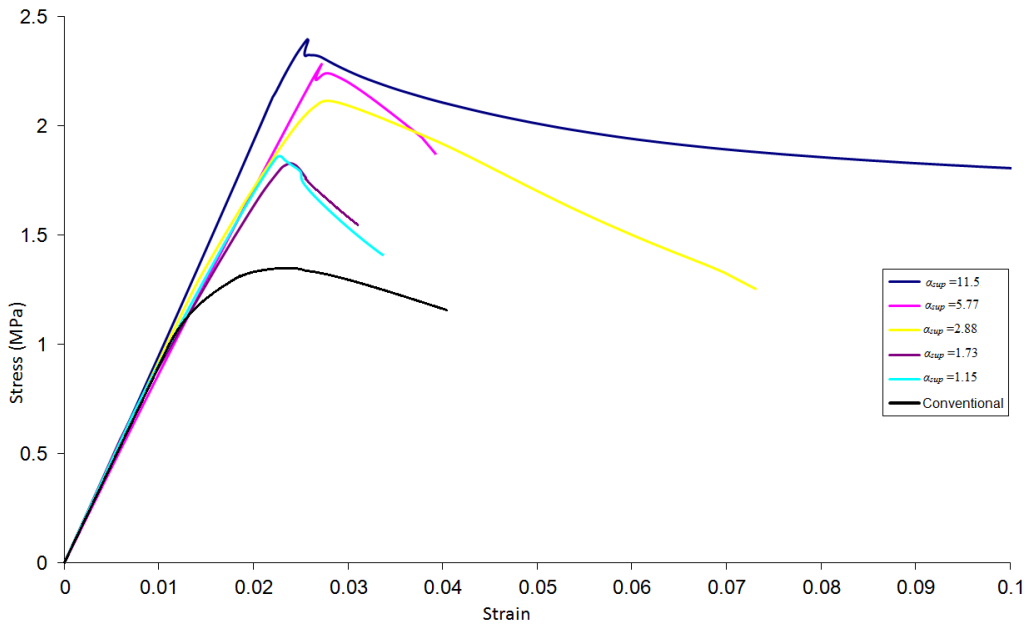


Figure 7.10: Out-of-plane stress strain response of hierarchical honeycombs that are functionally graded with super-structure aspect ratios of ($\alpha_{sup} = 11.5$, $\alpha_{sup} = 5.77$, $\alpha_{sup} = 2.88$, $\alpha_{sup} = 1.73$ and $\alpha_{sup} = 1.15$).

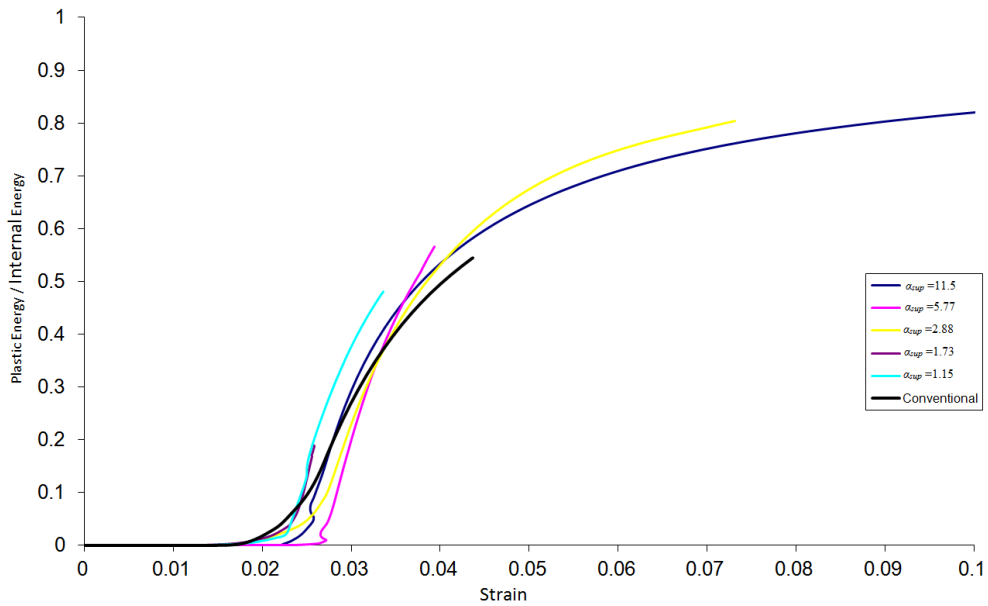


Figure 7.11: *Plastic Dissipation Energy / Internal Energy* for functionally graded hierarchical honeycombs compared to a conventional hexagonal honeycomb of the same relative density.

Looking at the conventional hexagonal honeycomb in the stress strain graph in Figure 7.10 it can be seen that the structure becomes non-linear at a strain of approximately 0.01 if you compare this result to the *Plastic Dissipation Energy / Internal Energy* in Figure 7.11 the structure experiences plastic dissipation energy at a strain of approximately 0.02 it can be deduced that the model elastically buckles at a strain of approximately 0.01 and a stress of approximately 1 MPa. Comparing this result to the functionally graded hierarchical honeycomb with a super-structure aspect ratio of $\alpha_{sup} = 11.5$ the constituent material plastically yields at a strain of approximately 0.022 and a stress of approximately 2.2 MPa. This is deduced as the stress strain graph plotted in Figure 7.10 does not show sign of nonlinearity until a strain of approximately 0.022 which is at the same strain that the hierarchical honeycomb shows signs of plasticity in the plastic energy / internal energy in Figure 7.11.

The internal energy of functionally graded hierarchical honeycombs against the applied strain is shown in Figure 7.12. As expected it can be seen that the initial elastic region is similar between all hierarchical honeycombs and the conventional hexagonal honeycomb, but the conventional hexagonal honeycomb diverges from the hierarchical models at a strain of approximately 0.01 in the region where it elastically buckles.

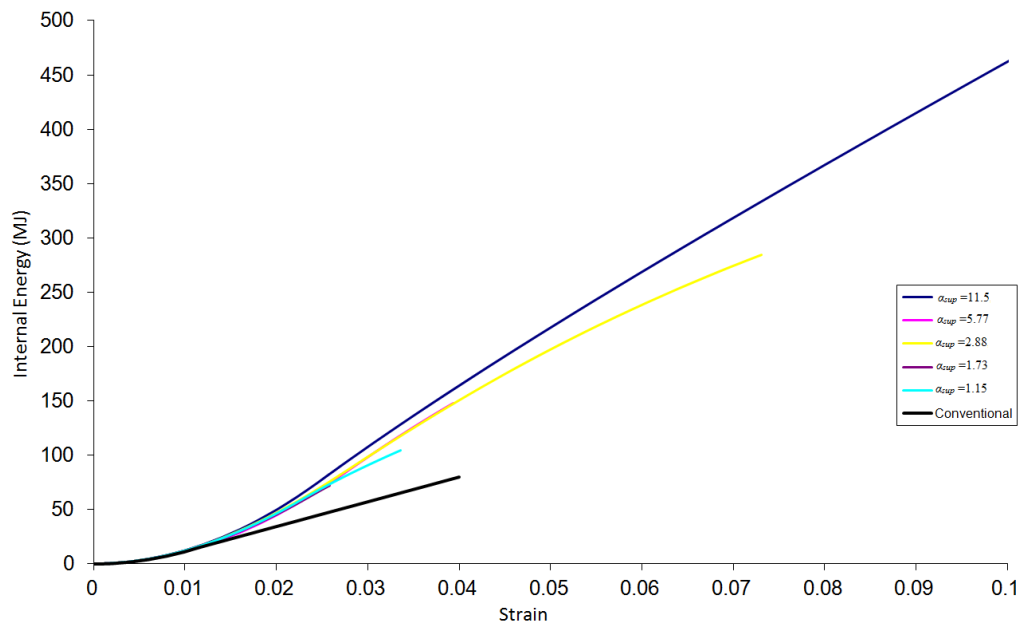


Figure 7.12: Internal energy of functionally graded hierarchical honeycombs against the applied strain compared to a conventional hexagonal honeycomb of the same relative

density. The hierarchical honeycombs investigated has aspect ratios of $\alpha_{sup} = 11.5$, $\alpha_{sup} = 5.77$, $\alpha_{sup} = 2.88$, $\alpha_{sup} = 1.73$ and $\alpha_{sup} = 1.15$.

It is possible to determine the first failure mode analytical of a hierarchical honeycombs loaded out-of-plane, for a given relative density of $\rho^* = 0.0577$ over a range of super-structure aspect ratios. This is achieved by plotting the elastic buckling stress of functionally graded hierarchical honeycombs along with the plastic yield stress against the super-structure thickness t_{sup} for a given super-structure length l_{sup} as shown in Figure 7.13. The predicted failure mode is the one that occurs at the lower stress. It can be seen that high super-structure thicknesses hierarchical honeycombs are more likely to elastically buckle, but lower super-structure thicknesses are more likely to plastically yield. For the case shown in Figure 7.13 for a relative density of $\rho^* = 0.0577$ and the material properties previously described in this chapter there is transfer from elastic buckling to plastic yield of the sub-structure as the dominant failure mechanism as a super-structure thickness of approximately $t_{sup} = 5.5$ for a super-structure length $l_{sup} = 10$.

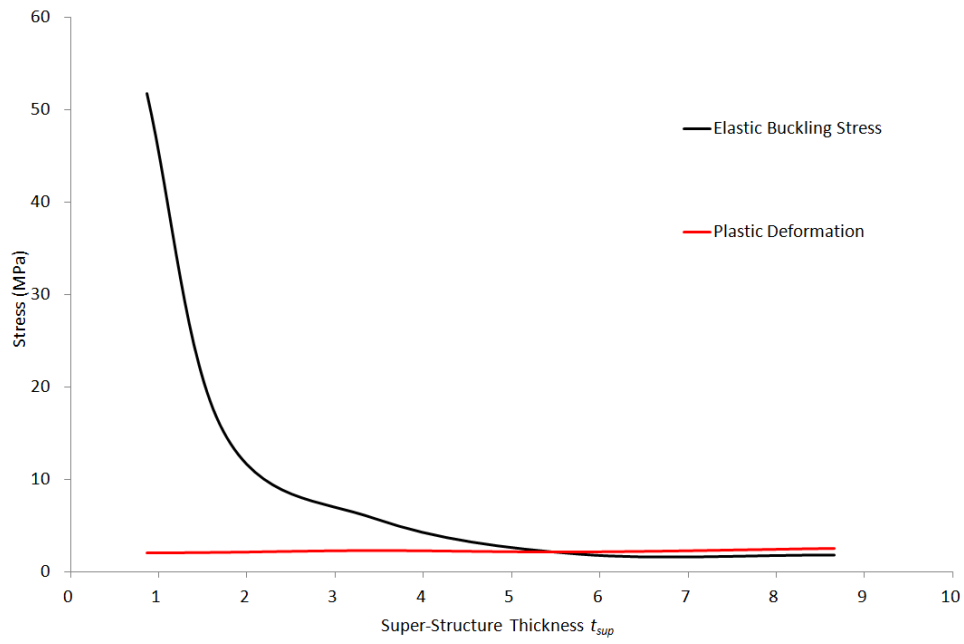


Figure 7.13: Elastic buckling stress of functionally graded hierarchical honeycombs along with the plastic yield stress against the super-structure thickness t_{sup} for a given super-structure length $l_{sup}=10$ and a relative density = 0.0577.

7.5 Discussion

7.5.1 Elastic Models, hierarchical Length Ratio and Super-Structure Aspect Ratio

The most apparent feature of the elastic out-of-plane compression results for functionally graded hierarchical honeycombs presented in Figure 7.8 is that there is little difference in their properties between the hierarchical honeycombs and the conventional hexagonal honeycombs and that the hierarchical length ratio has no effect on the Young's Modulus. This result could be expected as all such structures are stretch dominated in the out-of-plane direction. Since all models have the same relative density the ribs can be described as columns loaded in parallel thus the Young's modulus remains unchanged. This explanation can also be used to describe the results in Figure 7.9 where changing the super-structure aspect has no effect on the out-of-plane Young's modulus of hierarchical honeycombs vs that of a conventional hexagonal honeycomb.

7.5.2 Plasticity and Non-Linear Geometry Models

The effects of introducing plastic material properties and non-linear geometry for functionally graded hierarchical honeycombs on the out-of-plane stress strain response are shown in Figure 7.10. It can be seen that out-of-plane elastic buckling is delayed by the introduction of hierarchy in honeycombs and is highlighted in the results. It is shown that the conventional hexagonal honeycomb experiences elastic buckling at a stress of approximately 1 MPa this concurs with the analytical presented in Equation 7-5 that predicts that the convention hexagonal honeycomb would elastically buckle at stress of 1.02 MPa which is at a lower stress than the plastic yield of the constituent material of 2.54 MPa. It is a similar case for two hierarchical honeycombs when the super-structure aspect ratio is $\alpha_{sup} = 1.15$ and $\alpha_{sup} = 1.73$ which also experience elastic buckling at stresses of approximately 1.5 MPa and 1.6 MPa respectively according to the FEA modelling this is at lower stresses than the onset of plasticity within the model, which occurs at stresses of 1.62 MPa and 1.75 MPa respectively, the strain at which plasticity occurs is shown in Figure 7.11. This results shows close agreement with analytical predictions presented in Equation 7-9 that predicts the elastic buckling stress of the hierarchical honeycombs with super-structure aspect ratios of $\alpha_{sup} = 1.15$ and $\alpha_{sup} = 1.73$ to be 1.80 MPa and 1.90 MPa respectively, both models have an analytical

prediction for the onset of plasticity to be the same as the conventional hexagonal honeycomb of 2.54 MPa, which is greater than that of elastic buckling.

The hierarchical honeycombs that have super-structure aspect ratios of $\alpha_{sup} = 11.5$, $\alpha_{sup} = 5.77$ and $\alpha_{sup} = 2.88$ all experience plastic yield of the constituent material prior to buckling of the structure. According to the FEA the hierarchical honeycombs with super-structure aspect ratio of $\alpha_{sup} = 11.5$, $\alpha_{sup} = 5.77$ and $\alpha_{sup} = 2.88$ initially experience plasticity at stresses of 2.13 MPa, 1.94 MPa and 1.87 MPa respectively the analytical provides an over estimate for the onset of plasticity the same as a conventional hexagonal honeycomb of 2.54 MPa. These results are accurate to within 15 - 30 %; the deviation could be due to stress concentrations being experienced in the sub-structure ribs due to boundary condition couplings or the absence of connecting ribs which have been removed, which is inherent to creating the hierarchical structure.

The early onset of elastic buckling of the conventional hexagonal honeycomb has an effect of reducing the internal energy absorption of the structure as can be seen in Figure 7.12 where the initial response is similar to that of hierarchical honeycombs, but on elastically buckling the internal energy to strain increases at a reduced rate when compared the hierarchical honeycombs.

The marked ability of the hierarchical honeycombs to delay the onset of elastic buckling is due to the increased thickness of sub-structure ribs compared to the sub-structure length. This effectively decreases the sub-structure aspect ratio. As can be seen in Equation 7-5 and Equation 7-6 the elastic buckling of sub-structure ribs is predominantly determined by the $(t_{sub}/l_{sub})^3$ which explains the non-linear response for the elastic buckling stress prediction presented in Figure 7.13, so a small change in the sub-structure aspect ratio has a great effect on the elastic buckling stress. The elastic buckling stress of hierarchical honeycombs is increased as the super-structure thickness t_{sup} decreases as this allows an increase of the sub-structure thickness t_{sub} , hence decreasing the sub-structure aspect ratio. Conversely the plastic yield stress is determined by the (t_{sub}/l_{sub}) as shown in Equation 7-10 and Equation 7-11 resulting in no change in the plastic yield stress of hierarchical honeycomb, also shown in Figure 7.13.

This analysis suggests that there is little to be gained in terms of the out-of-plane plastic collapse stress from the introduction of hierarchy, since plastic yield of the constituent material is independent of the in-plane geometry for a honeycomb, but dependent on the constituent material properties and the cell's relative density. There are however benefits from introducing hierarchy into low relative density honeycombs where the elastic buckling occurs prior to the onset of plastic collapse as is the case for the examples presented. Conventional hexagonal honeycomb with a relative density of 0.0577 would experience failure via elastic buckling at a stress of approximately 1 MPa, but due to the introduction of hierarchy on an equal density basis it can be made to fail via plastic collapse at a stress of approximately 2.2 MPa an increase of 120%.

7.6 Conclusion

The aim of this chapter was to investigate the effects on elastic buckling and plastic collapse in the out-of-plane direction of functionally graded hierarchical honeycombs by changing the super-structure aspect ratio α_{sup} , and to compare to conventional hexagonal honeycombs of the same relative density. It has been shown that there is no change in the elastic properties arising from the introduction of hierarchy, as could be expected. This is due to a honeycomb behaving out-of-plane as columns loaded in parallel and being dependent on the constituent material properties and the density of the honeycomb (Gibson & Ashby 1997). It has also been shown that there is no change in the onset of plastic collapse arising from the introduction of hierarchy, as expected, due to the reliance on the relative density.

There are considerable increases in stress at which the onset of elastic buckling which is shown can occur at lower stresses than plastic collapse. The elastic buckling stress is inversely dependent on the aspect ratio of the sub-structure. The sub-structure is dependent on the aspect ratio of the super-structure and relative density of hierarchical honeycomb. It is possible by the introduction of hierarchy into honeycombs to increase the elastic buckling of honeycombs up to the limit of when plastic collapse occurs in the honeycomb. This is more important on low relative density honeycombs as for higher relative density conventional honeycombs it is more likely that the first mode of failure is via plastic collapse opposed to elastic buckling. It has been shown that there is a delay in the onset of elastic buckling for hexagonal honeycombs, but the same introduction of hierarchy could show increased resistance to elastic buckling for triangular and square honeycombs that would be more prone to elastic buckling than conventional hexagonal honeycomb at low relative densities. For the case shown it can be seen that there is over a 100% increase in the failure stress of the honeycomb due to the introduction of hierarchy.

Chapter 8. Experimental Validation

8.1 Introduction

The aim of this chapter is to experimentally validate the finite element models that have been used in the previous chapters. This was achieved by developing a manufacturing technique to produce hierarchical honeycombs which can then be experimentally tested and compared to finite element models. As is the inherent problem when fabricating hierarchical materials, manufacture of hierarchical honeycombs proved to be difficult and time consuming, limiting the number of samples that could be produced, and a reasonable range was provided to validate the finite element models.

The effect of introducing hierarchy into honeycombs was only investigated for hierarchical honeycombs with 100% mass distribution within the sub-structure, as other mass distributions would be too difficult to accurately manufacture. The same is also true of honeycombs with square and triangular geometry. So the experimental was also limited to hexagonal hierarchical honeycombs. The experimental investigation was undertaken for in-plane and out-of-plane hierarchical honeycombs.

8.2 Method

The in-plane and out-of-plane elastic and plastic response of functionally graded hierarchical honeycomb was determined via experimental models which considered each unit cell as a discrete structure, and made no assumptions about sub-cells as continua.

8.2.1 Manufacture of Hierarchical Honeycombs

Initially it was thought that hierarchical honeycombs could be manufactured via additive layer manufacture, but due to the limitation of wall thicknesses available and the size of unit cells it was not viable. Instead a method more similar to the manufacture of conventional hexagonal honeycombs was chosen as described in Chapter 1 (Wadley 2006). This involved the creation of corrugated aluminium sheet, initially formed by creating a press from two blocks of aluminium with mating hexagonal profile as can be seen in Figure 8.1.



Figure 8.1: Press used to forge corrugated strips

This was later replaced with a rotary method to corrugate strips of aluminium using gears similar to the process described by (Wadley 2006). An image of the machine used is shown in Figure 8.2, which was designed and made with the help of Christophe Scoumaque.



Figure 8.2: Rotary corrugating machine

Following the corrugation process, strips were then attached using adhesive (Araldite 2000+) to create a single row of conventional honeycombs. The rows of honeycombs were then assembled to form an array followed by selective removal of cells to form a hierarchical honeycomb or assembled directly to form a hierarchical honeycomb. An example hierarchical honeycomb manufacture by this process is shown in Figure 8.3

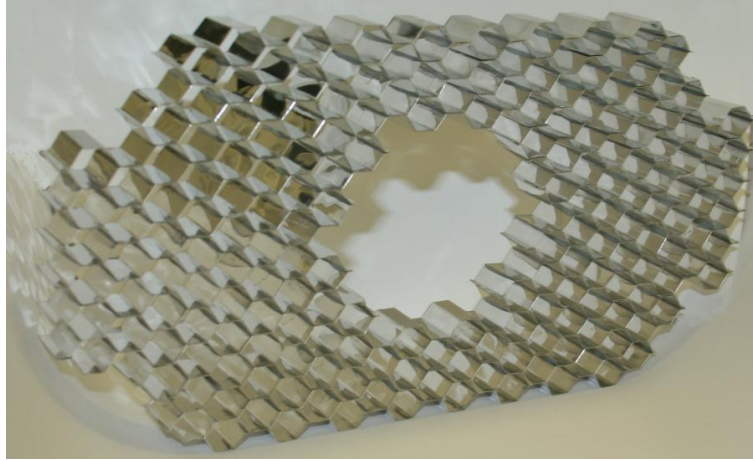


Figure 8.3: An example hierarchical honeycomb manufactured by the process described in this section. Characterisation

8.2.2 Characterisation of Continuum Material

The characterisation of aluminium sheet (constituent material) was done in accordance to ASTM E 8 - 04 using the INSTRON tensile test machine. The 0.13mm thick aluminium sheet was investigated in two axis's in-plane to ensure it was isotropic. A stress-strain plot is shown in Figure 8.4 for an example of the experimental test data, which shows almost exact correlation in the two directions investigated. Also shown is the approximated discretised data used to input material properties into the FE program (Abaqus) (Papka & Kyriakides 1994).

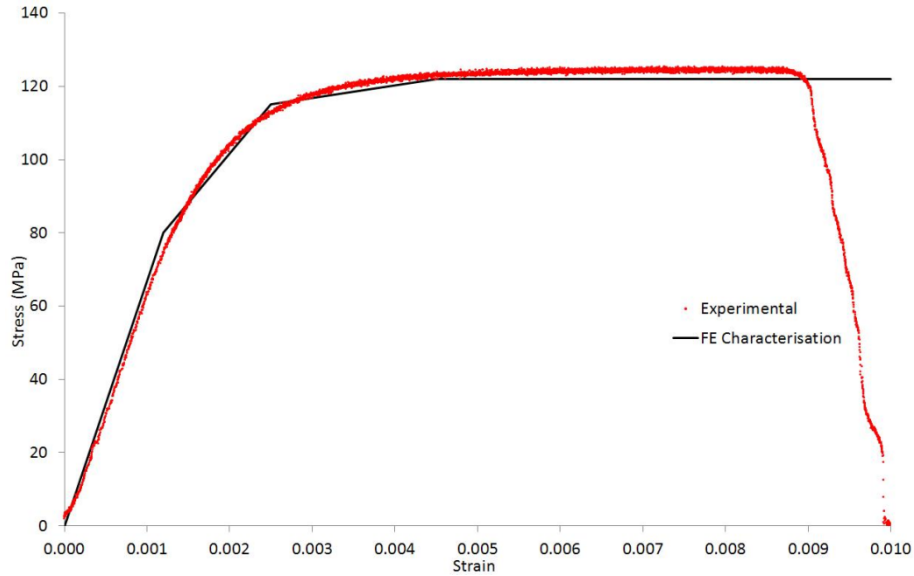


Figure 8.4: Material characterisation of the aluminium sheet used in the manufacture of hierarchical honeycombs along with a discretisation of the material for input into FE models.

8.2.3 In-plane Change in the HLR Experimental

Hierarchical honeycombs used to investigate the change in the HLR were manufactured by the previously described technique. The aluminium hierarchical honeycombs were 20mm deep in the z-axis and all had a super-structure aspect ratio $\alpha_{sup} = 1.15$ and a sub structure aspect ratio $\alpha_{sub} = 53.8$. The number of cells spanning the super-structure was iteratively increased from 2 up to 6 changing the super-structure length to maintain a constant super-structure aspect ratio and relative density. A table showing how the HLR and the relative density changes as the number of sub-cells spanning the super-structure changes is shown in Table 8.1. It can be seen that the relative density varies from $\rho^* = 0.0217$ to $\rho^* = 0.0232$ with a percentage difference of 6.56%. The change in relative density was due to a limited range in thickness of aluminium honeycomb. Hierarchical honeycombs were directly compared to finite element models for each structure investigated and had the same relative density. It was not possible to manufacture honeycombs via the chosen method whilst maintaining constant rib thickness of all sub-structure ribs. It was necessary for horizontal ribs to have thickness $2t$, consistent with honeycombs manufacture by (Kooistra *et al* 2007). This double thickness was replicated in the FE model, assigning appropriate ribs a thickness $2t$. Images of the hierarchical honeycombs described in Table 8.1 are shown in Figure 8.5 to Figure 8.9. Unfortunately

due to the complexity of the introduction of hierarchy and the limitation of sub and super-cell size it was not realistically viable to produce large arrays of hierarchical honeycombs. Instead a single unit cell was investigated and compared to a single cell hierarchical honeycomb finite element model with the same boundary conditions applied.

Sample Number	Number of sub-cells spanning the super-structure	Hierarchical Length Ratio λ	Relative Density ρ^*
1	2	0.250	0.0232
2	3	0.167	0.0226
3	4	0.125	0.0220
4	5	0.1	0.0220
5	6	0.0833	0.0217

Table 8.1: Shows how the HLR and the relative density changes as the number of sub-cells spanning the super-structure changes.



Figure 8.5: Hierarchical honeycomb with 2 sub-cells spanning the super-structure and hierarchical length ratio $\lambda = 0.25$.

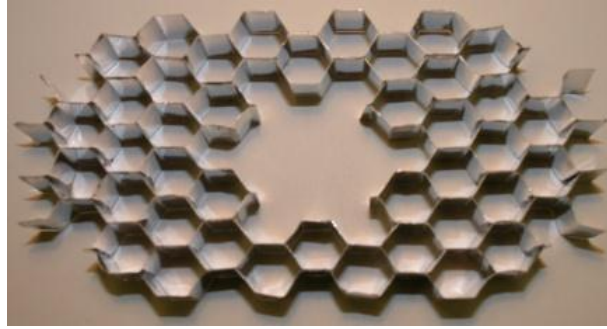


Figure 8.6: Hierarchical honeycomb with 3 sub-cells spanning the super-structure and hierarchical length ratio $\lambda = 0.167$.



Figure 8.7: Hierarchical honeycomb with 4 sub-cells spanning the super-structure and hierarchical length ratio $\lambda = 0.125$.

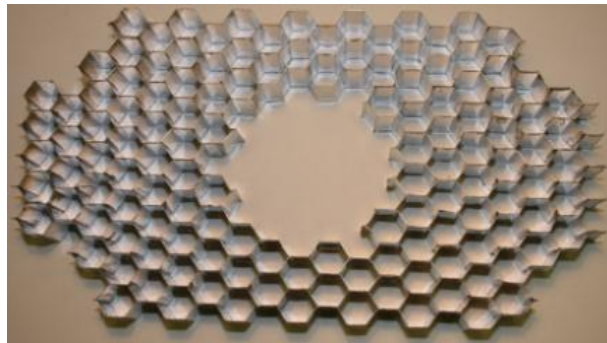


Figure 8.8: Hierarchical honeycomb with 5 sub-cells spanning the super-structure and hierarchical length ratio $\lambda = 0.1$.

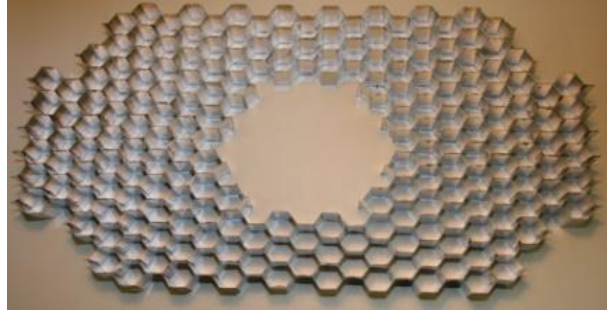


Figure 8.9: Hierarchical honeycomb with 6 sub-cells spanning the super-structure and hierarchical length ratio $\lambda = 0.0833$.

8.2.4 In-plane Change in the Super-Structure Aspect Ratio α_{sup} Experimental

To validate the in-plane finite element models hierarchical honeycombs were manufactured in the same way as the previous honeycombs but for a range of super-structure aspect ratios α_{sup} specifically ($\alpha_{sup} = 1.15$, $\alpha_{sup} = 1.73$, $\alpha_{sup} = 2.89$, $\alpha_{sup} = 5.77$ and $\alpha_{sup} = 7.51$). To change the super-structure aspect ratio the number of ribs spanning the super structure was maintained at 1 cell, instead the length l_{sup} was varied by changing the number of sub-cells running along the length of the super-structure. Unfortunately due to the limited availability of aluminium sheet thicknesses available it was not possible to ensure all models were of an equal density basis and were not compared as such. Instead hierarchical honeycombs were directly compared to finite element models of each aspect ratio investigated. As in the previous section it was not possible to manufacture honeycombs via the chosen method whilst maintaining constant rib thickness of all sub-structure ribs. It was necessary for horizontal ribs to have thickness $2t$. This double thickness was replicated in the FE model, assigning appropriate ribs a thickness $2t$. A table showing how the HLR and the relative density changes as the super-structure aspect ratio α_{sup} changes is shown in Table 8.2. Images of the hierarchical honeycombs described in Table 8.2 are shown in Figure 8.10 to Figure 8.14. Due to the complexity of the introduction of hierarchy and the limitation of sub and super-cell size it was not realistically viable to produce large arrays of hierarchical honeycombs. Instead a single unit cell was investigated and compared to a single cell hierarchical honeycomb finite element model with the same boundary conditions.

Sample Number	Super-Structure Aspect Ratio α_{sup}	Hierarchical Length Ratio λ	Relative Density ρ^*
1	1.15	0.500	0.0300
2	1.73	0.333	0.0267
3	2.89	0.200	0.0160
4	5.77	0.100	0.00901
5	7.51	0.077	0.00687

Table 8.2 Shows how the HLR and the relative density changes as the super-structure aspect ratio α_{sup} changes.

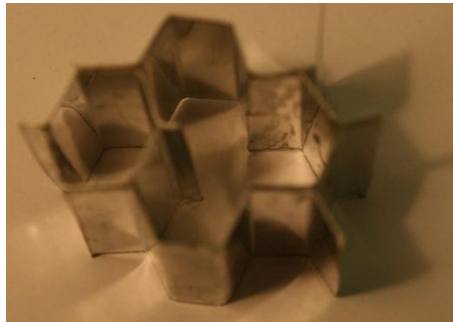


Figure 8.10: Hierarchical honeycomb with a super-structure aspect ratio $\alpha_{sup} = 1.15$ and a hierarchical length ratio $\lambda = 0.5$.



Figure 8.11: Hierarchical honeycomb with a super-structure aspect ratio $\alpha_{sup} = 1.73$ and a hierarchical length ratio $\lambda = 0.333$.

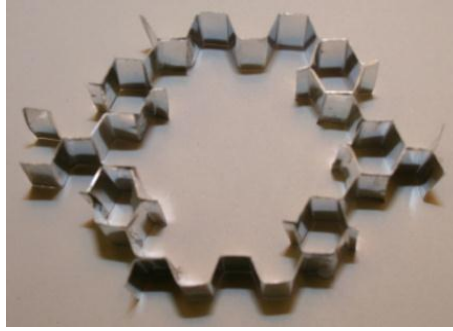


Figure 8.12: Hierarchical honeycomb with a super-structure aspect ratio $\alpha_{sup} = 2.89$ and a hierarchical length ratio $\lambda = 0.1$.

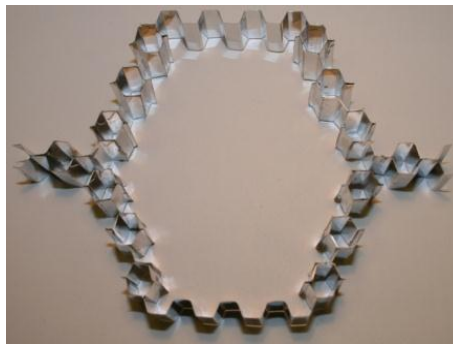


Figure 8.13: Hierarchical honeycomb with a super-structure aspect ratio $\alpha_{sup} = 5.77$ and a hierarchical length ratio $\lambda = 0.2$.



Figure 8.14: Hierarchical honeycomb with a super-structure aspect ratio $\alpha_{sup} = 7.51$ and a hierarchical length ratio $\lambda = 0.077$.

8.2.5 In-plane Discussion of Experimental Procedure

Aluminium hierarchical honeycombs were subjected to an in-plane quasi-static compression test with a displacement rate of 1mm/min. The upper and lower faces of the hierarchical honeycombs were attached to aluminium sheet 0.26mm thick to prevent

the upper and lower horizontal ribs from bowing due to the bending moment created by the connecting ribs. This created a more realistic boundary condition of a periodic honeycomb by restricting the axial displacement and rotation, but over constrained the transverse displacement. This also allowed simple boundary conditions to be replicated in FE where friction between the sample and load plate could be ignored. The horizontal ribs in the middle of the cell were free from end constraints and could be easily replicated in the FE analysis. This resulted in a direct comparison between FE and Experimental boundary conditions. As previously stated only a single cell hierarchical honeycomb was investigated, otherwise the test procedure complied with ASTM C 364.

The specimen size only had a modest effect on the main parameters of the corresponding load displacement responses

(Papka & Kyriakides 1994) pointed out that whilst the size of specimen had an effect on events associated with the crushing of honeycombs the specimen size only had a modest effect on the main parameters of the corresponding load-displacement responses

8.2.6 In-plane Discussion of Finite Element models

Two dimensional finite element models were generated for each unique unit cell in the finite element software ABAQUS. The cell geometry was the same as those previously described in the experimental section and assumed to be made of perfect hexagons free from imperfections (Papka & Kyriakides 1994 & 1998 (1)) and can be seen in Figure 8.15 and Figure 8.16 for the change in HLR and change in the super-structure aspect ratio respectively.

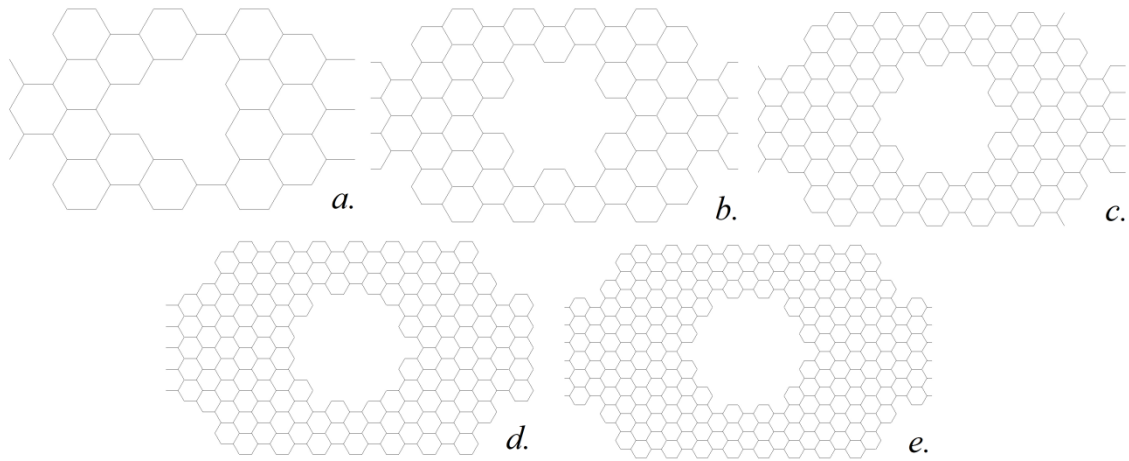


Figure 8.15: Shows how the sub and super-structure dimensions change for a hexagonal super-structure and hexagonal sub-structure hierarchical honeycomb for a) when the super-structure aspect ratio $\alpha_{sup} = 1.15$, b) when the super-structure aspect ratio $\alpha_{sup} = 1.73$, c) when the super-structure aspect ratio $\alpha_{sup} = 2.88$, d) when the super-structure aspect ratio $\alpha_{sup} = 5.77$ and e) when the super-structure aspect ratio $\alpha_{sup} = 7.51$

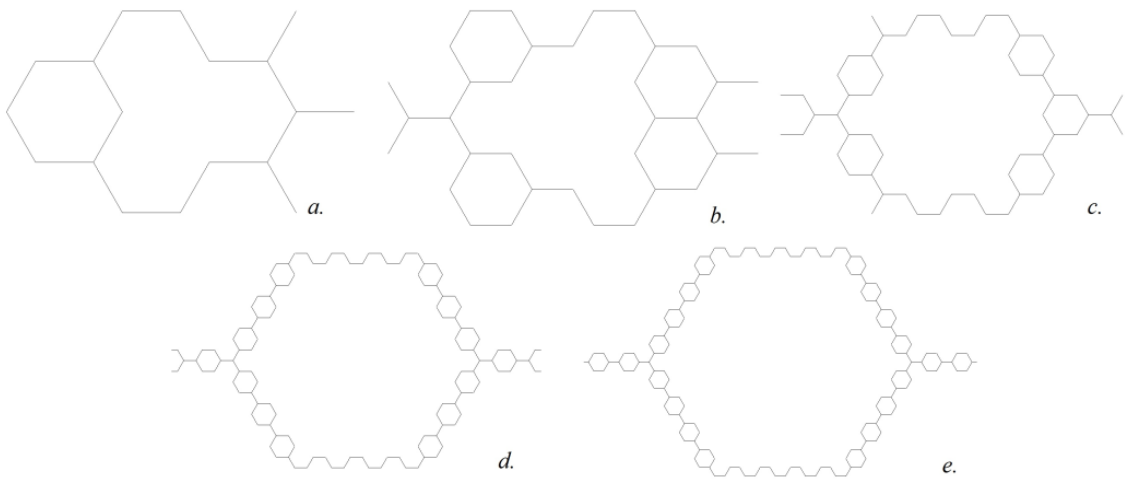


Figure 8.16: Shows how the sub and super-structure dimensions change for a hexagonal super-structure and hexagonal sub-structure hierarchical honeycomb for a) when the super-structure aspect ratio $\alpha_{sup} = 1.15$, b) when the super-structure aspect ratio $\alpha_{sup} = 1.73$, c) when the super-structure aspect ratio $\alpha_{sup} = 2.88$, d) when the super-structure aspect ratio $\alpha_{sup} = 5.77$ and e) when the super-structure aspect ratio $\alpha_{sup} = 7.51$

The constitutive material (Aluminium Sheet) is initially elastic and then exhibits plastic behaviour, to model this a set of linear isotropic elastic constants were defined

consistent with the characterisation of the aluminium sheet and used for all cases (specifically $E_s = 50$ GPa and $\nu_s = 0.36$) the non-linear material behaviour was specified as a plastic response. The nonlinear material behaviour was modelled by strain increments and assumed to consist of an elastic part and an inelastic part similar to that proposed (Chung & Waas 2001) (Papka & Kyriakides 1994 & 1998 (1)). The plastic material properties were defined as a yield stress corresponding to a plastic strain and can be seen in Table 8.3. Non-linear geometry was also specified.

Yield Stress	Plastic Strain
80	0
115	0.0013
122	0.0020
122	0.0055

Table 8.3: Shows how the plastic strain response was inputted into Abaqus

The step used was specified as ‘*Static, Riks*’ which uses the load magnitude as an additional unknown and solves simultaneously for loads and displacements. The ‘*Static Riks*’ step is used due to the issues involved with buckling or collapse behaviour of geometrically non-linear static problems, where the load-displacement response shows a negative stiffness resulting in the structure releasing strain energy to remain in equilibrium similarly to (Shariati & Rokhi 2008, Waas 2002 and Kim & Lee 2002). The Riks method allows static equilibrium states during the unstable phase of the response and is used to predict unstable, geometrically nonlinear collapse of a structure including the nonlinear material behaviour. The strain applied to the model was increased from 0.1% in the elastic regime to 50% to investigate the plastic regime, but due to use of ‘*Static Riks*’ it was not possible to specify the exact strain on the model as an arc length is used to define the progress of the model not a force or a displacement. The sub and super-cells were modelled using a minimum of 20 2D Timoshenko beam elements (B22: a 3-node quadratic beam) per cell rib (Papka & Kyriakides 1994 & 1998 (1)) (Chung & Waas 2001) using a commercial Finite Element (FE) analysis package (ABAQUS, version 6.9. Dassault Systèmes). Boundary sharing ribs had either half thickness or half-lengths, corresponding to the experimental samples.

History outputs were created to extract data from the models. Specifically the displacement and reaction force for each increment on the displaced face. The reaction force normal to the displaced face and the displacement were used to create the stress strain graph as the projected area was known along with the original height of the model from the initial geometry.

Whilst the inclusion of non-linear geometry and material properties were incorporated into the model, this was the extent of the model. The aim of the study was to compare the non-linear elastic response and plastic yield of hierarchical honeycombs to experimental samples. The problem complexity is reduced by neglecting the presence of the adhesive used to connect honeycomb ribs assuming a perfect bond along with changes in the mechanical properties and residual stresses due to the forging process used to manufacture the corrugated honeycomb. The rounding of the corners of the actual cells is also neglected and an idealised geometry assumed, similar to the models created in (Wilbert *et al* 2011). The models show large strains and a large post yield response with no sign of further fracture or failure; this is a limitation of the model. No attempt to predict the possible areas of fracture have been made depending on the initial onset of plasticity as due to the complex nature of the structures stress concentrations could change move post yield. It is also true to say that imperfections that may occur due to manufacture and the onset of fracture were ignored, but the models can be validated against the experimental samples which obviously take into account the above simplifications.

8.2.7 Out-of-plane Change in the Super-Structure Aspect Ratio α_{sup} Experimental

To validate the out-of-plane finite element models hierarchical honeycombs were manufacture in the same way as the previous honeycombs for a range of super-structure aspect ratios α_{sup} specifically ($\alpha_{sup} = 1.15$, $\alpha_{sup} = 1.73$, $\alpha_{sup} = 2.89$ and $\alpha_{sup} = 5.77$). The super structure aspect ratio was changed in the same way as the in-plane investigation by maintaining 1 sub-cell spanning the super-structure and changing the number of sub cells along the length of the super-structure. Again as in the in-plane investigation, due to the limited availability of aluminium sheet thicknesses available it was not possible to ensure all models were of an equal density basis and were not compared as such. Instead

hierarchical honeycombs were directly compared to finite element models of each aspect ratio investigated. As in the previous sections it was not possible to manufacture honeycombs via the chosen method whilst maintaining constant rib thickness of all sub-structure ribs. It was necessary for horizontal ribs to have thickness $2t$. This double thickness was replicated in the FE model, assigning appropriate ribs a thickness $2t$. A table showing how the HLR and the relative density changes as the super-structure aspect ratio α_{sup} changes is shown in Table 8.4. Images of the hierarchical honeycombs described in Table 8.4 are shown in Figure 8.17. Due to the complexity of the introduction of hierarchy and the limitation of sub and super-cell size it was not realistically viable to produce large arrays of hierarchical honeycombs. Instead a single unit cell was investigated and compared to a single cell hierarchical honeycomb finite element model with the same boundary conditions.

Sample Number	Super-Structure Aspect Ratio α_{sup}	Hierarchical Length Ratio λ	Relative Density ρ^*
1	1.15	0.500	0.0300
2	1.73	0.333	0.0267
3	2.89	0.200	0.0160
4	5.77	0.100	0.00901

Table 8.4 Shows how the HLR and the relative density changes as the super-structure aspect ratio α_{sup} changes.

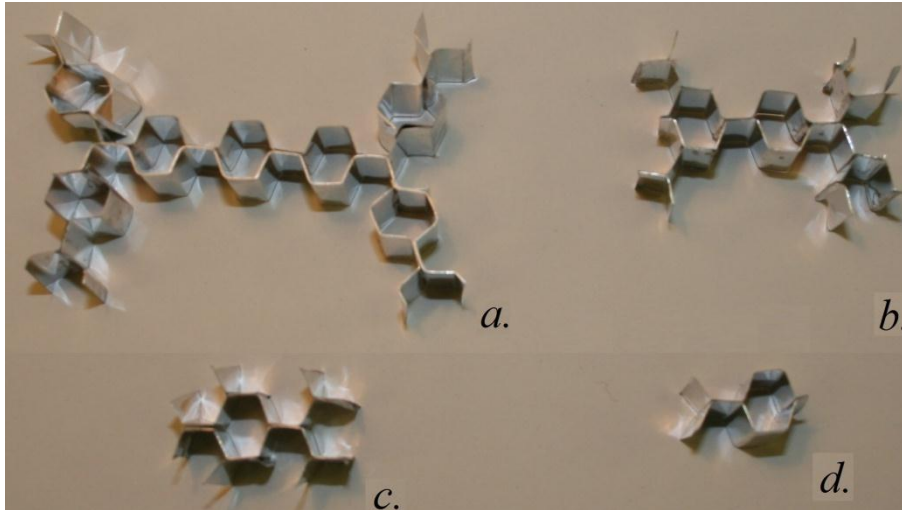


Figure 8.17: Hierarchical honeycombs with a) a super-structure aspect ratio $\alpha_{sup} = 1.15$ and a hierarchical length ratio $\lambda = 0.5$, b) a super-structure aspect ratio $\alpha_{sup} = 1.73$ and a hierarchical length ratio $\lambda = 0.333$, c) a super-structure aspect ratio $\alpha_{sup} = 2.88$ and a hierarchical length ratio $\lambda = 0.1$ and d) a super-structure aspect ratio $\alpha_{sup} = 5.77$ and a hierarchical length ratio $\lambda = 0.2$.

8.2.8 Out-of-plane Discussion of Experimental Procedure

Aluminium hierarchical honeycombs were subjected to an out-of-plane quasi-static compression test with a displacement rate of 1mm/min. The upper and lower faces of the hierarchical honeycombs were attached to aluminium sheet 0.26mm thick to simulate the face sheet of a sandwich panel ideally resulting in fixed end for the upper and lower faces of the sample. The face sheet was attached using Araldite 2000+. The addition of the face sheet allowed simple boundary conditions to be replicated in FE where friction between the sample and load plate could be ignored. The free ends from boundary sharing ribs were free from end constraints and could be easily replicated in the FE analysis. This resulted in a direct comparison between FE and Experimental boundary conditions. As previously stated only a single cell hierarchical honeycomb was investigated, otherwise the test procedure complied with ASTM C 365

8.2.9 Out-of-plane Discussion to Finite Element models

Models of functionally graded hierarchical structures were developed by producing a 3D part in the finite element software ABAQUS. The cell geometry was the same as

those previously described in the out-of-plane experimental section and can be seen in Figure 8.18.

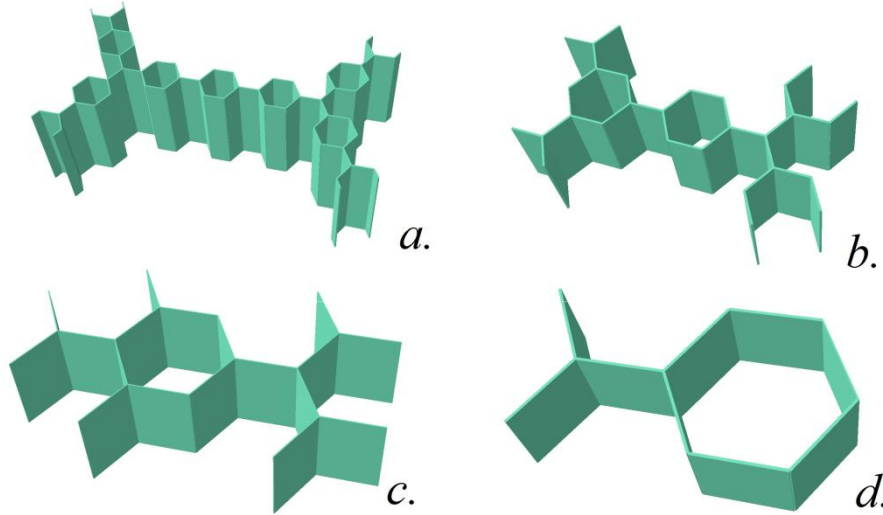


Figure 8.18: Shows how the sub and super-structure dimensions change for a hexagonal super-structure and hexagonal sub-structure hierarchical honeycomb for a) when the super-structure aspect ratio $\alpha_{sup} = 5.77$, b) when the super-structure aspect ratio $\alpha_{sup} = 2.88$, c) when the super-structure aspect ratio $\alpha_{sup} = 1.73$ and d) when the super-structure aspect ratio $\alpha_{sup} = 1.15$

The constitutive material (Aluminium Sheet) is initially elastic and then exhibits plastic behaviour, to model this a set of linear isotropic elastic constants were defined consistent with the characterisation of the aluminium sheet and used for all cases (specifically $E_s = 50$ GPa and $\nu_s = 0.36$) the non-linear material behaviour was specified as a plastic response. The nonlinear material behaviour was modelled by strain increments and assumed to consist of an elastic part and an inelastic part similar to that proposed (Chung & Waas 2001) (Papka & Kyriakides 1994 & 1998 (1)). The plastic material properties were defined as a yield stress corresponding to a plastic strain and can be seen in Table 8.3. Non-linear geometry was also specified. Similar to the in-plane models a ‘*Static, Riks*’ step was used for the same reasons previously described.

The models used to determine the out-of-plane properties of a hierarchical honeycomb were the same half unit cell as the experimental and a 2D plan view of a conventional hexagonal honeycomb array along with a unit and half unit cell highlighted is shown in

Figure 7.5. The unit cell used to model the out-of-plane response were consistent with the unit cell used in (Wilbert *et al* 2011) to model the out-of-plane buckling of aluminium conventional hexagonal honeycombs and showed that the half unit cell with the correct boundary conditions replicated well the response of larger honeycomb arrays.

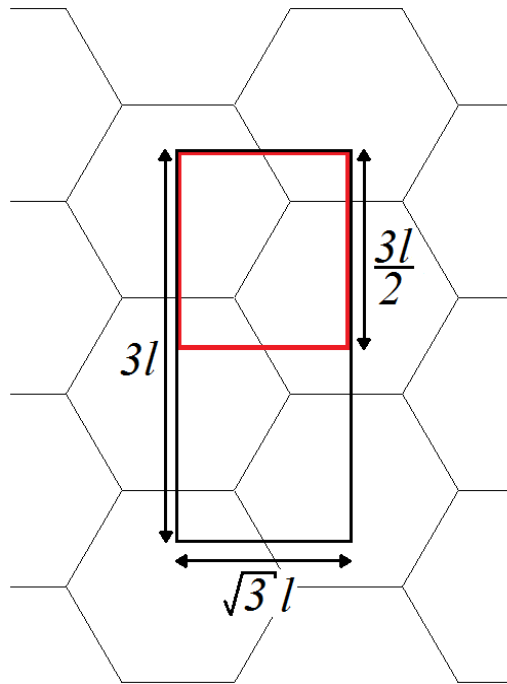


Figure 8.19: 2D plan view of a hexagonal honeycomb array along with a highlighting repeatable unit cell in black and half a repeatable unit cell in red. The global dimensions of the unit cell are also shown.

History outputs were created to extract data from the models. Specifically the displacement and reaction force for each increment on the displaced face. The reaction force normal to the displaced face and the displacement were used to create the stress strain graph as the projected area was known along with the original height of the model from the initial geometry.

Whilst the inclusion of non-linear geometry and material properties were incorporated into the model, this was the extent of the model. The aim of the study was to compare the non-linear elastic response and plastic yield of hierarchical honeycombs to experimental samples. The problem complexity is reduced by neglecting the presence of the adhesive used to connect honeycomb ribs assuming a perfect bond along with

changes in the mechanical properties and residual stresses due to the forging process used to manufacture the corrugated honeycomb. The rounding of the corners of the actual cells is also neglected and an idealised geometry assumed, similar to the models created in (Wilbert *et al* 2011). The models show large strains and a large post yield response with no sign of further fracture or failure; this is a limitation of the model. No attempt to predict the possible areas of fracture have been made depending on the initial onset of plasticity as due to the complex nature of the structures stress concentrations could be move post yield. It is also true to say that imperfections that may occur due to manufacture and the onset of fracture were ignored, but the models can be validated against the experimental samples which obviously take into account the above simplifications.

Boundary conditions applied to the model were comparable to those of a sandwich panel in that the bottom face of the model was restrained to zero displacement in the X, Y and Z axis's along with zero rotation around the X, Y and Z axis's effectively encastred. The top face of the model had similar boundary conditions as the bottom but a uniform displacement was applied negatively in the Z axis applying a strain of 0.1% normal to the face, putting the model in compression. These boundary conditions can be seen in Figure 7.6, for simplicity a conventional honeycomb is shown, but boundary conditions are exactly the same as those applied to hierarchical honeycombs. The half-length beams at the side of the structure were modelled as free end in that no boundary conditions were applied replicating the experimental tests.

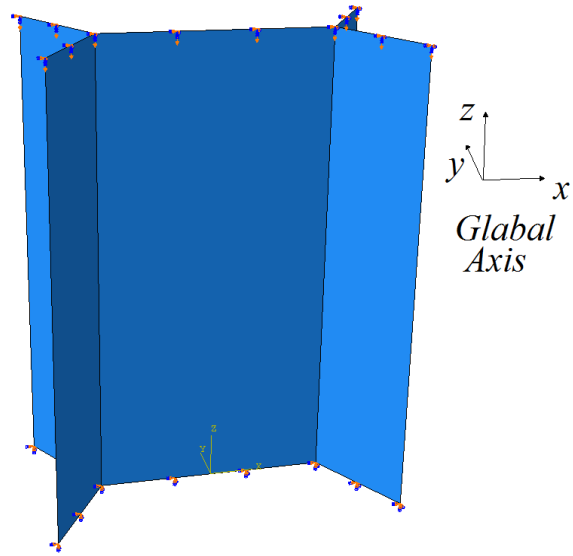


Figure 8.20: Boundary conditions applied to the top and bottom face of a conventional honeycomb.

8.3 Results

8.3.1 In-plane Change in the HLR Experimental

The in-plane results of changing the HLR for a super-structure aspect ratio $\alpha_{sup} = 1.15$ are shown, firstly for a comparison in the elastic regime between the experimental and FE followed by stress strain plots for each hierarchical honeycomb as the number of sub-cells spanning the super-structure rib thickness changes. Also shown are deformation plots FE analysis of models compared to experimental deformation images.

The in-plane Young's modulus normalised to the relative density is plotted against the number of sub-cells spanning the super-structure in Figure 8.21. It can be seen that there is a correlation between the experimental and the FE analysis, but there is a percentage difference of 9% when there are 2 sub-cells spanning the super-structure rib thickness to a percentage difference of 6% when there are 6 sub-cells spanning the super-structure rib thickness. Error bars are shown in Figure 8.21 for the normalised Young's modulus for 10%, taking into account measurement errors and imperfections in the Geometry of the unit cell. The same approach was taken into account when calculating uncertainty in Figure 8.32 and Figure 8.43.

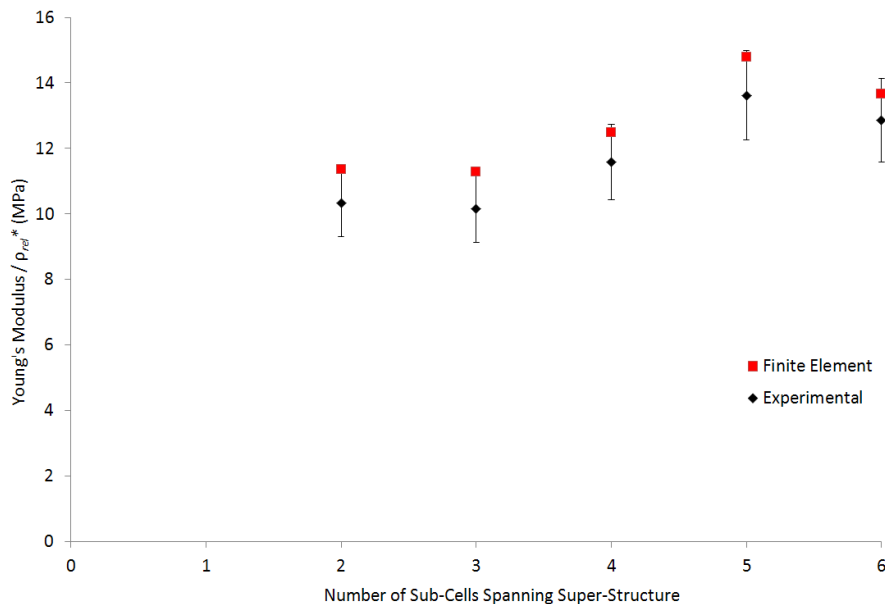


Figure 8.21 Young's modulus normalised to the relative density against the number of sub-cells spanning the super-structure for experimental and finite element results for

hierarchical honeycombs. The experimental results show an error bar of 10% for the normalised Young's.

Stress strain plots are shown in Figure 8.22, Figure 8.24, Figure 8.26, Figure 8.28 and Figure 8.30 for changes in the number of sub-cells spanning the super-structure for a super-structure aspect ratio $\alpha_{sup} = 1.15$. There is a clear correlation between the FE and experimental data although the FE consistently overestimates the stress for low strains. This is due to a bedding in region for the samples that is not allowed for in the FE. There is a clear correlation between the two sets of results, which is reiterated in the FE and experimental deformation images also shown for each hierarchical honeycomb in Figure 8.23, Figure 8.25, Figure 8.27, Figure 8.29 and Figure 8.31.

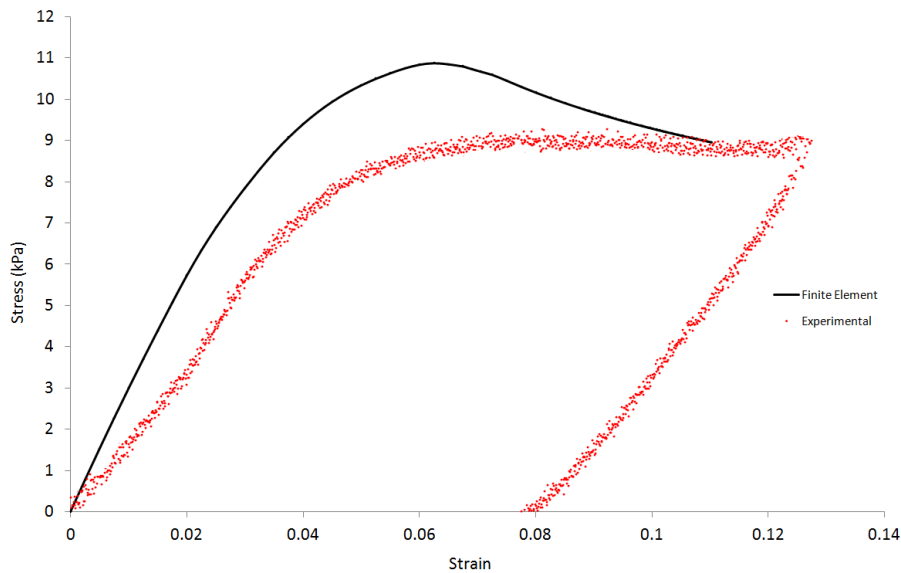


Figure 8.22: Stress strain response for experimental and finite element results for a hierarchical honeycomb with a super-structure aspect ratio $\alpha_{sup} = 1.15$, a relative density of 0.0232 and 2 sub-cells spanning the super-structure giving a HLR = 0.25.

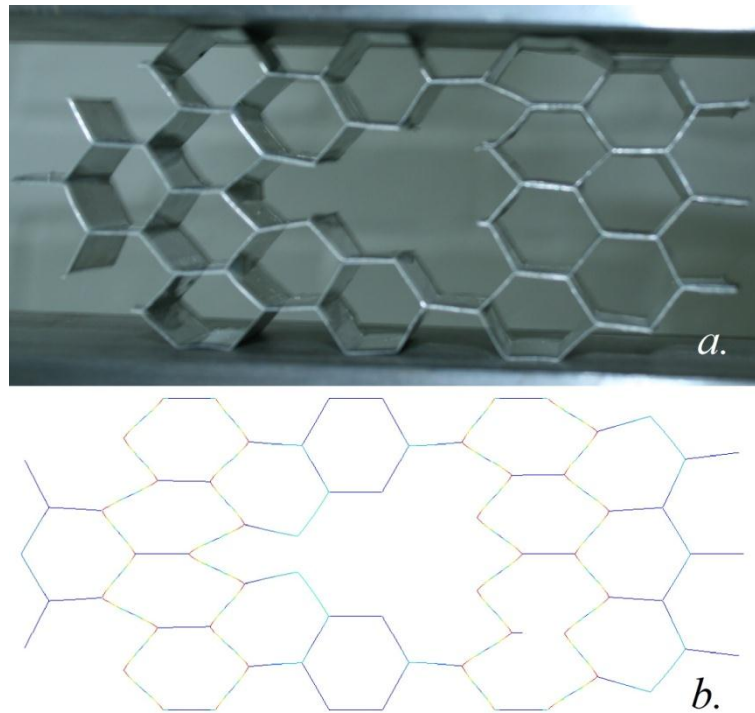


Figure 8.23: Comparison of the deformation between FE analysis and experimental test for a hierarchical honeycomb with a super-structure aspect ratio $\alpha_{sup} = 1.15$, a relative density of 0.0232 and 2 sub-cells spanning the super-structure giving a HLR = 0.25.

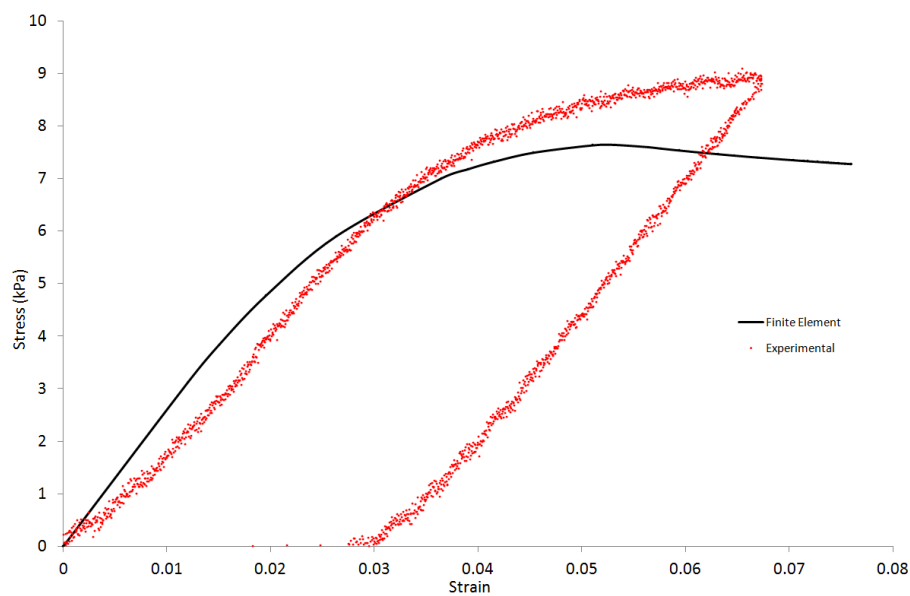


Figure 8.24: Stress strain response for experimental and finite element results for a hierarchical honeycomb with a super-structure aspect ratio $\alpha_{sup} = 1.15$, a relative density of 0.0226 and 3 sub-cells spanning the super-structure giving a HLR = 0.167.

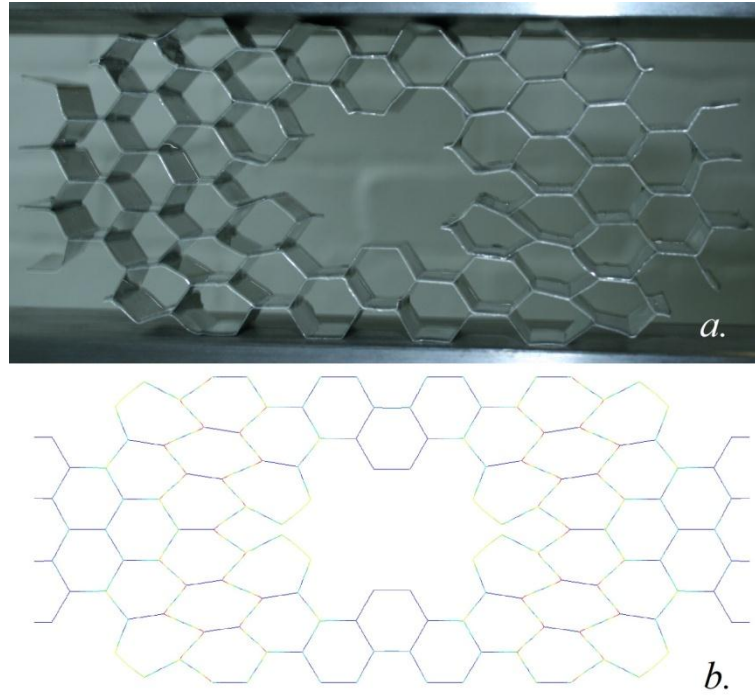


Figure 8.25: Comparison of the deformation between FE analysis and experimental test for a hierarchical honeycomb with a super-structure aspect ratio $\alpha_{sup} = 1.15$, a relative density of 0.0226 and 3 sub-cells spanning the super-structure giving a HLR = 0.167.

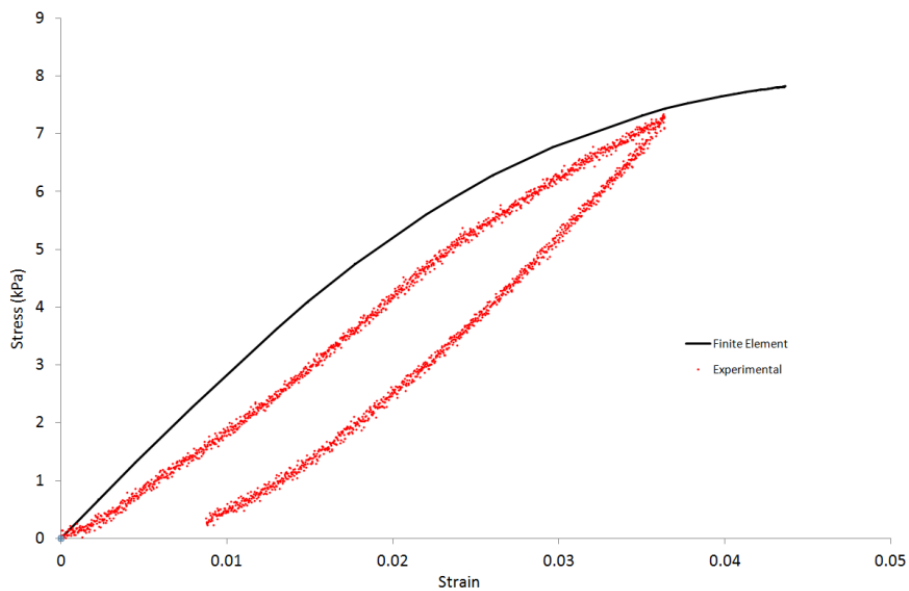


Figure 8.26: Stress strain response for experimental and finite element results for a hierarchical honeycomb with a super-structure aspect ratio $\alpha_{sup} = 1.15$, a relative density of 0.0220 and 4 sub-cells spanning the super-structure giving a HLR = 0.125.

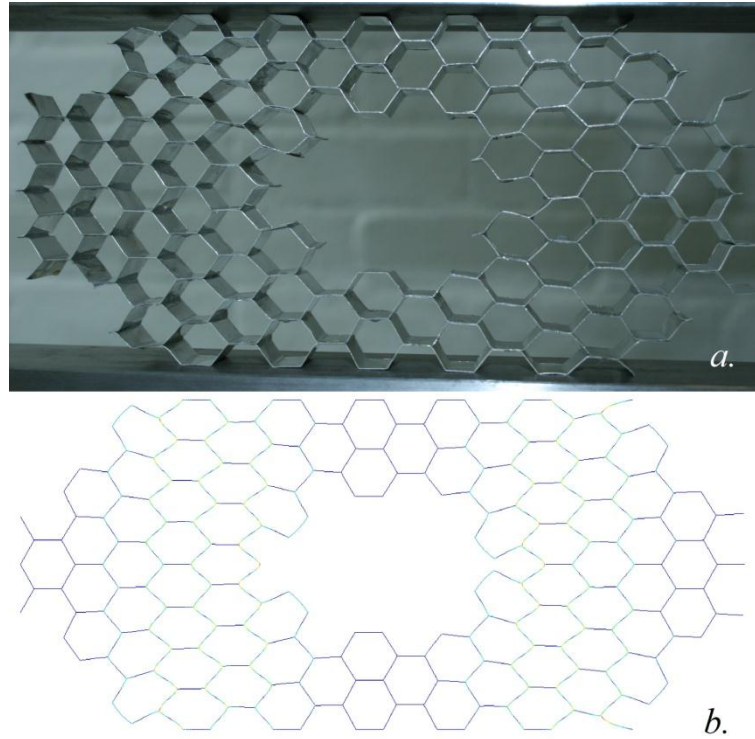


Figure 8.27: Comparison of the deformation between FE analysis and experimental test for a hierarchical honeycomb with a super-structure aspect ratio $\alpha_{sup} = 1.15$, a relative density of 0.0220 and 4 sub-cells spanning the super-structure giving a HLR = 0.125.

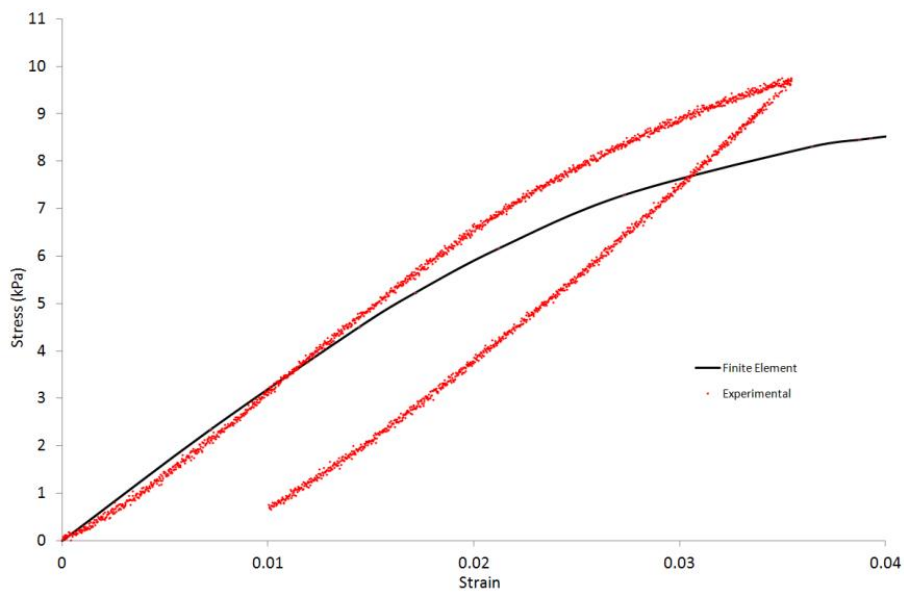


Figure 8.28: Stress strain response for experimental and finite element results for a hierarchical honeycomb with a super-structure aspect ratio $\alpha_{sup} = 1.15$, a relative density of 0.0220 and 5 sub-cells spanning the super-structure giving a HLR = 0.100.

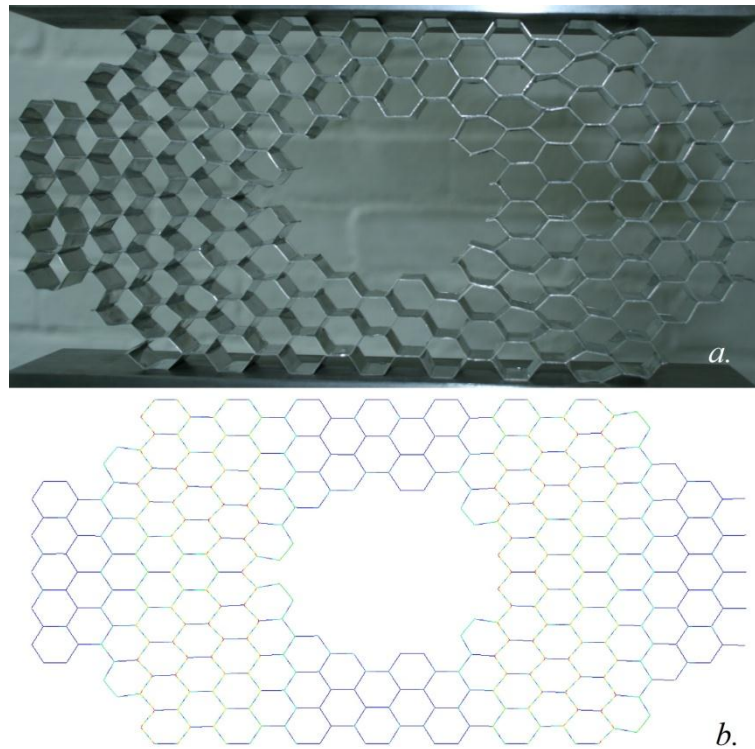


Figure 8.29: Comparison of the deformation between FE analysis and experimental test for a hierarchical honeycomb with a super-structure aspect ratio $\alpha_{sup} = 1.15$, a relative density of 0.0220 and 5 sub-cells spanning the super-structure giving a HLR = 0.100.

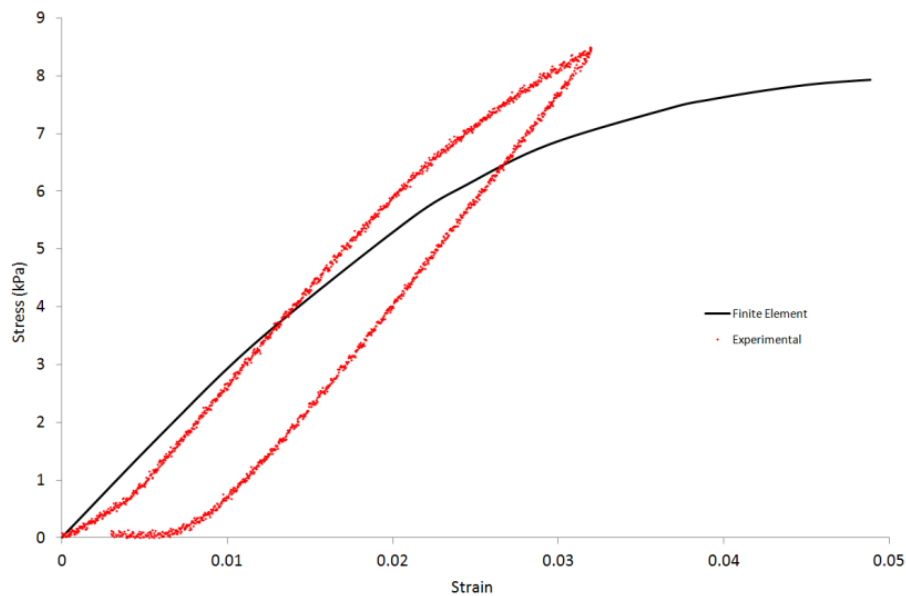


Figure 8.30: Stress strain response for experimental and finite element results for a hierarchical honeycomb with a super-structure aspect ratio $\alpha_{sup} = 1.15$, a relative density of 0.0218 and 6 sub-cells spanning the super-structure giving a HLR = 0.0833.

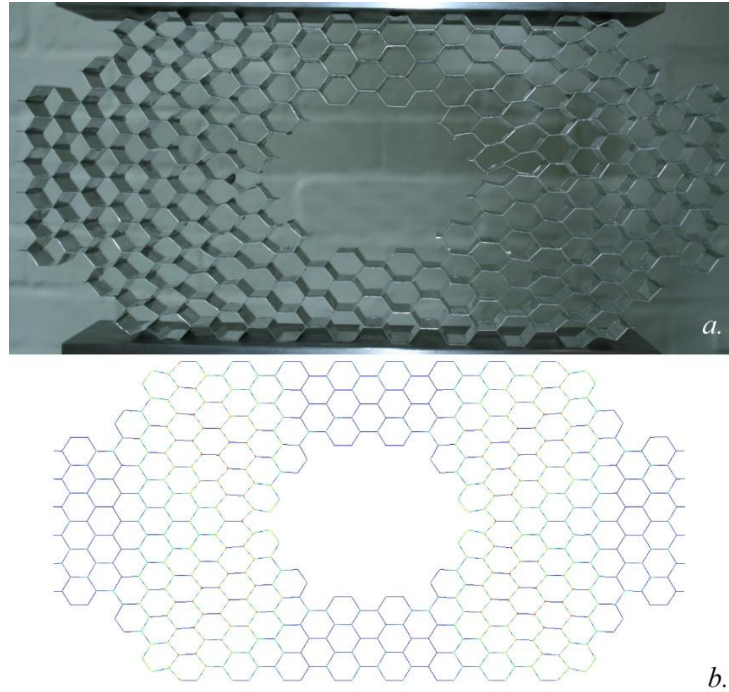


Figure 8.31: Comparison of the deformation between FE analysis and experimental test for a hierarchical honeycomb with a super-structure aspect ratio $\alpha_{sup} = 1.15$, a relative density of 0.0218 and 6 sub-cells spanning the super-structure giving a HLR = 0.0833.

8.3.2 In-plane Change in the Super-Structure Aspect Ratio α_{sup} Experimental

The in-plane results of changing the super-structure aspect ratio α_{sup} are shown, firstly for a comparison in the elastic regime between the experimental and FE followed by stress strain plots for each hierarchical honeycomb. Also shown are experimental deformation images compared to FE analysis deformation plots.

The in-plane Young's modulus normalised to the relative density is plotted against the super-structure aspect ratio α_{sup} in Figure 8.21. It can be seen that there is a correlation between the experimental and the FE analysis, but there is a percentage difference of 9.7% when the super structure aspect ratio $\alpha_{sup} = 1.73$ to a percentage difference of -4.7% when the super structure aspect ratio $\alpha_{sup} = 5.77$.

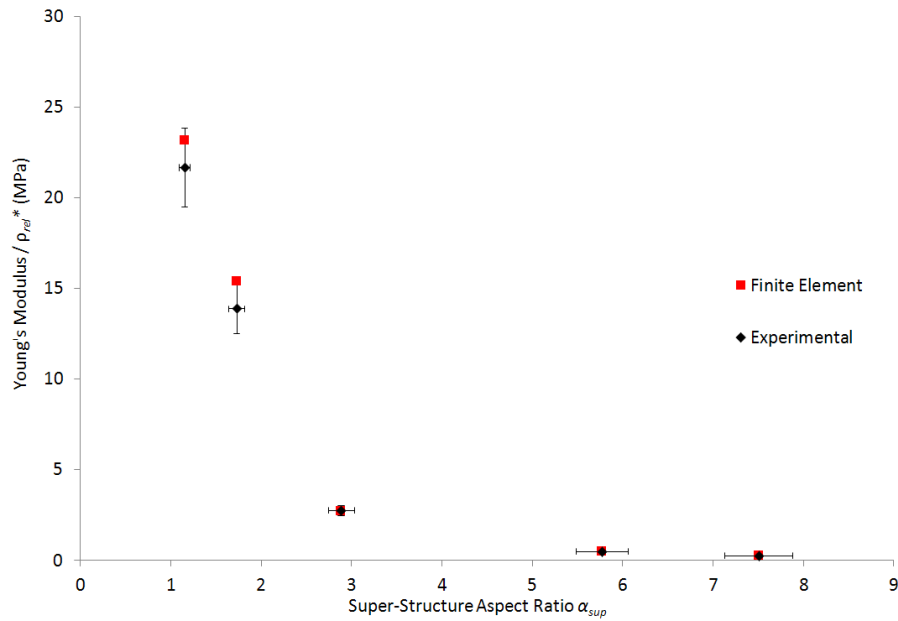


Figure 8.32: In-plane Young's modulus normalised to the relative density against the super-structure aspect ratio for experimental and finite element results for hierarchical honeycombs. The experimental results show error bars of 10% for the normalised Young's modulus and 5% for the super-structure aspect ratio.

Stress strain plots are shown in Figure 8.33, Figure 8.35, Figure 8.37, Figure 8.39 and Figure 8.41 for changes in the super-structure aspect ratio α_{sup} . Again there is a clear correlation between the FE and experimental data although the FE consistently overestimates the stress for low strains. This is due to a bedding in region for the samples that is not allowed for in the FE. There is a clear correlation between the two sets of results, which is reiterated in the FE and experimental deformation images also shown for each hierarchical honeycomb in Figure 8.34, Figure 8.36, Figure 8.38, Figure 8.40 and Figure 8.42.

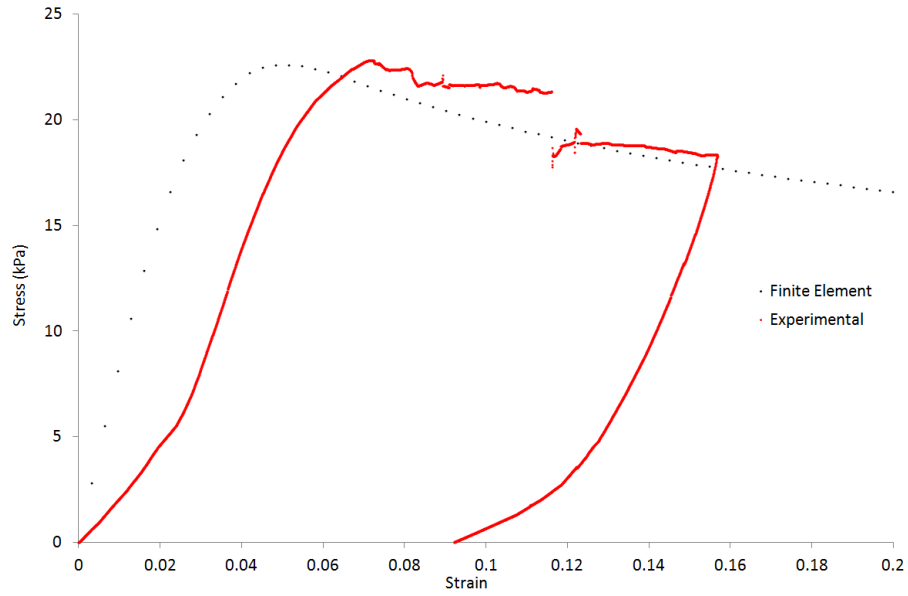


Figure 8.33: Stress strain response for experimental and finite element results for a hierarchical honeycomb with a super-structure aspect ratio $\alpha_{sup} = 1.15$, a relative density of 0.0300 and a HLR = 0.5.

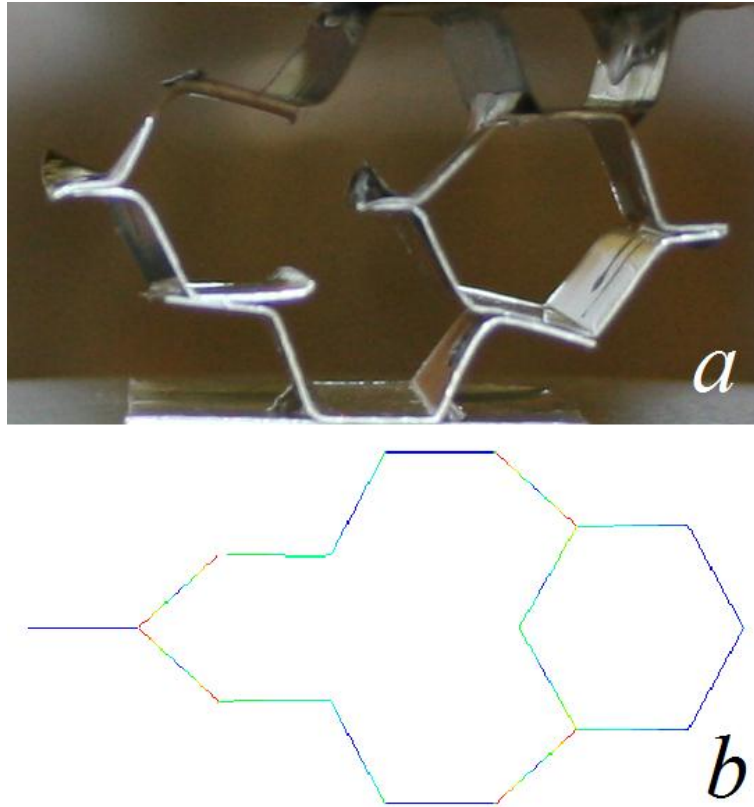


Figure 8.34: Comparison of the deformation between FE analysis and experimental test for a hierarchical honeycomb with a super-structure aspect ratio $\alpha_{sup} = 1.15$, a relative density of 0.0300 and a HLR = 0.5.

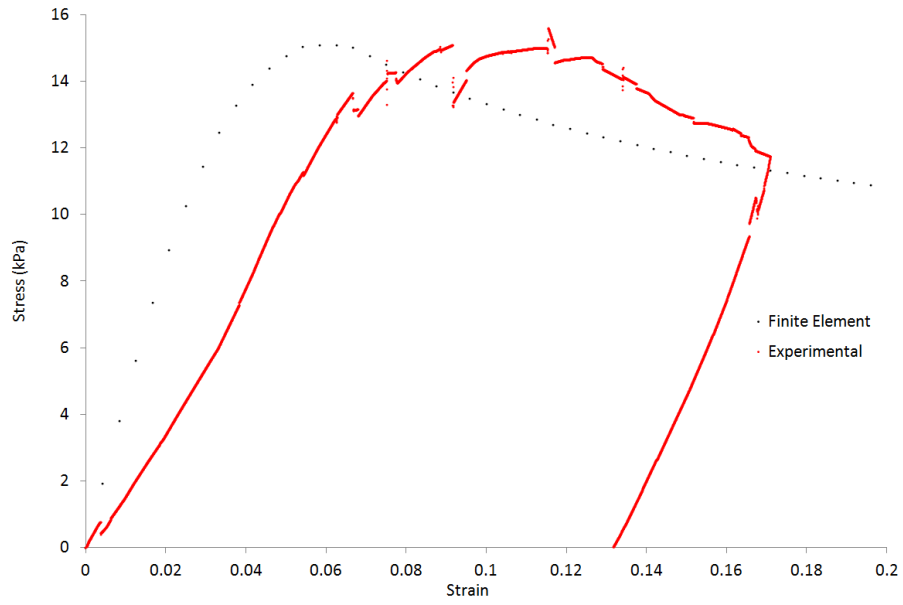


Figure 8.35: Stress strain response for experimental and finite element results for a hierarchical honeycomb with a super-structure aspect ratio $\alpha_{sup} = 1.73$, a relative density of 0.0267 and a HLR = 0.333.

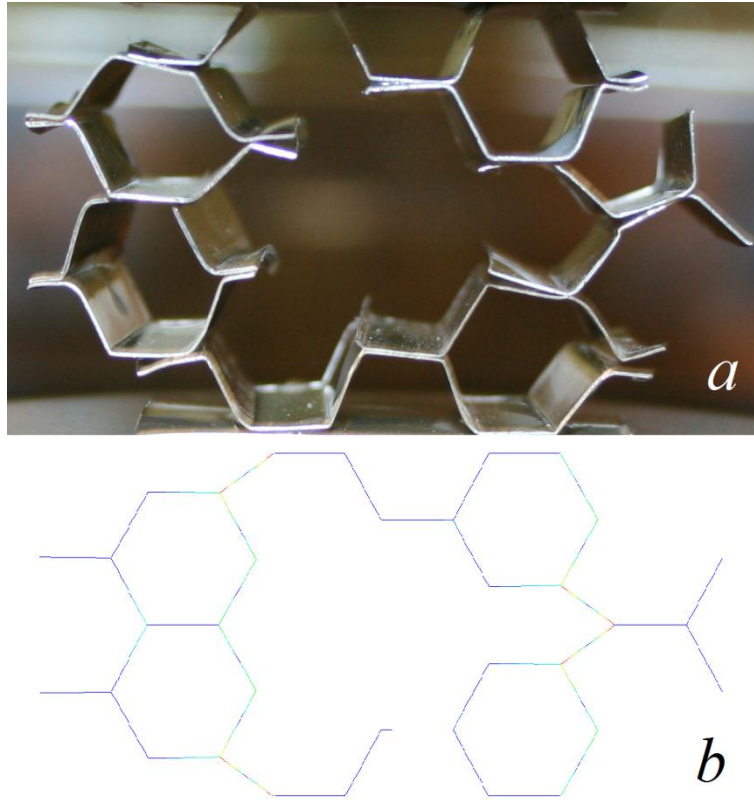


Figure 8.36: Comparison of the deformation between FE analysis and experimental test for a hierarchical honeycomb with a super-structure aspect ratio $\alpha_{sup} = 1.73$, a relative density of 0.0267 and a HLR = 0.333.

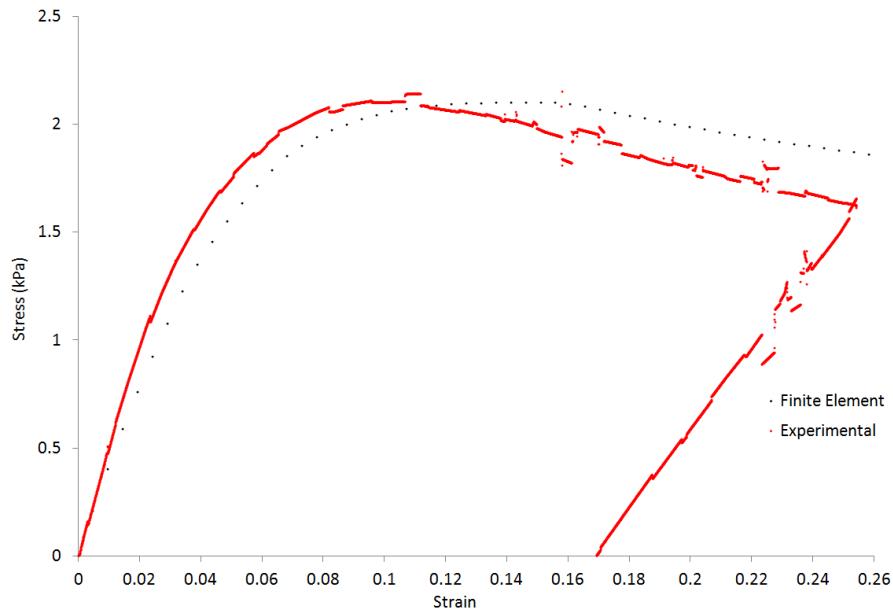


Figure 8.37: Stress strain response for experimental and finite element results for a hierarchical honeycomb with a super-structure aspect ratio $\alpha_{sup} = 2.89$, a relative density of 0.0160 and a HLR = 0.2.

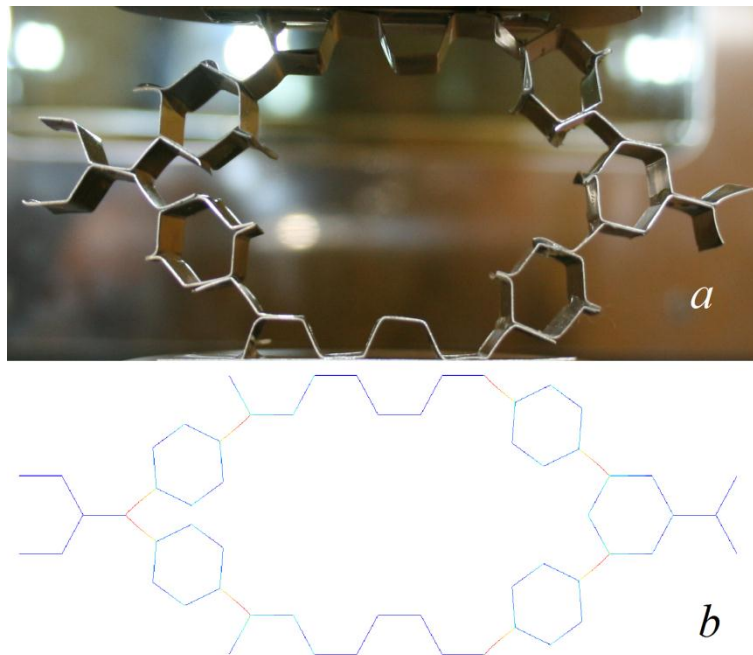


Figure 8.38: Comparison of the deformation between FE analysis and experimental test for a hierarchical honeycomb with a super-structure aspect ratio $\alpha_{sup} = 2.89$, a relative density of 0.0160 and a HLR = 0.2.

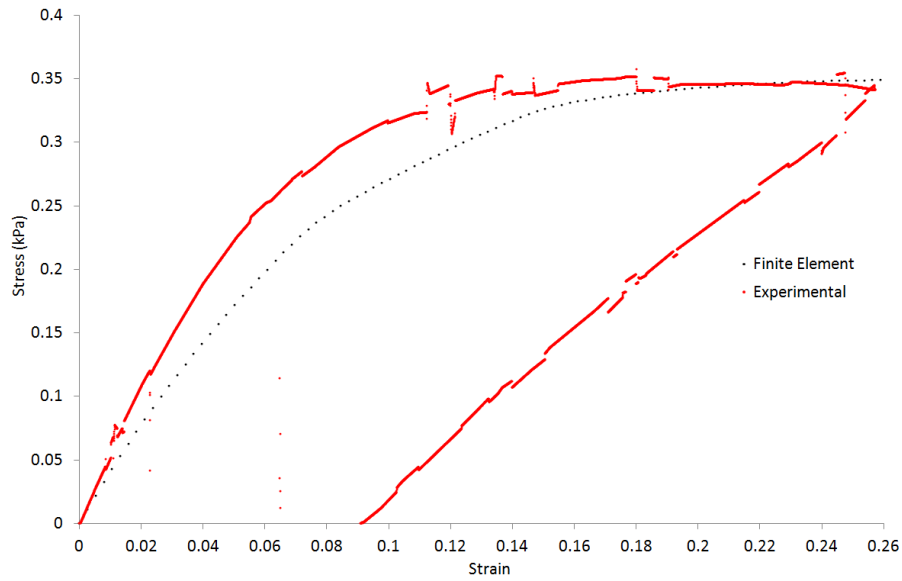


Figure 8.39: Stress strain response for experimental and finite element results for a hierarchical honeycomb with a super-structure aspect ratio $\alpha_{sup} = 5.77$, a relative density of 0.00901 and a HLR = 0.1.

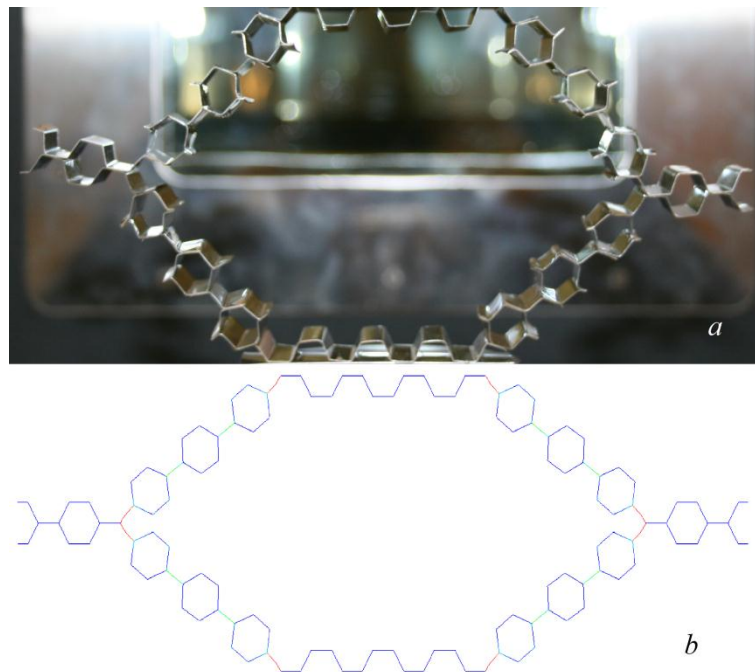


Figure 8.40: Comparison of the deformation between FE analysis and experimental test for a hierarchical honeycomb with a super-structure aspect ratio $\alpha_{sup} = 5.77$, a relative density of 0.00901 and a HLR = 0.1.

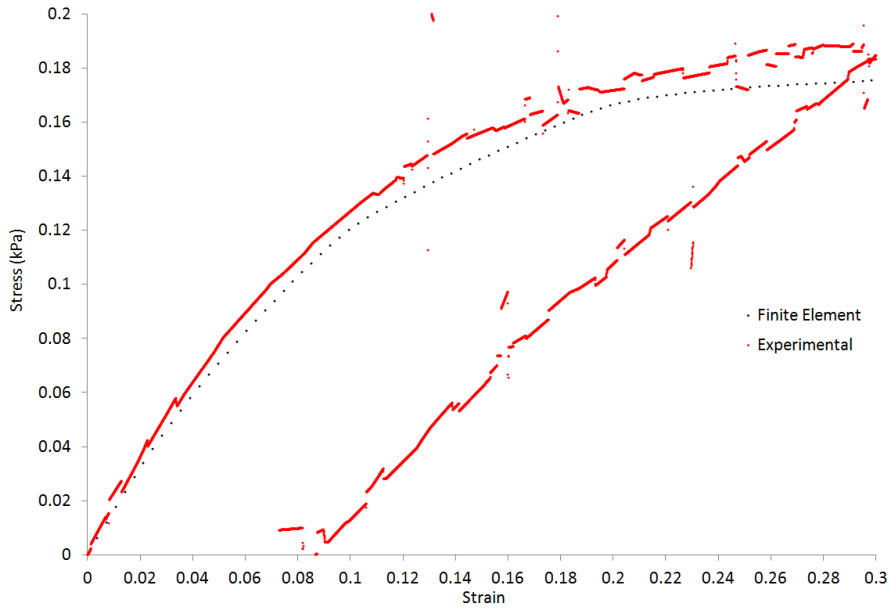


Figure 8.41: Stress strain response for experimental and finite element results for a hierarchical honeycomb with a super-structure aspect ratio $\alpha_{sup} = 7.51$, a relative density of 0.00687 and a HLR = 0.0769.

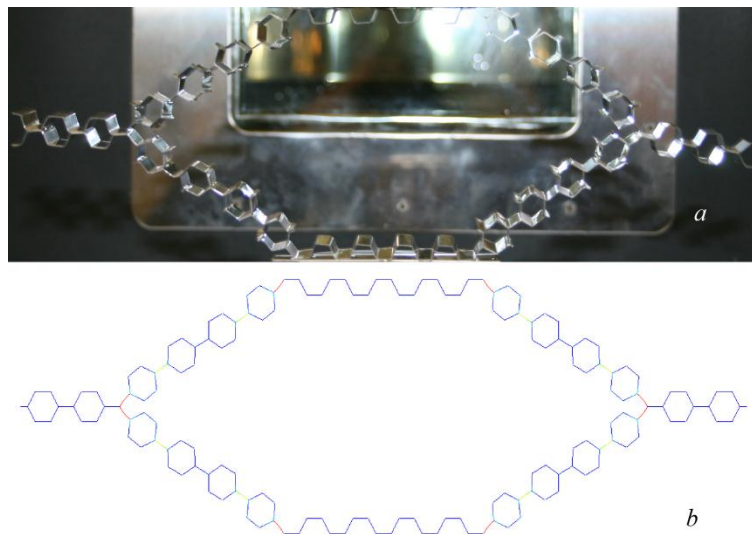


Figure 8.42: Comparison of the deformation between FE analysis and experimental test for a hierarchical honeycomb with a super-structure aspect ratio $\alpha_{sup} = 7.51$, a relative density of 0.00687 and a HLR = 0.0769.

8.3.3 Out-of-plane Change in the Super-Structure Aspect Ratio α_{sup} Experimental

The out-of-plane results of changing the super-structure aspect ratio α_{sup} are shown, firstly for a comparison in the elastic regime between the FE, experimental and analytical followed by FE and experimental stress strain plots for each hierarchical honeycomb. Also shown are experimental deformation images compared to FE analysis deformation plots for each sample.

The out-of-plane Young's modulus normalised to the relative density is plotted against the super-structure aspect ratio α_{sup} in Figure 8.43. It can be seen that there is a clear agreement between the FE and analytical with approximately 2% percentage difference between the two results. There is however a marked difference between the FE and the experimental where the experimental is approximately 60% of the FE and analytical.

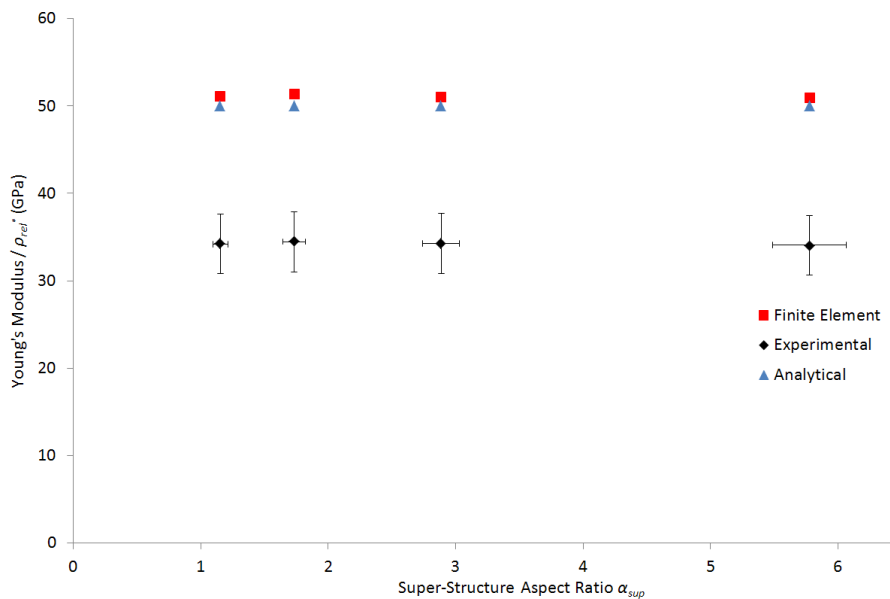


Figure 8.43: In-plane Young's modulus normalised to the relative density against the super-structure aspect ratio for FE, experimental and analytical results for hierarchical honeycombs. The experimental results show error bars of 10% for the normalised Young's modulus and 5% for the super-structure aspect ratio.

Stress strain plots are shown in Figure 8.44, Figure 8.46, Figure 8.48 and Figure 8.50 for changes in the super-structure aspect ratio α_{sup} . Again there is a clear correlation between the FE and experimental data although the FE consistently overestimates the

stress for low strains. This is due to bedding in region for the samples that is not allowed for in the FE. There is a clear correlation between the two sets of results, which is reiterated in the FE and experimental deformation images also shown for each hierarchical honeycomb in Figure 8.45, Figure 8.47, Figure 8.49 and Figure 8.51.

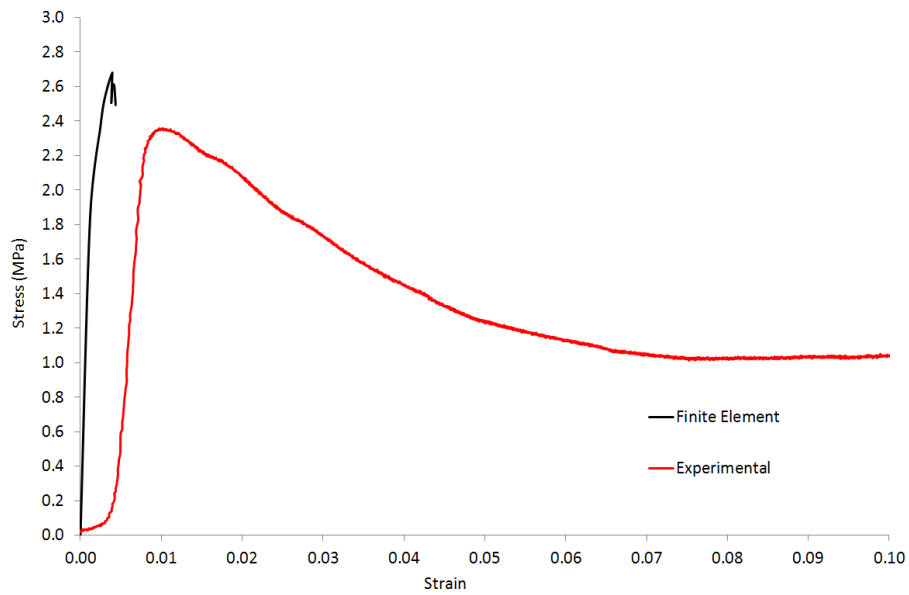


Figure 8.44: Stress strain response for experimental and finite element results for a hierarchical honeycomb with a super-structure aspect ratio $\alpha_{sup} = 1.15$, a relative density of 0.0300 and a HLR = 0.5.

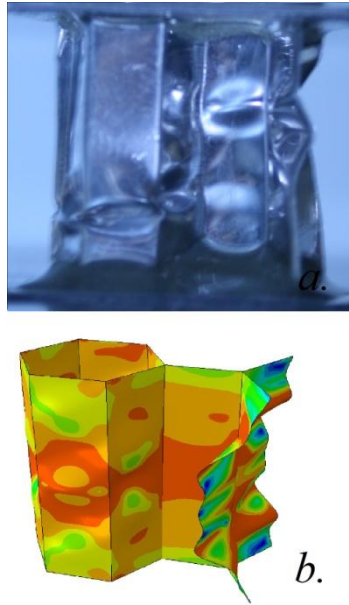


Figure 8.45: Comparison of the deformation between FE analysis and experimental test for a hierarchical honeycomb with a super-structure aspect ratio $\alpha_{sup} = 1.15$, a relative density of 0.0300 and a HLR = 0.5.

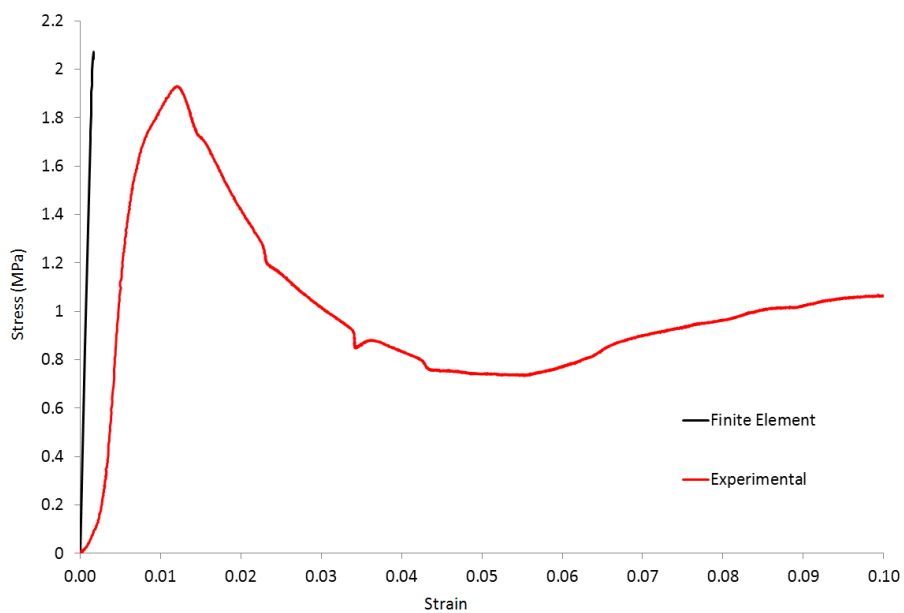


Figure 8.46: Stress strain response for experimental and finite element results for a hierarchical honeycomb with a super-structure aspect ratio $\alpha_{sup} = 1.73$, a relative density of 0.0267 and a HLR = 0.333.

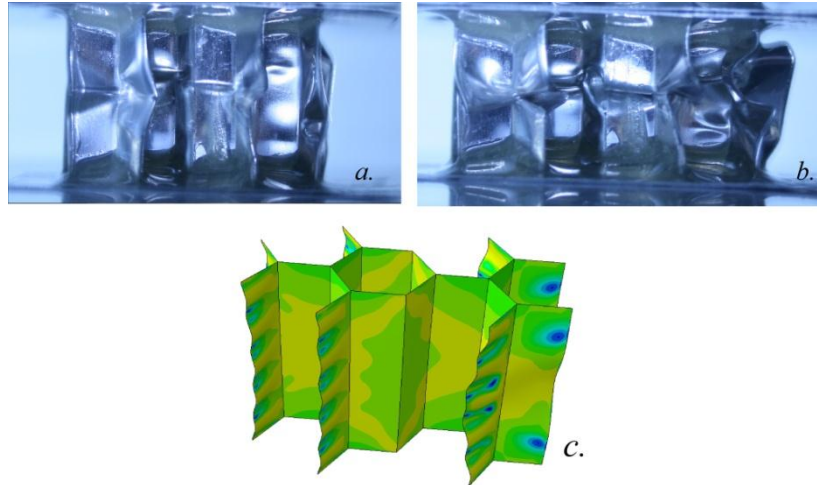


Figure 8.47: Comparison of the deformation between FE analysis and experimental test for a hierarchical honeycomb with a super-structure aspect ratio $\alpha_{sup} = 1.73$, a relative density of 0.0267 and a HLR = 0.333.

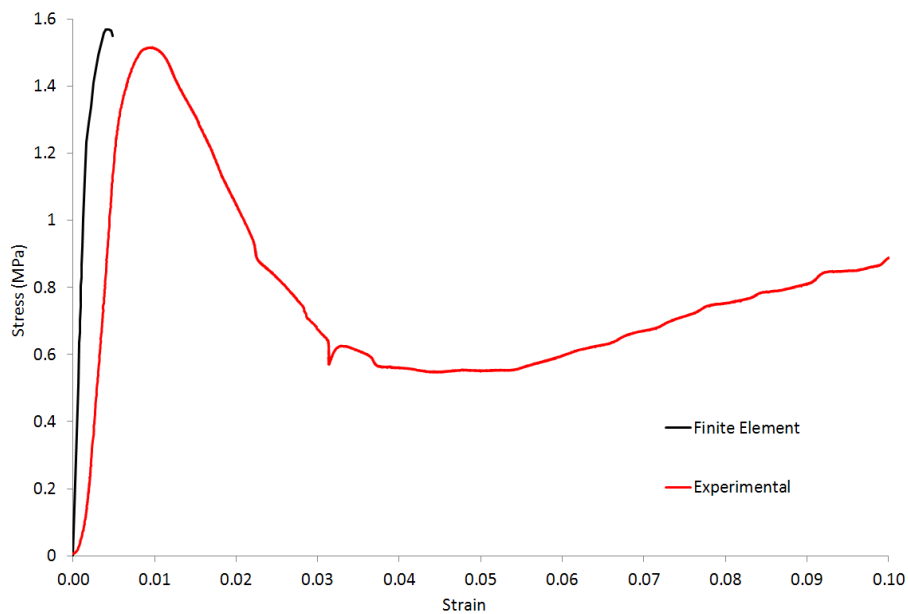


Figure 8.48: Stress strain response for experimental and finite element results for a hierarchical honeycomb with a super-structure aspect ratio $\alpha_{sup} = 2.89$, a relative density of 0.0160 and a HLR = 0.2.

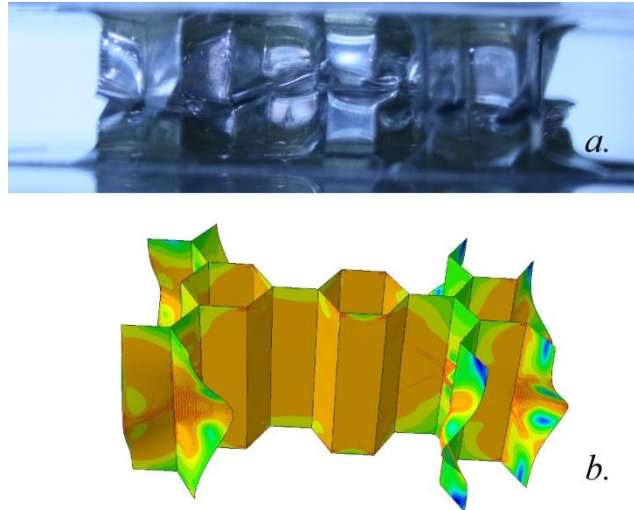


Figure 8.49: Comparison of the deformation between FE analysis and experimental test for a hierarchical honeycomb with a super-structure aspect ratio $\alpha_{sup} = 2.88$, a relative density of 0.0160 and a HLR = 0.2.

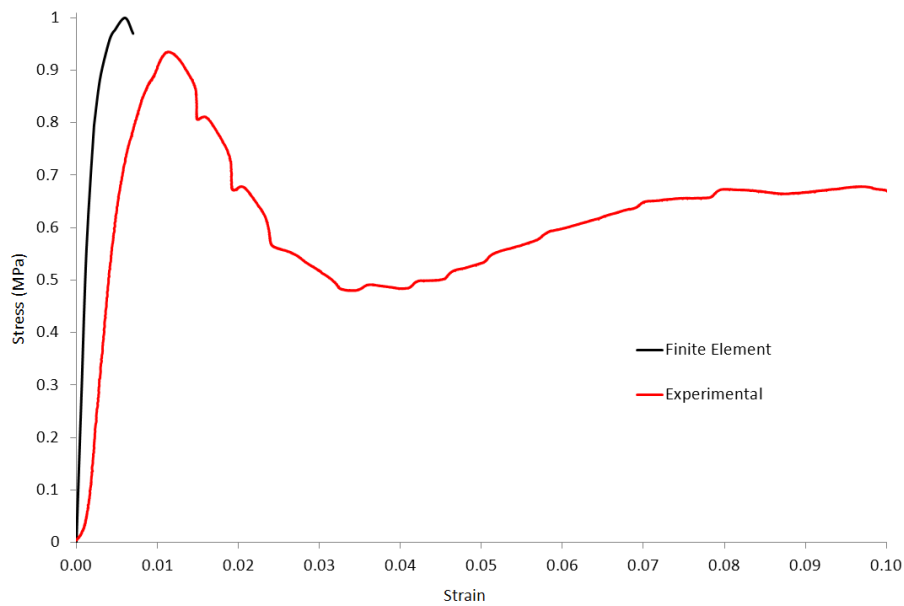


Figure 8.50: Stress strain response for experimental and finite element results for a hierarchical honeycomb with a super-structure aspect ratio $\alpha_{sup} = 5.77$, a relative density of 0.00901 and a HLR = 0.1.

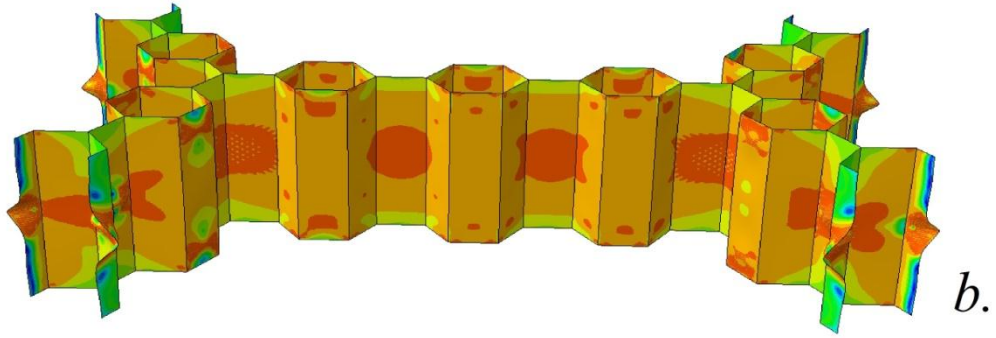
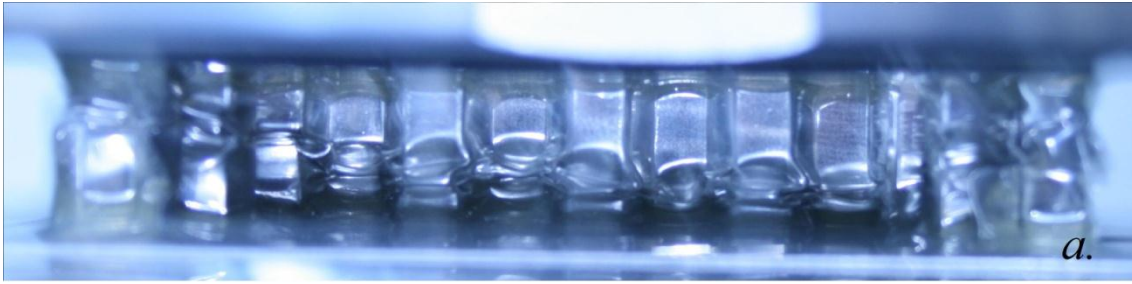


Figure 8.51: Comparison of the deformation between FE analysis and experimental test for a hierarchical honeycomb with a super-structure aspect ratio $\alpha_{sup} = 5.77$, a relative density of 0.00901 and a HLR = 0.1.

8.4 Discussion

8.4.1 In-plane change in HLR

The most apparent feature investigating the In-plane Young's modulus normalised to relative density in Figure 8.21 is the clear correlation between the experimental and FE results for a change in the number of sub-cells spanning the super-structure validating FE models in the elastic regime. The normalised experimental results consistently underestimate the normalised FE modulus by 6% to 13% similar overestimates are also seen in (Gibson *et al* 1982) for metal honeycombs (Papka & Kyriakides 1994, 1998 (1) and 1998 (2)) when comparing FE and experimental results. This can be explained due to imperfections in the geometry of experimental samples whereas the FE analysis uses perfectly defined geometry for l_{sub} , h_{sub} , θ_{sub} , l_{sub} , h_{sub} and θ_{sub} . Another contributing factor could be the plastic deformation at each node of the sub-structure inherent of the manufacturing process also negated in the FE analysis. The above effects were not taken into account in the FE models and could account for small deviations between the FE and experimental results. The defects could be assumed to occur uniformly within the structure as investigated by (Papka & Kyriakides 1994) who quantified that the inclusion of such defects had negligible effect on the FE response when modelling conventional hexagonal honeycombs. They concluded that the honeycomb also has random imperfection in the structure along with imperfections not characterising in the discretisation and homogenisation of the constituent material (aluminium sheet) which is more likely the reason for the small discrepancies between the FE and experimental results.

Looking at the elastic plastic response of hierarchical honeycombs for changes in the HLR in Figure 8.22 to Figure 8.31 it is clear that the FE models were able to predict accurately the elastic and plastic deformation mechanisms. The elastic plastic response seen is similar to that described by (Papka & Kyriakides 1994) for elastic plastic models of conventional honeycombs where an elastic region is followed by a gradual reduction in stiffness. In Figure 8.22 and Figure 8.24 there is also a sign of the peak stress seen in (Papka & Kyriakides 1994) followed by a negative slope defined by the nonlinear material properties and the nonlinear geometry. This was not seen in other hierarchical honeycombs with lower HLR as the applied strain was not great enough to induce a

peak stress. The change in global strain applied to each model is due to stress concentration causing a greater local deformation at the super-structure nodes, resulting in greater distortion of the cells in the local area. FE models did not take into account contact between ribs and was not modelled, therefore contact was avoided in experiments for an accurate comparison. The local distortion was greater in hierarchical honeycombs with a lower HLR in terms of cells size, which is why the higher HLR hierarchical honeycombs have a greater applied strain.

The comparison between experimental and FE results can be used to validate the in-plane modelling used to investigate the elastic regime, the onset of plasticity and the initial post yield response of hierarchical honeycombs used in the presented work. This is due to the close proximity of the FE and experimental stress strain graphs and is highlighted in the clear relationship in the deformation plots where it is clear to see stress concentrations and maximum displacements.

8.4.2 In-plane Change in Super-Structure Aspect Ratio α_{sup}

The results presented in Figure 8.32 investigating the In-plane Young's modulus normalised to relative density against the super-structure aspect ratio, show a clear correlation between the experimental and FE results validating FE model in the elastic regime, whilst changing the super-structure aspect ratio. It can be seen that even though the Young's modulus is normalised to the relative density there is still an exponential relationship between the modulus and the super-structure aspect ratio. This is due to the in-plane Young's modulus being dependent on the $(t/l)^3$ function (Gibson *et al* 1982), even though the results are normalised the exponential relationship is still present. The normalised experimental results deviated from the FE normalised modulus by -4.7% to 9.7% similar overestimates are also seen in (Gibson *et al* 1982) for metal honeycombs (Papka & Kyriakides 1994, 1998 (1) and 1998 (2)) when comparing FE and experimental results. The overestimates of the FE are due to the reinforcement of sub-structure ribs due to excess adhesive creating a filet at sub-structure node not accounted for in the models. The deviations can be explained due to imperfections in the geometry and plastic deformation at each node of the sub-structure intrinsic of the manufacturing process and is explained and quantified in the previous section and (Papka & Kyriakides 1994). It is more likely that the random imperfection in the structure along with

imperfections not characterising in the discretisation and homogenisation of the constituent material are the reason for the discrepancies (Papka & Kyriakides 1994).

Looking at the elastic plastic response of hierarchical honeycombs for changes in the super-structure aspect ratio in Figure 8.33 to Figure 8.42 it is clear that the FE models were able to predict accurately the elastic and plastic deformation mechanisms. This is shown by the close proximity of the FE and experimental stress strain graphs and is highlighted in the clear relationship in the deformation plots where it is clear to see parallel stress concentrations and maximum displacements. Unlike in the previous investigation on the HLR the results for changing the super-structure aspect ratio show clear jumps in stress post yield. This is due to the fracture of the adhesive connecting sub-structure ribs and is not allowed for in FE analysis and as such is not present in the FE results. The fracture of the adhesive is more prominent in the changing super-structure aspect ratio as all super-structure ribs are composed of a single sub-cell in thickness and therefore stress concentrations are focused on single sub-structure cells. Another reason for the failure of the adhesive is the limited area allowed for some sub-structure nodes where only two sub-structure ribs meet to conform to the super-structure geometry.

8.4.3 Out-of-plane Change in Super-Structure Aspect Ratio α_{sup}

The most apparent feature when looking at the out-of-plane Young's modulus normalised to the relative density in Figure 8.43 is the discrepancy between the experimental and the FE results with a percentage difference of approximately 30%. Another distinguishing feature of the graph is the close proximity between the FE results and the analytical derived in Chapter 7, with a percentage difference of less than 2% consistent for all models. The close proximity between the FE and analytical results highlights the underestimate of the experimental out-of-plane Young's modulus. There are many reasons for the discrepancies in the out-of-plane experimental, such as imperfections in the geometry of experimental samples, whereas the FE analysis uses perfectly defined geometry for l_{sub} , h_{sub} , θ_{sub} , l_{sub} , h_{sub} , θ_{sub} and the depth of the sample d . The stretch dominated response of honeycombs loaded out-of-plane means that the structure is more sensitive to such imperfections which could result in the underestimate. There is also the fact that the experimental samples were not perfectly

vertical or normal to the loading plate due to imperfections of the manufacturing process. Another major contributing factor to the disagreement is that the heights of sub-structure cells were not exact. Where aluminium samples maybe cut via water cutting (Aktay *et al* 2008) avoiding damage to the honeycomb and an accurate geometry, investigated samples were cut via a slicing method meaning a $\pm 0.5\text{mm}$ in the width of aluminium strips. This combined with a difficult assembly process resulted in some beams being proud of others resulting in the consistent underestimate of the Young's modulus. Similar discrepancies in the Young's modulus were seen in (Miller *et al* 2009 and Aktay *et al* 2008) whilst much work investigates the out-of-plane response of honeycombs it is focused on the crush behaviour and it is difficult to note the elastic response due to the presentation of graphs focusing on the post yield response or due to the removal of the experimental elastic regime from the results altogether. There is however a close correlation in the peak stresses between the FE and experimental results with a percentage difference less than approximately 10% for all samples.

Despite the difference in the Young's modulus and the small deviation in peak stresses of the experimental samples it is thought that the consistent underestimate for all samples can be explain by imperfections due to the manufacturing process. Thus the experimental results can be used to validate that of the FE models.

8.5 Conclusion

The aim of this chapter was to validate numerical models against experimental results. It has been shown that whilst there is a small amount of deviation for in-plane results, FE models accurately predict the response of hierarchical honeycombs. Where there are discrepancies between the results, they can be explained by assumptions made in the models. The out-of-plane results show larger discrepancies in the elastic region which can be explained by the sensitivity of the stretch dominated nature of the structure to imperfections and also shows a close correlation to peak stresses. As such the experimental results can be used to validate the FE models developed in the previous chapters.

Chapter 9. Discussion

Seminal work by Lakes in his pioneering paper (Lakes 1993a), presented a new bio inspired class of materials, due to the introduction of hierarchy. Lakes also showed the potential benefits of hierarchical material of combining strength and toughness. The aim of the current work has been to further develop the work of Lakes and subsequent studies (Kooistra *et al* 2007), (Fan *et al* 2008), by investigating how hierarchy can be introduced into cellular materials, specifically honeycombs, with potential manufacture in mind. The work addresses issues such as the use of continuum theories proposed in (Lakes 1993a) and (Carpinteri *et al* 2009), which assume that the size scale of the sub-structure is negligible to that of the super-structure. The present work also investigates the multitude of variables that arise due to the introduction of hierarchy and aims at determining their effects on the material properties of the structure. Finite element models and analytical predictions have been developed for hierarchical honeycombs and were compared to experimental results, which showed close correlation validating the findings. Hierarchical structures were also bench marked against conventional first order honeycombs using the same models and techniques. The results obtained for conventional honeycombs were compared to existing well established analytical predictions (Gibson and Ashby 1997), which also showed close correlation, further validating the models and techniques used.

9.1 In-Plane

The introduction of hierarchy by the redistribution of mass from a conventional honeycomb rib to create a sub-structure of a different length scale failed to increase the in-plane stiffness of the honeycomb. The results showed that when changing the mass distribution between the sub and super-structure the (3-3) hierarchical honeycomb was heavily dependent on the mass distribution, due to its bending dominated nature Figure 3.21. The (3-3) hierarchical honeycomb showed a minimum in terms of in-plane Young's modulus when the mass distribution was 50% by a reduction of 75% (Gibson and Ashby 1982) (Gibson and Ashby 1997). The (6-6) hierarchical honeycomb however is stretch dominated and remained relatively unaffected by the change in mass distribution. This result highlights the exponential dependence of the bending dominated hexagonal honeycomb on the redistribution of mass and the effect the

distribution of mass has on the aspect ratio of sub and super-structure ribs whereas the stretch dominated triangular honeycomb structure has a linear relation to the aspect ratio of sub and super-structure ribs (Deshpande *et al* 2001).

Another interesting point was the independence between the Hierarchical Length Ratio (HLR) and the in-plane Young's modulus when the sub-structure is allowed to fill the entire void between super-structure ribs as in Figure 3.1 & Figure 3.2. This independence was also seen when investigating the HLR whilst changing the Poisson's ratio of the sub-structure relative to that of the super-structure as in Chapter 4 Figure 4.3, Figure 4.4 & Figure 4.5. This result is expected as similar work by (Gibson and Ashby 1982 & 1997) showed that the material properties of conventional honeycombs were independent of the size of the considered cells, but dependant on the aspect ratio of ribs and the geometry of the unit cell. The fact that the length scale between the sub and super-structure has no effect on the response of the unit cell, has important implications when considering the feasibility of manufacturing hierarchical honeycombs of this nature. As the HLR has no effect, the length scales used to produce such hierarchical honeycombs could be relatively similar meaning conventional manufacturing methods could be used such as the expansion method followed by a cell removal process.

The work was further developed to investigate hierarchical honeycombs where the mass distribution was entirely contained within the sub-structure, and the super-structure is defined by the global geometry of the sub-structure. The first stage of this investigation was to answer a question raised by Lakes in his 1993 paper (Lakes 1993a); at what length scale can the sub-structure be considered to be negligible to the super-structure? This was answered for multiple co-ordination numbers, specifically (3-3), (3-6), (6-6) and (6-3). It was found that the sub-structure can be considered a continuum to the super-structure when the number of sub-cells spanning the super-structure is 8 as can be seen in Figure 3.24 to Figure 3.27. The results showed that whilst length ratios such as the HLR had an effect on the global response. The HLR could not be used to determine a ratio when the sub-structure could be considered a continuum for all considered geometries and investigated parameters.

Subsequent FE and analytical work investigating the effect of change in the super-structure aspect ratio on the in-plane Young's modulus showed clear correlation. The

results showed that hierarchical honeycombs with stretch dominated triangular sub and super-structure were superior in terms of Young's modulus, by three orders of magnitude when compared to a conventional hexagonal honeycomb of the same relative density (Deshpande *et al* 2001) and can be seen in Figure 3.28 to Figure 3.31. Significant improvements were also seen in hierarchical honeycombs with hexagonal sub-structures (3-3 and 6-3) due to the introduction of hierarchy by up to 400% in investigated geometries. This increased of in-plane Young's modulus due to introduction of hierarchy was also seen in work by (Kooistra *et al* 2007), (Fan *et al* 2008), (Chen and Pugno 2012) and (Ajdari *et al* 2012).

It is important to remember that although hierarchical honeycombs with a triangular sub-structure have a greater in-plane Young's modulus, the manufacture of such structures can be difficult. The (3-3) and (6-3) co-ordinations however are based on a hexagonal sub-structure and could be manufacture by the conventional adhesive and expansion method, followed by cell removal process. These results could drastically increase the potential use for hierarchical honeycombs for their in-plane properties, with combined advantage of increased Young's modulus over conventional hexagonal honeycombs whilst maintaining the ease of manufacture. Hexagonal honeycombs are already commonly used as the core of sandwich panels. The increased in-plane properties could impart additional increases to the performance of such sandwich panels in out-of-plane bending. This is due to the fact that the upper and lower faces are loaded in tension and compression; as such the higher in-plane properties would further stiffen the structure. The increase to the core alone would be proportional to the increase stiffness of the structure, but would be less prominent when face sheets of the sandwich panel are applied. Another obvious advantage to the increased Young's modulus over conventional hexagonal honeycombs is that the same in-plane properties could be achieved with the use of the same constituent material but at a lower relative density. This would have the advantage of reducing the weight of the structure, which is often considered advantageous in sectors such as the transport industry where weight reduction often leads to increased performance and reduced fuel consumption.

The results presented in Chapter 4 show the effect of changing the sub-structure Poisson's ratio in relation to that of the super-structure. The introduction a NPR sub-

structure has the effect of increasing the on axis properties by approximately two orders of magnitude at the expense of introducing in-plane anisotropy in the hierarchical honeycomb as can be seen in Figure 4.10 to Figure 4.12. This type of hierarchical honeycomb could be utilised when there is a known and constant direction of loading. The results show that it is not necessary for there to be a difference in length scale between the sub and super-structure when introducing a NPR sub-structure as previously discussed. This has important implication when considering the feasibility of manufacturing hierarchical structures, i.e. hierarchical honeycombs could be manufactured with minor changes to conventional methods as opposed to relying on new and relatively expensive methods such as additive layer manufacture.

It has been shown that it is further possible to optimise the in-plane Young's modulus of a hierarchical honeycomb by functional grading the mass of the sub-structure in relation to the super-structure rib as in Chapter 5. The results showed that it was possible to increase the in-plane Young's modulus of a (3-3) hierarchical honeycomb by up to 200% when compared to a conventional hexagonal honeycomb as can be seen in Figure 5.5. Numerical simulations were performed to investigate the effect of redistributing the mass across the thickness of the super-structure rib and compared to analytical models. The implementation of functional grading and hierarchy in this manner would no doubt incur manufacturing cost and could not be done via conventional processes and would be reliant on processes such as additive layer manufacture to produce the complicated geometries. The future of functionally graded hierarchical honeycombs is very much dependent on the manufacturing implications and would tend towards introduction of such hierarchy into parts that are already dependant on processes such as additive layer manufacture and use the hierarchy to further optimise the structure.

The investigation into the in-plane plastic and non-linear response of hierarchical honeycombs showed that it is possible to tailor the response of hierarchical honeycombs specifically to delay the onset of elastic buckling and the extent of plasticity in the structure. The results compared hierarchical honeycombs of different co-ordination numbers specifically (3-3), (3-6), (6-6) and (6-3) to conventional hexagonal and triangular honeycombs. It was found that the stretch dominated conventional triangular honeycombs were the stiffest, but elastically buckled at a low strain compared to the

bending dominated conventional hexagonal honeycomb which was one of the most compliant structures of those investigated and can be seen in Figure 6.5 to Figure 6.27.

For the lower relative density $\rho_{rel}^* = 0.00577$ investigated, the first mode of failure of conventional honeycombs is elastic bending or elastic buckling of ribs, it is possible for hierarchical honeycombs to increase the buckling stress due to an increase in the second moment of area of the sub and super-structure ribs. The same is also true for the higher relative density $\rho_{rel}^* = 0.0577$ also investigated. The results showed that the introduction of hierarchy into honeycombs can have the effect of delaying the onset of elastic buckling, which is most prominent for low relative density structures, but is less apparent in higher relative density structures due to the onset of plasticity becoming the first mode of failure. Hierarchical honeycombs have the advantage of being able to be tailored to the required demands of a certain application for a given relative density. This can be achieved by changing parameters such as the co-ordination number, mass distribution and the aspect ratio of the super-structure for functionally graded hierarchical honeycombs or the internal angle or mass distribution for NPR sub-structure hierarchical honeycombs. The (3-6) co-ordination hierarchical honeycomb shows a particular transition from the bending dominated hexagonal honeycomb to the stretch dominated triangular honeycomb as the super-structure aspect ratio is decreased as shown in Figure 6.8 & Figure 6.9.

Honeycombs are currently used in the packaging industry to protect products from impact and damage. The use of hierarchical honeycombs could be used to tailor specific material response to protect against the most likely impacts. Similarly the automotive industry relies on crumple zones to absorb energy in the event of impact to protect the passengers or haulage. The tailored response of hierarchical honeycombs could be used to deliver the required material response especially when a certain constituent material or relative density is necessary, enabling a designer to have more freedom. The work investigating the in-plane plastic non-linear response of hierarchical honeycomb shows that due to the introduction of hierarchy it is possible to combine the advantage of the bending and stretch dominated hexagonal and triangular honeycombs respectively. The high Young's modulus of stretch dominated structures is shown by the comparable modulus of the hierarchical honeycomb, but combine with the higher failure strain

intrinsic with the bending dominated hexagonal honeycomb. The work presented on functional grading a unit cell to alter the global response could be used to implement functional grading over a domain as suggested by (Adjari 2012) who shows that such functional grading can be used to increase the damage tolerance of a structure.

9.2 Out-of-Plane

The investigation into the out-of-plane elastic response of hierarchical honeycombs showed that the introduction of hierarchy had no effect on the out-of-plane Young's modulus of the honeycomb, following a to rule of mixtures, type behaviour, and the fact that the same amount of material remained in direct compression between cases. The same was also true when changing the HLR which had no effect on the out-of-plane properties. There was however considerable increase to the out-of-plane stress at which elastic buckling occurred due to the introduction of (3-3) hierarchy into a honeycomb. The analysis suggests that there is little to be gained in terms of the out-of-plane plastic collapse stress from the introduction of hierarchy, since plastic yield of the constituent material is independent of the in-plane geometry for a honeycomb, but dependent on the constituent material properties and the cell's relative density. There are benefits from introducing hierarchy into low relative density honeycombs where the elastic buckling occurs prior to the onset of plastic collapse as is the case for the examples presented. The introduction of hierarchy yielded an increase of up to 60% for the out-of plane elastic buckling stress, when compared to conventional hexagonal honeycomb of the same relative density as can be seen in Figure 7.10 to Figure 7.13. It is difficult to quantify the potential increase to the elastic buckling stress as it is dependent on the relative density and the material properties, specifically the relationship between the Young's modulus and the plastic yield stress of the constituent material. Although the results suggest that the potential increase is exponential, as the relative density decreases. As previously discussed honeycombs are used as core for sandwich panels which are commonly used with in the aerospace and automotive industry. Whist there is no out-of-plane benefit it terms of the linear elastic regime by the introduction of hierarchy, the delayed onset of elastic buckling could be beneficial to sandwich structure especially when a low relative density core maybe required. A similar result is seen in (Long *et al* 2012) due to the introduction of hierarchy by the increased second moment of area.

Chapter 10. Conclusion

The main aim of this project was to examine the effects of introducing hierarchy into honeycombs and determining the variables that preside over the global response of the structure. Specifically to understand how the in and out-of-plane elastic and non-linear plastic properties of honeycombs were affected by hierarchy. The initial investigation focused on finding if the elastic modulus could be maintained or improved on an equal density basis due to the introduction of hierarchy. It is clear that honeycombs are sensitive to hierarchical sub-structures, particularly the fraction of mass shared between the super- and sub-structures. Introduction of an additional level of hierarchy without reducing performance is difficult. However it is possible by functionally grading such hierarchies to improve the in-plane modulus, in this case by up to 400% (6-3) compared to a similar density first order hierarchy (conventional) and increase of two orders of magnitudes due to the introduction of triangular sub-structures.

Another exciting result was that it was determined when the sub-structure could be assumed to be a continuum of the super-structure. The material properties from a single unit sub-cell could be used to describe the super-structure material properties, enabling the assumptions of the continuum theory used when modelling the sub-structure being modelled as in previous work by (Lakes 1993) and (Carpinteri *et al* 2009) for example. This has implication when developing analytical models to predict the response of hierarchical materials and can be used in further work to determine the feasibility of hierarchical structure. Previous works that have used continuum theory for hierarchical structures to develop analytical models have done little to determine at what point the models are valid.

Work investigating the in-plane, non-linear plastic response of hierarchical honeycombs showed that the introduction of hierarchy into honeycombs can have the effect of delaying the onset of elastic buckling, which is a common failure mechanism for low relative density structures. As such it was possible to achieve a marked increase in the recoverable energy absorbed by hierarchical honeycombs prior to elastic buckling or plastic yield. The potential benefits are less apparent in higher relative density structures due to the onset of plasticity becoming the first mode of failure. The out-of-plane properties also investigated showed no increase in the elastic properties due to the

introduction of hierarchy, but showed a marked increase in the out-of-plane elastic buckling stress of 60% when compared to a conventional hexagonal honeycomb of the same relative density. Further investigation in to constituent materials and relative densities used, other than those investigated in the present work, could result in further improvements to the in and out-of-plane material properties when compared to conventional honeycombs.

Hierarchical honeycombs have the advantage of being able to be tailored to the required demands of a certain application for a give relative density or constituent material by changing parameters such as the co-ordination number, mass distribution and the aspect ratio of the super-structure for functionally graded hierarchical honeycombs or the internal angle or mass distribution for NPR sub-structure hierarchical honeycombs. The further development or implementation of hierarchical honeycombs could result in improved performance over conventional honeycombs. The modelling and analytical approach taken in the present work focuses on honeycomb structure, but a similar approach could be taken with other cellular materials such as foams and truss structures to introduce hierarchy. The beam mechanics used to describe both the bending and stretch dominated hexagonal and triangular honeycombs respectively could be used for foams and truss structure. For example the foam model developed in (Gibson and Ashby 1997) uses similar equations to that of the hexagonal honeycomb, but is obviously 3D.

10.1 Further Work

The out-of-plane Young's has been determined along with the elastic buckling and plastic yield stress. It would be interesting to investigate the out-of-plane shear modulus as it is suspected that changes in the aspect ratio of sub and super-structure ribs could yield positive results due to the bending dominated nature of the loading conditions, taking advantage of the $(t/l)^3$ term. The same is true when investigating the plastic yield and elastic buckling (also dependent on the $(t/l)^3$ term) stress of the structure in shear.

The introduction of hierarchy has been shown to increase the amount of recoverable energy absorbed by the structure prior to the onset of failure, when compared to conventional honeycombs of the same relative density. It could be worthwhile further investigating the effect that the introduction of hierarchy has on the damage tolerance of

the structure. This has been done to a certain extent, but current models are only reliable up to elastic collapse and plastic yield and shortly after. This is due to the simplified models focusing on the structure of the hierarchical honeycombs and ignoring such effects as contact and adhesion between ribs, work hardening via manufacture (although consider negligible) and dynamic effect along with wave propagations. Another area of possible interest could be the effect of hierarchy on the vibration response of the structure given the change in aspect ratio of sub and super-structure ribs.

As previously mentioned the presented work could be used to describe simplified foams and truss structures. It would therefore be interesting to further investigate the effect that hierarchy has on the other types of cellular materials.

References

A

Aizenberg J., Weaver J.C., Thanawala M.S., Vikram C. Sundar V.C., Daniel E. Morse D.E. and Fratzi P., 2005. Skeleton of *Euplectella* sp.: Structural Hierarchy from the Nanoscale to the Macroscale, *Science*. 309, 5732, 275-278.

Ajdari A., Jahromi B.H., Papadopoulos J., Nayeb-Hashemi H., Vaziri A., 2012, Hierarchical honeycombs with tailorable properties, *International Journal of Solids and Structures* 49 (2012) 1413–1419.

Aktay L, Johnson A.F, Kroplin B-H, 2008, Numerical modelling of honeycomb core crush behaviour, *Engineering Fracture Mechanics*, 75, 2616–2630.

Ashby, M. F., 1983, The mechanical properties of cellular solids. *Metallurgical Transactions*, 14A, 1755-1769.

Ashby, M. F., 1991, Materials and Shape, *Acta metall, mater.* 39, 6, 1025-1039.

B

Bhat T, Wang T.G, Gibson L.J, 1989, Micro-sandwich honeycomb, *SAMPE J*, 25:43–5.

Bitzer, T, 1994. Honeycomb marine applications. *Journal of Reinforced Plastics and Composites* 13 (4), 355–360.

Bitzer T., 1997. *Honeycomb technology*. London: Chapman & Hall.

Buehler M.J., 2006. Nature designs tough collagen: Explaining the nanostructure of collagen fibrils, *The National Academy of Sciences of the USA*.

Burlayenko, V.N, Sadowski, T, 2009, Analysis of structural performance of sandwich plates with foam-filled aluminum hexagonal honeycomb core. *Computational Materials Science* 45, 658–662

C

Carpinteri A, 1994a Fractal nature of material microstructure and size effects on apparent mechanical properties, *Mech Mater*, 18, 89–101.

Carpinteri A, 1994b, Scaling laws and renormalization groups for strength and toughness of disordered materials, *Int J Solids Struct*, 31, 291–302.

Carpinteri A & Pugno N, 2005, Are scaling laws on strength of solids related to mechanics or geometry?, *Nat Mater*, 4:421–23.

Carpinteri A, Pugno N.M, 2008, Mechanics of hierarchical materials, *Int J Fract* 150:221–226

Carpinteri A, Cornetti P, Pugno N, Sapora A, 2009, Strength of hierarchical materials, *Microsyst Technol*, 15:27-31

Caulfield B, McHugh PE, Lohfeld S, 2007, Dependence of mechanical properties of polyamide components on build parameters in the SLS process. *J Mater Process Technol*;182:477–88.

Chen D.H, Ozaki S, 2009, Analysis of in-plane elastic modulus for a hexagonal honeycomb core: Effect of core height and proposed analytical method, *Composite Structures*, 88, 17–25

Chen Q & Pugno N, 2012a, Mechanics of hierarchical 3-D nanofoams, *EPL*, 97, 2,

Chen Q & Pugno N, 2012b, In-plane elastic buckling of hierarchical honeycomb materials, *European Journal of Mechanics A/Solids*, 34, 120-129

Chung J and Waas A.M, 2001, In-plane biaxial crush response of polycarbonate honeycombs, *Journal of Engineering Mechanics*, 180-193

Coelho PG; Fernandes PR; Guedes JM, Rodrigues HC, 2008, A hierarchical model for concurrent material and topology optimisation of three-dimensional structures, *Structural and Multidisciplinary Optimization*, 35(2):107.

Coté F, Deshpande V.S, Fleck N.A, Evans A.G, 2004, The out-of-plane compressive behavior of metallic honeycombs, *Materials Science and Engineering A*, 380, 272–280.

D

Deshpande V.S, Fleck N.A, 2000, High strain rate compressive behavior of aluminum alloy foams, *International Journal of Impact Engineering*, 24, 277–298.

Deshpande V.S., Ashby M.F., and Fleck N.A., 2001. Foam topology bending versus stretching dominated architectures, *Acta mater.* 49, 1035–1040

E

Euler L, 1746, Thoughts on the elements of bodies, *Memoirs of the Prussian academy of science*, Berlin.

Evans K.E., 1991, The design of doubly curved sandwich panels with honeycomb cores. *Composite Structures* 17, 95–111.

Evans K.E., Nkansah M.A., Hutchinson I.J. and Rogers S.C., 1991. Molecular network design. *Nature*, 353, 124.

Evans K. E. and Alderson A., 2000, Auxetic Materials: Functional Materials and Structures from Lateral Thinking! *Adv. Mater*, 12, 9.

F

Fan, H.L., Jin, F.N., Fang, D.N., 2008. Mechanical properties of hierarchical cellular materials. Part i: Analysis. *Composites Science and Technology*, 68, 3380–3387.

Fan H, Fang D, Jin F, 2008. Mechanical properties of lattice grid composites, *Acta Mech Sin.* 24, 409–418.

Fratzl, P., Weinkamer, R., 2007. Nature's hierarchical materials. *Progress in Materials Science* 52, 1263–1334.

G

Gao, H., 2006. Application of fracture mechanics concepts to hierarchical biomechanics of bone and bone-like materials. *International Journal of Fracture*, 138, 101–137.

Gibson L. J, Ashby M. F, Schajer G. S, Robertson C. I, 1982, *The Mechanics of Two-Dimensional Cellular Materials*, Proceedings of the Royal Society of London. Series A, Mathematical and Physical Sciences, Vol. 382, pp. 25-42.

Gibson L.J. and Ashby M.F, 1997, *Cellular solids, structures and properties*, Cambridge University Press, second edition.

Gibson L.J. and Ashby M.F, 1988, *Cellular solids, structures and properties*, Pergamon Press, first edition.

Gibson L.J, Ashby M.F, Zhang. J, Traintafillou T.C, 1989, Failure surfaces for cellular materials under multiaxial loads i. modelling. *Int.J.Mech.Sci*, 31(9):635.

Gibson L.J; Ashby M.F; Schajer G.S and Robertson C.I, 1982, The mechanics of two-dimensional cellular materials. *Proceedings of the Royal Society of London*, 382(1782):28.

Goldsmith, W, Louie, D.L, 1995, Axial perforation of aluminum honeycombs by projectiles, *International Journal of Solids and Structures* 32, 1017–1046.

Goldsmith, W, Sackman, J.L, 1992. An experimental study of energy absorption in impact on sandwich plates, *International Journal of Impact Engineering*, 12, 241–262.

Grediac, M., 1993, A Finite Element Study of the Transverse Shear in Honeycomb Cores, *Int. J. Solids Struct*, 30, 13, pp. 1777–1788.

Gupta V., Bastias P., Hahn G.T. and Rubin C.A., 1993. Elasto-plastic finite-element analysis of 2-D rolling-plus-sliding contact with temperature-dependent bearing steel material properties, *Wear*, 169, 251-256.

H

Halsey C, Jensen M, Kadanoff L, Procaccia I, Shraiman B, 1986, Fractal measures and their singularities: the characterization of strange sets, *Phy Rev A*, 33(2):1141–1151.

Hatch J.E., 1984. *Aluminium: properties and physical metallurgy*, American Society for Metals.

Hong S.T, Pan J, Tyan T, Prasad P, 2008, Dynamic crush behaviors of aluminium honeycomb specimens under compression dominant inclined loads, *International Journal of Plasticity* 24, 89–117.

I

Inco Ltd. Product data sheet of incofoam. <http://www.inco.com>, 1998.Canada.

J

Jichun Y., Han B.Q., Lee Z., Ahn B., Nutt S.R., Schoenung J.M., 2005. A tri-modal aluminum based composite with super-high strength, *Scripta Materialia*, 53,481.

K

Kanzaki S., Shimada M., Komeya K. & Tsuge A., 1999, *Key Engineering Materials, The Science of Engineering Ceramics II*, 437-442.

Kelsey, S, Gellatly, R. A., and Clark, B. W., 1958, The Shear Modulus of Foil Honeycombs Cores, *Aircraft Eng.*, 30, pp. 294–302.

Kim S-E. & Lee D-H., Second-order distributed plasticity analysis of space steel frames, *Engineering Structures*, 24, 2002 735–744.

Klintonworth, J. W. and Stronge, W. J. (1988) Elasto-plastic yield limits and deformation laws for transversely crushed honeycombs. *International Journal of Mechanical Sciences*, 30, 273-292.

Kooistra, G.W., Deshpande, V., Wadley, H.N.G., 2007. Hierarchical corrugated core sandwich panel concepts. *Journal of Applied Mechanics* 74, 259–268.

L

Lakatos I, 1976, *Proofs and Refutations, the Logic of Mathematical Discovery*, Cambridge University Press, Cambridge, ed J. Worall and E. Zahar.

Lakes R., 1987. Foam structures with a negative Poisson's ratio, *Science*. 235, 1038–1040.

Lakes R., 1993a. Materials with structural hierarchy. *Nature* 361, 511–515.

Lakes R., 1993b. Advances in Negative Poisson's Ratio Materials, *Adv. Mater.* 5, No. 4.

Lakes R., 2002. High Damping Composite Materials: Effect of Structural Hierarchy, *Journal of Composite Materials*. 36, 03.

Liu, B., Feng, X., Zhang, S., 2009. The effective Young's modulus of composites beyond the Voigt estimation due to the Poisson effect. *Composites Science and Technology* 69, 2198–2204.

Love A.E.H., 1892, *A treatise on the mathematical theory of elasticity*, Cambridge University Press.

Loyrette H., *Gustave Eiffel* (Rizolli, New York) 1985.

M

Maiti S.K, Ashby M.F, Gibson L.J, 1984, Fracture toughness of brittle cellular solids

Masters, I.G., Evans, K.E., 1996. Models for the elastic deformation of honeycombs, *Composite Structures*, 35, 403–422.

McFarland R. K, 1963, *AIAA*, 1, 1380.

Miller, W., Smith, C.W., MacKenzie, D.S., Evans, K.E., 2009. Negative thermal expansion: A review, *Journal of Materials Science*. 44, 20, 5441-5451.

Miller W, Smith C.W, Scarpa F, Evans K.E, 2010a. Flatwise buckling optimization of hexachiral and tetrachiral honeycombs, *Composites Science and Technology*. 70, 7, 1049–1056.

Miller W, Smith C.W, Evans K.E, 2010b. Honeycomb cores with enhanced buckling strength, *Composite Structures*, 93, 1072–1077.

Murphey T, Hinkle J, 2003, Some performance trends in hierarchical truss structures, In: 44th AIAA/ASME/ASCE/AHS/ASC conference, Norfolk, p 1903.

O

Odegard G.M., 2004, Constitutive modelling of piezoelectric polymer composites, *Acta Materialia*, 52, 18, 5315-5330.

P

Papka S.D and Kyriakides S, 1994, In-plane compressive response and crushing of honeycomb, *J. Mech. Phys. Solids*, Vol. 42, No. 10, pp. 1499-1532.

Papka S.D and Kyriakides S, 1998a, experiments and full-scale numerical simulations of in-plane crushing of a honeycomb, *Acta mater.* Vol. 46, No. 8, pp. 2765.

Papka S.D and Kyriakides S, 1998b, in-plane crushing of a polycarbonate honeycomb, *Int. J. Solids Structures* Vol. 35. Nos. 3-4, pp. 239-267.

Papka S.D and Kyriakides S, 1999a, Biaxial crushing of honeycombs*Part I] Experiments, *International Journal of Solids and Structures*, 36, pp. 4367-4396.

Papka S.D and Kyriakides S, 1999b, In-plane biaxial crushing of honeycombs*Part II] Analysis, 36, pp. 4397-4423

Parkhouse J.G., 1984. Structuring: a process of material dilution, 3rd Int. Conf. on Space Structures. 367.

Parkhouse, J.G, 1987, Damage accumulation in structures, *Reliability Engineering*. 17, 2, 97–109.

Prall, D., Lakes, R.,S, 1996. Properties of a chiral honeycomb with a Poisson's ratio -1. *International Journal of Mechanical Sciences* 39, 305–314.

Price T, Timbrook R.L, 2001, Structural honeycomb panel building system, Patent number US 6,253,530 B1.

Pugno N, 2006, Mimicking nacles with super-nanotubes for producing optimized super-composites, *Nanotechnology*, 17:5480-5484.

Pugno N & Carpinteri A, 2008, Design of micro-nanoscale bio-inspired hierarchical materials, *Philosophical Magazine Letters*.

Pugno N, Chen Q, 2011, In-plane elastic properties of hierarchical cellular solids, 11th International Conference on the Mechanical Behavior of Materials, *Procedia Engineering* 10, 3026

Q

Qing H., Mishnaevsky Jr L, 2009a. 3D hierarchical computational model of wood as a cellular material with fibril reinforced, heterogeneous multiple layers, *Mechanics of Materials*. 41, 1034–1049.

Qing H., Mishnaevsky Jr L, 2009b. Unidirectional high fiber content composites: Automatic 3D FE model generation and damage simulation, *Computational Materials Science*. 47, 548–555.

R

Rodrigues H., Guedes J.M. and Bendse M.P., 2002, Hierarchical optimization of material and structure, *Structural and Multidisciplinary Optimization*, 24(1):1.

Rolls-Royce. *The Jet Engine*. Rolls-Royce, 1986. ISBN 0 902121 04 9.

S

Scarpa F, Blain S, Lew T, Perrott D, Ruzzene M, Yates J.R, 2007, Elastic buckling of hexagonal chiral cell honeycombs, *Composites: Part A*, 38, 280–289.

Shariati M & Rokhi M.M., 2008. Numerical and experimental investigations on buckling of steel cylindrical shells with elliptical cutout subject to axial compression, *Thin-Walled Structures*. 46, 11, 1251-1261.

Shaw, M. C. and Sata, T. 1966, The plastic behaviour of cellular materials. *International Journal of Mechanical Sciences*, 8,469-478.

Sypeck, D.J., 2005. Cellular truss core sandwich structures. *Applied Composite Materials*, 12, 229–246.

T

Taylor CM, Smith CW, Miller W, Evans KE, 2011, The effects of hierarchy on the in-plane elastic properties of honeycombs. *Int J Solid Struct*;48:1330–9.

Taylor CM, Smith CW, Miller W, Evans KE, 2012. Functional grading in hierarchical honeycombs: Density specific elastic performance, *Composite Structures*.

Thompson, R.W., Matthews, F.L., 1995. Load attachments for honeycomb panels in racing cars. *Materials and Design* 16 (3), 131–150.

Traintafillou. T.C, Zhang. J; Shercli T.L; Gibson L.J; Ashby M.F, 1989, Failure surfaces for cellular materials under multiaxial loads - ii. Comparison of models with experiment. *Int.J.Mech.Sci*, 31(9):665.

Traintafillou T.C; Schraad M.W, 1998, Onset of failure in aluminum honeycombs under general in-plane loading, *J. Mech. Phys Solids*, Vol. 46, No. 6, pp. 1089-1 124.

W

Waas A.M., 2002, Size effects in the compressive crushing of honeycombs, *Structures, Structural Dynamics, and Materials Con*

Wadley, H.N.G., 2006. Multifunctional periodic cellular metals. *Philosophical Transactions of the Royal Society of London Series A* 364, 31–68.

Wang A, McDowell D.L, 2003, Effects of defect on the in-plane properties of periodic metal Honeycombs, *International Journal of Mechanical Science*, 46, 1799-1813,

Wang A, McDowell D.L, 2004, In-Plane Stiffness and Yield Strength of Periodic Metal Honeycombs, *Journal of Engineering Materials and Technology*, 126, 137-156

Wang A, McDowell D.L, 2005, Yield surfaces of various periodic metal honeycombs at intermediate relative density, *International Journal of Plasticity*, 21, 285–320.

Wang Y, 1991, Elastic collapse of honeycombs under out-of-plane pressure, *Int. J. Mech Sci*, 33, 8, 637-644.

Wierzbicki T, 1983, *Int. J. Impact Eng*, 1, 157.

Wilson, S., 1990, A new face of aerospace honeycomb, *Materials and Design*, 11, 6, 323–326.

Wilbert A, Jang W.-Y, Kyriakides S, Floccari J.F, 2011, Buckling and progressive crushing of laterally loaded honeycomb, *International Journal of Solids and Structures* 48, 803–816

Wilson, S, 1990. A new face of aerospace honeycomb. *Materials and Design* 11 (6), 323–326.

Wu E and Jiang W.S, 1997, Axial crush of metallic honeycombs, *Int. J. Impact Engng*, 19, 5, 439-456.

X

Xia R, Feng XQ, Wang GF, 2011, Effective elastic properties of nanoporous materials with hierarchical structure, *Acta Materialia*, 59, 6801–6808

Z

Zhang J. & Ashby M. F, 1992a, Buckling of honeycombs under in-plane biaxial stresses, *Int. J. Mech. Sci.* Vol. 34, No. 6, pp. 491 509.

Zhang J. & Ashby M. F, 1992b, The out-of-plane properties of honeycombs, *Int. J. Mech. Sci*, 34, 6, 475~189.

Zhao H, Elnasri I, Abdennadher S, 2005, An experimental study on the behaviour under impact loading of metallic cellular materials, *International Journal of Mechanical Sciences* 47, 757–774.

Zhou, Q., Mayer, R.R., 2002. Characterization of aluminum honeycomb material failure in large deformation compression, shear, and tearing. *Journal of Engineering Materials and Technology*. 124, 412–420.

